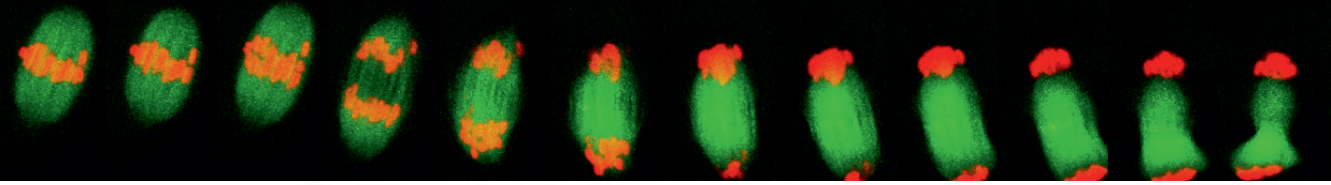

MUNI SCI

Department of Experimental Biology

MASARYK UNIVERSITY
FACULTY OF SCIENCE
DEPARTMENT OF EXPERIMENTAL BIOLOGY

Control of chromosome segregation in mammalian female meiosis

Martin Anger

Habilitation thesis
Field: Animal physiology

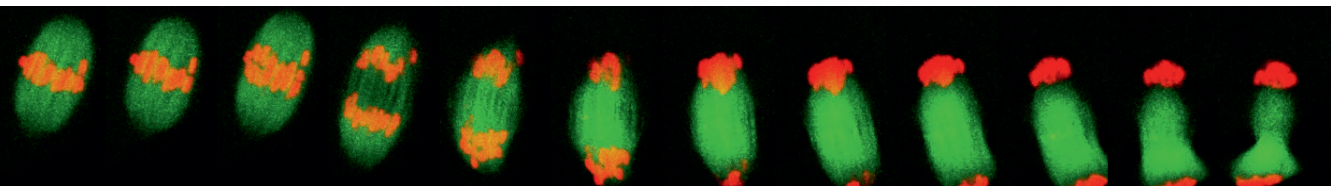

MUNI SCI Department of Experimental Biology

MASARYK UNIVERSITY
FACULTY OF SCIENCE
DEPARTMENT OF EXPERIMENTAL BIOLOGY

Control of chromosome segregation in mammalian female meiosis

Habilitation thesis
Field: Animal physiology

BRNO 2019

Martin Anger

I would like to thank all people who helped me on my way to this habilitation thesis. My first scientific mentor Josef Derka, my PhD and postdoc supervisors Jan Motlik, Michal Kubelka, Richard Schultz, Kim Nasmyth and Bela Novak. I would like to thank further to all my colleagues from laboratory at UPENN in Philadelphia, IMP in Vienna and Oxford University and to all current as well as former students and postdocs in my laboratory. I would like to express my gratitude to Czech Academy of Sciences, Veterinary Research Institute in Brno and of course Masaryk University for providing scientifically stimulating environment. And the last but not least, I would like to thank my wife Katerina and my family. Without their support I would not have achieved anything.

TABLE OF CONTENTS:

Abstract:

Chromosome segregation in mammalian oocytes and embryos is prone to errors, which might lead into numerical chromosomal aberrations or aneuploidy. Such conditions are linked with either termination of development or severe mental and developmental disorders, such as Down syndrome. Molecular mechanisms responsible for the higher incidence of chromosome segregation errors in oocytes or embryos, in comparison to the somatic cells, are still not completely understood. However, it seems that the acentrosomal spindle assembly, location of chiasmata on chromosome arms, reduction of cohesin related to maternal age, failure of protection of centromeric cohesion and limited functionality of spindle assembly checkpoint might all contribute to the high incidence of aneuploidy. And also let's not forget other remarkable differences between oocytes and almost any other cell in the body. First is their very special live cycle, oocytes are sometimes decades old when engaging into reproduction. Then there is also their enormously large volume in comparison to other cells in the body. And both prolonged maternal age and large cellular volume were shown to be affecting the aneuploidy as well. We might conclude that several mechanisms, which might, together or separately, cause chromosome segregation errors and contribute to the frequent failure of embryonic development, were identified so far. And the objective for our future studies should be to focus more closely on those, which are more important and perhaps also on possibilities how to prevent such conditions and preserve healthy gametes and embryos.

Abstrakt:

Dělení chromozomů v savčích oocytech a embryích je náchylné k chybám, které mohou vést k numerickým chromozomálním aberacím nebo též aneuploidii. Tyto stavy jsou často spojovány s předčasným ukončením vývoje nebo s těžkými mentálními a vývojovými poruchami, jako je například Downův syndrom. Molekulární mechanismy, odpovědné za vyšší výskyt aneuploidií v oocytech a embryích, ve srovnání se somatickými buňkami nejsou dosud úplně probádány. Nicméně se zdá, že sestavování dělícího vřeténka bez centrozomů, pozice chiazmat na ramenech chromozomů, redukce kohezínu v závislosti na věku matky, selhání ochrany centromerického kohezínu a nedostatečná funkce kontrolního bodu sestavení dělícího vřeténka mohou přispívat k vyšší aneuploidii u těchto buněk. A nezapomínejme také na dva další významné rozdíly mezi oocyty a téměř všemi ostatními somatickými buňkami. Jejich specializovaný životní cyklus způsobuje že někdy jsou tyto buňky staré desítky let v okamžiku, když vstupují do reprodukce. Pak také jejich enormní velikost ve srovnání s ostatními buňkami. A obě tyto vlastnosti, kterými se liší od ostatních buněk, hrají roli při vzniku aneuploidie. Můžeme konstatovat, že doposud bylo identifikováno několik mechanismů, které mohou společně nebo každý zvlášť, přispět ke vzniku aneuploidie. A úkolem dalších studií bude zaměřit se na ty nejdůležitější z nich a také na možnosti, jak těmto poruchám předcházet a zachovat zdravé gamety a embrya.

CONTROL OF CHROMOSOME SEGREGATION IN MAMMALIAN FEMALE MEIOSIS

ABSTRACT:

1. A brief overview of life cycle of mammalian oocyte

Oocytes are highly differentiated and specialized cells and notably the largest cells in a body by their volume. Together with sperm, which is on the opposite side of the size spectra, being one of the smallest cells in the body, they fuse during fertilization in order to create a genetically unique individual. Primordial germ cells appear relatively early during embryogenesis and after series of mitotic divisions they give rise to oogonia, which undergo premeiotic S phase. During S phase chromosomes are replicated and simultaneously protein complex called cohesin, which holds together sister chromatids until their separation in anaphase, is loaded on the chromosomes (Nasmyth and Haering, 2009). Cohesin complex in mammalian meiosis contains several subunits, which are not present in mitosis, namely kleisins Rec8 and Rad21L, SMC1β and SA3 (Ishiguro, 2019). This demonstrates that premeiotic S phase is unique and the germ cells are already committed to the reductional division during this stage. After completion of chromosome replication, cells undergo a unique chain of events focused on recognition and pairing of homologous chromosomes and formation of chiasmata facilitating exchange of genetic material between homologs (Gray and Cohen, 2016). The processes taking place during leptotene, zygotene and pachytene stages of prophase I are extremely complex and not yet fully understood. They are however essential and serve many important functions, such as maintaining genetic variability or providing barrier against hybridization of genetically diverse individuals during speciation. Our laboratory participated on a study leading into elucidation of a molecular mechanism behind postzygotic sterility of interspecific hybrids (Bhattacharyya *et al.*, 2013). The study revealed that the asynapsis of homologous chromosomes, consequently leading into pachytene arrest and sterility, is caused by an incomplete pairing of heterospecific homologous chromosomes. The correct formation of bivalents plays therefore also an important role in controlling speciation. In the diplotene stage of prophase I, the progression of meiosis is arrested and the oocytes remain in this stage until puberty, after which the oocytes with follicular cells are being periodically stimulated by FSH/LH hormonal waves to resume meiosis (Channing *et al.*, 1978). It is crucial to keep in mind that oocytes in mammals are unable to initiate meiosis after birth. Although it was repeatedly challenged, the provided arguments were unconvincing and this theory is still widely accepted (Johnson *et al.*, 2004). Inevitable consequence for long-living mammals, such as human, is that the prolonged meiotic arrest, which in some species lasts for decades, leads into increased frequency of chromosome segregation errors and aneuploidy in eggs (Hassold and Hunt, 2001).

2. Aneuploidy is a leading cause of termination of early development

The goal of chromosome division in mitosis, as well as in meiosis, is to achieve equal distribution of chromosomes between daughter cells. In case of chromosome segregation errors leading into unequal chromosome distribution, the resulting cells do not possess a complete set of chromosomes. Such situation is called aneuploidy and it has usually severe consequences (Santaguida and Amon, 2015; Naylor and van Deursen, 2016; Chunduri and Storchová, 2019). It needs to be mentioned there are tissues and organs in our bodies, such as liver or developing brain, which contain aneuploid cells physiologically (Rehen *et al.*, 2005; Yurov *et al.*, 2007; Duncan, 2013). However, from the long-term perspective, aneuploidy has deleterious effects mainly caused by an imbalance of the gene expression and is often associated with various pathological conditions, such as cancer and aging. Aneuploidy in mammalian germ cells is far more frequent then in somatic cells and it represents the most frequent single cause of the termination of development with incidence 2%, 20%, 20% and 35% in sperm, oocytes, embryonic blastomeres and spontaneous abortions respectively (Hassold and Hunt, 2001; Nagaoka *et al.*, 2012). There are studies showing the incidence of aneuploidy in

human embryos is as high as 73% (van Echten-Arends *et al.*, 2011). Aneuploidy can arise either during meiosis in germ cells or during mitosis in embryos. In case the aneuploidy was inherited from the germ cells all blastomeres in the embryo are affected and the development is terminated early, with exception of allosomes and trisomies (presence of extra chromosomal copy) of specific autosomes. Trisomies of chromosomes 13, 18 and 21, known as Patau, Edwards and Down syndrome respectively and aneuploidy of sex chromosomes (Lee and Kiessling, 2017) are compatible with embryonic development. The incidence of all three autosomal trisomies in human oocytes increases with maternal age, with trisomy of chromosome 13 being elevated in late twenties and 18 and 21 in thirties (Nagaoka *et al.*, 2012). Similar pattern of increasing incidence of aneuploidy in correlation with maternal age was observed also in mouse (Pan *et al.*, 2008). In our laboratory, we were interested whether there is any strain-specific variability of aneuploidy in meiosis II mouse oocytes. In order to analyse this we selected three frequently used mouse laboratory strains, namely inbred strains C57BL/6 and C3H/HeJ and outbred CD-1 strain and scored their aneuploidy in meiosis II eggs after *in vitro* maturation (Danylevska *et al.*, 2014) and [A1]. Our experiments revealed that the overall aneuploidy among these strains was similar, 2.97% 3.06 % and 3.68 % in C57BL/6, CD1 and C3H/HeJ mice respectively [A1, Figure 2B and C]. However, scoring prematurely separated sister chromatids (PSSC) in metaphase II arrested eggs revealed that all three mouse strains had different frequency of PSSC with the highest frequency 18,97 % in C3H/HeJ, 11,57 % in CD-1 and 3,72 % in C57BL/6 [A1, Figure 3A and B]. Since the chances for separated sister chromatids to segregate properly during anaphase are very low, the precociously separated sister chromatids represent a precondition for aneuploidy after fertilization. Our results demonstrated clearly that the incidence of PSSC in mouse is affected by genetic background. It is known that various mouse strains show variability in essential processes linked to cell cycle progression and chromosome segregation, for example in the level of cyclin B synthesis (Polanski *et al.*, 1998). We have no information about molecular mechanisms leading into premature loss of cohesion between sister chromatids more frequently in one strain or another, but we suspect that strain–specific levels of cohesins or factors involved in protection of cohesion, such as Sgo2, might play a role in this phenomenon.

For many applications in research, human reproduction and applications in biotechnology of farm animals, it is necessary to culture mammalian oocytes *in vitro*, sometimes for prolonged time period. We were interested whether *in vitro* culture conditions have an effect on frequency of chromosome segregation errors and aneuploidy in oocytes. In our study we focused on the effect of suboptimal temperature on the frequency of chromosome segregation errors in mouse oocytes during their *in vitro* maturation (Danadova *et al.*, 2016) and [A2]. Our initial experiments showed that the duration of meiosis I and the timing of anaphase entry were both significantly affected by the culture temperature [A2, Figure 1 and 2]. Incubating oocytes in temperature only 1.5°C lower than the optimal culture temperature showed already detectable defects, and the 3°C difference caused significant increase in misaligned chromosomes and aneuploidy [A2, Figure 4 and 5]. This illustrates clearly how cell division, particularly in oocytes, is extremely sensitive to the outside conditions, and that any disturbances of this process might lead into chromosome segregation errors.

On the contrary, it seems that not all mammals are suffering from the maternal age-related aneuploidy. We studied the incidence of this phenomenon in pigs (Hornak *et al.*, 2011) and [A3]. In contrast to mouse oocytes, in which for scoring aneuploidy we use a procedure originally developed by Francesca Duncan (Duncan *et al.*, 2009), involving disruption of meiotic spindle and 3D scanning of the whole cell volume, for porcine oocytes we had to develop an assay based on comparative genomic hybridization (CGH) [A3 Figure 1]. This allowed us to score chromosomes in non-transparent porcine oocytes. Using this protocol, we scored the number of chromosomes in metaphase II eggs and also in the corresponding polar bodies as the controls. Oocytes were obtained from pigs of various age categories. Our results surprisingly showed that the frequency of aneuploidy in young animals was quite high, around 10 – 12% in comparison to the human or mouse oocytes, in which the aneuploidy is under 5% in young individuals. However, this frequency of aneuploidy remained

similar and showed no increase with maternal age in our experiments, for up to 10 years of age [A3 Table 2]. This demonstrated that the maternal age related aneuploidy might be affecting some species more then others and therefore it would be interesting to study other species and their ability to cope with the aging of the germ cells.

3. The control of chromosome segregation during meiosis

The meiosis, as well as mitosis, is completed by segregation of chromosomes and cell division (Alberts, 2017). There are however fundamental differences in how this goal is achieved between mitosis and meiosis. In mitosis, following dissolution of the nuclear membrane a bipolar spindle assembles and kinetochores of all chromosomes are attached in such manner that the sister kinetochores are attached to the opposite poles. Then the connection between sister chromatids is abolished allowing equal segregation of chromosomes to the daughter cells. Main goal of meiosis, besides increasing genetic variability by exchange of genetic material between arms of the homologous chromosomes, is to prepare cells that fuse during fertilization, which means that they have to reduce their number of chromosomes to haploid. In order to achieve this, in meiosis there are two consecutive divisions with supressed DNA replication in between, which inevitably leads into reduction of chromosome number. Also, the configuration of the chromosomes in cells entering division differs between meiosis and mitosis. Mammals are diploid and changes in ploidy have usually fatal consequences (Otto, 2007). The cells in both divisions are therefore diploid and replicate their chromosomes during preceding S phase, reaching four copies of each autosome. During mitosis, cohesin holding sister chromatids together is removed by two-step mechanism. The first from the chromosome arms during prophase (see below the prophase pathway) and the second from the centromeres during anaphase by proteolysis. In germs cells however, paternal and maternal chromosomes, each consisting of two sister chromatids, form bivalents or tetrads connected via chiasmata and after their resolution by the cohesin complex located distally to the chiasmata (Petronczki *et al.*, 2003). Homologous chromosomes are segregated during the first meiotic division and the cohesin on chromosome arms must therefore survive until anaphase I. Separation of the homologous chromosomes is then achieved by removal of this portion of cohesin complex, while the cohesin at the kinetochores, holding together sister chromatids, must survive until meiosis II. This pool of cohesion is protected by PP2A phosphatase, transported to the kinetochores by shugoshin protein (Kitajima *et al.*, 2006; Riedel *et al.*, 2006). The cohesion holding sister chromatids around the centromeres is then dissolved during anaphase II. As I mentioned before, the bulk of cohesin complex from chromosome arms is in vertebrate mitosis removed early after entry in mitosis in a process called prophase pathway (Waizenegger *et al.*, 2000). This pathway requires activity of CDK1, Plk1 and Aurora B kinases and also protein called Wapl and it removes bulk of cohesins from chromosome arms without cleavage of any of cohesin subunit (Peters and Nishiyama, 2012). In contrast to the prophase pathway, the remaining cohesin is removed during anaphase by cohesin cleavage, and the enzyme responsible for cleavage of kleisin subunit of cohesin ring upon anaphase entry is called Separase (Uhlmann *et al.*, 1999; Uhlmann *et al.*, 2000; Waizenegger *et al.*, 2000; Hauf *et al.*, 2001). It was soon recognized that Separase is also required for segregation of homologous chromosomes in meiosis I (Siomos *et al.*, 2001; Terret *et al.*, 2003). However, it was not entirely clear, whether together with Separase cleavage a mechanism similar to the prophase pathway is operating in mammalian meiosis. In order to resolve this question, we prepared a mouse line with flox sites inserted in both alleles of Separase. The region between flox sites was then removed by CRE recombinase, and since the Separase is essential, CRE expression was controlled by ZP3 promoter, limiting the expression of CRE recombinase only to the oocytes (Kudo *et al.*, 2006) and [A4]. We first confirmed that mouse oocytes without Separase are unable to extrude the first polar body (A4, Figure 2 and 3). More importantly, our results showed that the depletion of Separase prevented removal of cohesin from chromosomes and conversion of bivalents into univalents (A4, Figure 4 C and D, Figure 5B). This was conceptually important result

demonstrating that removal of cohesin from chromosome arms during meiosis I in mammalian oocytes, which leads into separation of homologue chromosomes, requires proteolytic cleavage by Separase instead of the prophase pathway. The target of Separase cleavage during meiosis in yeast is the α–kleisin cohesin subunit called Rec8 (Klein *et al.*, 1999; Watanabe and Nurse, 1999). In order to find out whether Rec8 is also a Separase target in mouse oocytes, we constructed Rec8 with mutated Separase cleavage sites and studied the effect of overexpression of this version in mouse male and female germ cells (Kudo *et al.*, 2009) and [A5, Figure 1]. Our data suggested that the Rec8 cleavage is indeed essential for chiasmata resolution during meiosis I and also there is a difference between male and female meiosis in terms of timing of Rec8 cleavage [A5, Figures 3-9].

As mentioned earlier, the cohesin complex is removed from meiotic chromosomes in two steps, from the arms in meiosis I and from the centromeres during meiosis II. The preservation of cohesin around centromeres during anaphase I requires protection. This is mediated by proteins called shugoshins, which brings trimeric complex of PP2A to the centromeres in order prevent Rec8 phosphorylation and Separase cleavage of centromeric cohesion (Marston, 2015). In order to study shugoshin – PP2A interaction, we analysed the crystal structure of Sgo1/2 and PP2A (Xu *et al.*, 2009) and [A6]. Our experiments revealed the important residues for binding of both molecules. Further, we discovered that the Sgo1 differs from Sgo2 in more restrictive interaction with PP2A, allowing the Sgo2/PP2A to dephosphorylate distinctive substrates. The results obtained by crystallography and molecular modelling were tested in mammalian oocytes and it was demonstrated clearly that the interaction between Sgo1 and PP2A is required to protect chromosome cohesion [A6 – Figure 6].

4. Spindle assembly control mechanisms in mammalian oocytes

Unlike in somatic cells, in which the assembly of the spindle is initiated from centrosomes, in animal oocytes the spindle is assembled from Microtubule Organising Centres (MTOCs) and controlled by the chromosomes themselves (Dumont and Desai, 2012; Clift and Schuh, 2013; Bennabi *et al.*, 2016; Severson *et al.*, 2016; Gruss, 2018). In mouse embryos, the transition from the MTOC based to the centrosome based spindle assembly is completed around blastocyst stage (Courtois *et al.*, 2012). Whereas in human embryos the centrosome is inherited from the sperm and the first mitosis is already centrosomal (Sathananthan *et al.*, 1991), although all details about how the centrosome is duplicated or quadruplicated in the zygote are not available yet (Fishman *et al.*, 2018). In mouse oocytes, the spindle is assembled in the vicinity of the condensed meiotic chromosomes (Schuh and Ellenberg, 2007; Bennabi *et al.*, 2018) and the stabilization of the bipolar spindle structure involves several rounds of MTOC sorting and fragmentation (Clift and Schuh, 2015). There are also studies indicating that an exposure to *in vitro* conditions might change certain properties of the spindle itself. It is known for a relatively long time that the morphology of the spindles of *in vitro* and *in vivo* maturing oocytes is slightly different (Sanfins *et al.*, 2003; Ibáñez *et al.*, 2005; Barrett and Albertini, 2007). In order to study differences between *in vivo* and *in vitro* oocytes, we focused on spindle bipolarization and maintenance of bipolar spindle (Kovacovicova *et al.*, 2016) and [A7]. Our study was inspired by an effect of drug called monastrol, which is an inhibitor of molecule called Eg5 or Kif11, and shows different effect on *in vivo* and *in vitro* oocytes [A7, Figure 1]. Contrary to our first assumption, those *in vitro* oocytes, which were more sensitive to the Eg5 inhibitor, had significantly more Eg5 localized on the spindle [A7, Figure 2]. Our key experiment revealed that the sensitivity to Eg5 inhibitor could be induced also in the oocytes matured *in vivo* by forcing them to rebuild their spindles *in vitro* by nocodazole. As this procedure takes only several minutes, it is likely that the differences in Eg5 spindle localization and increased sensitivity to Eg5 inhibitor between oocytes matured in culture does not require gene expression. It is therefore clear the spindles built outside of the ovary use different repertoire of molecules to maintain spindle bipolarity then cells in the ovary. Given the redundancy of kinesins and their activities (Hancock, 2014) the *in vitro* and the *in vivo* spindles might be functionally similar, although fine differences might be identified by future studies.

The assembly of the meiotic spindle (or perhaps also mitotic spindle) is somehow connected to the molecular machinery involved in DNA replication. This connection is not clear, but it was shown for example that the ORC1 protein, which is essential for assembly of prereplication complexes on DNA, is also involved in control of centriole or centrosome copy number (Hemerly *et al.*, 2009). It was also shown that another protein, which is required for DNA replication and which is called CDC6, controls repression of DNA replication between meiosis I and meiosis II (Lemaître *et al.*, 2002; Whitmire *et al.*, 2002). Specifically, the absence of CDC6 is presumably important to prevent DNA replication. This was interesting and therefore we aimed to analyse whether CDC6 has similar function also in mammalian oocytes (Anger *et al.*, 2005) and [A8]. We overexpressed or knocked down the CDC6 in mouse oocytes and somewhat surprisingly our experiments revealed that this molecule is required for the spindle assembly in oocytes. Most importantly, the RNAi knockdown of CDC6 in oocytes prevented normal chromosome condensation and spindle assembly and caused arrest in meiosis I [A8, Figure 4 and 5]. Our finding was later confirmed in Xenopus oocytes (Narasimhachar *et al.*, 2012). Moreover, recently it was shown in somatic cells that DNA replication controls the timing of mitosis by regulating the activity of mitotic kinases CDK1 and Plk1 (Lemmens *et al.*, 2018). All above demonstrates that the DNA replication, spindle assembly and chromosome segregation, are linked together and controlled via shared signalling cascades.

Mammalian oocytes are dividing asymmetrically during both meiotic divisions, giving rise to a large cell, which will be eventually fertilized and to two significantly smaller polar bodies, which are extruded after each division (Figure 1A). During meiosis I, the spindle in mouse oocyte is assembled in the centre and then it moves to the cortex, where it remains also during the second meiotic division. The movement to the cortex is required for the asymmetric division of mouse oocyte, in contrast to the division of the zygote, in which the spindle is positioned centrally (Almonacid *et al.*, 2014; Chaigne *et al.*, 2017; Mogessie *et al.*, 2018) and (Figure 1B). Faithful chromosome segregation, as well as asymmetric position of the spindle in cells such as oocytes, requires proper control over the length of the spindle (Dumont *et al.*, 2007; Choi and McCollum, 2012). If the spindle length is greater than certain optimal length, it might represent a problem for the polar body extrusion (Figure 2A).

FIGURE 1

A

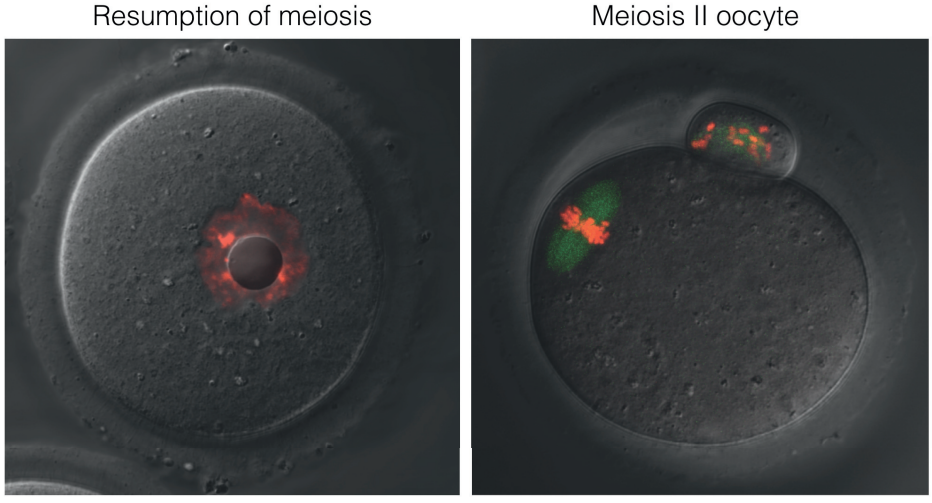

B

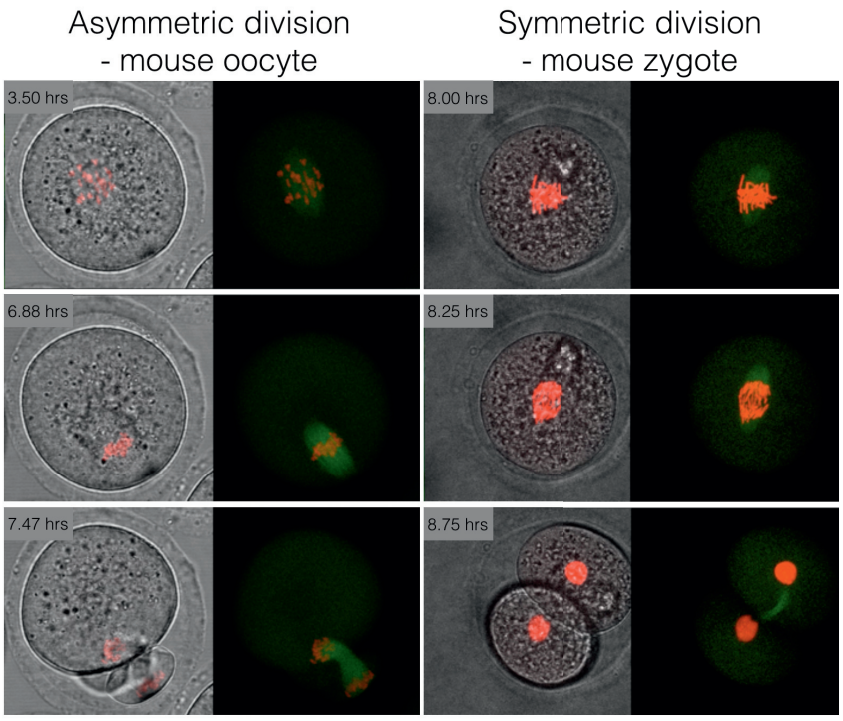

Figure 1: The asymmetric division of mouse oocyte versus symmetric division of zygote

(A): The illustrative image of mouse oocyte during resumption of meiosis (left panel) and arrested in metaphase II (right panel). Oocyte was microinjected with cRNAs encoding beta tubulin fused to EGFP and histone H2B fused to mCherry.

(B): The difference between position of the spindle in oocyte meiosis I (left panel) and the mitosis (right panel). Cells were microinjected with cRNAs encoding beta tubulin fused to EGFP and histone H2B fused to mCherry, frames from the time-lapse experiments are shown.

In comparison to the mouse oocyte, the spindle in bovine oocyte is significantly smaller (Figure 2B) demonstrating that in contrast to the larger spindle size, the smaller size of the spindle does not represent a problem for the asymmetric division.

FIGURE 2

A

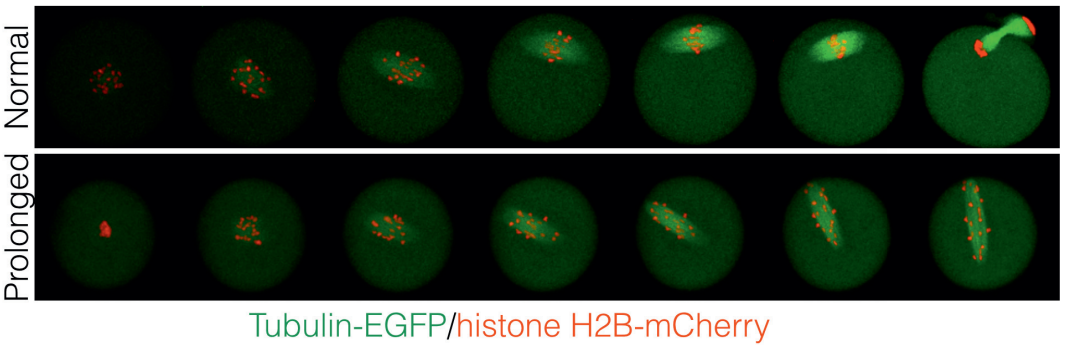

B

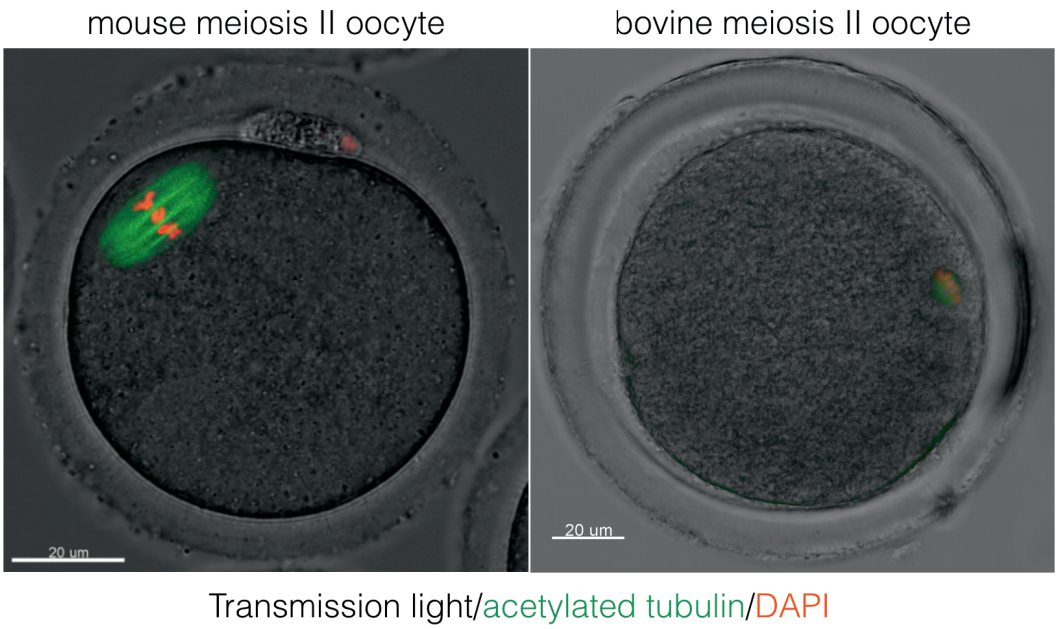

Figure 2: Spindle length in oocytes is regulated and varies between species

(A): Examples of cells with a physiological length of the meiotic spindle (top panel) and the elongated spindle, which does not support oocyte division (lower panel). Cells were microinjected with cRNAs encoding beta tubulin fused to EGFP and histone H2B fused to mCherry, frames from the time-lapse experiments are shown, the duration of the experiment was the same for both cells.

(B): Comparison of spindle length in mouse and bovine oocyte. The spindle and the chromosomes are visualized either by microinjection of tagged versions of beta tubulin and histone H2B encoding cRNAs (mouse oocyte) or by primary antibody recognizing acetylated tubulin and DAPI (bovine oocyte).

The spindle in oocytes, and also in embryos during initial cleavage cycles, is not stretched throughout the entire cell volume (Courtois *et al.*, 2012; Yamagata and FitzHarris, 2013) and Figure 1B. This changes later during development, when the spindle size is more closely adjusted to the cell size. It was shown that large cells, such as *Xenopus* eggs, have the upper limit to the spindle size (Wühr *et al.*, 2008). We were interested to find how the size of the spindle is regulated in mouse oocytes and embryos. As a model system we used blastomeres of mouse 2 cell embryos and we aimed to elucidate whether the spindle length is limited also in mammals (Novakova *et al.*, 2016) and [A8]. Using cell to cell fusion we discovered that by enlarging cell volume up to three times, the spindle size is still changing accordingly and therefore it is very unlikely that there is a limit to the spindle length in mammalian early embryos [A8, Figure 1]. Our subsequent experiments, in which we used manipulation of cell volume, nuclear volume or both, revealed that the length of the spindle is affected by the proportion between the nuclear and cytoplasmic volume [A8, Figure 2 and 3]. Our data could be probably best interpreted using recently published results, which showed that in *Xenopus* oocyte more that 80% of the total proteins are located exclusively either in the nucleus or in the cytoplasm (Wühr *et al.*, 2015). Only about 17% of total proteins are distributed evenly in both compartments. It is therefore possible that by altering the proportion between nuclear and cytoplasmic volumes we shifted a balance between both groups of proteins, which might have further effect on multiple processes in the cell, including the control over the spindle length.

5. Regulation of APC/C activity in mammalian oocytes

The assembly of the spindle in mitosis is controlled by the activity of a pathway called Spindle Assembly Checkpoint (SAC) (London and Biggins, 2014; Musacchio, 2015; Marston and Wassmann, 2017). This pathway postpones activation of a multiunit protein ligase called Anaphase Promoting Complex (APC/C), until all kinetochores are attached to the spindle and the sister kinetochores face its opposite poles (Sivakumar and Gorbsky, 2015; Kimata, 2019) (Figure 3A).

Figure 3

A

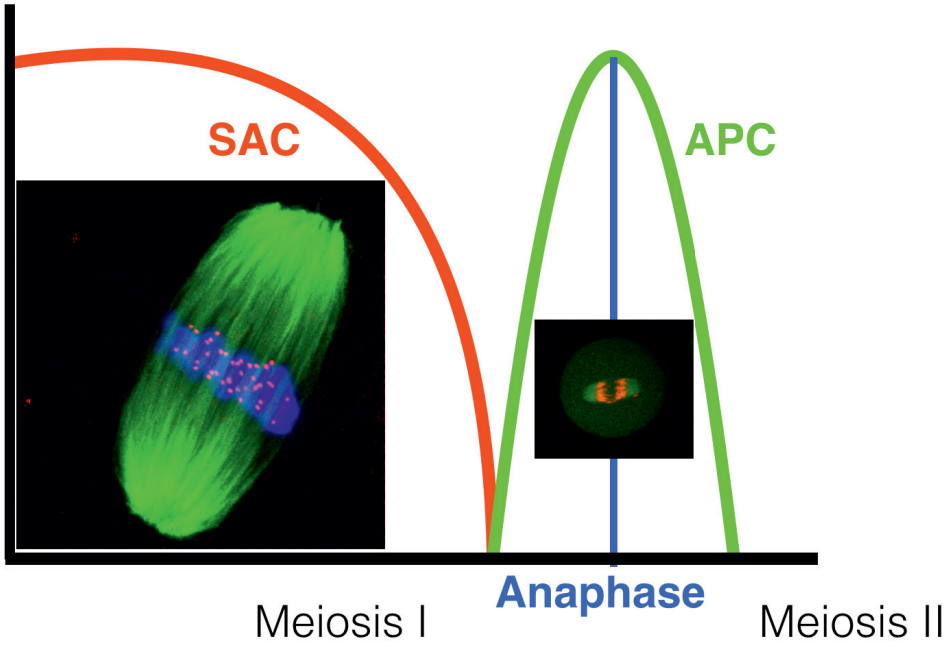

B

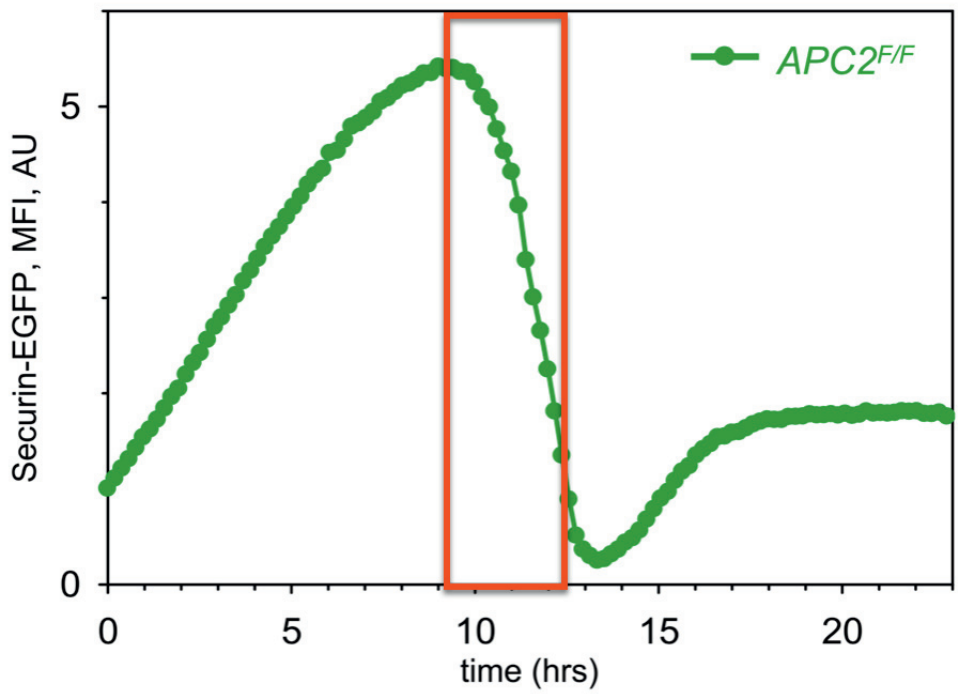

Figure 3: The relationship between SAC and APC/C activity in mouse meiosis I

(A) Schematic view of duration of the activity of Spindle Assembly Checkpoint (SAC) and Anaphase promoting complex (APC) during mouse meiosis illustrating that only after SAC is inactivated, the APC activity increases

(B) The prolonged APC/C activity during meiosis is illustrated on the expression curve of Securin (green), which, upon activation of APC/C, is destroyed within 2 – 3 hours (picture adapted from McGuinness et al. 2009).

Without this checkpoint, cells are unable to segregate chromosomes correctly and the resulting aneuploidy have severe consequences. There are three main components essential for the correct function of SAC. The first is the existence of a cohesion between sister chromatids, which is holding them together from the DNA replication in S phase, and which is also opposing to the pulling forces of the spindle allowing to create a tension. Then there is the spindle apparatus itself, providing a mechanical connection between the spindle poles and the kinetochores and pulling sister kinetochores apart. And finally, SAC requires mechanisms capable to detect and correct improper connections between kinetochores and the spindle microtubules. The spindle assembly is then based on establishing microtubule - kinetochore connections, which are dynamically dissolved in case they are incorrect, and the whole process is not finished until two main conditions are fulfilled – attachment of all kinetochores to the spindle and the tension between sister kinetochores. We have significant knowledge concerning the activation of SAC by unattached kinetochores. On the unattached kinetochores the proteins from Bub ("budding uninhibited by benzimidazole" - identified in genetic screen using budding yeast (Hoyt *et al.*, 1991)) and Mad ("mitotic arrest deficient" identified in the same model species (Li and Murray, 1991)) families catalyse a formation of a complex called mitotic checkpoint complex (MCC), which is composed of BubR1 (called Mad3 in some species), Bub3, Mad2 and CDC20 (Hardwick *et al.*, 2000; Faesen *et al.*, 2017). The CDC20, which is a coactivator of APC/C during mitosis (Watson *et al.*, 2019), is inhibited by complex with BubR1, Bub3 and Mad2, which prevents its binding to APC/C and anaphase entry. However,

significantly less clear is how SAC senses a tension between sister kinetochores (Pinsky and Biggins, 2005; Khodjakov and Pines, 2010; Salmon and Bloom, 2017). The problem is partially caused by interconnection of SAC ability to sense the improper connections, which does not cause sufficient tension, and correcting mechanisms, based on the activity of Aurora B kinase, which are able to dissolve such connections (Krenn and Musacchio, 2015). Our understanding of how the spindle pulling forces on kinetochores are being detected is still quite limited and will perhaps require more detailed knowledge about the structure of the kinetochore itself. It is however really important that we understand this process, since without it, cells are unable to establish bi-orientation of the sister kinetochores.

It was recognized some time ago that SAC function is essential also in mammalian oocyte meiosis (Brunet *et al.*, 2003; Wassmann *et al.*, 2003; Tsurumi *et al.*, 2004; Homer *et al.*, 2005a; Homer *et al.*, 2005b; Niault *et al.*, 2007). However, as most of the studies were done by knockdown or overexpression approaches, and the results were sometimes not so clear. We targeted Bub1 protein, which is essential for the SAC function, and prepared oocytes without this protein by ZP3/Cre-lox system (McGuinness *et al.*, 2009) and [A10]. Our results showed that targeting Bub1 caused premature anaphase onset without congression of chromosomes on the metaphase plate [A10, Figure 1 and 2]. And importantly, virtually all oocytes were aneuploid [A10, Figure 2]. To address whether SAC is required for postponing APC/C activity, we developed an assay based on overexpression of tagged Securin, which is an APC/C substrate, and which allowed us to analyse the APC/C activity in live cells undergoing meiotic divisions [A10, Figure 3 and 4]. These experiments clearly showed that the precocious segregation of homologues was preceded by activation of APC/C. The results provided therefore a direct evidence that SAC is required to postpone APC/C activity also in oocytes. However, the results also showed that the duration APC/C activity in oocytes is remarkably longer, about 2-3 hours (Figure 3B), in comparison to the somatic cells, in which the destruction of cyclins and securin takes tens of minutes (Hagting *et al.*, 2002).

Above mentioned results from our laboratory, as well as other laboratories, demonstrated without doubt, that SAC in oocytes is essential for postponing APC/C activity and thus for timely entry into anaphase. It is less clear however, whether SAC in meiosis poses all the functions known from somatic cells. For example, it is not uncommon to observe mouse oocytes entering anaphase with uncongressed chromosomes (Figure 4A and B).

FIGURE 4

A

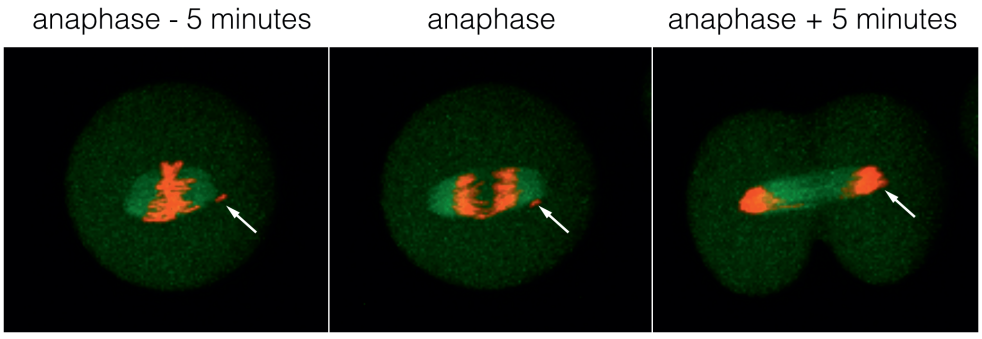

B

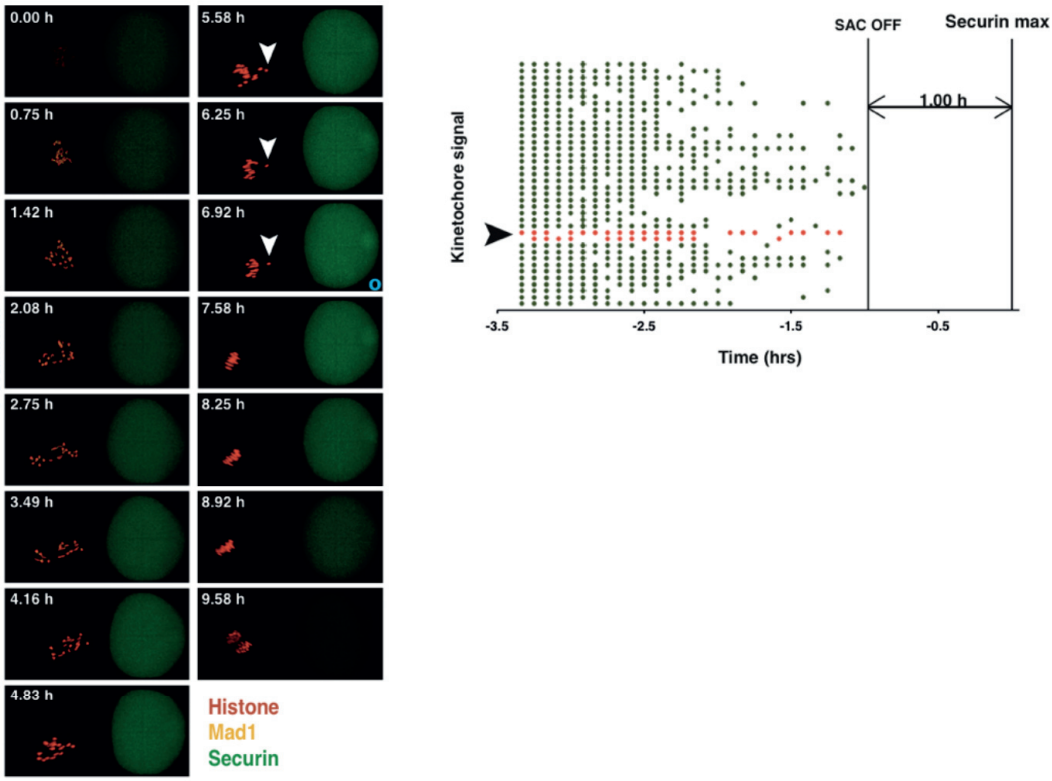

Figure 3: The impact of congression defects on SAC activity

(A) The illustrative image of mouse embryonic blastomere undergoing anaphase with congression defect. Oocyte was microinjected with cRNAs encoding beta tubulin fused to EGFP and histone H2B fused to mCherry

(B) Simultaneous detection of positions of chromosomes (red), Mad1 signal on the kinetochores (yellow) and Securin expression levels (green). (Left) lagging chromosome is indicated by arrowhead in several time frames, however the Mad1 signal from such chromosome disappears in similar time interval as form the other chromosomes (left). Oocyte was microinjected with cRNAs encoding Securin, Histone H2B and Mad1 fused to fluorescent proteins (preliminary results).

Such situation, as depicted in Figure 3, inevitably leads into chromosome segregation errors and aneuploidy in meiosis II. In fact, the inability of SAC to postpone APC/C in case of congression defects, was reported from several laboratories, including our laboratory (Nagaoka *et al.*, 2011; Lane *et al.*, 2012; Sebestova *et al.*, 2012) and [A11]. In our study we used an exceptional model system based on hybrids between two mouse species, namely *M. musculus* and *M. spretus*. The hybrids are known to be sterile and it was also shown that the aneuploidy rates in oocytes from hybrid females are extraordinarily high (Koehler *et al.*, 2006). First goal was to assess whether the hybrid oocytes poses intact SAC. For this we used treatment of oocytes with a low level of nocodazole, which does not disrupt the spindle, but it challenges the SAC and causes a permanent SAC activity. This experiment surprisingly revealed that the hybrid oocytes pose normal SAC activity, comparable to control CD1 oocytes [A11]. Despite this, as well as despite the similar duration of meiosis I between control and hybrid oocytes, they enter anaphase with severely misaligned chromosomes and multiple congression defects [A11, Figure 4 and 6]. Our recent follow-up study showed furthermore that

the oocytes from hybrid animals harbour chromosomes with unattached kinetochores undergoing nondisjunction, during which the whole tetrad is co-segregated. (Sodek *et al.*, 2017) and [A12, Figure 2 and 3]. And strikingly, such defects merely delayed anaphase onset and polar body extrusion [A12, Figure 1]. Our study [A12] provided another evidence, that the SAC in oocytes is not capable of preventing APC/C activation in case of an unattached or uncongressed kinetochores, although it was clearly demonstrated that SAC in somatic cells delays APC/C activation, even in case of a single unattached kinetochore (Rieder *et al.*, 1994).

6. Conclusions and future directions

Cell division, which involves segregation of chromosomes, is a risky affair. Even in somatic cells it comes with a chance of errors, which can be demonstrated by the correlation between the frequency of stem cell divisions in given tissue and an incidence of cancer in this tissue (Tomasetti and Vogelstein, 2015). The incidence of chromosome segregation errors in mammalian oocytes and embryos is significantly higher with aneuploidy being the leading cause of termination of development, mental or developmental disorders (Hassold and Hunt, 2001). It is my opinion that in order to gain insight why mammalian oocytes and embryos are so prone to chromosome segregation errors, we need to focus on differences between somatic cells and germs cells in the molecular mechanisms controlling chromosome segregation. One obvious difference being the cell size, both oocytes and early embryonic blastomeres are one of the largest cells in the body in terms of their cell volume. Regarding this, it was recently shown that the large amount of cytoplasm might be responsible for the lower fidelity of SAC in *C. elegans* early embryonic blastomeres (Galli and Morgan, 2016). The idea is that the strength of SAC is dependent on the number of kinetochores, whereas the APC/C machinery is determined by the cell volume. While cell volume changes, the number of kinetochores is constant for the species, and therefore SAC become weaker in larger cells. Attempts to verify the relationship between the strength of SAC and the cell volume in mouse oocytes gave inconclusive results (Kyogoku and Kitajima, 2017) (Lane and Jones, 2017) and therefore it seems we need more experiments in order to fully understand this phenomenon.

Another striking difference between the somatic cells and the germ cells and embryos, is in the regulation of the gene expression, namely the regulatory role of transcription and translation. In fully-grown oocytes the transcription is repressed (De La Fuente and Eppig, 2001) and resumes again during the activation of the zygotic genome (ZGA) (Schulz and Harrison, 2018). This means the regulation of several consecutive cell cycles is accomplished without transcription. According to our knowledge, the transcription plays an essential role in the cell cycle control in mitosis (Simmons Kovacs *et al.*, 2008; Bertoli *et al.*, 2013). In mammalian oocytes and early embryos, the absence of a regulatory role of transcription is fulfilled by regulated translation (Susor *et al.*, 2016). In case of certain molecules, this mechanism was extensively studied. We know for example that the mRNA encoding cyclin B is specifically recruited for translation, thanks to a specific sequence in its 3'UTR, and this process takes place during the initiation of meiosis I (Yang *et al.*, 2017). Another example is a molecule called Incenp, which is a member of Chromosome Passenger Complex regulating activity of Aurora B kinase (Leblond *et al.*, 2012). However, since ubiquitination is an essential part of regulation of the transition between cell cycle stages, it still remains a mystery how oocytes and early embryonic blastomeres compensate for the loss of many proteins during each cell cycle, when the transcription is being repressed. And our aim is to explore, whether the fidelity of SAC in oocytes and embryos is not affected by the absence of transcription. In fact, it is not even clear yet, whether the chromosome segregation control mechanisms, known from somatic cells, are even operational during the initial cleavage cycles of the embryo (Radonova *et al.*, 2019).

REFERENCES:

ALBERTS B (2017). Molecular Biology of the Cell.

ALMONACID M, TERRET M É, and VERLHAC M H (2014). Actin-based spindle positioning: new insights from female gametes. *J Cell Sci* 127: 477-483.

ANGER M, STEIN P, and SCHULTZ R M (2005). CDC6 requirement for spindle formation during maturation of mouse oocytes. *Biol Reprod* 72: 188-194.

BARRETT S L, and ALBERTINI D F (2007). Allocation of gamma-tubulin between oocyte cortex and meiotic spindle influences asymmetric cytokinesis in the mouse oocyte. *Biol Reprod* 76: 949-957.

BENNABI I, QUÉGUINER I, KOLANO A, BOUDIER T, MAILLY P, VERLHAC M H, and TERRET M E (2018). Shifting meiotic to mitotic spindle assembly in oocytes disrupts chromosome alignment. *EMBO Rep*

BENNABI I, TERRET M E, and VERLHAC M H (2016). Meiotic spindle assembly and chromosome segregation in oocytes. *J Cell Biol*

BERTOLI C, SKOTHEIM J M, and DE BRUIN R A (2013). Control of cell cycle transcription during G1 and S phases. *Nat Rev Mol Cell Biol* 14: 518-528.

BHATTACHARYYA T, GREGOROVA S, MIHOLA O, ANGER M, SEBESTOVA J, DENNY P, SIMECEK P, and FOREJT J (2013). Mechanistic basis of infertility of mouse intersubspecific hybrids. *Proc Natl Acad Sci U S A* 110: E468-77.

BRUNET S, PAHLAVAN G, TAYLOR S, and MARO B (2003). Functionality of the spindle checkpoint during the first meiotic division of mammalian oocytes. *Reproduction* 126: 443-450.

CHAIGNE A, TERRET M E, and VERLHAC M H (2017). Asymmetries and Symmetries in the Mouse Oocyte and Zygote. *Results Probl Cell Differ* 61: 285-299.

CHANNING C P, HILLENSJO T, and SCHAERF F W (1978). Hormonal control of oocyte meiosis, ovulation and luteinization in mammals. *Clin Endocrinol Metab* 7: 601-624.

CHOI S H, and MCCOLLUM D (2012). A role for metaphase spindle elongation forces in correction of merotelic kinetochore attachments. *Curr Biol* 22: 225-230.

CHUNDURI N K, and STORCHOVÁ Z (2019). The diverse consequences of aneuploidy. *Nat Cell Biol* 21: 54–62.

CLIFT D, and SCHUH M (2013). Restarting life: fertilization and the transition from meiosis to mitosis. *Nat Rev Mol Cell Biol* 14: 549-562.

CLIFT D, and SCHUH M (2015). A three-step MTOC fragmentation mechanism facilitates bipolar spindle assembly in mouse oocytes. *Nat Commun* 6: 7217.

COURTOIS A, SCHUH M, ELLENBERG J, and HIIRAGI T (2012). The transition from meiotic to mitotic spindle assembly is gradual during early mammalian development. *J Cell Biol* 198: 357-370.

DANADOVA J, MATIJESCUKOVA N, DANYLEVSKA A M, and ANGER M (2016). Increased frequency of chromosome congression defects and aneuploidy in mouse oocytes cultured at lower temperature. *Reprod Fertil Dev*

DANYLEVSKA A, KOVACOVICOVA K, AWADOVA T, and ANGER M (2014). The frequency of precocious segregation of sister chromatids in mouse female meiosis I is affected by genetic background. *Chromosome Res* 22: 365-373.

DE LA FUENTE R, and EPPIG J J (2001). Transcriptional activity of the mouse oocyte genome: companion granulosa cells modulate transcription and chromatin remodeling. *Dev Biol* 229: 224-236.

DUMONT J, and DESAI A (2012). Acentrosomal spindle assembly and chromosome segregation during oocyte meiosis. *Trends Cell Biol* 22: 241-249.

DUMONT J, PETRI S, PELLEGRIN F, TERRET M E, BOHNSACK M T, RASSINIER P, GEORGET V, KALAB P, GRUSS O J, and VERLHAC M H (2007). A centriole- and RanGTP-independent spindle assembly pathway in meiosis I of vertebrate oocytes. *J Cell Biol* 176: 295-305.

DUNCAN A W (2013). Aneuploidy, polyploidy and ploidy reversal in the liver. *Semin Cell Dev Biol* 24: 347–356.

DUNCAN F E, CHIANG T, SCHULTZ R M, and LAMPSON M A (2009). Evidence that a defective spindle assembly checkpoint is not the primary cause of maternal age-associated aneuploidy in mouse eggs. *Biol Reprod* 81: 768-776.

FAESEN A C, THANASOULA M, MAFFINI S, BREIT C, MÜLLER F, VAN GERWEN S, BANGE T, and MUSACCHIO A (2017). Basis of catalytic assembly of the mitotic checkpoint complex. *Nature*

FISHMAN E L, JO K, NGUYEN Q P H, KONG D, ROYFMAN R, CEKIC A R, KHANAL S, MILLER A L, SIMERLY C, SCHATTEN G, LONCAREK J, MENNELLA V, and AVIDOR-REISS T (2018). A novel atypical sperm centriole is functional during human fertilization. *Nat Commun* 9: 2210.

GALLI M, and MORGAN D O (2016). Cell Size Determines the Strength of the Spindle Assembly Checkpoint during Embryonic Development. *Dev Cell* 36: 344-352.

GRAY S, and COHEN P E (2016). Control of Meiotic Crossovers: From Double-Strand Break Formation to Designation. *Annu Rev Genet* 50: 175-210.

GRUSS O J (2018). Animal Female Meiosis: The Challenges of Eliminating Centrosomes. *Cells* 7:

HANCOCK W O (2014). Mitotic kinesins: a reason to delve into kinesin-12. *Curr Biol* 24: R968-70.

HARDWICK K G, JOHNSTON R C, SMITH D L, and MURRAY A W (2000). MAD3 encodes a novel component of the spindle checkpoint which interacts with Bub3p, Cdc20p, and Mad2p. *J Cell Biol* 148: 871-882.

HASSOLD T, and HUNT P (2001). To err (meiotically) is human: the genesis of human aneuploidy. *Nat Rev Genet* 2: 280-291.

HAUF S, WAIZENEGGER I C, and PETERS J M (2001). Cohesin cleavage by separase required for anaphase and cytokinesis in human cells. *Science* 293: 1320-1323.

HAGTING A, DEN ELZEN N, VODERMAIER H C, WAIZENEGGER I C, PETERS J M, and PINES J (2002). Human securin proteolysis is controlled by the spindle checkpoint and reveals when the APC/C switches from activation by Cdc20 to Cdh1. *J Cell Biol* 157: 1125-1137.

HEMERLY A S, PRASANTH S G, SIDDIQUI K, and STILLMAN B (2009). Orc1 controls centriole and centrosome copy number in human cells. *Science* 323: 789-793.

HOMER H A, MCDOUGALL A, LEVASSEUR M, MURDOCH A P, and HERBERT M (2005a). Mad2 is required for inhibiting securin and cyclin B degradation following spindle depolymerisation in meiosis I mouse oocytes. *Reproduction* 130: 829-843.

HOMER H A, MCDOUGALL A, LEVASSEUR M, YALLOP K, MURDOCH A P, and HERBERT M (2005b). Mad2 prevents aneuploidy and premature proteolysis of cyclin B and securin during meiosis I in mouse oocytes. *Genes Dev* 19: 202-207.

HORNAK M, JESETA M, MUSILOVA P, PAVLOK A, KUBELKA M, MOTLIK J, RUBES J, and ANGER M (2011). Frequency of aneuploidy related to age in porcine oocytes. *PLoS One* 6: e18892.

HOYT M A, TOTIS L, and ROBERTS B T (1991). S. cerevisiae genes required for cell cycle arrest in response to loss of microtubule function. *Cell* 66: 507-517.

IBÁÑEZ E, SANFINS A, COMBELLES C M, OVERSTRÖM E W, and ALBERTINI D F (2005). Genetic strain variations in the metaphase-II phenotype of mouse oocytes matured in vivo or in vitro. *Reproduction* 130: 845-855.

ISHIGURO K I (2019). The cohesin complex in mammalian meiosis. *Genes Cells* 24: 6-30.

JOHNSON J, CANNING J, KANEKO T, PRU J K, and TILLY J L (2004). Germline stem cells and follicular renewal in the postnatal mammalian ovary. *Nature* 428: 145-150.

KHODJAKOV A, and PINES J (2010). Centromere tension: a divisive issue. *Nat Cell Biol* 12: 919-923.

KIMATA Y (2019). APC/C Ubiquitin Ligase: Coupling Cellular Differentiation to G1/G0 Phase in Multicellular Systems. *Trends Cell Biol*

KITAJIMA T S, SAKUNO T, ISHIGURO K, IEMURA S, NATSUME T, KAWASHIMA S A, and WATANABE Y (2006). Shugoshin collaborates with protein phosphatase 2A to protect cohesin. *Nature* 441: 46-52.

KLEIN F, MAHR P, GALOVA M, BUONOMO S B, MICHAELIS C, NAIRZ K, and NASMYTH K (1999). A central role for cohesins in sister chromatid cohesion, formation of axial elements, and recombination during yeast meiosis. *Cell* 98: 91-103.

KOEHLER K E, SCHRUMP S E, CHERRY J P, HASSOLD T J, and HUNT P A (2006). Near-human aneuploidy levels in female mice with homeologous chromosomes. *Curr Biol* 16: R579-80.

KOVACOVICOVA K, AWADOVA T, MIKEL P, and ANGER M (2016). In Vitro Maturation of Mouse Oocytes Increases the Level of Kif11/Eg5 on Meiosis II Spindles. *Biol Reprod*

KRENN V, and MUSACCHIO A (2015). The Aurora B Kinase in Chromosome Bi-Orientation and Spindle Checkpoint Signaling. *Front Oncol* 5: 225.

KUDO N R, ANGER M, PETERS A H, STEMMANN O, THEUSSL H C, HELMHART W, KUDO H, HEYTING C, and NASMYTH K (2009). Role of cleavage by separase of the Rec8 kleisin subunit of cohesin during mammalian meiosis I. *J Cell Sci* 122: 2686-2698.

KUDO N R, WASSMANN K, ANGER M, SCHUH M, WIRTH K G, XU H, HELMHART W, KUDO H, MCKAY M, MARO B, ELLENBERG J, DE BOER P, and NASMYTH K (2006). Resolution of chiasmata in oocytes requires separase-mediated proteolysis. *Cell* 126: 135-146.

KYOGOKU H, and KITAJIMA T S (2017). Large Cytoplasm Is Linked to the Error-Prone Nature of Oocytes. *Dev Cell* 41: 287-298.e4.

LANE S I, YUN Y, and JONES K T (2012). Timing of anaphase-promoting complex activation in mouse oocytes is predicted by microtubule-kinetochore attachment but not by bivalent alignment or tension. *Development* 139: 1947-1955.

LANE S I R, and JONES K T (2017). Chromosome biorientation and APC activity remain uncoupled in oocytes with reduced volume. *J Cell Biol*

LEBLOND G G, SARAZIN H, LI R, SUZUKI M, UENO N, and LIU X J (2012). Translation of incenp during oocyte maturation is required for embryonic development in Xenopus laevis. *Biol Reprod* 86: 161, 1-8.

LEE A, and KIESSLING A A (2017). Early human embryos are naturally aneuploid-can that be corrected. *J Assist Reprod Genet* 34: 15-21.

LEMAÎTRE J M, BOCQUET S, and MÉCHALI M (2002). Competence to replicate in the unfertilized egg is conferred by Cdc6 during meiotic maturation. *Nature* 419: 718-722.

LEMMENS B, HEGARAT N, AKOPYAN K, SALA-GASTON J, BARTEK J, HOCHEGGER H, and LINDQVIST A (2018). DNA Replication Determines Timing of Mitosis by Restricting CDK1 and PLK1 Activation. *Mol Cell* 71: 117-128.e3.

LI R, and MURRAY A W (1991). Feedback control of mitosis in budding yeast. *Cell* 66: 519-531.

LONDON N, and BIGGINS S (2014). Signalling dynamics in the spindle checkpoint response. *Nat Rev Mol Cell Biol* 15: 736-747.

MARSTON A L (2015). Shugoshins: tension-sensitive pericentromeric adaptors safeguarding chromosome segregation. *Mol Cell Biol* 35: 634-648.

MARSTON A L, and WASSMANN K (2017). Multiple Duties for Spindle Assembly Checkpoint Kinases in Meiosis. *Front Cell Dev Biol* 5: 109.

MCGUINNESS B E, ANGER M, KOUZNETSOVA A, GIL-BERNABÉ A M, HELMHART W, KUDO N R, WUENSCHE A, TAYLOR S, HOOG C, NOVAK B, and NASMYTH K (2009). Regulation of APC/C activity in oocytes by a Bub1-dependent spindle assembly checkpoint. *Curr Biol* 19: 369-380.

MOGESSIE B, SCHEFFLER K, and SCHUH M (2018). Assembly and Positioning of the Oocyte Meiotic Spindle. *Annu Rev Cell Dev Biol*

MUSACCHIO A (2015). The Molecular Biology of Spindle Assembly Checkpoint Signaling Dynamics. *Curr Biol* 25: R1002-18.

NAGAOKA S I, HASSOLD T J, and HUNT P A (2012). Human aneuploidy: mechanisms and new insights into an age-old problem. *Nat Rev Genet* 13: 493-504.

NAGAOKA S I, HODGES C A, ALBERTINI D F, and HUNT P A (2011). Oocyte-specific differences in cell-cycle control create an innate susceptibility to meiotic errors. *Curr Biol* 21: 651-657.

NARASIMHACHAR Y, WEBSTER D R, GARD D L, and COUÉ M (2012). Cdc6 is required for meiotic spindle assembly in Xenopus oocytes. *Cell Cycle* 11: 524-531.

NASMYTH K, and HAERING C H (2009). Cohesin: its roles and mechanisms. *Annu Rev Genet* 43: 525-558.

NAYLOR R M, and VAN DEURSEN J M (2016). Aneuploidy in Cancer and Aging. *Annu Rev Genet* 50: 45-66.

NIAULT T, HACHED K, SOTILLO R, SORGER P K, MARO B, BENEZRA R, and WASSMANN K (2007). Changing Mad2 levels affects chromosome segregation and spindle assembly checkpoint control in female mouse meiosis I. *PLoS One* 2: e1165.

NOVAKOVA L, KOVACOVICOVA K, DANG-NGUYEN T Q, SODEK M, SKULTETY M, and ANGER M (2016). A Balance between Nuclear and Cytoplasmic Volumes Controls Spindle Length. *PLoS One* 11: e0149535.

OTTO S P (2007). The evolutionary consequences of polyploidy. *Cell* 131: 452-462.

PAN H, MA P, ZHU W, and SCHULTZ R M (2008). Age-associated increase in aneuploidy and changes in gene expression in mouse eggs. *Dev Biol* 316: 397-407.

PETERS J M, and NISHIYAMA T (2012). Sister chromatid cohesion. *Cold Spring Harb Perspect Biol* 4:

PETRONCZKI M, SIOMOS M F, and NASMYTH K (2003). Un ménage à quatre: the molecular biology of chromosome segregation in meiosis. *Cell* 112: 423-440.

PINSKY B A, and BIGGINS S (2005). The spindle checkpoint: tension versus attachment. *Trends Cell Biol* 15: 486-493.

POLANSKI Z, LEDAN E, BRUNET S, LOUVET S, VERLHAC M H, KUBIAK J Z, and MARO B (1998). Cyclin synthesis controls the progression of meiotic maturation in mouse oocytes. *Development* 125: 4989-4997.

RADONOVA L, SVOBODOVA T, and ANGER M (2019). Regulation of the cell cycle in early mammalian embryos and its clinical implications. *Int J Dev Biol*

REHEN S K, YUNG Y C, MCCREIGHT M P, KAUSHAL D, YANG A H, ALMEIDA B S, KINGSBURY M A, CABRAL K M, MCCONNELL M J, ANLIKER B, FONTANOZ M, and CHUN J (2005). Constitutional aneuploidy in the normal human brain. *J Neurosci* 25: 2176-2180.

RIEDEL C G, KATIS V L, KATOU Y, MORI S, ITOH T, HELMHART W, GÁLOVÁ M, PETRONCZKI M, GREGAN J, CETIN B, MUDRAK I, OGRIS E, MECHTLER K, PELLETIER L, BUCHHOLZ F, SHIRAHIGE K, and NASMYTH K (2006). Protein phosphatase 2A protects centromeric sister chromatid cohesion during meiosis I. *Nature* 441: 53-61.

RIEDER C L, SCHULTZ A, COLE R, and SLUDER G (1994). Anaphase onset in vertebrate somatic cells is controlled by a checkpoint that monitors sister kinetochore attachment to the spindle. *J Cell Biol* 127: 1301-1310.

SALMON E D, and BLOOM K (2017). Tension sensors reveal how the kinetochore shares its load. *Bioessays*

SANFINS A, LEE G Y, PLANCHA C E, OVERSTROM E W, and ALBERTINI D F (2003). Distinctions in meiotic spindle structure and assembly during in vitro and in vivo maturation of mouse oocytes. *Biol Reprod* 69: 2059-2067.

SANTAGUIDA S, and AMON A (2015). Short- and long-term effects of chromosome mis-segregation and aneuploidy. *Nat Rev Mol Cell Biol* 16: 473-485.

SATHANANTHAN A H, KOLA I, OSBORNE J, TROUNSON A, NG S C, BONGSO A, and RATNAM S S (1991). Centrioles in the beginning of human development. *Proc Natl Acad Sci U S A* 88: 4806-4810.

SCHUH M, and ELLENBERG J (2007). Self-organization of MTOCs replaces centrosome function during acentrosomal spindle assembly in live mouse oocytes. *Cell* 130: 484-498.

SCHULZ K N, and HARRISON M M (2018). Mechanisms regulating zygotic genome activation. *Nat Rev Genet*

SEBESTOVA J, DANYLEVSKA A, NOVAKOVA L, KUBELKA M, and ANGER M (2012). Lack of response to unaligned chromosomes in mammalian female gametes. *Cell Cycle* 11: 3011-3018.

SEVERSON A F, VON DASSOW G, and BOWERMAN B (2016). Oocyte Meiotic Spindle Assembly and Function. *Curr Top Dev Biol* 116: 65-98.

SIMMONS KOVACS L A, ORLANDO D A, and HAASE S B (2008). Transcription networks and cyclin/CDKs: the yin and yang of cell cycle oscillators. *Cell Cycle* 7: 2626-2629.

SIOMOS M F, BADRINATH A, PASIERBEK P, LIVINGSTONE D, WHITE J, GLOTZER M, and NASMYTH K (2001). Separase is required for chromosome segregation during meiosis I in Caenorhabditis elegans. *Curr Biol* 11: 1825-1835.

SIVAKUMAR S, and GORBSKY G J (2015). Spatiotemporal regulation of the anaphase-promoting complex in mitosis. *Nat Rev Mol Cell Biol* 16: 82-94.

SODEK M, KOVACOVICOVA K, and ANGER M (2017). True Nondisjunction of Whole Bivalents in Oocytes with Attachment and Congression Defects. *Cytogenet Genome Res*

SUSOR A, JANSOVA D, ANGER M, and KUBELKA M (2016). Translation in the mammalian oocyte in space and time. *Cell Tissue Res* 363: 69-84.

TERRET M E, WASSMANN K, WAIZENEGGER I, MARO B, PETERS J-M, and VERLHAC M-H (2003). The Meiosis I-to-Meiosis II Transition in Mouse Oocytes Requires Separase Activity. *Current Biology* 13: 1797-1802.

TOMASETTI C, and VOGELSTEIN B (2015). Cancer etiology. Variation in cancer risk among tissues can be explained by the number of stem cell divisions. *Science* 347: 78-81.

TSURUMI C, HOFFMANN S, GELEY S, GRAESER R, and POLANSKI Z (2004). The spindle assembly checkpoint is not essential for CSF arrest of mouse oocytes. *J Cell Biol* 167: 1037-1050.

UHLMANN F, LOTTSPEICH F, and NASMYTH K (1999). Sister-chromatid separation at anaphase onset is promoted by cleavage of the cohesin subunit Scc1. *Nature* 400: 37-42.

UHLMANN F, WERNIC D, POUPART M-A, KOONIN E V, and NASMYTH K (2000). Cleavage of Cohesin by the CD Clan Protease Separin Triggers Anaphase in Yeast. *Cell* 103: 375-386.

VAN ECHTEN-ARENDS J, MASTENBROEK S, SIKKEMA-RADDATZ B, KOREVAAR J C, HEINEMAN M J, VAN DER VEEN F, and REPPING S (2011). Chromosomal mosaicism in human preimplantation embryos: a systematic review. *Hum Reprod Update* 17: 620-627.

WAIZENEGGER I C, HAUF S, MEINKE A, and PETERS J M (2000). Two distinct pathways remove mammalian cohesin from chromosome arms in prophase and from centromeres in anaphase. *Cell* 103: 399-410.

WASSMANN K, NIAULT T, and MARO B (2003). Metaphase I arrest upon activation of the Mad2-dependent spindle checkpoint in mouse oocytes. *Curr Biol* 13: 1596-1608.

WATANABE Y, and NURSE P (1999). Cohesin Rec8 is required for reductional chromosome segregation at meiosis. *Nature* 400: 461-464.

WATSON E R, BROWN N G, PETERS J M, STARK H, and SCHULMAN B A (2019). Posing the APC/C E3 Ubiquitin Ligase to Orchestrate Cell Division. *Trends Cell Biol* 29: 117-134.

WHITMIRE E, KHAN B, and COUÉ M (2002). Cdc6 synthesis regulates replication competence in Xenopus oocytes. *Nature* 419: 722-725.

WÜHR M, CHEN Y, DUMONT S, GROEN A C, NEEDLEMAN D J, SALIC A, and MITCHISON T J (2008). Evidence for an upper limit to mitotic spindle length. *Curr Biol* 18: 1256-1261.

WÜHR M, GÜTTLER T, PESHKIN L, MCALISTER G C, SONNETT M, ISHIHARA K, GROEN A C, PRESLER M, ERICKSON B K, MITCHISON T J, KIRSCHNER M W, and GYGI S P (2015). The Nuclear Proteome of a Vertebrate. *Curr Biol* 25: 2663-2671.

XU Z, CETIN B, ANGER M, CHO U S, HELMHART W, NASMYTH K, and XU W (2009). Structure and function of the PP2A-shugoshin interaction. *Mol Cell* 35: 426-441.

YAMAGATA K, and FITZHARRIS G (2013). 4D imaging reveals a shift in chromosome segregation dynamics during mouse pre-implantation development. *Cell Cycle* 12: 157-165.

YANG Y, YANG C R, HAN S J, DALDELLO E M, CHO A, MARTINS J P S, XIA G, and CONTI M (2017). Maternal mRNAs with distinct 3' UTRs define the temporal pattern of Ccnb1 synthesis during mouse oocyte meiotic maturation. *Genes Dev* 31: 1302-1307.

YUROV Y B, IOUROV I Y, VORSANOVA S G, LIEHR T, KOLOTII A D, KUTSEV S I, PELLESTOR F, BERESHEVA A K, DEMIDOVA I A, KRAVETS V S, MONAKHOV V V, and SOLOVIEV I V (2007). Aneuploidy and confined chromosomal mosaicism in the developing human brain. *PLoS One* 2: e558.

ATTACHMENTS:

[A1] Danylevska A, Kovacovicova K, Awadova T, Anger M. The frequency of precocious segregation of sister chromatids in mouse female meiosis I is affected by genetic background. Chromosome Res. 2014;22: 365–373.

[A2] Danadova J, Matijescukova N, Danylevska AM, Anger M. Increased frequency of chromosome congression defects and aneuploidy in mouse oocytes cultured at lower temperature. Reprod Fertil Dev. 2016

[A3] Hornak M, Jeseta M, Musilova P, Pavlok A, Kubelka M, Motlik J, et al. Frequency of aneuploidy related to age in porcine oocytes. PLoS One. 2011;6: e18892.

[A4] Kudo NR, Wassmann K, Anger M, Schuh M, Wirth KG, Xu H, et al. Resolution of chiasmata in oocytes requires separase-mediated proteolysis. Cell. 2006;126: 135–146.

[A5] Kudo NR, Anger M, Peters AH, Stemmann O, Theussl HC, Helmhart W, et al. Role of cleavage by separase of the Rec8 kleisin subunit of cohesin during mammalian meiosis I. J Cell Sci. 2009;122: 2686–2698.

[A6] Xu Z, Cetin B, Anger M, Cho US, Helmhart W, Nasmyth K, et al. Structure and function of the PP2A-shugoshin interaction. Mol Cell. 2009;35: 426–441.

[A7] Kovacovicova K, Awadova T, Mikel P, Anger M. In Vitro Maturation of Mouse Oocytes Increases the Level of Kif11/Eg5 on Meiosis II Spindles. Biol Reprod. 2016

[A8] Anger M, Stein P, Schultz RM. CDC6 requirement for spindle formation during maturation of mouse oocytes. Biol Reprod. 2005;72: 188–194.

[A9] Novakova L, Kovacovicova K, Dang-Nguyen TQ, Sodek M, Skultety M, Anger M. A Balance between Nuclear and Cytoplasmic Volumes Controls Spindle Length. PLoS One. 2016;11: e0149535.

[A10] McGuinness BE, Anger M, Kouznetsova A, Gil-Bernabé AM, Helmhart W, Kudo NR, et al. Regulation of APC/C activity in oocytes by a Bub1-dependent spindle assembly checkpoint. Curr Biol. 2009;19: 369–380.

[A11] Sebestova J, Danylevska A, Novakova L, Kubelka M, Anger M. Lack of response to unaligned chromosomes in mammalian female gametes. Cell Cycle. 2012;11: 3011–3018.

[A12] Sodek M, Kovacovicova K, Anger M. True Nondisjunction of Whole Bivalents in Oocytes with Attachment and Congression Defects. Cytogenet Genome Res. 2017

Danylevska A, Kovacovicova K, Awadova T, Anger M. The frequency of precocious segregation of sister chromatids in mouse female meiosis I is affected by genetic background. Chromosome Res. 2014;22: 365–373

Impact Factor/Quartile: 2.909/Q2
Times cited (Wos May 2019): 7
Significance: First report showing genetic - based differences in frequency of aneuploidy
Contribution of the author: Experimental design, interpretation of experiments manuscript preparation, securing funding

Chromosome Res
DOI 10.1007/s10577-014-9428-6

The frequency of precocious segregation of sister chromatids in mouse female meiosis I is affected by genetic background

Anna Danylevska · Kristina Kovacovicova · Thuraya Awadova · Martin Anger

Received: 22 April 2014 / Revised: 16 May 2014 / Accepted: 2 June 2014

Abstract Mammalian female gametes frequently suffer from numerical chromosomal aberrations, the main cause of miscarriages and severe developmental defects. The underlying mechanisms responsible for the development of aneuploidy in oocytes are still not completely understood and remain a subject of extensive research. From studies focused on prevalence of aneuploidy in mouse oocytes, it has become obvious that reported rates of aneuploidy are strongly dependent on the method used for chromosome counting. In addition, it seems likely that differences between mouse strains could influence the frequency of aneuploidy as well; however, up till now, such a comparison has not been available. Therefore, in our study, we measured the levels of aneuploidy which has resulted from missegregation in meiosis I, in oocytes of three commonly used mouse strains—CD-1, C3H/HeJ, and C57BL/6. Our results revealed that, although the overall chromosomal numerical aberration rates were similar in all three strains, a different number of oocytes in each strain contained prematurely segregated sister chromatids (PSSC). This indicates that a predisposition for this type of chromosome segregation error in oocyte meiosis I is dependent on genetic background.

Keywords Meiosis · Oocyte · Aneuploidy · Numerical chromosomal aberrations · Precocious segregation of sister chromatids · Chromosomes · Univalents

Abbreviations

CGH	Comparative genomic hybridization
CSF	Cytostatic factor
FISH	Fluorescence in situ hybridization
GV	Germinal vesicle
GVBD	Germinal vesicle breakdown
PB	Polar body
PSSC	Prematurely segregated sister chromatids/ precociously separated sister chromatids
SAC	Spindle assembly checkpoint

Introduction

Meiosis is a unique type of cell division, during which the male and female haploid gametes are generated. Male germ cells are continuously entering meiosis during almost the entire lifespan of the individual. In contrast, the onset of meiotic division in oocytes, during the intrauterine development, is separated in time from the resumption of meiosis after reaching puberty. During this interval, oocytes are arrested in the prophase of the first meiotic division. In certain species, this might last for decades and is most likely a cause for high levels of chromosome segregation errors and subsequent

Responsible Editor: Fengtang Yang

Electronic supplementary material The online version of this article (doi:10.1007/s10577-014-9428-6) contains supplementary material, which is available to authorized users.

A. Danylevska · K. Kovacovicova · T. Awadova · M. Anger (✉)
Veterinary Research Institute,
Hudcova 70, 621 00 Brno, Czech Republic
e-mail: anger@vri.cz

Published online: 17 June 2014

aneuploidy. It has been reported that 5–10 % of the clinically recognized pregnancies in humans are afflicted by monosomy or trisomy, which originates in oocytes (Hassold et al. 2007; Nagaoka et al. 2012). Other mammalian species seem to share this predisposition with humans, with levels reaching up to 12 % in porcine oocytes (Hornak et al. 2011) and 7.1 % in cattle (Lechniak and Switonski 1998). In contrast, the rate of chromosomal segregation errors during meiosis in lower eukaryotes such as *Saccharomyces cerevisiae* is 1 to 10,000 (Sears et al. 1992). The vast majority of human aneuploid pregnancies terminate without ever being diagnosed, and thus, the actual level of aneuploidy in human oocytes and embryos is much higher. Detailed studies on human oocytes and embryos, which were meant for IVF, have demonstrated levels of aneuploidy reaching 20–40 % (Martin et al. 1991; Jacobs 1992; Jamieson et al. 1994; Eichenlaub-Ritter 1998; Hunt and Hassold 2010; Munne et al. 2007; Fragouli et al. 2011; Fragouli et al. 2013). It has also been shown that there is a strong correlation between maternal age and the occurrence of aneuploidy, with up to 50 % of the eggs of females over 40 years old containing an incorrect number of chromosomes (Hassold and Jacobs 1984; Hassold and Chiu 1985; Hassold and Hunt 2001; Kuliev et al. 2005; Hassold and Hunt 2009; Gianaroli et al. 2010; Hunt and Hassold 2010; Kuliev et al. 2011). In 60 % of cases, aneuploidy in female gametes results from predivision, the condition in which sister chromatids are already separated during the first meiotic division (Rosenbusch 2004; Rosenbusch 2006). Precociously separated sister chromatids are subsequently randomly segregated between the oocyte and the first polar body, creating an egg containing either one of the sister chromatids (and thus being aneuploid) or both separated sister chromatids (balanced predivision), predetermining the oocyte for aneuploidy after the second meiotic division in 50 % of cases (Angell 1997; Rosenbusch et al. 2001).

Although the causes of aneuploidy in oocytes have been studied for a relatively long time, the underlying mechanisms remain not completely understood (Eichenlaub-Ritter 2012; Howe and FitzHarris 2013; Jones and Lane 2013). Numerous studies have demonstrated that mouse oocytes do not only have a similar predisposition for aneuploidy as human oocytes (Golbus 1981; Zackowski and Martin-Deleon 1988; Zuccotti et al. 1998; Duncan et al. 2009; Sebestova et al. 2012), but also share patterns of increased aneuploidy levels relative to maternal age (Pan et al. 2008; Duncan et al. 2009; Merriman et al. 2011; Sebestova et al. 2012). This, together with the possibility to create animals with a disruption of a particular gene, makes mice an ideal model for research focused on the origins of aneuploidy in oocytes.

Based on previously published data, we can assume that the differences in reported rates of aneuploidy in mouse oocytes (Table 1) are predominantly dependent on the technique used for detection. The genetic background, however, should be taken into account as well, since, even within mice strains, differences can be observed (Aldinger et al. 2009). Moreover, recent studies have revealed that genetic background can influence the age-related aneuploidy rise in mice (Shomper et al. 2014; Yun et al. 2014b). The purpose of our study was to determine aneuploidy levels in in vitro matured oocytes of commonly used laboratory mouse strains. For this, we have selected the CD-1 outbred and the C57BL/6 and C3H/HeJ inbred mouse strains. The latter was chosen based on a comparison of previous studies, in which this strain was found to have the lowest aneuploidy rates (Hansmann 1974; Rohrborn and Hansmann 1974). To measure the levels of aneuploidy, we used a method which allowed us not only to score numbers of chromosomes but also to analyze the mutual positions of sister chromatids and the distance between their kinetochores in intact cells. Our results showed that assessing the configuration of sister chromatids in oocytes is at least as important as determining the overall number of chromosomes.

Materials and methods

Mice

The CD-1, C3H/HeJ, and C57BL/6 mouse strains were purchased from AnLab, Czech Republic, and the Animal Breeding and Experimental Facility, Faculty of Medicine, Masaryk University, Czech Republic. All animal work was conducted in accordance with Act No 246/1992 Coll., on the protection of animals against cruelty under the supervision of the Central Commission for Animal Welfare, approval ID 018/2010.

Table 1 Overview of previously published aneuploidy rates in mouse strains

Strain	Age of animals	Aneuploidy rate	Technique	Reference
CD-1	4–12 weeks	3–4 %	In vitro (hCG)/monastrol/CREST	Merriman et al. (2011)
	8–12 weeks	13.7 %	In vivo (PMSG)/C-banded	Mailhes et al. (2002)
	8–20 weeks	4.1 %	In vitro/monastrol/CREST	Sebestova et al. (2012)
C57BL/6	6–8 weeks	4.3 %	In vivo (PMSG)/spread	Cheng et al. (2011)
C3H/HeJ	10–12 weeks	3.6 %		Hansmann 1974

Oocyte harvesting and maturation

Adult (12–20 weeks) female mice were sacrificed and the ovaries were excised. The ovarian tissue was disaggregated in a drop of M2 medium (Sigma-Aldrich) with 100 μM 3-isobutyl-1-methylxanthine (IBMX, Sigma-Aldrich). Germinal vesicle (GV)-stage oocytes were subsequently incubated in a drop of M16 medium, (Sigma-Aldrich) containing 100 μM IBMX and covered with a mineral oil (Sigma-Aldrich), at 37 °C, 5 % CO_2, for at least 1 h prior to further procedures. Maturation was induced by the removal of the inhibitor from the media, and 1.5 h after the onset of maturation, the oocytes, which had not undergone germinal vesicle breakdown (GVBD), were discarded from further use.

Immunofluorescence and kinetochore counting assay

The immunofluorescence protocol and kinetochore counting assay were adopted from Duncan et al. (2009) and Sebestova et al. (2012). Twenty hours after the onset of maturation, MII-stage oocytes were selected, washed in M16 medium with 100 μM monastrol (Sigma-Aldrich) or 2 μM dimethylenastron (Sigma-Aldrich), and incubated at 37 °C, 5 % CO_2 for 2 h.

The zona pellucida and polar bodies (PBs) were subsequently removed by a short incubation in Pronase (Sigma-Aldrich). The oocytes were fixed with 2 % paraformaldehyde (Sigma-Aldrich) for 20 min and permeabilized with 0.1 % Triton for 15 min. The fixation was followed by immuno-staining with a human anti-centromere antibody (HCT-0100, Immunovision, 1:500) and an Alexa Flour 555 goat anti-human secondary antibody (A21433, 1:500, Invitrogen, Life Technologies). Vectashield with DAPI (H-1200, Vector Laboratories) was used as a mounting medium. The cells were scanned using a Leica AF 6000 inverted fluorescence microscope, equipped with a HCX PL APO ×100/1.4–0.7 oil objective. Leica A filter cube (exCitation filter

A

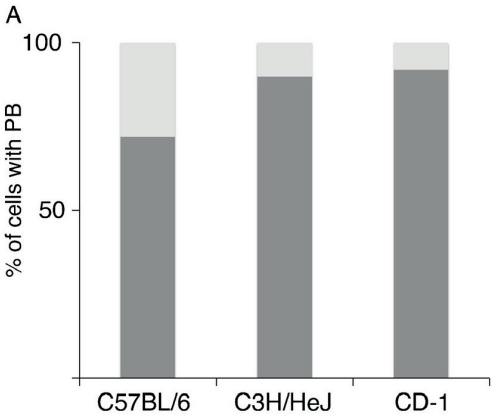

B

Mouse strain	Number of oocytes	Number of cells with PB after 20 hrs
C57BL/6	342	246
C3H/HeJ	241	217
CD-1	389	358

Fig. 1 Polar body extrusion during in vitro maturation of oocytes isolated from C57BL/6, C3H/HeJ, and CD-1 strains. **a** Oocytes from the C57BL/6, C3H/HeJ, and CD-1 mouse strains which have undergone GVBD within 1.5 h after the onset of maturation were scored for the presence of polar bodies after 20 h of maturation. Among the oocytes, 71.9 % from C57BL/6 (n=342), 90 % from C3H/HeJ (n=241), and 92 % from CD-1 (n=389) mice reached the MII-stage and extruded PB. The *light grey bars* indicate a portion of cells which have not reached the MII-stage. The *dark grey bars* indicate the percentage of oocytes with PB after 20 h of maturation. **b** The total numbers of oocytes from each strain used in the experiments are indicated in the *table*

BP 360/40) and Leica DsRed ET filter cube (exCitation filter BP 546/11) were used for the detection of DAPI and an Alexa Fluor 555, respectively. The Z-resolution was automatically optimized by LAS AF software. IMARIS software was used for 3D reconstruction.

Statistical analysis

Data were analyzed using Fisher's exact test. Statistical analysis was performed using Prism software, version 5.00 for Mac (GraphPad Software, San Diego, CA, USA, www.graphpad.com).

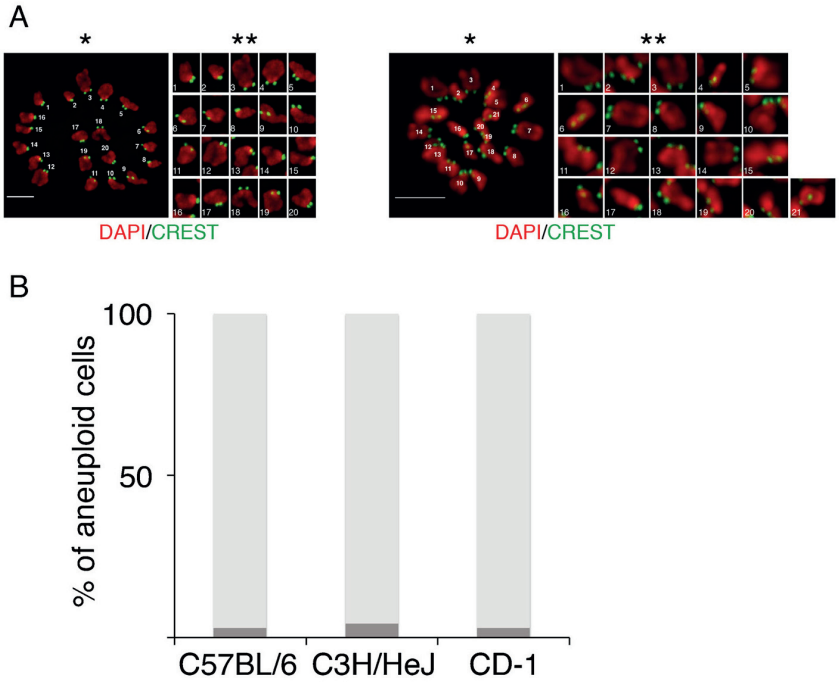

C

Mouse strain	Number of cells	Number of aneuploid cells
C57BL/6	236	7
C3H/HeJ	190	7
CD-1	327	10

Fig. 2 Aneuploidy rates are similar in C57BL/6, C3H/HeJ, and CD-1 mouse strains. **a** *left panel, single asterisk*: a euploid MII-stage oocyte fixed after monastrol treatment, with 20 pairs of closely positioned kinetochores; *left panel, double asterisks*: 20 individual univalents from the same cell reconstructed from selected z plains. *Right panel, single asterisk*: an aneuploid oocyte with an additional univalent; *right panel, double asterisks*: 21 individual pairs of attached sister chromatids. Chromosomes (in *red*) stained with DAPI, kinetochores (in *green*) labeled by CREST antiserum. *Scale bar* represents 5 μm. The chromosomes are numbered randomly. **b** The frequency of aneuploidy was scored in mice from inbred C57BL/6 (n=236) and C3H/HeJ (n=190) strains and the CD-1 outbred strain (n=327). Aneuploidy levels reached 2.97 % in C57BL/6, 3.68 % in C3H/HeJ, and 3.06 % in CD-1 mice. No significant difference was observed between the represented strains (p>0.05). The *light grey bars* represent the rate of euploid oocytes; the *dark grey bars* represent the rate of aneuploid cells. **c** The numbers of oocytes from each strain, which were analyzed for aneuploidy, are indicated in the *table*

Results

The ability to complete meiosis in vitro varies between selected mouse strains

We analyzed the ability of oocytes from adult mice (12–20 weeks) of all three strains to resume and complete meiosis in our culture conditions (see "Materials and methods"). Most of the oocytes resumed meiosis within 1.5 h after the onset of maturation, and only the oocytes which accomplished GVBD within this time were selected for further analysis. Twenty hours after the onset of maturation, oocytes from each strain were scored for polar body extrusion (PBE). The lowest maturation rate, 71.9 %, was observed in C57BL/6 oocytes, in contrast to 90 % in the C3H/HeJ and 92 % in the CD-1 strains (Fig. 1a, b). Moreover, the ovaries of C57BL/6 mice contained a lower number of fully grown GV oocytes compared to those of the other strains in our study. On average, we were able to obtain 22 fully grown GV oocytes per mice from the C57BL/6 strain and 35 and 45 in the C3H/HeJ and CD-1 strains, respectively (data not shown).

The frequency of aneuploidy in MII-stage oocytes is similar for CD-1, C57BL/6, and C3H/HeJ strains

After PBE and the formation of the second meiotic spindle, oocytes arrest at the metaphase II due to the activity of the cytostatic factor (CSF) (Madgwick and Jones 2007). At this time point, we scored the outcome of the first meiotic division. To establish the number of chromosomes in the MII-stage oocytes, we employed the kinetochore counting assay (Duncan et al. 2009; Sebestova et al. 2012). Oocytes which contained 40 kinetochores were scored as euploid (Fig. 2a, left panel). Cells with a different number of kinetochores were scored as aneuploid (Fig. 2a, right panel). Thanks to the optimization of cell coverage by z stacks and the subsequent 3D reconstruction of the entire cell by Imaris software, we were able to resolve the superimposed or closely associated kinetochores as well (Fig. S1). Our results revealed that the frequency of aneuploidy in oocytes of all three strains is similar, ranging from 2.97 % in C57BL/6 through 3.06 % in CD-1 and up to 3.68 % in C3H/HeJ (Fig. 2b, c). According to statistical analysis, the differences in aneuploidy levels between selected strains were statistically not significant. The aneuploidy rates obtained in our experiments were consistent with previously published results (Hansmann 1974; Duncan et al. 2009; Cheng et al. 2011; Merriman et al. 2011; Sebestova et al. 2012; Table 1).

The frequency of prematurely separated sister chromatids varies between selected mouse strains

While examining metaphase II oocytes for aneuploidy, we detected separated kinetochore signals of sister

A

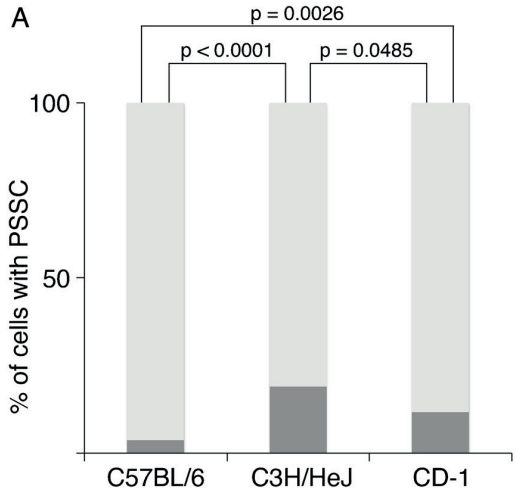

B

Mouse strain	Number of cells	Number of cells with PSSC
C57BL/6	215	8
C3H/HeJ	174	33
CD-1	242	28

Fig. 3 Levels of prematurely segregated sister chromatids in oocytes from C57BL/6, C3H/HeJ, and CD-1 mouse strains. **a** In 3.72 % of the C57BL/6 oocytes (n=215), 18.97 % of the C3H/HeJ (n=174), and 11.57 % of the CD-1 (n=242), PSSC were detected. There was a significant difference in the number of oocytes with prematurely segregated sister chromatids between all three strains (p<0.0001 for C57BL/6 vs. C3H/HeJ; p=0.0026 for C57BL/6 vs. CD-1 strains; p=0.0485 for C3H/HeJ vs. CD-1 strains). The *light grey bars* signify oocytes which did not contain PSSC; the *dark grey bars* indicate the rate of cells with PSSC. **b** The number of the oocytes from selected mouse strains containing PSSC is specified in the *table*

chromatids in some cells. The presence of single chromatids in MII-stage oocytes could lead to incorrect chromosome segregation in the following division and might impairs the subsequent development of an aneuploid embryo. Therefore, we decided to establish the number of cells containing prematurely segregated sister chromatids/precociously separated sister chromatids (PSSC), by scoring separated sister chromatids in the cells, which were previously analyzed for aneuploidy. Our results showed dramatic differences in the number of oocytes with PSSC between the selected strains (Fig. 3a, b). As shown in Fig. 4a, 11,57 % of CD-1 oocytes, 18,97 % of C3H/HeJ and 3,72 % of C57BL/6 oocytes contained at least one separated pair of kinetochores or a single kinetochore (Fig. 4a). However, we realized that cells with PSSC did not always contain a numerical chromosomal aberration. Therefore, the proportion of euploid versus aneuploid cells in the group of oocytes containing PSSC was established (Fig. 4b). Strikingly, the majority of the cells with prematurely segregated sister chromatids had a correct number of chromosomes, despite the fact that the actual proportion was different for each strain. More specifically, 37.5 % of oocytes from C57BL/6, 78.8 % from C3H/HeJ, and 78.6 % from CD-1 strains, which contained PSSC, were euploid.

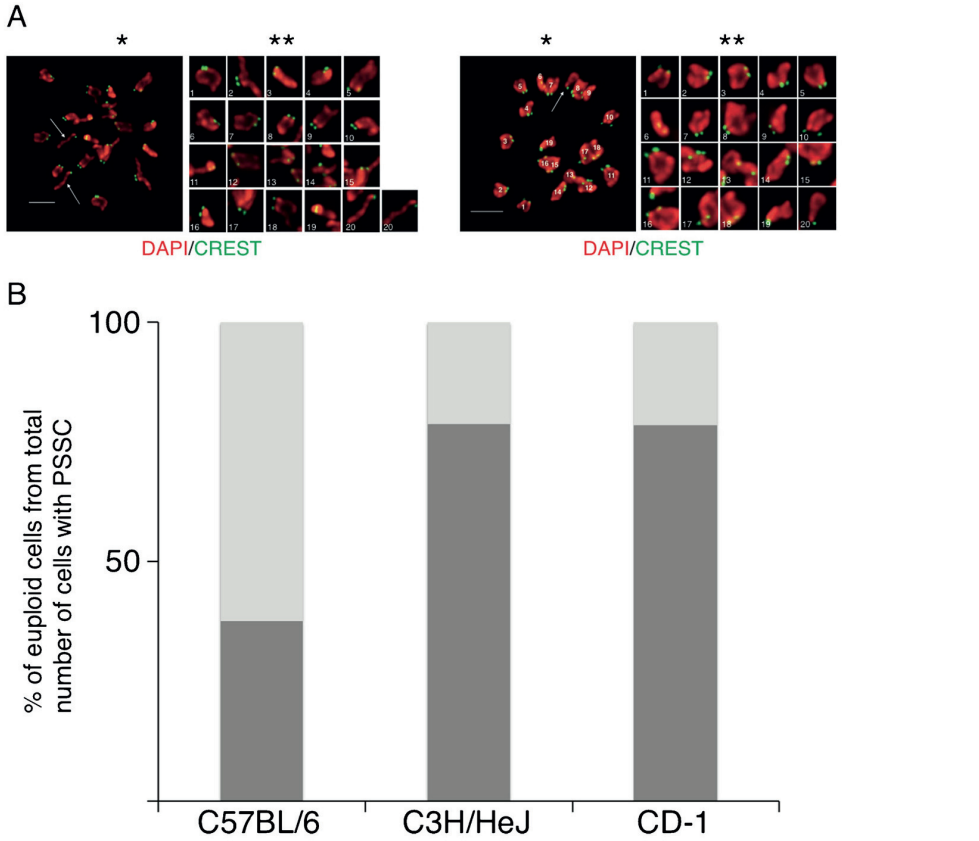

Fig. 4 Proportion of cells with balanced and unbalanced predivision in oocytes from C57BL/6, C3H/HeJ, and CD-1 mouse strains. **a** *Left panel, single asterisk*: predivision in the euploid oocyte; *left panel, double asterisks*: 19 univalents and 2 prematurely segregated sister chromatids. **a** *right panel, single asterisk*: oocyte with aneuploidy caused by predivision; *right panel*, *double asterisks*: 19 individual dyads and 1 single chromatid. Sister chromatids (marked by *arrows*) display one kinetochore signal each. Chromosome and kinetochore staining is like in Fig. 2a. *Scale bar* represents 5 μm. The chromosomes are numbered randomly. **b** The numbers of euploid oocytes from the total amount of oocytes with PSSC for each mouse strain were as follows: 37.5 % of the oocytes from the C57BL/6 strain (n=8), 78.8 % from the C3H/HeJ strain (n=33), and 78.6 % from the CD-1 (n=28). The *light grey bars* represent oocytes with unbalanced predivision: the *dark grey bars* represent cells with balanced predivision

Discussion

In our study, we analyzed the frequency of aneuploidy in the oocytes of three commonly used mouse strains. Thanks to the method we used, we were able to not only determine the number of chromosomes in each oocyte but also to evaluate the distance between all the sister chromatids and their relative positions. In comparison, conventional FISH is usually limited by the number of probes and routinely only three to six chromosomes per cell are detected (Nagaoka et al. 2012). Even when using the newest techniques, such as comparative genome hybridization (CGH) and array comparative genome hybridization (array-CGH), it is impossible to detect all the cells with PSSC since the cells with a balanced predivision are scored as euploid (Gutierrez-Mateo et al. 2011; Colls et al. 2012).

Our study revealed that the rates of numerical chromosomal aberrations in in vitro matured MII-stage oocytes were similar between the selected strains. However, more frequently than an incorrect number of chromosomes, oocytes harbored prematurely separated sister chromatids in metaphase II. Our results clearly show that the frequency of PSSC varies between the strains of our selection, and therefore, the predisposition for predivision depends on the genetic background. This finding is important because the precocious dissolution of the ties between sister chromatids is a major source of aneuploidy in oocytes and embryos, constituting more than half of the aneuploidy cases in humans (Rosenbusch 2004; Rosenbusch 2006). Moreover, PSSC is reported to be a main reason for age-related aneuploidy increase in both humans and mice (Vialard et al. 2006; Yun et al. 2014a). The precociously separated sister chromatids exploit a blind spot of the control mechanism called the spindle assembly checkpoint (SAC) by establishing a merotelic kinetochore-microtubule attachment, thus escaping detection by SAC (O'Connell et al. 2008; Gregan et al. 2011). Undetected by the surveillance mechanisms, sister chromatids are then distributed randomly between the polar body and the oocyte in anaphase II, causing a numerical abnormality in 50 % of cells (Angell 1997; Rosenbusch et al. 2001).

Our results are opening new avenues for studying the mechanisms responsible for predivision in oocytes. A comparison of mouse strains with different levels of PSSC might help our understanding of the mechanisms behind maternal age-related aneuploidy. There is, however, a possibility that the premature segregation of sister chromatids in in vitro cultured oocytes has a different underlying mechanism from PSSC in oocytes from animals of advanced age. Indeed, our preliminary results indicate that the amount of cohesin subunit Rec8 on chromosomes does not vary significantly between the strains used in this study (data not shown), although the deterioration of cohesion is most likely behind maternal age-related aneuploidy (Chiang et al. 2010; Lister et al. 2010; Revenkova et al. 2010; Tachibana-Konwalski et al. 2010) as well as aneuploidy in oocytes from young mice (Merriman et al. 2013).

The differences between mouse strains have been shown to interfere with the progression of female germ cells through meiosis (Polanski et al. 1998) or with the correlation of aneuploidy occurrence with the maternal age (Shomper et al. 2014; Yun et al. 2014a, b). Our results emphasize the importance of the careful selection of mouse strains for experiments, due to the influence, which the genetic background might have on the outcome of meiosis.

Acknowledgments We are grateful to Jiri Rubes for helpful discussion and useful comments. This work was supported by Czech science foundation project P502/12/2201 and by MEYS projects ED1.1.00/02.0068—CEITEC, CZ.1.07/2.3.00/20.0213—CeDiLa, and LH 13072—Kontakt II.

Ethical standards The authors declare that all experiments performed in this study comply with the current laws of the Czech Republic. All institutional and national guidelines for the care and use of laboratory animals were followed.

Conflict of interest The authors (A.D., K.K., T.A., and M.A.) declare that they have no conflict of interest.

References

Aldinger KA, Sokoloff G, Rosenberg DM, Palmer AA, Millen KJ (2009) Genetic variation and population substructure in outbred CD-1 mice: implications for genome-wide association studies. PLoS One 4:e4729

Angell R (1997) First-meiotic-division nondisjunction in human oocytes. Am J Hum Genet 61:23–32

Cheng PP, Xia JJ, Wang HL et al (2011) Islet transplantation reverses the effects of maternal diabetes on mouse oocytes. Reproduction 141:417–424

Chiang T, Duncan FE, Schindler K, Schultz RM, Lampson MA (2010) Evidence that weakened centromere cohesion is a leading cause of age-related aneuploidy in oocytes. Curr Biol 20:1522–1528

Colls P, Escudero T, Fischer J et al (2012) Validation of array comparative genome hybridization for diagnosis of translocations in preimplantation human embryos. Reprod BioMed Online 24:621–629

Duncan FE, Chiang T, Schultz RM, Lampson MA (2009) Evidence that a defective spindle assembly checkpoint is not the primary cause of maternal age-associated aneuploidy in mouse eggs. Biol Reprod 81:768–776

Eichenlaub-Ritter U (1998) Genetics of oocyte ageing. Maturitas 30:143–169

Eichenlaub-Ritter U (2012) Oocyte ageing and its cellular basis. Int J Dev Biol 56:841–852

Fragouli E, Alfarawati S, Goodall NN, Sanchez-Garcia JF, Colls P, Wells D (2011) The cytogenetics of polar bodies: insights into female meiosis and the diagnosis of aneuploidy. Mol Hum Reprod 17:286–295

Fragouli E, Alfarawati S, Spath K et al (2013) The origin and impact of embryonic aneuploidy. Hum Genet 132:1001–1013

Gianaroli L, Magli MC, Cavallini G et al (2010) Predicting aneuploidy in human oocytes: key factors which affect the meiotic process. Hum Reprod 25:2374–2386

Golbus MS (1981) The influence of strain, maternal age, and method of maturation on mouse oocyte aneuploidy. Cytogenet Cell Genet 31:84–90

Gregan J, Polakova S, Zhang L, Tolic-Norrelykke IM, Cimini D (2011) Merotelic kinetochore attachment: causes and effects. Trends Cell Biol 21:374–381

Gutierrez-Mateo C, Colls P, Sanchez-Garcia J et al (2011) Validation of microarray comparative genomic hybridization for comprehensive chromosome analysis of embryos. Fertil Steril 95:953–958

Hansmann I (1974) Chromosome aberrations in metaphase II-oocytes. Stage sensitivity in the mouse oogenesis to amethopterin and cyclophosphamide. Mutat Res 22:175–191

Hassold T, Chiu D (1985) Maternal age-specific rates of numerical chromosome abnormalities with special reference to trisomy. Hum Genet 70:11–17

Hassold T, Hunt P (2001) To err (meiotically) is human: the genesis of human aneuploidy. Nat Rev Genet 2:280–291

Hassold T, Hunt P (2009) Maternal age and chromosomally abnormal pregnancies: what we know and what we wish we knew. Curr Opin Pediatr 21:703–708

Hassold TJ, Jacobs PA (1984) Trisomy in man. Annu Rev Genet 18:69–1897

Hassold T, Hall H, Hunt P (2007) The origin of human aneuploidy: where we have been, where we are going. Hum Mol Genet 16(2):203–208

Hornak M, Jeseta M, Musilova P et al (2011) Frequency of aneuploidy related to age in porcine oocytes. PLoS One 6: e18892

Howe K, FitzHarris G (2013) Recent insights into spindle function in mammalian oocytes and early embryos. Biol Reprod 89:71

Hunt P, Hassold T (2010) Female meiosis: coming unglued with age. Curr Biol 20:699–702

Jacobs PA (1992) The chromosome complement of human gametes. Oxf Rev Reprod Biol 14:47–72

Jamieson ME, Coutts JR, Connor JM (1994) The chromosome constitution of human preimplantation embryos fertilized in vitro. Hum Reprod 9:709–715

Jones KT, Lane SI (2013) Molecular causes of aneuploidy in mammalian eggs. Development 140:3719–3730

Kuliev A, Cieslak J, Verlinsky Y (2005) Frequency and distribution of chromosome abnormalities in human oocytes. Cytogenet Genome Res 111:193–198

Kuliev A, Zlatopolsky Z, Kirillova I, Spivakova J, Cieslak Janzen J (2011) Meiosis errors in over 20,000 oocytes studied in the practice of preimplantation aneuploidy testing. Reprod BioMed Online 22:2–8

Lechniak D, Switonski M (1998) Aneuploidy in bovine oocytes matured in vitro. Chromosom Res 6:504–506

Lister LM, Kouznetsova A, Hyslop LA et al (2010) Age-related meiotic segregation errors in mammalian oocytes are preceded by depletion of cohesin and Sgo2. Curr Biol 20:1511–1521

Madgwick S, Jones KT (2007) How eggs arrest at metaphase II: MPF stabilisation plus APC/C inhibition equals cytostatic factor. Cell Div 2:4

Mailhes JB, Hilliard C, Lowery M, London SN (2002) MG-132, an inhibitor of proteasomes and calpains, induced inhibition of oocyte maturation and aneuploidy in mouse oocytes. Cell Chromosome 1:2

Martin RH, Ko E, Rademaker A (1991) Distribution of aneuploidy in human gametes: comparison between human sperm and oocytes. Am J Med Genet 39:321–331

Merriman JA, Jennings PC, McLaughlin EA, Jones KT (2011) Effect of aging on superovulation efficiency, aneuploidy rates, and sister chromatid cohesion in mice aged up to 15 months. Biol Reprod 86:49

Merriman JA, Lane SI, Holt JE et al (2013) Reduced chromosome cohesion measured by interkinetochore distance is associated with aneuploidy even in oocytes from young mice. Biol Reprod 88:31

Munne S, Chen S, Colls P et al (2007) Maternal age, morphology, development and chromosome abnormalities in over 6000 cleavage-stage embryos. Reprod BioMed Online 14:628–634

Nagaoka SI, Hassold TJ, Hunt PA (2012) Human aneuploidy: mechanisms and new insights into an age-old problem. Nat Rev Genet 13:493–504

O'Connell CB, Loncarek J, Hergert P, Kourtidis A, Conklin DS, Khodjakov A (2008) The spindle assembly checkpoint is satisfied in the absence of interkinetochore tension during mitosis with unreplicated genomes. J Cell Biol 183:29–36

Pan H, Ma P, Zhu W, Schultz RM (2008) Age-associated increase in aneuploidy and changes in gene expression in mouse eggs. Dev Biol 316:397–407

Polanski Z, Ledan E, Brunet S et al (1998) Cyclin synthesis controls the progression of meiotic maturation in mouse oocytes. Development 125:4989–4997

Revenkova E, Herrmann K, Adelfalk C, Jessberger R (2010) Oocyte cohesin expression restricted to predictyate stages provides full fertility and prevents aneuploidy. Curr Biol 20:1529–1533

Rohrborn G, Hansmann I (1974) Oral contraceptives and chromosome segregation in oocytes of mice. Mutat Res 26:535–544

Rosenbusch B (2004) The incidence of aneuploidy in human oocytes assessed by conventional cytogenetic analysis. Hereditas 141:97–105

Rosenbusch B (2006) The contradictory information on the distribution of non-disjunction and pre-division in female gametes. Hum Reprod 21:2739–2742

Rosenbusch B, Glaeser B, Schneider M (2001) Aneuploidy in human oocytes: nondisjunction or predivision? Cytogenet Cell Genet 94:241–243

Sears DD, Hegemann JH, Hieter P (1992) Meiotic recombination and segregation of human-derived artificial chromosomes in

Saccharomyces cerevisiae. Proc Natl Acad Sci U S A 89: 5296–5300

Sebestova J, Danylevska A, Novakova L, Kubelka M, Anger M (2012) Lack of response to unaligned chromosomes in mammalian female gametes. Cell Cycle 11:3011–3018

Shomper M, Lappa C, FitzHarris G (2014) Kinetochore microtubule establishment is defective in oocytes from aged mice. Cell Cycle 13:1171–1179

Tachibana-Konwalski K, Godwin J, van der Weyden L et al (2010) Rec8-containing cohesin maintains bivalents without turnover during the growing phase of mouse oocytes. Genes Dev 24:2505–2516

Vialard F, Petit C, Bergere M et al (2006) Evidence of a high proportion of premature unbalanced separation of sister chromatids in the first polar bodies of women of advanced age. Hum Reprod 21: 1172–1178

Yun Y, Lane SI, Jones KT (2014a) Premature dyad separation in meiosis II is the major segregation error with maternal age in mouse oocytes. Development 141:199–208

Yun Y, Holt JE, Lane SI, McLaughlin EA, Merriman JA, Jones KT (2014b) Reduced ability to recover from spindle disruption and loss of kinetochore spindle assembly checkpoint proteins in oocytes from aged mice. Cell Cycle 13

Zackowski JL, Martin-Deleon PA (1988) Second meiotic nondisjunction is not increased in postovulatory aged murine oocytes fertilized in vitro. In vitro Cell Dev Biol 24:133–137

Zuccotti M, Boiani M, Garagna S, Redi CA (1998) Analysis of aneuploidy rate in antral and ovulated mouse oocytes during female aging. Mol Reprod Dev 50:305–312

Danadova J, Matijescukova N, Danylevska AM, Anger M. Increased frequency of chromosome congression defects and aneuploidy in mouse oocytes cultured at lower temperature. Reprod Fertil Dev. 2016

Impact Factor/Quartile: 2.105/Q1
Times cited (Wos May 2019): 2
Significance: Report showing the impact of culture conditions on the frequency of aneuploidy – important for human IVF.
Contribution of the author: Experimental design, interpretation of experiments manuscript preparation, securing funding

CSIRO PUBLISHING

Reproduction, Fertility and Development
http://dx.doi.org/10.1071/RD15306

Increased frequency of chromosome congression defects and aneuploidy in mouse oocytes cultured at lower temperature

Jitka Danadova[A], *Natalie Matijescukova*[A], *Anna Mac Gillavry Danylevska*[A] *and Martin Anger*[A,B]

[A]Central European Institute of Technology, Veterinary Research Institute, Hudcova 70, 621 00 Brno, Czech Republic.
[B]Corresponding author. Email: anger@vri.cz

Abstract. Optimal culture conditions are essential for successful IVM of mammalian oocytes and for their further development into an embryo. In the present study we used live cell imaging microscopy to assess the effects of suboptimal culture temperature on various aspects of IVM, including duration of meiosis I, dynamics of polar body extrusion, chromosome congression, anaphase-promoting complex/cyclosome (APC/C) activation and aneuploidy. The data showed that even a small deviation from the optimal incubation temperature causes marked changes in the duration and synchronicity of meiosis, APC/C activity and the frequency of chromosome congression and segregation errors. *In vitro* manipulation and maturation of germ cells is widely used in both human and animal artificial reproduction techniques. Mammalian oocytes are naturally prone to chromosomal segregation errors, which are responsible for severe mental and developmental disorders. The data presented herein demonstrate that exposure of mouse oocytes to suboptimal temperature during manipulation and maturation could further increase the frequency of chromosome segregation defects in these cells.

Additional keywords: anaphase-promoting complex/cyclosome, chromosome misalignment, culture temperature, IVM.

Received 29 July 2015, accepted 19 January 2016, published online 9 March 2016

Introduction

Mammalian oocytes mature spontaneously after removal from the follicle (Pincus and Enzmann 1935). Since the first attempts on IVM of oocytes, efforts have been made to define culture conditions, which are optimal for supporting their further development into embryos (Edwards 1965). Understandably, most studies were focused on culture media and their components, including energy sources and biologically active compounds, such as hormones. However, another important factor in optimisation of IVM of the gametes is temperature. Traditionally, this has been selected with regard to the average core body temperature of each particular species. The effect of lower temperature on meiotic maturation has been studied and some effects are already known. Using porcine oocytes, it was shown that the frequency of first polar body extrusion (PBE) and the duration of meiosis I change with lower culture media temperatures (Eng *et al.* 1986; Abeydeera *et al.* 2001; Ye *et al.* 2007). Conversely, exposure to temperatures higher than body temperature was shown to have a negative effect on porcine oocytes, resulting in decreased meiotic and developmental competence, a lower fertilisation rate and fewer cells progressing to the blastocyst stage (Tong *et al.* 2004; Barati *et al.* 2008). Such damage can be introduced relatively rapidly, for example during transient exposure of animals to higher temperatures during slaughtering procedures (hot water treatment and flame sterilisation before removal of organs).

It was shown that the subcellular structure that is particularly sensitive to changes in culture temperature is the meiotic spindle, and spindle disassembly has been observed upon exposure to lower temperatures in mouse (Pickering and Johnson 1987) and human (Wang *et al.* 2001) oocytes. Because an intact spindle with all kinetochores correctly attached to the microtubules is a prerequisite for faithful chromosome segregation in all cells studied so far (Foley and Kapoor 2013), it is conceivable that a disruption of the spindle microtubules in cells exposed to lower temperatures may lead to incorrect distribution of chromosomes and aneuploidy in resulting MII oocytes. Considering the fact that virtually all procedures used in human and animal assisted reproduction use manipulation of gametes and embryos outside the incubator, where temperature control is limited, these findings are particularly important.

The effect of lower culture temperature on chromosome segregation has not been studied thus far. Therefore, in the present study we used time-lapse microscopy to investigate how suboptimal culture temperature affects important aspects of chromosome segregation, such as chromosome congression

and initiation of anaphase. The results reveal that an increased frequency of cells with chromosome congression and segregation defects and lower anaphase-promoting complex/cyclosome (APC/C) efficiency are consequences of a relatively small deviation from the optimal culture temperature. We believe that these results will contribute to knowledge of the origin of aneuploidy in mammalian oocytes cultured *in vitro* and will be important for further improvements of IVM and manipulation techniques.

Materials and methods

Animals

Oocytes were collected from CD-1 female mice aged 9–20 weeks (Animal Breeding and Experimental Facility, Faculty of Medicine, Masaryk University, Brno, Czech Republic). All animal work was conducted according to Act No. 246/1992 Coll., on the protection of animals against cruelty under supervision of the Central Commission for Animal Welfare (Approval ID 1504/2013, 1566/2014).

Oocyte collection, manipulation, microinjection and live cell imaging

Unless stated otherwise, all reagents were purchased from Sigma-Aldrich (Czech Republic). Mice were killed and oocytes were collected by mechanical disruption of ovarian tissue in M2 medium containing 100 μM 3-isobutyl-1-methylxanthine (IBMX). Cells were cultured in M16 medium (Merck Millipore, Czech Republic), supplemented with 100 μM IBMX and covered with mineral oil, at 37°C in the presence of 5% CO_2. Microinjection was performed in M2 medium supplemented with 100 μM IBMX, covered with mineral oil, using an I-10 microinjector (Narishige, Tokyo, Japan) on a Leica (Wetzlar, Germany) DMIL inverted microscope. cRNA constructs for microinjection encoding mouse Histone H2B and Securin tagged with mCherry and Venus, respectively, were used as described previously (Sebestova *et al.* 2012). After microinjection, oocytes were cultured in M16 medium with 100 μM IBMX at 37°C under 5% CO_2 for 2 h to allow synthesis of injected proteins and then matured by removal of IBMX from the medium. Time-lapse imaging was performed on a Leica AF 6000B inverted fluorescence microscope with an HC PL APO 20x/0.7 IMM CORR CS objective, or on a Leica SP5 laser scanning microscope with an HCX PL APO 20 × /0.7 IMM CORR λ_{BL} objective; both objectives were equipped with differential interference contrast (DIC). For detection of the tagged proteins, a Leica *Discosoma* sp. red fluorescent protein (DsRed) ET filter cube (excitation filter BP 546/11) and a green fluorescent protein (GFP) ET filter cube (excitation filter BP 470/40) were used. Images were acquired every 5 min for 18 h. Both microscopes were equipped with a European Molecular Biology Laboratory (EMBL) environmental box allowing temperature and CO_2 to be controlled during the experiment. The temperature in the vicinity of the culture chamber was further monitored with an external probe (Pt1000TG8/E, model SN 105E; Comet System, Roznov pod Radhostem, Czech Republic). Temperature was recorded during each experiment and temperature fluctuations were <1°C over a period of 24 h.

Immunofluorescence and kinetochore counting assay

The protocols used for immunofluorescence and kinetochore counting were those described by Duncan *et al.* (2009) and Sebestova *et al.* (2012). Oocytes were isolated and cultured for 16 h in M16 medium, then washed in M16 medium supplemented with 100 μM monastrol and incubated for 2 h at either 35°C or 37°C in the presence of 5% CO_2. MII oocytes were fixed using 2% paraformaldehyde for 25 min, permeabilised with 0.1% Triton X-100 for 20 min and blocked in blocking solution composed of phosphate-buffered saline (PBS) containing 0.3% bovine serum albumin (BSA) and 0.01% Tween-20, for 15 min. Immunostaining was performed with a 1 : 500 dilution of human anti-centromere primary antibody (HCT-0100; Immunovision, Springdale, AR, USA) and a 1 : 500 dilution of an Alexa Flour 555 goat anti-human secondary antibody (A21433; Invitrogen, Life Technologies, Prague, Czech Republic). Cells were mounted in Vectashield with 4′,6′-diamidino-2-phenylindole (DAPI; H-1200; Vector Laboratories, Burlingame, CA, USA).

Samples were scanned on a Leica AF 6000B inverted fluorescence microscope, equipped with an HCX PL APO × 100/1.4– 0.7 oil objective. For detection of DAPI and Alexa Fluor 555, a Leica A filter cube (excitation filter BP 360/40) and a Leica DsRed ET filter cube (excitation filter BP 546/11) were used. The Z-resolution was automatically optimised by LAS AF software (Leica, Wetzlar, Germany).

Image and statistical analysis

Data analysis was performed using ImageJ (http://rsb.info.nih.gov/ij/) and Imaris software (http://www.bitplane.com), with statistical analyses performed using Prism version 5.00 for Mac (GraphPad Software, San Diego, CA, USA). Mean ± s.d. values were calculated using MS Excel (Microsoft, Bellevue, WA, USA). The statistical significance of differences was tested using Chi-squared tests, one-way analysis of variance (ANOVA) with post hoc Tukey's multiple comparison test and Mann–Whitney *U*-tests, as appropriate. Two-tailed $P < 0.05$ was considered significant.

Results

Impact of lower culture temperature on meiosis I duration and anaphase entry

To analyse the effect of culture temperature on meiosis I progression, groups of oocytes were matured at 35°C, 36°C, 37°C and 37.5°C. A temperature of 37°C was used as the control, because it represents average mouse core body temperature (Sanchez-Alavez *et al.* 2011) and is thus conventionally used for IVM of mouse oocytes (Brinster 1969; Hong *et al.* 2014). Prior to meiotic maturation, germinal vesicle (GV) oocytes were injected with cRNA encoding Histone H2B fused to mCherry. After a period of time sufficient for the translation of injected cRNA, the resumption of meiosis was induced by removal of IBMX from the culture medium and oocytes were subsequently transferred to the microscope stage. Chromosome segregation and PBE were monitored using time-lapse imaging for 18 h and stacks of images were acquired in 5-min intervals. The duration of meiosis I was analysed in each individual cell by measuring the time interval between disassembly of the nuclear membrane

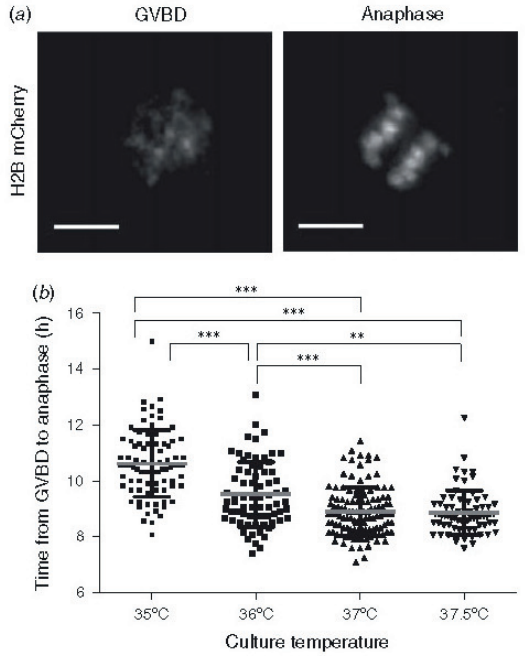

Fig. 1. The duration of meiosis I is dependent on culture temperature. Oocytes were microinjected with cRNA of Histone H2B fused with mCherry fluorescent protein and the time from germinal vesicle breakdown (GVBD) until the onset of anaphase was measured. (*a*) Representative time-lapse frames showing chromatin during GVBD and chromosomal mass segregation indicating the onset of anaphase in oocytes matured at 37°C. Scale bars = 15 μm. (*b*) Scatter dot plot of the length of the interval from GVBD until the onset of anaphase in individual oocytes. Oocytes were cultured at 35°C ($n = 84$), 36°C ($n = 72$), 37°C ($n = 118$) or 37.5°C ($n = 72$). Mean ± s.d. values (horizontal grey line and black whiskers, respectively) are indicated. Statistical significance was estimated using analysis of variance and Turkey's post hoc multiple comparison test (***$P < 0.001$, **$P < 0.01$). Significant differences were found between all groups, except those cultured at 37°C and 37.5°C. For each temperature, the experiments were repeated four (35°C, 36°C and 37.5°C) or six (37°C) times.

(germinal vesicle breakdown (GVBD)) and anaphase, visible by separation of chromosomal masses (Fig. 1*a*). The duration of meiosis I in oocytes cultured at 35°C and 36°C was significantly longer (10.62 ± 1.19 and 9.52 ± 1.15 h, respectively) than that in oocytes cultured at 37°C and 37.5°C (8.91 ± 0.87 and 8.88 ± 0.79 h, respectively; Fig. 1*b*). The increase in the duration of meiosis I was inversely correlated with culture temperature, although oocytes matured at 37°C and 37.5°C spent a similar time in meiosis I (Fig. 1*b*). These observations support previously published data (Abeydeera *et al.* 2001; Ye *et al.* 2007) and confirm that the length of meiosis I is significantly affected by the temperature of the culture medium. Compared with previously published data (Abeydeera *et al.* 2001; Ye *et al.* 2007) the data presented herein show that even a relatively subtle change in culture temperature has a surprisingly marked

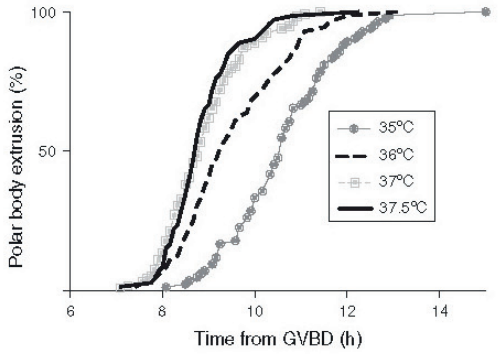

Fig. 2. Dynamics of polar body extrusion (PBE) after oocyte culture at different temperatures. Oocytes were microinjected with cRNA of Histone H2B fused with mCherry fluorescent protein and scored for PBE using time-lapse microscopy. The curves show the proportion of oocytes that had extruded the first polar body at particular time points during meiosis I. Timing of PBE was determined from data obtained in experiments shown in Fig. 1. The duration of meiosis I is dependent on culture temperature. GVBD, germinal vesicle breakdown.

effect. Decreasing the temperature just 1°C from the standard culture temperature prolonged the first meiotic division by 0.6 h; a 2°C decrease resulted in meiosis I that was 1.7 h longer. Using the same set of data, we also analysed the dynamics of PBE (Fig. 2). Approximately 90% of oocytes cultured at 37°C and 37.5°C entered anaphase within 2 h of the first cell in the group entering anaphase. Interestingly, in oocytes cultured at 35°C and 36°C, this time interval was extended to 4–5 h (Fig. 2), demonstrating that the lower temperature emphasised individual differences between cells and unsynchronised meiosis I progression. In addition, oocytes matured at 35°C started PBE with an approximate 1 h delay compared with all other groups (Fig. 2).

Effects of lower culture temperature on APC/C activity

In order to monitor APC/C activity in oocytes during meiosis I, we used its substrate Securin (McGuinness *et al.* 2009; Sebestova *et al.* 2012). The highest Securin fluorescence intensity followed by its relatively rapid decline coincides with the onset of APC/C activity in each cell. cRNAs encoding Securin and Histone H2B fused to fluorescent tags were microinjected into oocytes and Securin fluorescence intensity was subsequently detected in each cell individually throughout meiosis I. For this experiment, we restricted the culture temperatures to 35°C and 37°C (Fig. 3*a*). Although the Securin fluorescence intensity profiles were similar in both groups, alignment to the points of maximum fluorescence intensity demonstrated that the degradation of Securin required a longer time in cells cultured at 35°C (Fig. 3*b*). To confirm this, we measured the time interval from the highest Securin fluorescence intensity to anaphase in individual cells (Fig. 3*c*); this interval was significantly longer in the group cultured at 35°C compared with 37°C (2.35 ± 0.36 vs 2.12 ± 0.45 h, respectively; $P < 0.01$), indicating that the degradation of Securin by APC/C is less efficient in the oocytes cultured at a lower temperature.

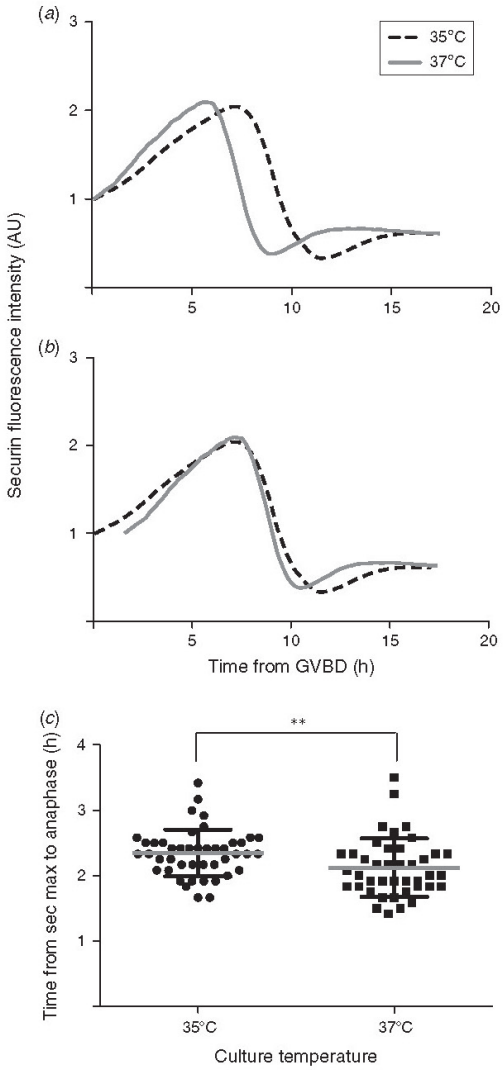

Fig. 3. Anaphase-promoting complex/cyclosome (APC/C) activity is affected by culture temperature. Oocytes were microinjected with cRNA of Securin tagged with Venus fluorescent protein to visualise APC/C activity. (*a*) Curves showing mean fluorescence intensity of Securin–Venus at particular time points during meiosis I in oocytes cultured at 35°C ($n=44$) or 37°C ($n=41$). The fluorescence intensity of Securin–Venus was measured as mean grey value and normalised against the time of germinal vesicle breakdown (GVBD). (*b*) Curves shown in (*a*) aligned to the point of maximum Securin fluorescence intensity. (*c*) Scatter dot plot of time between maximum Securin fluorescence intensity (activation of APC/C) and onset of anaphase I for individual oocytes. Mean ± s.d. values (horizontal grey line and black whiskers, respectively) are indicated. The difference is significant (**$P<0.01$). Data were obtained from two replicates for each temperature.

Impact of lower culture temperature on APC/C activity

It has been demonstrated previously that the frequency of aneuploidy in mammalian oocytes corresponds to the occurrence of misaligned chromosomes shortly before anaphase (Nagaoka *et al.* 2011; Sebestova *et al.* 2012). To determine whether culture temperature affects the occurrence of this phenomenon, we analysed chromosome congression defects in oocytes cultured at different temperatures. Oocytes injected with cRNA encoding histone H2B fused to mCherry were matured on the microscope stage. Misaligned chromosomes were scored individually in each cell using images acquired during the last time interval before anaphase (Fig. 4*a*). The number of cells in each group in which at least one chromosome was visibly separated from the others clearly demonstrated that chromosome congression is impaired by lower culture temperature. Although only 2.5% of oocytes cultured at 37°C and 4.2% of oocytes cultured at 36°C contained misaligned chromosomes at the given time point, this number was almost sevenfold higher in oocytes at 35°C, reaching 16.7% (Fig. 4*b*). In oocytes cultured at 37.5°C, no congression defects were detected (Fig. 4*b*). The degree of congression defects in oocytes with misaligned chromosomes is shown in Fig. 4*c*. Whereas cells cultured at 36°C and 37°C that contained misaligned chromosomes had mostly a single chromosome separated from the metaphase plate, chromosome segregation defects in oocytes cultured at 35°C usually involved multiple chromosomes. These results demonstrate that culture temperature affects the alignment of chromosomes and that the extent of this defect is correlated with the degree of deviation from the normal culture temperature.

Effects of lower culture temperature on chromosome segregation errors

In order to test whether more frequent chromosome congression defects are reflected in chromosome segregation defects, we scored aneuploidy levels in cells maturing at 37°C and 35°C. GV oocytes after isolation were divided into two groups and cultured in the incubator for 20 h at either 37°C and 35°C until they reached the MII stage. Then, using the kinesin 5 inhibitor monastrol, bipolar spindles were disrupted, cells were stained for kinetochores and DNA and chromosome content was scored in each intact cell (Duncan *at al.* 2009). Fig. 5*a* shows an example of the chromosome content of euploid cell, whereas Fig. 5*b* shows an example of hypoploid cell with 19 univalents after meiosis I. The results showed that aneuploidy is more frequently detected in cells cultured at 35°C than in cells that matured at more physiological temperatures (Fig. 5*c*, *d*). However, the absence of aneuploid cells in the group cultured at 37°C was definitely caused by the small number of cells because we know from previous studies that some basal aneuploidy is always present even in cells cultured under relatively ideal culture conditions (Danylevska *et al.* 2014).

Discussion

The aim of the present study was to describe the effect of lower culture temperatures on meiosis I progression and chromosome segregation in mouse oocytes. The temperatures chosen for the

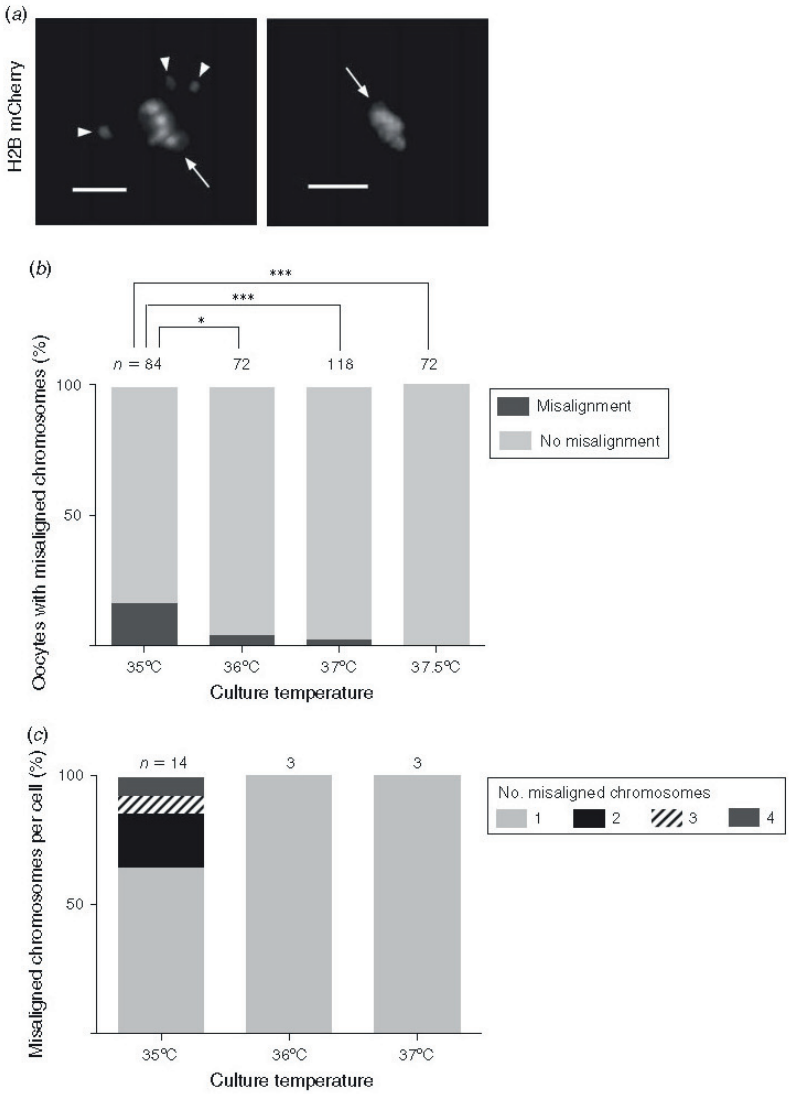

Fig. 4. Increased frequency of chromosome misalignment in oocytes matured at lower culture temperature. Oocytes were microinjected with cRNA of Histone H2B fused with mCherry fluorescent protein and scored for the presence and number of chromosomes visibly dissociated from the metaphase plate. (*a*) Representative images showing congression defects in an oocyte one frame prior to anaphase (left) and an oocyte with all the chromosomes properly aligned on the metaphase plate one frame prior to anaphase (right). Oocytes were matured at 35°C. Arrowheads indicate misaligned chromosomes, arrows indicate chromosomes aligned at the metaphase plate. Scale bars = 15 μm. (*b*) Percentage of oocytes with misaligned chromosomes in groups matured at 35°C ($n = 84$), 36°C ($n = 72$), 37°C ($n = 118$) or 37.5°C ($n = 72$). Significant differences were found between oocytes cultured at 35°C and the other three groups (***$P < 0.001$, *$P < 0.05$). No misalignment was detected in oocytes matured at 37.5°C. (*c*) Number of misaligned chromosomes in oocytes with congression defects. Misalignment defects were scored in four replicates for each temperature.

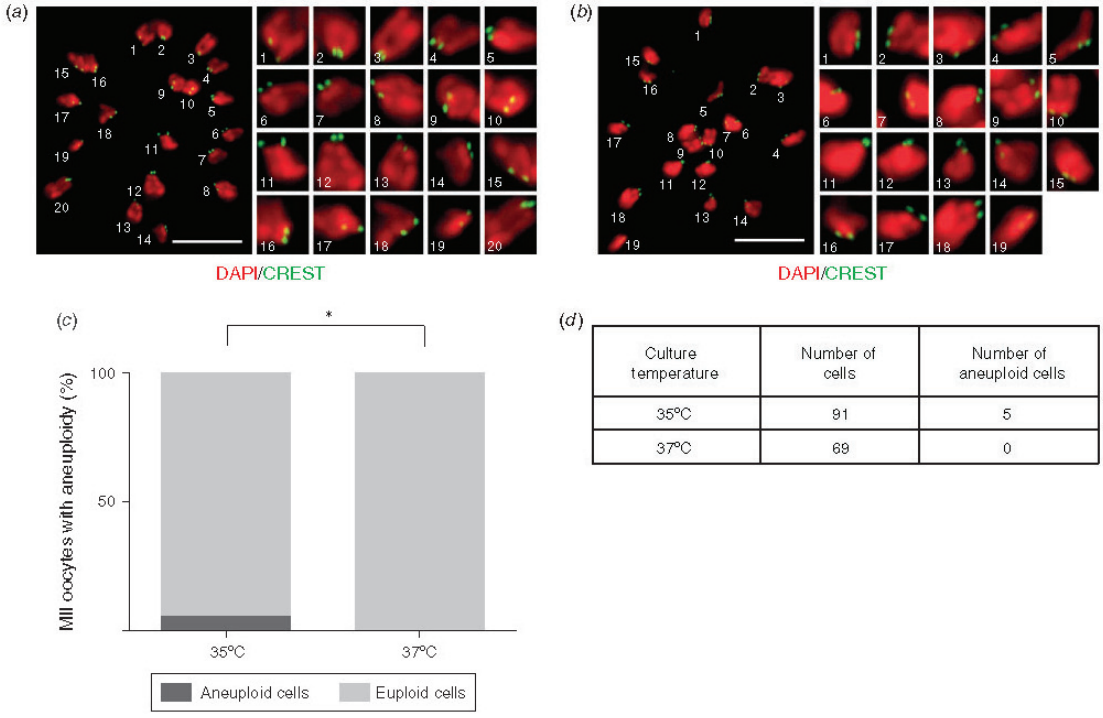

Culture temperature	Number of cells	Number of aneuploid cells
35°C	91	5
37°C	69	0

Fig. 5. Increased frequency of aneuploidy in MII oocytes matured at lower culture temperature. Oocytes were matured at 35°C and 37°C until the MII stage and treated with monastrol for 2 h to spread chromosomes, followed by immunostaining to visualise DNA and kinetochores. (*a*) Representative image showing a euploid cell with 20 individual univalent, which are shown enlarged to the right, and (*b*) an aneuploid cell with 19 individual univalent, also enlarged on the right. Scale bars = 12 μm. (*c*) Percentage of MII oocytes with aneuploidy. Cells were matured at 35°C ($n = 91$) and 37°C ($n = 69$). Significant difference was found (* $P < 0.05$). (*d*) The number of oocytes from both groups analysed for aneuploidy is indicated in the table. Aneuploidy was scored in three independent experiments.

present study were, in fact, reasonably close to the standard culture temperature and therefore it is conceivable that such conditions may be reached during regular oocyte manipulation or culture. Despite the relatively small temperature differences between groups, the effects on various aspects of meiosis I were correlated with the level of deviation from the standard temperature. From previously published studies, we know that short-term exposure to a lower temperature causes prolongation of meiosis I and instability of the spindle microtubules (Eng *et al.* 1986; Pickering and Johnson 1987; Abeydeera *et al.* 2001; Wang *et al.* 2001; Tong *et al.* 2004; Ye *et al.* 2007). The results of the present study revealed, quite surprisingly, that a decrease in culture temperature as little as 1°C already negatively affects meiosis I completion rates and PBE timing. However, this effect was much stronger when the lower temperature (35°C) was used. Thanks to the techniques used in the present study, we were able to detect other consequences of the lower culture temperature, some of which have not been reported previously, namely effects on the synchronicity of anaphase entry, deceleration of APC/C substrate degradation and, importantly, chromosomal congression and segregation defects.

During exit from mitosis, APC/C activity is essential for targeting important regulators of the cell cycle, such as Cyclin B and Securin, for destruction, which makes the metaphase to anaphase transition irreversible (Pesin and Orr-Weaver 2008). The results of the present study indicate that this pathway is less efficient in cells cultured at the lower temperature, which was reflected by slower degradation of Securin. However, whether other important substrates, such as mitotic cyclins, are also affected needs to be tested. It is conceivable that any change to the processes required for an exit from meiosis I could also potentially contribute to oocyte aneuploidy. During meiosis I, the APC/C is active for approximately 2–3 h during the metaphase I to anaphase I transition, which is much longer compared with the somatic cell cycle. To test whether oocytes are more sensitive to temperature changes during APC/C activity could be important for our understanding of the origin of aneuploidy in cells cultured *in vitro*. However, the most important observation is the increase in errors of both chromosome congression and segregation with the lower culture temperature. This is particularly important because oocytes are known to be prone to chromosome segregation errors (Nagaoka *et al.* 2011) and congression defects were shown to worsen this even further

(Nagaoka *et al.* 2011; Sebestova *et al.* 2012). It is clear from the results of the present study that most chromosome congression defects caused by the lower culture temperature are only transient and are not converted into chromosome segregation defects. However, we have demonstrated here that the lower temperature also significantly increased chromosome segregation defects causing aneuploidy, which would be incompatible with subsequent embryonic development. The number of cells scored was relatively small and the data presented herein are not sufficient to reflect overall aneuploidy levels in each group. To obtain such information, a much larger cohort of cells needs to be analysed for each culture temperature (Danylevska *et al.* 2014). However, the numbers shown here clearly demonstrate the effect of lower culture temperature on the occurrence of chromosome segregation errors. Because *in vitro* manipulation of oocytes and embryos has become a basic method used not only for scientific research, but also as a routine procedure in human and animal assisted reproduction, we believe the findings of the present study are highly relevant. Exposure of cells to the lower temperature obviously increased chromosome congression errors and therefore the findings of the present study are important for future improvement of techniques used in human and animal reproduction. It remains to be determined whether, for example, shorter exposure of cells to conditions outside the incubator has similar effects as the long-term exposure to different temperatures as reported in this paper.

Acknowledgements

The authors are grateful to all members of the Martin Anger laboratory (Mammalian Reproduction Laboratory, Veterinary Research Institute, Brno, Czech Republic) for helpful discussion and useful comments. This work was supported by Czech Science Foundation Projects P502/12/ 2201 and 15-04844S and by the Ministry of Education, Youth and Sports of the Czech Republic under the project CEITEC 2020 (LQ1601) and project LH 13072–Kontakt II.

References

Abeydeera, L. R., Wang, W. H., Prather, R. S., and Day, B. N. (2001). Effect of incubation temperature on *in vitro* maturation of porcine oocytes: nuclear maturation, fertilisation and developmental competence. *Zygote* **9**, 331–337. doi:10.1017/S0967199401001381

Barati, F., Agung, B., Wongsrikeao, P., Taniguchi, M., Nagai, T., and Otoi, T. (2008). Meiotic competence and DNA damage of porcine oocytes exposed to an elevated temperature. *Theriogenology* **69**, 767–772. doi:10.1016/J.THERIOGENOLOGY.2007.08.038

Brinster, R. L. (1969). *In vitro* cultivation of mammalian ova. *Adv. Biosci.* **4**, 199–233.

Danylevska, A., Kovacovicova, K., Awadova, T., and Anger, M. (2014). The frequency of precocious segregation of sister chromatids in mouse female meiosis I is affected by genetic background. *Chromosome Res.* **22**, 365–373. doi:10.1007/S10577-014-9428-6

Duncan, F. E., Chiang, T., Schultz, R. M., and Lampson, M. A. (2009). Evidence that a defective spindle assembly checkpoint is not the primary cause of maternal age-associated aneuploidy in mouse eggs. *Biol. Reprod.* **81**, 768–776. doi:10.1095/BIOLREPROD.109.077909

Edwards, R. G. (1965). Maturation *in vitro* of mouse, sheep, cow, pig, rhesus monkey and human ovarian oocytes. *Nature* **208**, 349–351. doi:10.1038/208349A0

Eng, L. A., Kornegay, E. T., Huntington, J., and Wellman, T. (1986). Effects of incubation temperature and bicarbonate on maturation of pig oocytes *in vitro*. *J. Reprod. Fertil.* **76**, 657–662. doi:10.1530/JRF.0.0760657

Foley, E. A., and Kapoor, T. M. (2013). Microtubule attachment and spindle assembly checkpoint signalling at the kinetochore. *Nat. Rev. Mol. Cell Biol.* **14**, 25–37. doi:10.1038/NRM3494

Hong, K. H., Lee, H., Forman, E. J., Upham, K. M., and Scott, R. T. J. (2014). Examining the temperature of embryo culture in *in vitro* fertilization: a randomized controlled trial comparing traditional core temperature (37 degrees C) to a more physiologic, cooler temperature (36 degrees C). *Fertil. Steril.* **102**, 767–773. doi:10.1016/J.FERTNSTERT.2014.06.009

McGuinness, B. E., Anger, M., Kouznetsova, A., Gil-Bernabe, A. M., Helmhart, W., Kudo, N. R., Wuensche, A., Taylor, S., Hoog, C., Novak, B., and Nasmyth, K. (2009). Regulation of APC/C activity in oocytes by a Bub1-dependent spindle assembly checkpoint. *Curr. Biol.* **19**, 369–380. doi:10.1016/J.CUB.2009.01.064

Nagaoka, S. I., Hodges, C. A., Albertini, D. F., and Hunt, P. A. (2011). Oocyte-specific differences in cell-cycle control create an innate susceptibility to meiotic errors. *Curr. Biol.* **21**, 651–657. doi:10.1016/J.CUB.2011.03.003

Pesin, J. A., and Orr-Weaver, T. L. (2008). Regulation of APC/C activators in mitosis and meiosis. *Annu. Rev. Cell Dev. Biol.* **24**, 475–499. doi:10.1146/ANNUREV.CELLBIO.041408.115949

Pickering, S. J., and Johnson, M. H. (1987). The influence of cooling on the organization of the meiotic spindle of the mouse oocyte. *Hum. Reprod.* **2**, 207–216.

Pincus, G., and Enzmann, E. V. (1935). The comparative behavior of mammalian eggs *in vivo* and *in vitro*: I. the activation of ovarian eggs. *J. Exp. Med.* **62**, 665–675. doi:10.1084/JEM.62.5.665

Sanchez-Alavez, M., Alboni, S., and Conti, B. (2011). Sex- and age-specific differences in core body temperature of C57Bl/6 mice. *Age (Dordr.)* **33**, 89–99. doi:10.1007/S11357-010-9164-6

Sebestova, J., Danylevska, A., Novakova, L., Kubelka, M., and Anger, M. (2012). Lack of response to unaligned chromosomes in mammalian female gametes. *Cell Cycle* **11**, 3011–3018. doi:10.4161/CC.21398

Tong, G. Q., Heng, B. C., Chen, N. Q., Yip, W. Y., and Ng, S. C. (2004). Effects of elevated temperature *in vivo* on the maturational and developmental competence of porcine germinal vesicle stage oocytes. *J. Anim. Sci.* **82**, 3175–3180.

Wang, W. H., Meng, L., Hackett, R. J., Odenbourg, R., and Keefe, D. L. (2001). Limited recovery of meiotic spindles in living human oocytes after cooling–rewarming observed using polarized light microscopy. *Hum. Reprod.* **16**, 2374–2378.

Ye, J., Coleman, J., Hunter, M. G., Craigon, J., Campbell, K. H., and Luck, M. R. (2007). Physiological temperature variants and culture media modify meiotic progression and developmental potential of pig oocytes *in vitro*. *Reproduction* **133**, 877–886. doi:10.1530/REP-06-0318

Hornak M, Jeseta M, Musilova P, Pavlok A, Kubelka M, Motlik J, et al. Frequency of aneuploidy related to age in porcine oocytes. PLoS One. 2011;6: e18892.

Impact Factor/Quartile: 4.411/Q1
Times cited (Wos May 2019): 18
Significance: The important discovery showing that not all mammalian species are suffering from maternal – age related aneuploidy.
Contribution of the author: Experimental design, interpretation of experiments manuscript preparation, securing funding

OPEN ACCESS Freely available online

PLoS one

Frequency of Aneuploidy Related to Age in Porcine Oocytes

Miroslav Hornak[2☯], Michal Jeseta[2☯], Petra Musilova[2], Antonin Pavlok[1], Michal Kubelka[1], Jan Motlik[1], Jiri Rubes[2], Martin Anger[1,2*]

1 Institute of Animal Physiology and Genetics, Libechov, Czech Republic, **2** Veterinary Research Institute, Brno, Czech Republic

Abstract

It is generally accepted that mammalian oocytes are frequently suffering from chromosome segregation errors during meiosis I, which have severe consequences, including pregnancy loss, developmental disorders and mental retardation. In a search for physiologically more relevant model than rodent oocytes to study this phenomenon, we have employed comparative genomic hybridization (CGH), combined with whole genome amplification (WGA), to study the frequency of aneuploidy in porcine oocytes, including rare cells obtained from aged animals. Using this method, we were able to analyze segregation pattern of each individual chromosome during meiosis I. In contrast to the previous reports where conventional methods, such as chromosome spreads or FISH, were used to estimate frequency of aneuploidy, our results presented here show, that the frequency of this phenomenon was overestimated in porcine oocytes. Surprisingly, despite the results from human and mouse showing an increase in the frequency of aneuploidy with advanced maternal age, our results obtained by the most accurate method currently available for scoring the aneuploidy in oocytes indicated no increase in the frequency of aneuploidy even in oocytes from animals, whose age was close to the life expectancy of the breed.

Citation: Hornak M, Jeseta M, Musilova P, Pavlok A, Kubelka M, et al. (2011) Frequency of Aneuploidy Related to Age in Porcine Oocytes. PLoS ONE 6(4): e18892. doi:10.1371/journal.pone.0018892

Editor: Ziyin Li, University of Texas-Houston Medical School, United States of America

Received January 1, 2011; **Accepted** March 24, 2011; **Published** April 27, 2011

Funding: This study was supported by Grant Agency of AS CR grant no. IAA501620801, Czech Science Foundation grant no. 523/09/0743, EMBO installation grant no. 1817, Marie Curie ERG no. 224931 and Purkyne Fellowship to M.A. The funders had no role in study design, data collection and analysis, decision to publish, or preparation of the manuscript.

Competing Interests: The authors have declared that no competing interests exist.

* E-mail: anger@iapg.cas.cz

☯ These authors contributed equally to this work.

Introduction

Development of human embryo is affected by a high frequency of aneuploidy, which has severe consequences, namely pregnancy loss, incidence of abortions, developmental disorders and mental retardation [1]. Search for the potential source of these defects showed, that the female gametes are more susceptible to the accumulation of chromosome segregation errors during meiosis I division, and therefore the egg is the major contributor to the embryo aneuploidy [2 4].

Data obtained from other mammals show that their oocytes are also frequently affected by aneuploidy. In mouse, where this phenomenon was extensively studied, the frequency of aneuploidy at metaphase II, estimated by chromosome spreads or by counting CREST signals after monastrol treatment in intact oocytes, varies from 3% to 8% [5 7]. In cattle, the differences between individual reports are even greater, with estimated aneuploidy rate in MII oocytes varying from 7.1% up to 30%, using either chromosome spreads and counting hyperhaploid oocytes [8] or counting chromosomes X and 5 detected by FISH [9]. Analysis of porcine oocytes based on the hyperhaploid chromosome spreads showed aneuploidy in 4.9% of cells [10] or 11.9% cells [11], whereas counting chromosomes 1 and 10 using FISH led to the estimated aneuploidy ranging from 27% up to 57% of oocytes [12,13].

The development of mammalian female gametes is characterized by a relatively long interruption, lasting from the formation of oocytes during early embryonic development until their recruitment to complete meiosis after puberty. The length of this period, during which are the oocytes arrested in the prophase of the first meiotic division, varies dramatically between species and can last from months to decades. It seems that the frequency of aneuploidy increases significantly with declining reproduction, which places increased maternal age within the potential risk factors of developing embryo suffering from aneuploidy. Analysis of the correlation between age of human female donors and oocyte aneuploidy showed that in young women relatively small fraction, around 3 10% of oocytes, are aneuploid, whereas in women in their forties and later, the frequency of aneuploidy exceeds 50% [14 16]. To our knowledge, the only non-human mammalian species, in which the correlation between maternal ageing and oocyte aneuploidy was systematically studied, was mouse. In this species, the low overall initial aneuploidy 3 8% in animals around age of 8 10 weeks increases to 12% at the age of 32 to 35 weeks and even further increases to 25% at the age of 70 weeks, these results were obtained by counting chromosomes on chromosome spreads [6,7]. The high frequency of aneuploidy in animals advanced in age was confirmed also by a different method, namely disruption of the metaphase II spindle by monastrol and counting kinetochores on chromosomes stained by DAPI and CREST [5]. Using this method authors showed that the incidence of aneuploidy in oocytes from animals at the age of 16 19 months (64 76 weeks) is as high as 35%.

Due to the differences between various techniques used for scoring aneuploidy in oocytes, the reported frequencies are sometimes highly heterogeneous [17]. The objective of our study was to obtain the most accurate picture of the incidence of aneuploidy in porcine oocytes, since the previously published data are rather inhomogeneous. We were also keen to know, whether in this species the frequency of aneuploidy in oocytes increases in correlation to the maternal age. Our aim was to obtain physiologically more relevant model system to study maternal age-related aneuploidy in oocytes, because the meiosis in porcine oocytes resembles much more the situation in human than in rodent oocytes, generally used for such studies. For scoring the aneuploidy in oocytes in our study, we employed comparative genomic hybridization (CGH), which proved to be more accurate for scoring chromosomal abnormalities than FISH [18].

Our data presented here show that the incidence of aneuploidy in porcine oocytes is lower than the most frequent estimations reported previously. Surprisingly, comparison of the frequency of aneuploidy in groups of animals of age more than 6 years apart showed that this species does not suffer from age-related increase of aneuploidy in oocytes, known in human and mouse.

Results

In vitro maturation of oocytes from various age categories

Oocytes isolated from two groups of miniature pigs and a group of Landrace and Czech Large White crossbreed (LxCLW), were matured in vitro. First group of miniature pigs consisted of three young animals at average age around 15 months. Animals in the second group were significantly older, with average age around 92 months. Oocytes in the third group, obtained from the LxCLW, were in average 69 months old at the time of oocyte isolation. GV stage oocytes, with intact cumulus (COCs), were isolated after prior PMSG stimulation. Within each group, similar number of COCs per animal was obtained, 14.67 from young miniature pigs, 19.34 from aged miniature pigs and 27 from the group of aged LxCLW (Table 1). After 44 hours of maturation in vitro, 77.3, 82.8 and 87.7% of oocytes isolated from the young miniature pigs, aged miniature pigs and LxCLW extruded the first polar body (PB) (Table 1). The rate of polar body extrusion is comparable to the data from other groups indicating that our culture conditions were supporting oocyte maturation in vitro [13]. For subsequent analysis, the polar bodies were detached from oocytes and frozen separately.

Comparative genomic hybridization (CGH) of the entire chromosome content of individual oocytes

CGH method, when DNA template comes from a single cell, represents a technical challenge, since the amount of template DNA in the reaction is drastically reduced. To solve this problem, we used amplification of the whole genome using commercially available PicoPlex^{TM} WGA kit (Rubicon Genomics). This technology was succesfully validated for aneuploidy detection in human blastomeres and polar bodies [19,20]. Our preliminary results showed that CGH from a single porcine oocyte is feasible and reproducible. We have observed a strong correlation between aneuploidy detected in the oocyte and the corresponding polar body (data not shown). In Figure 1, we summarized representative results of CGH analysis. Oocyte with normal chromosomal set and the corresponding polar body is shown on panel A. The yellow mixed hybridization signal, consisting of green (Green 496-dUTP) signal from control cumulus cell and red (Cyanine 3-dUTP) signal from the oocyte or the polar body, is uniformly covering each chromosome (ratio close to 1:1). A result of a segregation error, when the whole bivalents were not disjoined during meiosis I, is illustrated on panel B. Chromosomes 7, 8, 11 and 15 are predominantly labeled in red in the oocyte and entirely green in the polar body (see corresponding ratio profile), indicating that those chromosomes remained in the oocyte during the first meiotic division. Panel C illustrates situation, when sister chromatids separated prematurely during meiosis I. The red signal of chromosome 12 is not completely missing, however, the green signal of competing control DNA is more apparent (signal ratio shifted to green, see ratio profile). Importantly, the color of the signal from the same chromosome in the corresponding PB represents the dominant signal from tested cell (signal ratio shifted to red, see ratio profile). Presented results demonstrate, that when using our assay we are able to detect the most frequent sources of aneuploidy in mammalian oocytes failure to disjoin the whole bivalent or premature segregation of sister chromatids.

Frequency of aneuploidy related to the donor age

The chromosome content was analyzed in 141 oocytes. From the final score, three cells from the group of aged LxCLW were excluded, because of the failure of the sample preparation (more than half of the chromosomes missing in the oocyte with euploid PBs), and the result of CGH analysis of 138 oocytes are summarized in Table 2 and 3. Altogether, we have identified 14 oocytes with incorrect chromosome content. In 9 cases, the aneuploidy was confirmed by CGH of the corresponding polar body. In two cases, amplification of DNA from the polar body failed and in three cases the profile of the polar body did not confirm the aneuploidy found in the oocyte. In the cases, where we were able to confirm the aneuploidy by analyzing the chromosome content in PBs, the affected chromosomes in the oocyte were accurately reflected in the corresponding PB. Both major causes of oocyte aneuploidy were present, 4 cells showed nondisjoined chromosomes and 10 cells suffered from premature segregation of sister chromatids (PSSC) (Table 3). When we divided the oocytes

Table 1. In vitro maturation of porcine oocytes isolated from various experimental groups.

Experimental group	Animals per group	Average age (months ± SD)	Number of isolated oocytes	Maturation rate number/% of PBs
Miniature pigs young	3	15.33+4.16	44	34/77.3
Miniature pigs old	3	92.00+21.66	58	48/82.8
LxCLW old	3	69.00+1.73	81	71/87.7

The number of animals per group, their average age, total number of isolated oocytes and the maturation rate scored after 44 hours of in vitro culture represented by absolute number of oocytes with polar bodies and frequency of polar body extrusion per group is indicated for each group. LxCLW stands for crossbred of Landrace and Czech Large White pigs.

doi:10.1371/journal.pone.0018892.t001

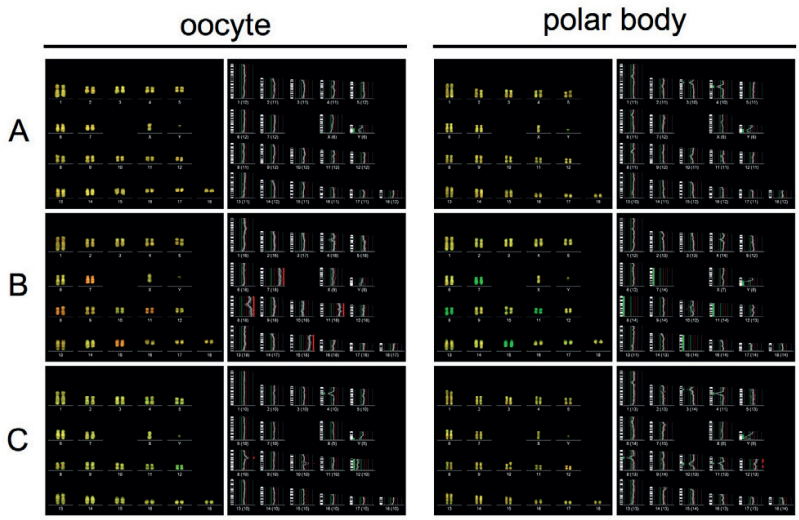

Figure 1. Detection of chromosome segregation errors by comparative genomic hybridization (CGH). Panel A: CGH analysis of euploid oocyte (left panel) and the corresponding polar body (right panel). Panel B: CGH analysis of oocyte (left panel) and the corresponding polar body (right panel) with non-disjunction of chromosomes 7, 8, 11 and 15. Panel C: CGH analysis of oocyte (left panel) and the corresponding polar body (right panel) with premature segregation of sister chromatids of chromosome 12.
doi:10.1371/journal.pone.0018892.g001

according to the age of donor animals, the frequency of aneuploidy was similar in oocytes from young miniature pigs, (12.1%), in oocytes from aged miniature pigs (8.7%) and in oocytes obtained from aged farm animals (LxCLW 10.2%) (Table 2).

Discussion

We show for the first time the CGH analysis of the whole chromosome content of a single female germ cell from non-human species. According to our results the frequency of aneuploidy in 138 analyzed porcine oocytes is 10.1%. These findings correspond to the large karyotyping survey of 1,397 human metaphase II oocytes, in which the frequency of aneuploidy was 10.8% [16]. Surprisingly, we were not able to detect increased frequency of aneuploidy in oocytes isolated from aged animals. In the group of oocytes isolated from young animals, 12.1% were aneuploid compared to aneuploidy ranging from 8.7% to 10.2% scored in oocytes isolated from two different breeds of aged animals. The low level of aneuploidy in oocytes from aged animals was unexpected and surprising; since in human and in mouse it seems that the level of aneuploidy increases with maternal age [1,6]. The simplest explanation could be that the animals, which we used for our analyses, were still relatively young and therefore the rate of aneuploidy was still low. Although we cannot exclude this possibility completely, it is very unlikely. Firstly, the estimated lifespan of miniature pig breed is between 10 15 years [21] and in our group of aged animals of this breed we have individuals 6, 8 and 9.5 years old, which should be close to the end of the expected lifespan. Secondly, we do not see any increase of the frequency of aneuploidy between young and aged animals, although in our study we are comparing animals separated by, on average, 6.39 years (average age in the group of young miniature pigs was 15.33 ± 4.16 months and in the group of old miniature pigs 92.00±24.66 months) with the biggest difference being 8.5 years (data not shown). It is reasonable to assume that such substantial age difference would somehow influence the frequency of aneuploidy, even if our animals were not at the end of their lifespan yet. We can also exclude a possibility that the data are reflecting only conditions within a particular breed of animals, since we are comparing two breeds with different genetic background - miniature pigs and a crossbreed of Landrace and Czech Large White and the results in both groups are similar.

The CGH seems to be very reliable tool compared to the highly variable results produced by traditional methods used for scoring aneuploidy in oocytes [17]. Although this method was successfully used before to analyze the level of aneuploidy in porcine embryos [22], for the analysis of a single oocyte or polar body presented here, it was necessary to modify several steps, including whole genomic amplification (WGA) procedure. The major advantage of CGH over traditional methods is that the chromosomes are not extracted before cell lysis and WGA, therefore the problem of loosing the chromosomes during procedure, a major drawback of

Table 2. The frequency of aneuploidy in oocytes from young donors versus oocytes from aged donors.

Experimental group	Total number of oocytes analyzed by CGH	Total number of oocytes with aneuploidy	Frequency of aneuploidy (%)
Miniature pigs young	33	4	12.1
Miniature pigs old	46	4	8.7
LxCLW old	59	6	10.2

Table summarizing the frequency of aneuploidy in oocytes isolated from various age categories. The total number of oocytes analyzed by comparative genomic hybridization (CGH) together with the number of oocytes with incorrect chromosomal counts and their frequency per group is indicated. LxCLW stands for crossbred of Landrace and Czech Large White pigs.
doi:10.1371/journal.pone.0018892.t002

Table 3. The analysis of the chromosomal segregation errors of porcine oocytes matured in vitro.

Experimental group	Chromosomes contributing to the aneuploidy - oocytes		Chromosomes contributing to the aneuploidy - PBs
	nondisjunction	PSSC	
Miniature pigs young	−2, −8, −15		Euploid
	+13, +14, +15		Unsuccessful amplification
		+15	−15
		−9	+9
Miniature pigs old	+7,+8,+11,+15		−7, −8, −11, −15
	+5		−5
		+12	−12
		−12	+12
LxCLW old		−6	Euploid
		−8, −13	Unsuccessful amplification
		−13	Euploid
		−1	+1
		−2	+2
		+X	−X

Oocytes with incorrect number of chromosomes are shown for each group. The origin of aneuploidy (chromosome non-disjunction versus premature segregation of sister chromatids - PSSC), chromosomes contributing to aneuploidy and the result of analysis of the corresponding polar body are shown for each cell. LxCLW stands for crossbred of Landrace and Czech Large White pigs.

doi:10.1371/journal.pone.0018892.t003

chromosome spreading techniques and SKY karyotyping, is eliminated here. Also, in contrast to the FISH method, when only few individual chromosomes could be detected, here we are able to analyze the entire chromosome set. This for example means that although we have analyzed chromosome content of merely 138 cells in our study, in fact we have analyzed precisely the segregation pattern of 2622 chromosomes. Additionally, most of the cases of aneuploidy detected in oocytes were confirmed also by analysis of the DNA in the corresponding polar body.

Chromosomes have various shapes, which is probably the reason why contribution of individual chromosomes to the aneuploidy is not random [23]. Because of the relatively small set of oocytes in this study, we are not able to provide statistical results of a contribution of different chromosomes into aneuploidy. However, we have noticed that chromosome 15 was involved more frequently in various cases in which aneuploidy was detected. In three cases the chromosome 15 was not disjoined and in one case sister chromatids of chromosome 15 segregated prematurely in meiosis I.

From our study we can conclude that the frequency of aneuploidy in porcine oocytes, measured by CGH, is lower than it was previously published. We were also unable to detect an increase in the frequency of aneuploidy in oocytes isolated from old animals, although it is important to emphasize the importance of future studies aiming to analyze this situation on larger number of animals and also different breeds. This might reflect some fundamental differences between human, mouse and pig folliculogenesis and meiosis resulting in low frequency of aneuploidy in aged pigs. Although human and mouse oocytes both show increased frequency of aneuploidy related to donor age, whether the etiology of aneuploidy in both cases is the same, is not so clear [24]. The low level of aneuploidy detected in porcine oocytes might be also a result of the constant pressure and selection focused on reproduction and fertility in farm animals, which could eventually eliminate individuals with potential problems. The maternal age-related aneuploidy in oocytes is an important issue in human reproductive medicine, although our results presented here indicate, that some mammalian species might not be affected. In order to find out how widely is this phenomenon spread among other mammals and also to identify species which would complement the rodent model system for studying this problem, we need to analyze carefully the incidence of this phenomenon in other mammals with longer lifespan using methods allowing for analysis of the whole set of chromosomes, such as CGH.

Materials and Methods

All animal work was conducted according to Act No 246/1992 Coll., on the protection of animals against cruelty under supervision of Central Commission for Animal Welfare, approval ID 018/2010.

Isolation of cumulus oocyte complexes (COCs) and in vitro maturation

A total of 6 of laboratory miniature pig cycling gilts and 3 Landrace x Czech Large White animals were used as oocyte donors. Their estrus cycle was synchronized by intramuscular injection of 750 IU and 1000 IU for miniature pigs and large animals respectively PMSG on the 15th day of cycle. Ovaries were collected 62 64 hr after PMSG stimulation. COCs were isolated from large preovulatory follicles and washed three times in M-199 (Sevac, Prague, Czech Republic), buffered with 6.25 mM HEPES and 26 mM sodium bicarbonate and supplemented with 0.91 mM sodium pyruvate, 1.62 mM calcium lactate, and antibiotics. COCs surrounded by compact multilayered cumulus were cultured in the above mentioned basic culture medium supplemented with 10% inactivated estrous cow serum (prepared in our laboratory) and 5 IU mL gonadotropins PG600 (Intervet, International B.V. Boxmeer, Holland) in 0.5 ml volume per one well, in 4-well culture dishes (Nunclon, Roskilde, Denmark) for 44 hours at 38.5°C, 5% CO_2 and 7.5% O_2.

Preparation of oocytes and polar bodies (PBs) for analysis

Before harvesting, the COCs were treated shortly by 0.1% (w/v) hyaluronidase (Sigma Aldrich) in culture media to remove cumulus cells. Denuded oocytes were washed five times in 10 µl droplets of PBS with 0.4% bovine serum albumin (BSA). Only oocytes with visible PB were used for analysis. Zona pellucida was removed using 0.1% (w/v) Pronase (Sigma Aldrich). During this step, PBs were separated from oocytes using very narrow-bore glass pipette and after washing in three 10 µl drops Tris-HCl (10 mM, pH 8.5), both were transferred into individual PCR tubes containing 2 µl Tris-HCl and stored at −80°C before analysis. Precautions against DNA contamination were taken when handling and sampling oocytes and corresponding PBs.

Whole genome amplification and comparative genomic hybridization

Oocytes or polar bodies (PBs) underwent lysis and whole genome amplification using PicoPlex™ WGA kit (Rubicon

Genomics) according to the manufacturer's instructions. Successful amplification of the samples was checked by agarose gel electrophoresis. A blank sample was included as a negative control with every amplification batch. Amplified DNA from oocytes and PBs was labelled by BioPrime® Array CGH Genomic labeling System (Invitrogen) using Cyanine 3-dUTP (Enzo Life Sciences) fluorescent dye. Reference DNA, prepared from single diploid cumulus cell, was also amplified and labeled using Green 496-dUTP (Enzo Life Sciences) fluorescent dye. Subsequently, comparative genomic hybridization was performed according to previously published protocol [22]. CGH analysis criteria were as follows: red signal: green signal ratio of >1.25:1 was indicative of chromosomal material gain, while ratio of <0.75:1 indicated loss. These criteria allow us to detect the non-disjunction of the whole bivalents as well as the pre-division of sister chromatids. The procedure of analysis of digital images was described in [22].

Acknowledgments

We are grateful to Stefan Juhas and Martin Pavlik for their assistance with isolation of ovaries from donor animals.

Author Contributions

Conceived and designed the experiments: MA JR JM MK. Performed the experiments: MH MJ PM AP. Analyzed the data: MH MJ PM MA. Wrote the paper: MA.

References

1. Hassold T, Hunt P (2001) To err (meiotically) is human: the genesis of human aneuploidy. Nat Rev Genet 2: 280 291.
2. Pacchierotti F, Adler ID, Eichenlaub-Ritter U, Mailhes JB (2007) Gender effects on the incidence of aneuploidy in mammalian germ cells. Environ Res 104: 46 69.
3. Hunt P, Hassold T (2002) Sex matters in meiosis. Science (New York, NY) 296: 2181 2183.
4. Pellestor F (1991) Differential distribution of aneuploidy in human gametes according to their sex. Hum Reprod 6: 1252 1258.
5. Duncan FE, Chiang T, Schultz RM, Lampson MA (2009) Evidence that a defective spindle assembly checkpoint is not the primary cause of maternal age-associated aneuploidy in mouse eggs. Biol Reprod 81: 768 776.
6. Pan H, Ma P, Zhu W, Schultz R (2008) Age-associated increase in aneuploidy and changes in gene expression in mouse eggs. Dev Biol 316: 397 407.
7. Zuccotti M, Boiani M, Garagna S, Redi C (1998) Analysis of aneuploidy rate in antral and ovulated mouse oocytes during female aging. Mol Reprod Dev 50: 305 312.
8. Lechniak D, Switonski M (1998) Aneuploidy in bovine oocytes matured in vitro. Chromosome Res 6: 504 506.
9. Nicodemo D, Pauciullo A, Cosenza G, Peretti V, Perucatti A, et al. (2010) Frequency of aneuploidy in in vitro-matured MII oocytes and corresponding first polar bodies in two dairy cattle (Bos taurus) breeds as determined by dual-color fluorescent in situ hybridization. Theriogenology 73: 523 529.
10. Sosnowski J, Waroczyk M, Switonski M (2003) Chromosome abnormalities in secondary pig oocytes matured in vitro. Theriogenology 60: 571 581.
11. Koenig JL, Stormshak F (1993) Cytogenetic evaluation of ova from pubertal and third-estrous gilts. Biol Reprod 49: 1158 1162.
12. Vozdova M, Machatkova M, Kubickova S, Zudova D, Jokesova E, et al. (2001) Frequency of aneuploidy in pig oocytes matured in vitro and of the corresponding first polar bodies detected by fluorescent in situ hybridization. Theriogenology 56: 771 776.
13. Lechniak D, Warzych E, Pers-Kamczyc E, Sosnowski J, Antosik P, et al. (2007) Gilts and sows produce similar rate of diploid oocytes in vitro whereas the incidence of aneuploidy differs significantly. Theriogenology 68: 755 762.
14. Fragouli E, Escalona A, Gutierrez-Mateo C, Tormasi S, Alfarawati S, et al. (2009) Comparative genomic hybridization of oocytes and first polar bodies from young donors. Reprod Biomed Online 19: 228 237.
15. Kuliev A, Cieslak J, Verlinsky Y (2005) Frequency and distribution of chromosome abnormalities in human oocytes. Cytogenet Genome Res 111: 193 198.
16. Pellestor F, Andreo B, Arnal F, Humeau C, Demaille J (2003) Maternal aging and chromosomal abnormalities: new data drawn from in vitro unfertilized human oocytes. Hum Genet 112: 195 203.
17. Pellestor F, Anahory T, Hamamah S (2005) Effect of maternal age on the frequency of cytogenetic abnormalities in human oocytes. Cytogenet Genome Res 111: 206 212.
18. Keskintepe L, Sher G, Keskintepe M (2007) Reproductive oocyte/embryo genetic analysis: comparison between fluorescence in-situ hybridization and comparative genomic hybridization. Reprod Biomed Online 15: 303 309.
19. Gutierrez-Mateo C, Colls P, Sanchez-Garcia J, Escudero T, Prates R, et al. (2010) Validation of microarray comparative genomic hybridization for comprehensive chromosome analysis of embryos. Fertil Steril 95: 953 958.
20. Geraedts J, Collins J, Gianaroli L, Goossens V, Handyside A, et al. (2010) What next for preimplantation genetic screening? A polar body approach! Hum Reprod 25: 575 577.
21. Vodicka P, Smetana KJ, Dvorankova B, Emerick T, Xu Y, et al. (2005) The miniature pig as an animal model in biomedical research. Ann N Y Acad Sci 1049: 161 171.
22. Hornak M, Hulinska P, Musilova P, Kubickova S, Rubes J (2009) Investigation of chromosome aneuploidies in early porcine embryos using comparative genomic hybridization. Cytogenet Genome Res 126: 210 216.
23. Benzacken B, Martin-Pont B, Bergere M, Hugues J, Wolf J, et al. (1998) Chromosome 21 detection in human oocyte fluorescence in situ hybridization: possible effect of maternal age. J Assist Reprod Genet 15: 105 110.
24. Hunt P, Hassold T (2010) Female meiosis: coming unglued with age. Curr Biol 20: R699 702.

Kudo NR, Wassmann K, Anger M, Schuh M, Wirth KG, Xu H, et al. Resolution of chiasmata in oocytes requires separase-mediated proteolysis. Cell. 2006;126: 135–146.

Impact Factor/Quartile: 34,336/Q1
Times cited (Wos May 2019): 141
Significance: Essential paper showing that there is no prophase pathway in mammalian female meiosis.
Contribution of the author: Microinjection experiments, data interpretation, data analysis

Cell

Resolution of Chiasmata in Oocytes Requires Separase-Mediated Proteolysis

Nobuaki R. Kudo,[1,7] Katja Wassmann,[2,7] Martin Anger,[1,8] Melina Schuh,[3] Karin G. Wirth,[1,9] Huiling Xu,[4] Wolfgang Helmhart,[1,8] Hiromi Kudo,[1] Michael Mckay,[4] Bernard Maro,[2,5] Jan Ellenberg,[3] Peter de Boer,[6] and Kim Nasmyth[1,8,*]

[1]Research Institute of Molecular Pathology, Dr. Bohr-Gasse 7, A-1030 Vienna, Austria
[2]Biologie du Développement, CNRS UMR7622, IFR83, Université Pierre et Marie Curie, 9 quai Saint Bernard, F-75005 Paris, France
[3]Gene Expression and Cell Biology/Biophysics Units, European Molecular Biology Laboratory, Meyerhofstrasse 1, D-69117 Heidelberg, Germany
[4]Division of Radiation Oncology and Research, Peter MacCallum Cancer Centre, Melbourne, Victoria 8006, Australia
[5]Department of Cell and Developmental Biology, Sackler School of Medicine, Tel Aviv University, Ramat Aviv, 69978, Israel
[6]Department of Obstetrics and Gynaecology, University Medical Centre St. Radboud, PO Box 9101, N-6500 HB Nijmegen, The Netherlands
[7]These authors contributed equally to this work.
[8]Present address: University of Oxford, Department of Biochemistry, South Parks Road, Oxford, OX1 3QU, UK.
[9]Present address: Klinik und Poliklinik für Innere Medizin II, Klinikum der FSU Jena, Erlanger Allee 101, D-07747 Jena, Germany.
*Contact: kim.nasmyth@bioch.ox.ac.uk
DOI 10.1016/j.cell.2006.05.033

SUMMARY

In yeast, resolution of chiasmata in meiosis I requires proteolytic cleavage along chromosome arms of cohesin's Rec8 subunit by separase. Since activation of separase by the anaphase-promoting complex (APC/C) is supposedly not required for meiosis I in *Xenopus* oocytes, it has been suggested that animal cells might resolve chiasmata by a separase-independent mechanism related to the so-called "prophase pathway" that removes cohesin from chromosome arms during mitosis. By expressing Cre recombinase from a zona pellucida promoter, we have deleted a floxed allele of separase specifically in mouse oocytes. This prevents removal of Rec8 from chromosome arms and resolution of chiasmata. It also hinders extrusion of the first polar body (PBE) and causes female sterility. mRNA encoding wild-type but not catalytically inactive separase restores chiasma resolution. Both types of mRNA restore PBE. Proteolytic activity of separase is therefore essential for Rec8's removal from chromosome arms and for chiasma resolution but not for PBE.

INTRODUCTION

During the first meiotic division, sister centromeres from homologous chromosomes are held together by chiasmata produced by reciprocal recombination between maternal and paternal chromatids (Petronczki et al., 2003). This process is essential for the traction of maternal and paternal kinetochores toward opposite poles of the meiosis I spindles (co-orientation) and hence for their segregation to opposite poles at the first meiotic division (see Figure 1). Since physical linkage of homologous centromeres due to chiasmata is in fact mediated by sister chromatid cohesion distal to the crossover site (marked by green arrowheads in Figure 1) (Miyazaki and Orr-Weaver, 1994), sister chromatid cohesion along chromosome arms is essential for meiosis I co-orientation.

Sister chromatid cohesion is mediated during both mitosis and meiosis by a multisubunit complex called cohesin (Nasmyth and Haering, 2005). In yeast, resolution of chiasmata is mediated by cleavage (exclusively along chromosome arms) of cohesin's α-kleisin (Rec8) subunit (Buonomo et al., 2000; Kitajima et al., 2003) by a site-specific protease called separase (Uhlmann et al., 2000; Waizenegger et al., 2000), whose activity is kept in check by the binding of an inhibitory chaperone called securin (Ciosk et al., 1998). Separase is activated at the onset of anaphase through the sudden destruction of securin (Cohen-Fix et al., 1996; Funabiki et al., 1996) by a ubiquitin protein ligase called the anaphase-promoting complex or cyclosome (APC/C) along with an accessory protein called Cdc20 (Peters, 2002). In mammalian cells, separase is also inhibited by the binding of Cdk1-cyclin B (Gorr et al., 2005), which is destroyed at the same time as securin by the APC/C. Kinetochores that have not attached to mitotic spindles delay the destruction of sister chromatid cohesion by sequestering Cdc20 in an inactive complex with the Mad2 protein, which prevents destruction of both securin and cyclin B (Nasmyth, 2005).

The finding that both separase (Siomos et al., 2001) and the APC/C (Furuta et al., 2000) are needed for meiosis I

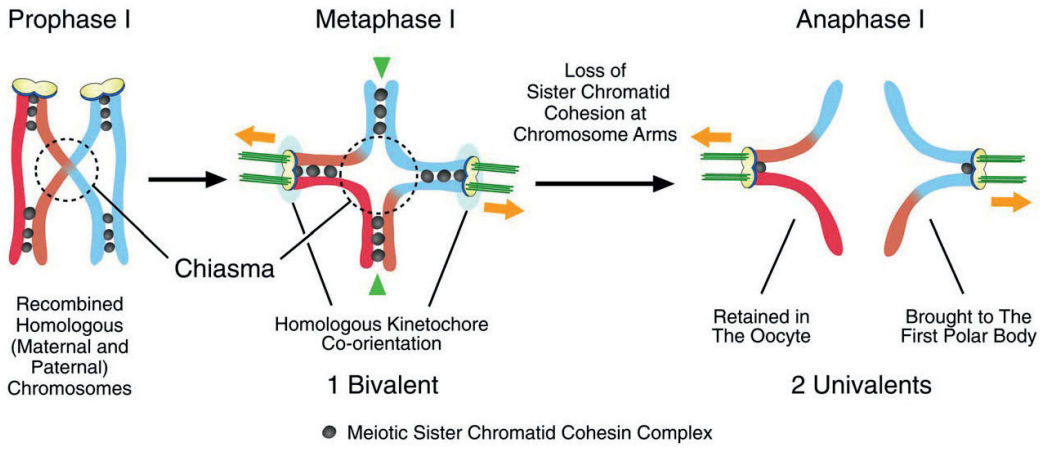

Figure 1. Chiasma Resolution Allows Chromosome Segregation in Meiosis I

Schematic diagrams of meiosis I chromosome segregation where only one chiasma is generated between a pair of homologous chromosomes. Red and sky-blue objects represent homologous chromosomes from maternal and paternal origins. Yellow and green objects represent kinetochores and microtubules, respectively. The meiotic sister chromatid cohesin complex (cohesin) is depicted by black disks. The physical connection between homologous centromeres due to chiasmata is mediated by cohesin molecules marked by green arrowheads distal (with regard to centromeres) to the crossover site. See main text for detail. See also Figure 5B for immunofluorescence images detecting centromeres and cohesin on chromosome spreads.

chromosome segregation in *Caenorhabditis elegans* suggested that chiasmata might be resolved by a common mechanism in all eukaryotic organisms. However, the finding that neither depletion of Cdc20 (Taieb et al., 2001) nor injection of antibodies against APC/C subunits (Peter et al., 2001) blocked meiosis I in *Xenopus laevis* oocytes raised the possibility that chiasmata in vertebrates might be resolved by a process that is independent of the APC/C-separase pathway. It has been suggested that they might instead be resolved by a mechanism related to the so-called "prophase pathway" (Losada et al., 1998; Sumara et al., 2000) that removes cohesin from chromosome arms during mitosis, not by kleisin cleavage but by phosphorylation of cohesin's Scc3-SA2 subunit (Hauf et al., 2005). This notion is controversial because microinjection of mRNA encoding nondegradable securin hinders both extrusion of the first polar body (PBE) and chromosome segregation at meiosis I in mouse oocytes (Herbert et al., 2003). The findings that a Mad2-dependent mechanism, which presumably inactivates the APC/C, blocks meiosis I (Wassmann et al., 2003) and that injection of an admittedly poorly characterized peptide-based separase inhibitor partially hinders chiasma resolution (Terret et al., 2003) also point to a role for the APC/C-separase pathway.

Since the resolution of chiasmata is such a fundamental process, it is essential to address the role of separase using a technique that eliminates the function of separase and no other protein specifically in oocytes. To do this, we used a transgene that expresses Cre recombinase from the *Zona pellucida 3* promoter (Lewandoski et al., 1997) active during growing oocytes to delete exons that encode separase's protease domain from a floxed allele of the gene (Wirth et al., 2006). We find that oocytes lacking active separase neither resolve chiasmata nor extrude permanently polar bodies. Crucially, mRNA encoding wild-type but not catalytically inactive separase restores chiasma resolution. Our data imply that proteolytic cleavage by separase is essential for Rec8's removal from chromosome arms and for chiasma resolution but not for PBE, which can be promoted by separase via a mechanism that does not involve proteolytic cleavage.

RESULTS

Oocytes Lacking Separase Fail to Segregate Chromosomes or to Extrude Polar Bodies Permanently in Meiosis I

Since separase is essential for mitosis, its deletion causes embryonic lethality in mice (Kumada et al., 2006; Wirth et al., 2006). To investigate separase function specifically during oocyte maturation, we tested whether Cre recombinase expressed during the growing oocyte stage from the *Zona pellucida 3* promoter (*Zp3-cre*) (Lewandoski et al., 1997) can cause efficient deletion of a floxed version of the gene (*Separase*^{flox}) in which exons encoding its protease domain are flanked by *loxP* sites (Wirth et al., 2006). Genotyping of offspring showed that 22 out of 22 *Separase*^{flox} alleles were converted to *Separase*$^{\Delta}$ in the female germline of *Separase*$^{flox/+}$ *Zp3-cre* mice. *Separase*$^{flox/+}$ *Zp3-cre* and *Separase*$^{flox/flox}$ females are fertile, but *Separase*$^{flox/flox}$ *Zp3-cre* females are sterile (n = 6). This

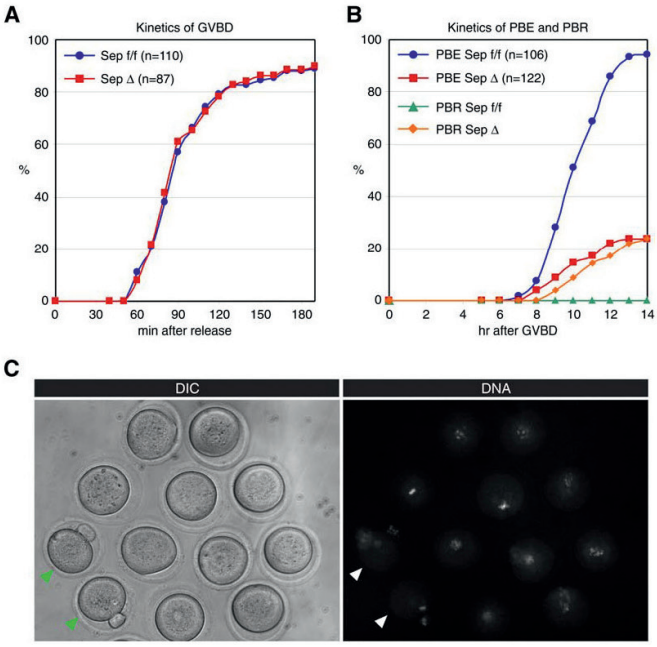

Figure 2. Oocytes Lacking Separase Fail to Extrude PBs Permanently in Meiosis I

In vitro maturation of *Separase*$^{flox/flox}$ *Zp3-cre* oocytes (Sep Δ) and control *Separase*$^{flox/flox}$ oocytes (Sep f/f) was characterized.

(A) Kinetics of germinal vesicle breakdown (GVBD). GV-stage oocytes were isolated in M2 medium containing dbcAMP that inhibits GVBD and released into inhibitor-free medium (at time = 0). Oocytes that had lost GVs were scored at 10 min intervals following release. The numbers of oocytes examined are indicated (n).

(B) Kinetics of polar body extrusion (PBE) and polar body retraction (PBR). Oocytes that had undergone GVBD within 1.5 hr after release into dbcAMP-free M16 medium were selected (at time = 0) and cultured further. PBE and PBR were scored at 1 hr intervals. The numbers of oocytes examined are indicated (n).

(C) Oocytes cultured in Hoechst-containing M2 medium for 15.3 hr after GVBD observed by time-lapse live microscopy. The DIC image and the corresponding DNA image of the identical field are shown. The two oocytes with PBs distinguished by an arrowhead are control Sep f/f; the other ten oocytes are Sep Δ oocytes. The images shown are selected from the original movie (Movie S1).

suggests that *Zp3-cre* causes efficient deletion of both *Separase*^{flox} alleles and that separase is essential for oocyte maturation. Despite their infertility, the ovaries of *Separase*$^{flox/flox}$ *Zp3-cre* females contain normal numbers of fully grown germinal vesicle (GV) stage oocytes surrounded by cumulus cells. Since *Separase*^{flox} deletion most likely occurs at the growing stage, when the *Zp3* promoter is active (Epifano et al., 1995), much oocyte growth must occur in the absence of any active separase gene.

When isolated from the follicle, fully grown mouse GV-stage oocytes resume meiosis when placed in culture medium. They break down germinal vesicles, form meiosis I spindles, and align bivalent chromosomes using their chiasmata (Figure 1; see also below). When all bivalents come under tension, chiasmata are resolved, and paternal and maternal centromeres (along with their associated parental and recombinant chromatids) segregate to opposite poles. One set of chromosomes is retained in the oocyte, while the other is segregated into the first PB. Oocytes subsequently enter meiosis II, form meiosis II spindles, biorient sister centromeres, and arrest at metaphase II awaiting fertilization. *Separase*$^{flox/flox}$ *Zp3-cre* (Sep Δ) oocytes containing GVs undergo germinal vesicle breakdown (GVBD) with the same efficiency and kinetics as *Separase*$^{flox/flox}$ (Sep f/f) oocytes (n = 87) (Figure 2A), which was confirmed by time-lapse live confocal microscopy (data not shown). Together, these results imply that separase is not required for the resumption of oocyte meiosis. In Sep f/f oocytes, PBE occurs between 8 and 12 hr after GVBD under our culture conditions (Figure 2B). Strikingly, only 20% of Sep Δ oocytes extruded PBs, and all PBs produced were retracted (PBR) within 1 hr (n = 122) (Figure 2B). The efficiency of transient PBE in Sep Δ oocytes was sensitive to culture conditions, occurring in only 3% of oocytes when M2 instead of M16 medium was used.

To visualize meiosis I chromosome segregation, we cultured Sep Δ and Sep f/f oocytes in medium containing Hoechst. Time-lapse live microscopy showed that chromosomes from Sep f/f oocytes aligned on metaphase plates 8–9 hr after GVBD and segregated to oocytes and PBs 9–10 hr after GVBD (see Figure S1 and Movie S1 in the Supplemental Data available with this article online). Under these culture conditions, few if any PBs were extruded in Sep Δ oocytes (n = 17). The chromosomes of Sep Δ oocytes failed to segregate and remained in a single group up to 15 hr after GVBD, by which time control oocytes would have arrested in metaphase II (Figure 2C and Movie S1).

We also used time-lapse confocal microscopy to follow chromosome movements in live oocytes that had been injected with mRNA encoding histone H2B fused to monomeric red fluorescent protein (mRFP). Separase depletion had little or no effect on the dynamics of formation of the metaphase plate, which started between 5 and 8 hr, or on the movement of chromosomes (Figure 3 and Movie S2). Strikingly, Sep Δ oocytes failed to segregate chromosomes and, under these culture conditions, also failed to extrude the first PB (n = 28). Control Sep f/f oocytes segregated chromosomes into the first PBs between 8 and 10 hr of the culture. Prolonged confocal microscopy showed

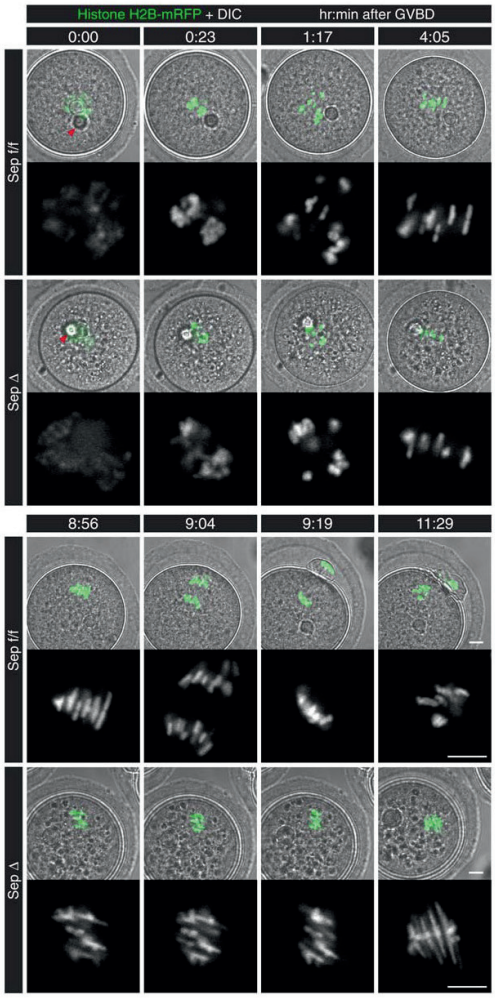

Figure 3. Oocytes Lacking Separase Fail to Segregate Chromosomes in Meiosis I

Chromosome movement and segregation of Sep Δ and Sep f/f oocytes expressing histone H2B-mRFP were observed by time-lapse live confocal microscopy. Upper panels show DIC images merged with images of the RFP channel pseudocolored in green; lower panels show magnified images of the RFP channel only in grayscale at higher magnification. Frames at the indicated times after GVBD were selected from the original time series (Movie S2), where images were acquired every 7 min 46 s with a resolution (xyz) of 160 nm × 160 nm × 5 μm. Time is shown in hr:min relative to GVBD (time = 0:00). An oil droplet resulting from the microinjection procedure is visible in the DIC images (arrowhead at 0:00). Scale bar = 10 μm.

that the chromosomes of Sep Δ oocytes remained in a single group up to 17 hr, by which time control oocytes would have arrested in metaphase II (data not shown). By the time Sep f/f oocytes had extruded PBs, chromosomes from Sep Δ oocytes were stretched, which presumably reflects persistent tractive forces exerted on unresolved bivalents (Figure 3, Sep Δ 11:29).

To observe spindle morphology and chromosomes simultaneously, we performed immunofluorescence confocal microscopy on oocytes fixed at various time points following GVBD (Figure 4A). Sep Δ oocytes established bipolar spindles and aligned most chromosomes on metaphase plates with kinetics similar to those of Sep f/f oocytes. Both reached this stage approximately 8 hr after GVBD. However, we noticed that Sep Δ oocytes had a greater tendency to form astral microtubules emanating from the bipolar spindle between 2 and 6.5 hr after GVBD (Figure 4A). The majority of Sep f/f oocytes underwent anaphase I between 8 and 10 hr after GVBD and reformed bipolar (meiosis II) spindles 12 hr after GVBD. In contrast, at 12 hr after GVBD, 7 out of 8 Sep Δ oocytes that had not extruded PBs did not possess bipolar spindles, while 13 out of 13 did by 17 hr (post-GVBD). This suggests that separase-deleted oocytes destroy their meiosis I bipolar spindles around the time that control oocytes would normally extrude PBs but may be slower than wild-type in re-forming meiosis II bipolar spindles. Most Sep Δ oocytes that transiently extruded PBs distributed chromosomal DNA unequally between oocytes and their PBs (n = 8; Figure 4B).

To address whether Sep Δ oocytes can resolve chiasmata, we examined chromosome spreads prepared at different stages after GVBD (Figures 4C and 4D). Between GVBD and metaphase I, homologous centromeres of different parental origin are connected by chiasmata that join all four homologous chromatids together, forming bivalent chromosomes. Resolution of chiasmata at anaphase I produces univalent chromosomes containing a pair of homologous chromatids connected solely by cohesion between sister centromeres (see Figure 1). Oocytes from Sep f/f mice invariably contained 20 bivalents before PBE and 20 univalents after PBE (Figure 4C). In contrast, Sep Δ oocytes contained only bivalent chromosomes with unresolved chiasmata at all stages after GVBD and irrespective of whether they had extruded PBs (Figures 4C and 4D). Even when PBs had been extruded, all bivalents remained in the oocyte in 60% of cases, while some bivalents were lost—presumably into the PBs—in 40% of cases (Figure 4D). These data imply that separase is necessary for the resolution of chiasmata as well as for proper PBE.

Separase Is Necessary for Removing Cohesin from Chromosome Arms at Anaphase I

In yeast, cleavage of cohesin's α-kleisin Rec8 subunit by separase is accompanied by and necessary for cohesin's disappearance from chromosome arms at anaphase I (Buonomo et al., 2000; Kitajima et al., 2003). This event destroys sister chromatid cohesion along chromosome arms, which presumably resolves chiasmata. To address whether a similar process occurs during oogenesis, we needed first to investigate whether the meiosis-specific α-kleisin presumed to be orthologous to yeast Rec8 (also known as Rec8 in mammals) (Xu et al., 2005) is

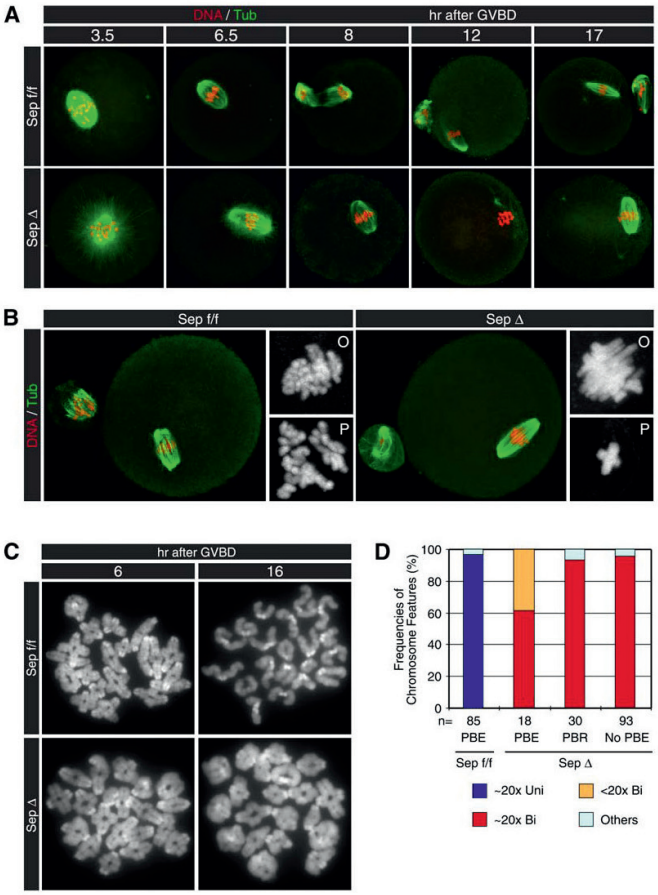

Figure 4. Oocytes Lacking Separase Fail to Segregate Bivalents into Univalents in Meiosis I

Sep Δ oocytes were characterized in comparison to the Sep f/f oocytes as control.

(A and B) Confocal microscopic images of oocytes fixed at the indicated time after GVBD. Microtubules were visualized by immunofluorescence staining with an anti-tubulin antibody (green), and DNA was counterstained with propidium iodide (red). Magnified DNA images of the oocyte (O) and the polar body (P) are shown in the right panels in (B).

(C) DAPI-stained chromosome spreads prepared at the indicated time after GVBD.

(D) Frequencies of different classes of chromosome features contained in the oocytes. Oocytes were harvested at 14 hr after GVBD, except for Sep Δ oocytes with PBs (Sep Δ PBE) because the presence of their PBs is transient. PBE: oocytes that had extruded and maintained PBs, No PBE: oocytes that had not extruded PBs, PBR: oocytes that had extruded PBs and retracted them. Chromosome features were classified into the following different categories: approximately 20 univalents (~20× Uni), approximately 20 bivalents (~20× Bi), apparently less than 20 bivalents (<20× Bi), or other (Others). Numbers of oocytes examined are indicated (n).

associated with chromosome arms at metaphase I. To do this rigorously, we visualized the distribution of a functional version of the Rec8 protein containing nine tandem myc epitopes at its C terminus, expressed at levels comparable to Rec8 protein from endogenous *Rec8* genes from a bacterial artificial chromosome (BAC) transgene (N.R.K. and K.N., unpublished data). This *Rec8-myc* transgene (*TG Rec8-myc*) fully complemented the female sterility caused by a homozygous deletion of the *Rec8* locus (Xu et al., 2005) (see details in Experimental Procedures). The use of an epitope-tagged protein is the only way of ensuring that signals are in fact due to the protein being investigated. This is particularly important in a field where it has been difficult and frequently impossible to detect cohesin on chromosomes at metaphase during mitosis or meiosis using conventional antibodies (Waizenegger et al., 2000).

We first analyzed the distribution of Rec8-myc during meiotic prophase. To do this, we prepared chromosome spreads from fetal ovaries of E13.5 embryos heterozygous for *TG Rec8-myc* and stained them with anti-Myc, anti-Smc3, and anti-Sycp3 antibodies. During pachytene, both Rec8-myc (Figure 5A) and Smc3 (Figure S2A) colocalized with Sycp3, a major component of the lateral element of the synaptonemal complex. The pattern of Rec8-myc staining was similar to that obtained using an anti-Rec8 antibody (Prieto et al., 2004). We next analyzed Rec8-myc in chromosome spreads prepared from oocytes at metaphase I and metaphase II. On metaphase I bivalents prepared 6 hr after GVBD, Rec8-myc localized to interchromatid axes both proximal and distal (with regard to centromeres) to chiasmata but not at the chiasmata themselves (Figure 5B), similar to the localization of another cohesin subunit, Stag3, at this stage (Hodges et al., 2005). On metaphase II univalents from oocytes fixed 18 hr after GVBD, where little is known about cohesin's localization, Rec8-myc was absent from chromosome arms but present at small foci between sister centromeres (Figure 5B). This distribution is similar to those observed on metaphase I and II chromosomes from

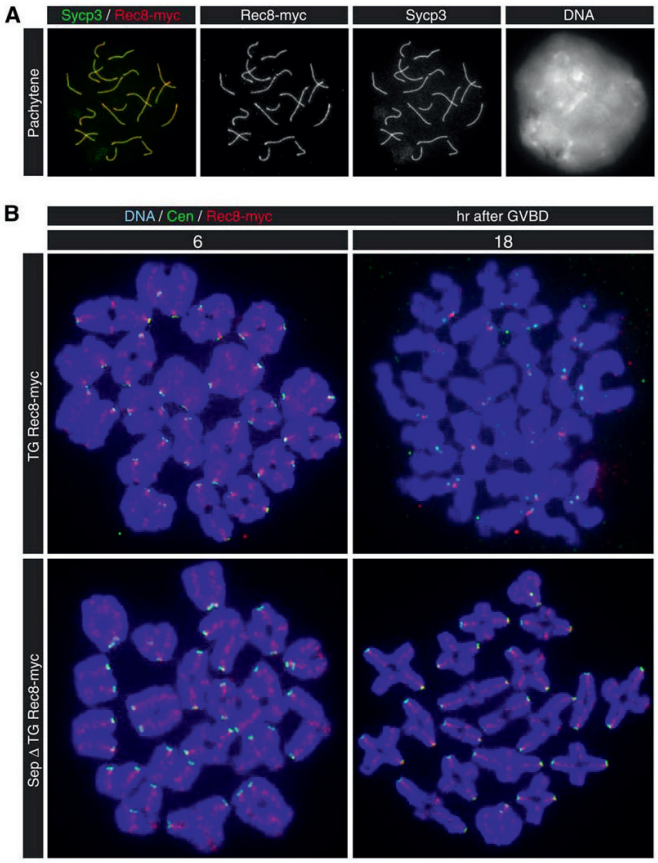

Figure 5. Separase Is Necessary for Removing Cohesin from Chromosome Arms at Anaphase I

(A) Localization of Rec8-myc on pachytene nuclei of oocytes expressing Rec8-myc. Chromosome spreads from fetal ovaries of E13.5 embryos heterozygous for the *Rec8-myc* transgene were prepared and stained with anti-Myc (green) and anti-Sycp3 (red) antibodies. DNA was counterstained with DAPI.

(B) Localization of Rec8-myc on chromosomes from *Separase*$^{flox/flox}$ oocytes also carrying a heterozygous *Rec8-myc* transgene (TG Rec8-myc) and *Separase*$^{flox/flox}$ *Zp3-cre* with *Rec8-myc* (Sep Δ TG Rec8-myc). Chromosome spreads were prepared from oocytes matured in culture for the indicated time after GVBD and stained with anti-Myc antibody (red) and CREST antiserum for marking centromeres (green). DNA was counterstained with DAPI (blue). Note that this spreading method produces large variations in chromosome morphology; we therefore refrain from drawing any more conclusions than are described in the Results.

mammalian spermatocytes (Eijpe et al., 2003; Lee et al., 2003). Crucially, no staining was observed on chromosomes obtained from mice lacking *TG Rec8-myc*. Signals attributable to Smc3 colocalized with Rec8-myc at least along the interchromatid axes in metaphase I (Figure S2B). These data are consistent with the notion that Rec8-containing cohesin complexes confer not only the sister chromatid cohesion distal to chiasmata that holds bivalents together during metaphase I but also the cohesion between sister centromeres that holds homologous chromatids together during metaphase II. The resolution of chiasmata that converts bivalents into univalents at anaphase I is accompanied by the selective loss of cohesin from chromosome arms in oocytes as well as in spermatocytes.

To address whether the lack of chiasma resolution in oocytes lacking separase is accompanied by a failure to remove cohesin from chromosome arms, we bred *Separase*$^{flox/flox}$ *Zp3-cre* females that were heterozygous for *TG Rec8-myc*. Localization of Rec8-myc on metaphase I bivalents was identical to that in oocytes of *Separase*$^{flox/flox}$ *TG Rec8-myc* control mice (Figure 5B). Importantly, we observed a similar if not identical localization on bivalents from *Separase*$^{flox/flox}$ *Zp3-cre TG Rec8-myc* mice when chromosomes were spread from oocytes incubated for 18 hr after GVBD (Figure 5B). At this stage, control oocytes contain only univalents. This implies that cohesin's removal from chromosome arms at anaphase I depends on separase. A corollary is that the nondisjunction of homologous chromosomes observed in oocytes lacking separase might be caused at least partly by their failure to cleave Rec8 along chromosome arms.

Oocytes Lacking Separase Are Not Arrested in Metaphase I

Since PBE is greatly impaired and neither chiasma resolution nor Rec8's removal from chromosome arms occurs in Sep Δ oocytes, it is theoretically possible that their lack of separase merely triggers a metaphase I arrest, possibly by activating a Mad2-dependent spindle assembly checkpoint (SAC). To investigate this, we examined the localization of Mad2 at kinetochores. Mad2 was recruited to the kinetochores of both Sep Δ and control Sep f/f oocytes 4 hr after GVBD (Figure 6A), as occurs in wild-type oocytes

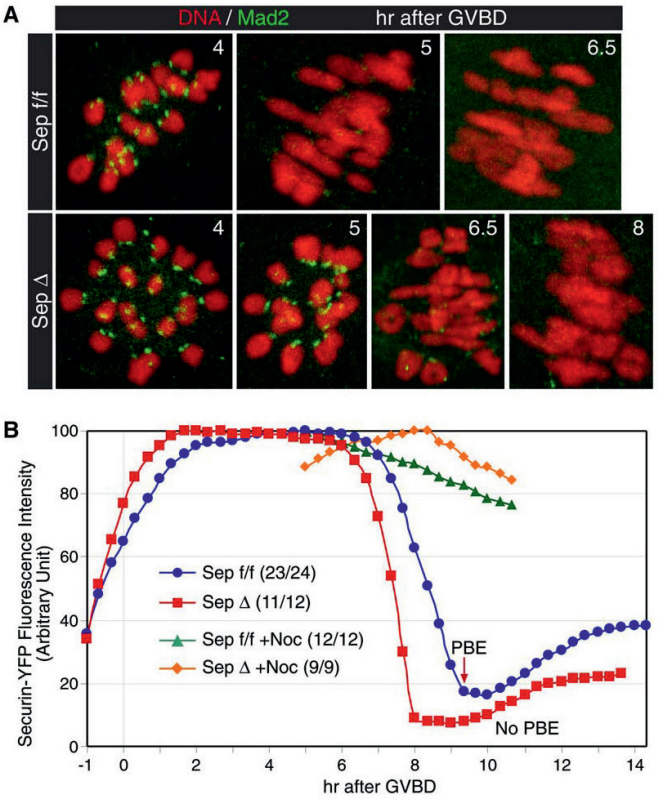

Figure 6. Oocytes Lacking Separase Are Not Arrested in Metaphase I

Sep Δ oocytes were characterized in comparison with control Sep f/f oocytes.

(A) Confocal microscopic images of immunofluorescence staining visualizing Mad2 at kinetochores before metaphase I. Oocytes were fixed at the indicated time in culture after GVBD. Mad2 was visualized by anti-Mad2 antibody (green), and DNA was counterstained with propidium iodide (red).

(B) Time-lapse fluorescence measurement of securin-YFP expressed from mRNA injected at GV stage. The maximum values of the YFP fluorescence signal in each oocyte during the time course were set to 100, and transitions of relative intensity in a representative oocyte were plotted. The ratio of the number of oocytes that showed a transition pattern similar to the indicated curve (n) to the number of oocytes successfully analyzed (N) is given as n/N in parentheses. Measurements in oocytes cultured in the presence of nocodazole (+Noc) were started from 5 hr after GVBD at the same time that the oocytes were transferred to 4 μM nocodazole-containing medium.

(Wassmann et al., 2003). In Sep f/f oocytes, the amount of Mad2 at kinetochores declined by 5 hr and was undetectable 6.5 hr after GVBD. This decline was modestly delayed in Sep Δ oocytes, in which some Mad2 persisted at kinetochores until 5 hr and small amounts even until 6.5 hr; nevertheless, none could be detected by 8 hr after GVBD. The modest delay in Mad2's departure from kinetochores was not accompanied by any major delay in activation of the APC/C because fluorescence due to injection of mRNA encoding a securin-yellow fluorescent protein (YFP) fusion protein declined dramatically 6–9 hr after GVBD in Sep Δ as well as Sep f/f oocytes (Figure 6B), as described in wild-type oocytes (Herbert et al., 2003). PBE accompanied the decline in Sep f/f but not Sep Δ oocytes. In both cases, activation of the SAC by the addition of nocodazole halted the decline (Figure 6B). We also measured histone H1 kinase activity, which is presumably associated with Cdk1-cyclin B1 complexes (Kubiak et al., 1992). We observed a decline in histone H1 kinase activity in Sep Δ oocytes irrespective of whether or not they extruded PBs (Figure S3). We conclude that many of the events normally associated with anaphase I (namely, disappearance of Mad2 from kinetochores, securin degradation, Cdk1 inactivation, and even early steps of PB formation) can occur in oocytes lacking separase. Despite this, chiasmata are never resolved.

Separase Proteolytic Activity Is Required for Chiasma Resolution but Not for PBE

To investigate whether removal of cohesin from chromosome arms at anaphase I depends on separase's proteolytic activity, we tested whether the meiotic defects of Sep Δ oocytes can be suppressed by injection (at the GV stage) of mRNA encoding wild-type or mutant separase (Figure 7A). Under the conditions used for these experiments, few if any Sep Δ oocytes were observed to extrude PBs. Neither mock injection nor injection of mRNA carrying a frameshift mutation at amino acid 212 (separase 1-212) had any effect, but injection of wild-type separase mRNA restored PBE in 57% (n = 169) of oocytes (Figure 7B). Strikingly, injection of mRNA encoding separase with a mutation of its catalytic cysteine residue (C2028S) (Stemmann et al., 2001; Uhlmann et al., 2000) caused 44% of oocytes (n = 144) to undergo PBE—an efficiency only slightly less than that of wild-type mRNA. Unlike wild-type oocytes and Sep Δ oocytes injected with wild-type mRNA, chromosomes were unequally distributed between oocytes and their PBs after

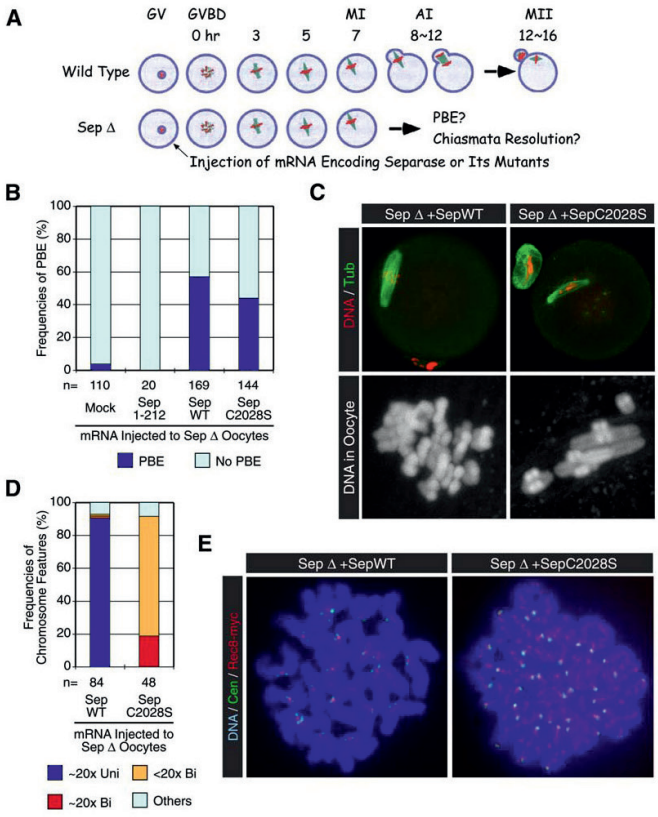

Figure 7. Separase Proteolytic Activity Is Required for Chiasma Resolution

(A) Schematic outline of the experimental procedure. Oocytes lacking separase (Sep Δ) at GV stage were injected with mRNA encoding wild-type or mutant separase. Injected mRNAs encoded wild-type separase (Sep WT), a mutant carrying a serine amino acid replacement at its catalytic cysteine residue (Sep C2028S), or a mutant carrying a frameshift mutation at amino acid residue 212 (Sep 1-212). Water (solvent of mRNA) was injected as a mock control (Mock). Injected oocytes were cultured for 16 hr after release into inhibitor-free medium, and PBE was scored. Chromosome spreads were prepared from oocytes that had extruded PBs and were stained with DAPI to classify chromosome features.

(B) PBE frequencies of either mRNA- or mock-injected oocytes. Numbers of oocytes examined are indicated (n).

(C) Confocal microscopic images of mRNA-injected Sep Δ oocytes fixed at 20 hr after release. Microtubules were visualized by immunofluorescence staining with an anti-tubulin antibody (green), and DNA was counterstained with propidium iodide (red). Magnified images of chromosomes in the oocytes are shown in the lower panels.

(D) Frequencies of different classes of chromosome features contained in the oocytes that had been injected with the indicated mRNAs and extruded PBs. Chromosome features were classified into the following different categories: approximately 20 univalents (~20× Uni), approximately 20 bivalents (~20× Bi), apparently less than 20 bivalents (<20× Bi), or other (Others). Numbers of oocytes examined are indicated (n).

(E) Localization of Rec8-myc on chromosomes from mRNA-injected *Separase*$^{flox/flox}$ *Zp3-cre TG Rec8-myc* oocytes that extruded PBs. Chromosome spreads were prepared at 16 hr after the release and stained with anti-Myc antibody (red) and CREST antiserum for marking centromeres (green). DNA was counterstained with DAPI (blue).

injection with C2028S mRNA and apparently present as bivalents rather than univalents (Figure 7C). To ascertain the state of chromosomes with greater certainty, we prepared chromosome spreads from Sep Δ oocytes injected with wild-type and C2028S mRNA. Ninety percent contained (approximately) 20 univalents after PBE when injected with wild-type mRNA, but none contained appreciable numbers of univalents when injected with C2028S mRNA. Instead, all post-PBE Sep Δ oocytes injected with C2028S mRNA contained only bivalent chromosomes, though usually fewer than 20 (Figure 7D). Importantly, this failure of chiasma resolution in oocytes stimulated to undergo PBE with C2028S mRNA was accompanied by the persistence of Rec8-myc protein along chromosome arms when the experiment was repeated with *Separase*$^{flox/flox}$ *Zp3-cre TG Rec8-myc* oocytes (Figure 7E) (n = 15). We conclude that a catalytically inactive separase can promote PBE but not the removal of cohesin from chromosome arms or the resolution of chiasmata.

DISCUSSION

We describe here a novel approach for studying the role of mitotic proteins during meiosis I in mouse oocytes. We show that expression of Cre recombinase from a zona pellucida promoter (*Zp3-cre*) causes efficient deletion of both maternal and paternal floxed alleles of the separase gene (*Separase*$^{flox/flox}$) specifically in oocytes. This prevents their first meiotic division and thereby causes complete female sterility without interrupting in any way the mitotic divisions required to produce the germ cells that give rise to oocytes. *Zp3-cre* is expressed only after completion of premeiotic DNA replication and meiotic recombination, which has both advantages and disadvantages. An important advantage is that it permits analysis of protein function during chromosome segregation without the potential complication of having interfered with a function that takes place earlier in the meiotic process, for example during recombination. A corollary is that the *Zp3-cre* system cannot be used to study early meiotic functions. As

a consequence, our finding that *Separase*$^{flox/flox}$ *Zp3-cre* mice produce normal numbers of oocytes with normal numbers of chiasmata does not imply that separase is not required for recombination. *Zp3-cre* causes inactivation of the separase gene only after recombination has already been completed. Another great advantage of the system is that the defects caused by gene deletion can be rescued by injection of mRNA made in vitro into oocytes, which enables analysis of the function of mutant forms of the protein in question without further strain construction. The *Zp3-cre* system should be applicable to many genes that have a function during later stages of oocyte maturation.

Our study of *Separase*$^{flox/flox}$ *Zp3-cre* oocytes has enabled us to answer in a definitive manner a long-standing and controversial question, namely whether proteolytic cleavage mediated by separase is required for resolving chiasmata at the onset of anaphase I in mammals. The resolution of chiasmata is one of the most important events during meiotic chromosome segregation. Moreover, it is a process that in human oocytes is accompanied by errors that give rise to aneuploidy, which causes Down's syndrome, miscarriages, and infertility (Hassold and Hunt, 2001). In yeast, cleavage by separase of cohesin's meiosis-specific α-kleisin subunit Rec8 is essential for destroying sister chromatid cohesion along chromosome arms that holds bivalent chromosomes together from the point at which crossovers are formed during pachytene until the onset of anaphase I (Buonomo et al., 2000; Kitajima et al., 2003). It is thought that Rec8 cleavage actually triggers meiosis I chromosome segregation. Therefore, it was somewhat surprising that meiosis I in *Xenopus* oocytes was unaffected either by depletion of the APC/C's activator Cdc20 using antisense RNA (Taieb et al., 2001) or by microinjection of antibodies against Cdc20 or the APC/C's Cdc27 subunit (Peter et al., 2001). These observations led to the proposal that chiasma resolution in vertebrates does not involve the APC/C-separase pathway and might instead be mediated by a process analogous to the prophase pathway that removes cohesin from chromosome arms in a separase-independent manner during mitosis (Hauf et al., 2005). The subsequent finding that meiosis I in mouse oocytes is blocked by microinjection of mRNA encoding nondegradable securin was inconsistent with the conclusion drawn from the *Xenopus* studies (Herbert et al., 2003). Nevertheless, the notion that meiosis I in vertebrates is triggered by a separase-independent process has still been given serious credence (Yu and Koshland, 2005).

Analysis of *Separase*$^{flox/flox}$ *Zp3-cre* oocytes (Sep Δ) has now finally settled this crucial issue. Depletion of separase using the *Zp3-cre* system clearly prevents resolution of chiasmata and the formation of permanent PBs. These effects cannot be caused by activation of the SAC because the kinetics of securin proteolysis appears unaffected by the lack of separase. Importantly, the resolution of chiasmata is restored in most oocytes by microinjection of mRNA encoding wild-type separase but not separase containing a frameshift mutation. PBE is also restored (though possibly not completely) by microinjection of mRNA encoding separase whose catalytic cysteine residue has been replaced by serine (C2028S). Crucially, all chromosomes persist as bivalents containing unresolved chiasmata and Rec8 along chromosome arms even when PBE has been promoted by C2028S mRNA. The lack of chiasma resolution in oocytes that express C2028S separase cannot therefore be due to a general block to meiotic progression and is very likely a direct consequence of separase failing to cleave proteins associated with meiosis I bivalents. Our work on oocytes leaves open the identity of these proteins. However, the finding that Rec8 persists on chromosome arms in these oocytes suggests that cohesin's α-kleisin subunits are likely targets of the protease. It is therefore possible (but still not fully proven) that the disjunction of chromosomes during anaphase involves the same fundamental chemistry during mitosis and meiosis in most eukaryotic organisms, namely cohesin cleavage.

One of our more surprising findings is the observation that Sep Δ oocytes often fail to extrude PBs. As expected, this defect is suppressed by injection of wild-type separase mRNA. More unexpectedly, it is also suppressed, albeit slightly less well, by mRNA encoding a catalytically dead protease (C2028S). This suggests that separase using a mechanism that does not rely on proteolytic cleavage has a role in triggering the formation of PBs following chiasma resolution. Since injection of mRNA encoding securin that cannot be degraded by the APC/C also hinders PBE (Herbert et al., 2003), it is likely that separase can only promote PBE once it has been liberated from its inhibitory chaperone. This implies that activation of separase by the APC/C, once bivalents have aligned on the meiotic spindle and the SAC has been turned off, triggers not only disjunction of bivalents but also the ensuing cell division that sequesters one half of the genome and extinguishes any further prospect of inheritance. This dual function of separase is reminiscent of the situation in budding yeast, where destruction of securin not only triggers sister chromatid separation but also releases the Cdc14 phosphatase from the nucleolus in a protease-independent manner (Buonomo et al., 2003; Stegmeier et al., 2002; Sullivan and Uhlmann, 2003). This event plays a role in downregulation of Cdk1, resolution of sister rDNAs, association of aurora B kinase with the midzone of anaphase spindles, and anaphase spindle stabilization (Higuchi and Uhlmann, 2005). Unlike mouse oocytes, separase is not essential for cytokinesis in yeast because Cdc14's release from the nucleolus is also supported by a separase-independent process called the mitotic exit network (Stegmeier et al., 2002). We have little idea at present how separase promotes PBE in oocytes. The finding that separase binds cyclin B1 and thereby inhibits Cdk1 (Gorr et al., 2005) suggests that its liberation from securin might help to lower Cdk1 activity, though whether separase is sufficiently abundant for such a function to be of physiological relevance is unclear.

Though it makes biological sense, our finding that PBE depends on separase is in fact surprising because elimination of separase function in mouse embryonic fibroblasts by inducing deletion of the very same floxed allele does not prevent cytokinesis despite eliminating sister chromatid separation (Wirth et al., 2006). Cytokinesis is likewise unaffected in fruit-fly embryos by mutations in *three rows* and *pimples* that compromise separase function (Pandey et al., 2005). This implies that, as in yeast, animal cells possess a separase-independent pathway capable of promoting cytokinesis following activation of the APC/C. For some reason, this pathway is insufficient for the equivalent task in oocytes. We suggest therefore that studying the process of cytokinesis in oocytes may be particularly revealing as to its physiology. We suspect that PBE is dependent on two or more processes, each of which is individually sufficient in somatic cells. If so, it may be easier to implicate particular proteins in the process of cytokinesis by studying the dependence of PBE on such proteins.

The recent finding that the sterility of SMC1β-deficient female mice is accompanied and very possibly caused by the precocious loss of chiasmata proves that sister chromatid cohesion has a key role in holding bivalents together during meiosis I, which is essential for co-orienting homologous centromeres (Hodges et al., 2005). The incidence of unpaired univalents and sometimes even single chromatids before the first meiotic division in SMC1β-deficient oocytes increases progressively with maternal age, which is reminiscent of human trisomy. Defects in maintaining sister chromatid cohesion might therefore contribute to the mistakes during meiosis I in human oocytes that give rise to trisomy. Such defects might be caused by a failure to maintain sufficient sister chromatid cohesion during the long arrest of oocytes in prophase. Our finding that separase mediates chiasma resolution in mammalian oocytes raises the possibility that misregulation of this key enzyme, possibly in conjunction with the inherent difficulty of maintaining sister chromatid cohesion for long periods, could also contribute to the mistakes during meiosis I that give rise to trisomy.

EXPERIMENTAL PROCEDURES

Mouse Strains and In Vitro Culture of Oocytes

Generation of the *Separase*^{flox} mice was recently described (Wirth et al., 2006). A transgenic mouse line that expresses Cre recombinase from the *Zona pellucida 3* promoter (*Zp3-cre*) (Lewandoski et al., 1997) was purchased from the Jackson Laboratory. A transgenic line that expresses Rec8 from a bacterial artificial chromosome (BAC), with nine tandem copies of the human c-*myc* epitope at its C terminus, will be described in a separate report (N.R.K. and K.N., unpublished data). Mouse strains used had mixed backgrounds of C57BL/6J, 129/Sv, and CBA/J. Fully grown mouse GV-stage oocytes surrounded by cumulus cells were isolated by disaggregating ovaries of females older than 11 weeks in M2 medium (Specialty Media or Sigma) supplemented with 100 μg/ml dibutyryl cyclic AMP (dbcAMP) (Sigma) at 37.5°C. Oocytes released from most of the surrounding cumulus cells were cultured in drops of medium (~50 μl) covered with mineral oil (Sigma). Oocytes were matured in M16 medium (Specialty Media or Sigma) at 37.5°C in the presence of 5% CO_2 or in M2 medium at 37.5°C in air. Only oocytes that had undergone GVBD within 90 min following release into dbcAMP-free medium were selected (time 0 after GVBD) and cultured further for experiments. Oocytes were cultured in medium containing nocodazole at different concentrations and for different lengths of time as indicated in the figure legends.

Examination of Functionality of the *Rec8-myc* Transgene

To test whether the *Rec8-myc* transgene is functional, we performed complementation tests using a *Rec8* null allele (*Rec8* $^{-}$) that causes complete sterility in homozygous mice of both sexes (Xu et al., 2005). We bred *Rec8* $^{-/-}$ mice that were heterozygous for *TG Rec8-myc*. The average litter size of crosses between *TG Rec8-myc Rec8* $^{-/-}$ females and C57BL/6J males was 9.7 (10 deliveries of 3 females). The average litter size of crosses between *TG Rec8-myc Rec8* $^{-/-}$ males and C57BL/6J females was 7.8 (7 deliveries of 2 males). These are comparable to the average litter size of 7.7 obtained from breeding C57BL/6J in our laboratory (28 deliveries of 10 breeding pairs). In addition, the heterozygous BAC-mediated *Rec8-myc* transgenic allele also suppresses late embryonic sublethality and severe postnatal growth defects seen in *Rec8* $^{-/-}$ mice (Xu et al., 2005). These results demonstrate that Rec8-myc is potentially as functional as wild-type Rec8 protein.

In Situ Immunofluorescence and Time-Lapse Live Microscopy

For in situ immunofluorescence studies, oocytes were harvested at the indicated time after GVBD and fixed following zona pellucida removal by Tyrode's acidic solution (Kubiak et al., 1992; Wassmann et al., 2003). For visualization of the spindle and Mad2, rat anti-α-tubulin antibody (clone YL1/2, Serotec) and rabbit anti-Mad2 antibody (Wassmann et al., 2003) were used as primary antibodies, respectively, and appropriate secondary antibodies conjugated with FITC (KPL or Biosystems) were used. Chromosomal DNA was counterstained with 2 μg/ml propidium iodide (Molecular Probes). Confocal microscopic images were acquired with a Leica TCS4D confocal microscope. Time-lapse live microscopy was performed with a Leica DM IRBE microscope equipped with a Micromax 1300 YHS CCD camera (Princeton Instruments). Fluorescence and DIC images were acquired using MetaMorph software (Universal Imaging) at 20 min intervals. For visualizing DNA, oocytes were cultured in M2 medium containing 2 ng/ml bisbenzimide *H* 33342 (Hoechst 33342) (Sigma) at 37°C following a 2 hr preculture in Hoechst-containing M2 medium. For quantification of the YFP signal, the excitation light of a 100 W mercury lamp was decreased to 10% by a neutral density filter and an exposure was taken for 300 ms. The signal intensity was calculated as the sum of pixels in a defined region against mean background levels using ImageJ 1.32j software (NIH).

Preparation and Staining of Chromosome Spreads

Chromosome spreads of mouse oocytes during prophase I and meiotic maturation were prepared using methods previously described (Hodges and Hunt, 2002; Peters et al., 1997); see Supplemental Data for further details. The dried chromosome spreads were stained with 1 μg/ml DAPI for DNA counterstaining, following immunofluorescence staining when required. Mouse anti-human c-*myc* epitope antibody (clone 4A6, Upstate), rabbit anti-Smc3 antibody (727, gift of J.-M. Peters, Vienna; Sumara et al., 2000), rabbit anti-Sycp3 antibody (Knuf, gift of C. Heyting, Wageningen, The Netherlands; Lammers et al., 1994), mouse anti-Sycp3 antibody (clone 10G11, Abcam), and CREST serum (gift of A. Kromminga, Hamburg, Germany) for marking centromeres were used as primary antibodies, and appropriate secondary antibodies conjugated with Alexa Fluor 488 or 568 (Molecular Probes) or Cy5 (Jackson ImmnoResearch) were used. Images were captured with an Axioplan 2 microscope (Carl Zeiss) equipped with an α Plan-FLUAR 100×/1.45 oil objective and a CoolSnap HQ CCD camera (Photometrics) and analyzed using MetaMorph software (Universal Imaging).

Synthesis and Microinjection of mRNAs

Mouse separase cDNA (GenBank/EMBL/DDBJ accession number AK129072) was identified by BLAST search using the amino acid sequences of its orthologs from other organisms. A cDNA clone encoding full-length mouse separase cDNA (clone name mKIAA0165) was kindly provided by the Kazusa DNA Research Institute (Chiba, Japan). Construction of plasmids for in vitro transcription of mRNAs encoding wild-type separase, a separase mutant with a site-directed mutation at its catalytic cysteine at amino acid 2028 replaced by serine (separase C2028S), and a truncated mutant with a frameshift mutation at amino acid 212 (separase 1-212) is described in the Supplemental Data. Construction of a plasmid for the mRNA encoding mouse securin (gene product of *Pttg1*, MGI ID 1353578) fused with YFP will be described elsewhere (K.W., unpublished data). Capped mRNAs were synthesized by in vitro transcription using an mMessage mMachine T3 kit (Ambion) and purified by RNeasy columns (QIAGEN). mRNAs prepared at a final concentration of 0.1 μg/μl in RNase-free water (Ambion) were microinjected using a FemtoJet microinjector (Eppendorf) with constant flow settings into the cytoplasm of GV-stage oocytes in M2 medium containing 100 μg/ml dbcAMP. Oocyte maturation was induced within 1 hr after microinjection. RNase-free water was injected as a mock control.

Time-Lapse Confocal Microscopy of Live Oocytes Expressing Histone H2B-mRFP

GV-stage oocytes were injected with 10 pl of 0.3 μg/μl mRNA encoding H2B-mRFP (M.S. and J.E., unpublished data) in M2 medium containing 250 μM dbcAMP using methods described elsewhere (Jaffe and Terasaki, 2004). Control Sep f/f oocytes were coinjected with 25 kDa Alexa 488-labeled dextran (Molecular Probes) to distinguish from Sep Δ oocytes. Following mRNA injection, oocytes were cultured for 2–3 hr at 37°C to allow H2B-mRFP expression and incorporation into chromosomes. Oocytes were cultured in M16 medium placed in an EMBL environmental microscope incubator (EMBL, GP 106), allowing cells to be maintained in a 5% CO_2 atmosphere at 37°C with humidity control during imaging. Time-lapse image acquisitions were performed using a customized Zeiss LSM510 META confocal microscope equipped with a 532 nm excitation laser, a long-pass 545 nm emission filter, a 40× C-Apochromat 1.2 NA water immersion objective lens (Carl Zeiss), and an in-house-developed 3D tracking macro (Rabut and Ellenberg, 2004).

Supplemental Data

Supplemental Data include Supplemental Results, Supplemental Experimental Procedures, Supplemental References, three figures, and two movies and can be found with this article online at http://www.cell.com/cgi/content/full/126/1/135/DC1/.

ACKNOWLEDGMENTS

We are grateful to A.H.F.M. Peters, H.-C. Theussl, A. Schleiffer, K. Paiha, S. Schneider-Maunoury, G. van der Heijden, A. Derijck, J. Tkadletz, the imaging facility of the IFR83 (V. Georget and R. Schwartzmann), and the Research Institute of Molecular Pathology (IMP) service and animal house staff for technical assistance and J.-M. Peters, C. Heyting, A. Kromminga, and Kazusa DNA Research Institute for materials. We also thank C. Jessus for valuable support; J.-M. Peters, K. Tachibana, B. McGuinness, and P. Arumugam for critical reading of manuscript; and members of the Nasmyth lab and Jessus lab for helpful discussions. The IMP is funded by Boehringer Ingelheim. This work was partly supported by grants from the Austrian Science Fund and the Austrian Industrial Research Promotion Fund (K.N.), a network grant from the European Community (contact number QLG1-CT-2001-02026, shared costs action U2P2) (K.N. and N.R.K.), the Japanese Society for the Promotion of Science (N.R.K.), INSERM Programme Avenir (K.W.), ARC (B.M., grant 3356; K.W., postdoctoral fellowship and grant 3883), and EC Fellowship MEIF-CT-2005-024429 (M.A.).

Received: December 9, 2005
Revised: March 20, 2006
Accepted: May 3, 2006
Published: July 13, 2006

REFERENCES

Buonomo, S.B., Clyne, R.K., Fuchs, J., Loidl, J., Uhlmann, F., and Nasmyth, K. (2000). Disjunction of homologous chromosomes in meiosis I depends on proteolytic cleavage of the meiotic cohesin Rec8 by separin. Cell *103*, 387–398.

Buonomo, S.B., Rabitsch, K.P., Fuchs, J., Gruber, S., Sullivan, M., Uhlmann, F., Petronczki, M., Toth, A., and Nasmyth, K. (2003). Division of the nucleolus and its release of CDC14 during anaphase of meiosis I depends on separase, SPO12, and SLK19. Dev. Cell *4*, 727–739.

Ciosk, R., Zachariae, W., Michaelis, C., Shevchenko, A., Mann, M., and Nasmyth, K. (1998). An Esp1/Pds1 complex regulates loss of sister chromatid cohesion at the metaphase to anaphase transition in yeast. Cell *93*, 1067–1076.

Cohen-Fix, O., Peters, J.-M., Kirschner, M.W., and Koshland, D. (1996). Anaphase initiation in Saccharomyces cerevisiae is controlled by the APC-dependent degradation of the anaphase inhibitor Pds1p. Genes Dev. *10*, 3081–3093.

Eijpe, M., Offenberg, H., Jessberger, R., Revenkova, E., and Heyting, C. (2003). Meiotic cohesin REC8 marks the axial elements of rat synaptonemal complexes before cohesins SMC1beta and SMC3. J. Cell Biol. *160*, 657–670.

Epifano, O., Liang, L.F., Familari, M., Moos, M.C., Jr., and Dean, J. (1995). Coordinate expression of the three zona pellucida genes during mouse oogenesis. Development *121*, 1947–1956.

Funabiki, H., Yamano, H., Kumada, K., Nagao, K., Hunt, T., and Yanagida, M. (1996). Cut2 proteolysis required for sister-chromatid seperation in fission yeast. Nature *381*, 438–441.

Furuta, T., Tuck, S., Kirchner, J., Koch, B., Auty, R., Kitagawa, R., Rose, A.M., and Greenstein, D. (2000). EMB-30: an APC4 homologue required for metaphase-to-anaphase transitions during meiosis and mitosis in Caenorhabditis elegans. Mol. Biol. Cell *11*, 1401–1419.

Gorr, I.H., Boos, D., and Stemmann, O. (2005). Mutual inhibition of separase and Cdk1 by two-step complex formation. Mol. Cell *19*, 135–141.

Hassold, T., and Hunt, P. (2001). To err (meiotically) is human: the genesis of human aneuploidy. Nat. Rev. Genet. *2*, 280–291.

Hauf, S., Roitinger, E., Koch, B., Dittrich, C.M., Mechtler, K., and Peters, J.M. (2005). Dissociation of cohesin from chromosome arms and loss of arm cohesion during early mitosis depends on phosphorylation of SA2. PLoS Biol. *3*, e69.

Herbert, M., Levasseur, M., Homer, H., Yallop, K., Murdoch, A., and McDougall, A. (2003). Homologue disjunction in mouse oocytes requires proteolysis of securin and cyclin B1. Nat. Cell Biol. *5*, 1023–1025.

Higuchi, T., and Uhlmann, F. (2005). Stabilization of microtubule dynamics at anaphase onset promotes chromosome segregation. Nature *433*, 171–176.

Hodges, C.A., and Hunt, P.A. (2002). Simultaneous analysis of chromosomes and chromosome-associated proteins in mammalian oocytes and embryos. Chromosoma *111*, 165–169.

Hodges, C.A., Revenkova, E., Jessberger, R., Hassold, T.J., and Hunt, P.A. (2005). SMC1beta-deficient female mice provide evidence that cohesins are a missing link in age-related nondisjunction. Nat. Genet. *37*, 1351–1355.

Jaffe, L.A., and Terasaki, M. (2004). Quantitative microinjection of oocytes, eggs, and embryos. Methods Cell Biol. *74*, 219–242.

Kitajima, T.S., Miyazaki, Y., Yamamoto, M., and Watanabe, Y. (2003). Rec8 cleavage by separase is required for meiotic nuclear divisions in fission yeast. EMBO J. *22*, 5643–5653.

Kubiak, J.Z., Weber, M., Geraud, G., and Maro, B. (1992). Cell cycle modification during the transitions between meiotic M-phases in mouse oocytes. J. Cell Sci. *102*, 457–467.

Kumada, K., Yao, R., Kawaguchi, T., Karasawa, M., Hoshikawa, Y., Ichikawa, K., Sugitani, Y., Imoto, I., Inazawa, J., Sugawara, M., et al. (2006). The selective continued linkage of centromeres from mitosis to interphase in the absence of mammalian separase. J. Cell Biol. *172*, 835–846.

Lammers, J.H., Offenberg, H.H., van Aalderen, M., Vink, A.C., Dietrich, A.J., and Heyting, C. (1994). The gene encoding a major component of the lateral elements of synaptonemal complexes of the rat is related to X-linked lymphocyte-regulated genes. Mol. Cell. Biol. *14*, 1137–1146.

Lee, J., Iwai, T., Yokota, T., and Yamashita, M. (2003). Temporally and spatially selective loss of Rec8 protein from meiotic chromosomes during mammalian meiosis. J. Cell Sci. *116*, 2781–2790.

Lewandoski, M., Wassarman, K.M., and Martin, G.R. (1997). Zp3-cre, a transgenic mouse line for the activation or inactivation of loxP-flanked target genes specifically in the female germ line. Curr. Biol. *7*, 148–151.

Losada, A., Hirano, M., and Hirano, T. (1998). Identification of Xenopus SMC protein complexes required for sister chromatid cohesion. Genes Dev. *12*, 1986–1997.

Miyazaki, W.Y., and Orr-Weaver, T.L. (1994). Sister-chromatid cohesion in mitosis and meiosis. Annu. Rev. Genet. *28*, 167–187.

Nasmyth, K. (2005). How do so few control so many? Cell *120*, 739–746.

Nasmyth, K., and Haering, C.H. (2005). The structure and function of smc and kleisin complexes. Annu. Rev. Biochem. *74*, 595–648.

Pandey, R., Heidmann, S., and Lehner, C.F. (2005). Epithelial re-organization and dynamics of progression through mitosis in Drosophila separase complex mutants. J. Cell Sci. *118*, 733–742.

Peter, M., Castro, A., Lorca, T., Le Peuch, C., Magnaghi-Jaulin, L., Doree, M., and Labbe, J.C. (2001). The APC is dispensable for first meiotic anaphase in Xenopus oocytes. Nat. Cell Biol. *3*, 83–87.

Peters, A.H., Plug, A.W., van Vugt, M.J., and de Boer, P. (1997). A drying-down technique for the spreading of mammalian meiocytes from the male and female germline. Chromosome Res. *5*, 66–68.

Peters, J.M. (2002). The anaphase-promoting complex: proteolysis in mitosis and beyond. Mol. Cell *9*, 931–943.

Petronczki, M., Siomos, M.F., and Nasmyth, K. (2003). Un menage a quatre: the molecular biology of chromosome segregation in meiosis. Cell *112*, 423–440.

Prieto, I., Tease, C., Pezzi, N., Buesa, J.M., Ortega, S., Kremer, L., Martinez, A., Martinez, A.C., Hulten, M.A., and Barbero, J.L. (2004). Cohesin component dynamics during meiotic prophase I in mammalian oocytes. Chromosome Res. *12*, 197–213.

Rabut, G., and Ellenberg, J. (2004). Automatic real-time three-dimensional cell tracking by fluorescence microscopy. J. Microsc. *216*, 131–137.

Siomos, M.F., Badrinath, A., Pasierbek, P., Livingstone, D., White, J., Glotzer, M., and Nasmyth, K. (2001). Separase is required for chromosome segregation during meiosis I in Caenorhabditis elegans. Curr. Biol. *11*, 1825–1835.

Stegmeier, F., Visintin, R., and Amon, A. (2002). Separase, polo kinase, the kinetochore protein Slk19, and Spo12 function in a network that controls Cdc14 localization during early anaphase. Cell *108*, 207–220.

Stemmann, O., Zou, H., Gerber, S.A., Gygi, S.P., and Kirschner, M.W. (2001). Dual inhibition of sister chromatid separation at metaphase. Cell *107*, 715–726.

Sullivan, M., and Uhlmann, F. (2003). A non-proteolytic function of separase links the onset of anaphase to mitotic exit. Nat. Cell Biol. *5*, 249–254.

Sumara, I., Vorlaufer, E., Gieffers, C., Peters, B.H., and Peters, J.-M. (2000). Characterization of vertebrate cohesin complexes and their regulation in prophase. J. Cell Biol. *151*, 749–762.

Taieb, F.E., Gross, S.D., Lewellyn, A.L., and Maller, J.L. (2001). Activation of the anaphase-promoting complex and degradation of cyclin B is not required for progression from meiosis I to II in Xenopus oocytes. Curr. Biol. *11*, 508–513.

Terret, M.E., Wassmann, K., Waizenegger, I., Maro, B., Peters, J.M., and Verlhac, M.H. (2003). The meiosis I-to-meiosis II transition in mouse oocytes requires separase activity. Curr. Biol. *13*, 1797–1802.

Uhlmann, F., Wernic, D., Poupart, M.A., Koonin, E., and Nasmyth, K. (2000). Cleavage of cohesin by the CD clan protease separin triggers anaphase in yeast. Cell *103*, 375–386.

Waizenegger, I., Hauf, S., Meinke, A., and Peters, J.M. (2000). Two distinct pathways remove mammalian cohesin from chromosome arms in prophase and from centromeres in anaphase. Cell *103*, 399–410.

Wassmann, K., Niault, T., and Maro, B. (2003). Metaphase I arrest upon activation of the Mad2-dependent spindle checkpoint in mouse oocytes. Curr. Biol. *13*, 1596–1608.

Wirth, K.G., Wutz, G., Kudo, N.R., Desdouets, C., Zetterberg, A., Taghybeeglu, S., Seznec, J., Ducos, G.M., Ricci, R., Firnberg, N., et al. (2006). Separase: a universal trigger for sister chromatid disjunction but not chromosome cycle progression. J. Cell Biol. *172*, 847–860.

Xu, H., Beasley, M.D., Warren, W.D., van der Horst, G.T., and McKay, M.J. (2005). Absence of mouse REC8 cohesin promotes synapsis of sister chromatids in meiosis. Dev. Cell *8*, 949–961.

Yu, H.G., and Koshland, D. (2005). Chromosome morphogenesis: condensin-dependent cohesin removal during meiosis. Cell *123*, 397–407.

Kudo NR, Anger M, Peters AH, Stemmann O, Theussl HC, Helmhart W, et al. Role of cleavage by separase of the Rec8 kleisin subunit of cohesin during mammalian meiosis I. J Cell Sci. 2009;122: 2686–2698.

Impact Factor/Quartile: 4,401/Q2
Times cited (Wos May 2019): 58
Significance: Important paper pointing to important differences between male and female mammalian meiosis.
Contribution of the author: Microinjection experiments, time -lapse imaging

Role of cleavage by separase of the Rec8 kleisin subunit of cohesin during mammalian meiosis I

Nobuaki R. Kudo[1,2,*], Martin Anger[1,3,‡], Antoine H. F. M. Peters[1,4], Olaf Stemmann[5,§], Hans-Christian Theussl[1], Wolfgang Helmhart[1,3], Hiromi Kudo[1,¶], Christa Heyting[6] and Kim Nasmyth[1,3,*]

[1]Research Institute of Molecular Pathology, A-1030 Vienna, Austria
[2]Institute of Reproductive and Developmental Biology, Imperial College London, London W12 0NN, UK
[3]University of Oxford, Department of Biochemistry, Oxford OX1 3QU, UK
[4]Friedrich Miescher Institute for Biomedical Research, CH-4058 Basel, Switzerland
[5]Department of Molecular Cell Biology, Max-Planck Institute of Biochemistry, D-82152 Martinsried, Germany
[6]Molecular Genetics Group, Wageningen University, NL-6703 BD Wageningen, The Netherlands

*Authors for correspondence (e-mails: n.kudo@imperial.ac.uk; kim.nasmyth@bioch.ox.ac.uk)
‡Present address: Institute of Animal Physiology and Genetics, AS CR, v.v.i., Rumburska 89, 277 21 Libechov, Czech Republic and Veterinary Research Institute, v.v.i., Hudcova 70, 621 00 Brno, Czech Republic
§Present address: Department of Genetics, University of Bayreuth, D-95440 Bayreuth, Germany
¶Present address: Division of Investigative Science, Imperial College London, London, W2 1PG, UK

Accepted 28 April 2009
Journal of Cell Science 122, 2686-2698 Published by The Company of Biologists 2009
doi:10.1242/jcs.035287

Summary

Proteolytic activity of separase is required for chiasma resolution during meiosis I in mouse oocytes. Rec8, the meiosis-specific α-kleisin subunit of cohesin, is a key target of separase in yeast. Is the equivalent protein also a target in mammals? We show here that separase cleaves mouse Rec8 at three positions in vitro but only when the latter is hyper-phosphorylated. Expression of a Rec8 variant (Rec8-N) that cannot be cleaved in vitro at these sites causes sterility in male mice. Their seminiferous tubules lack a normal complement of 2 C secondary spermatocytes and 1 C spermatids and contain instead a high proportion of cells with enlarged nuclei. Chromosome spreads reveal that Rec8-N expression has no effect in primary spermatocytes but produces secondary spermatocytes and spermatids with a 4 C DNA content, suggesting that the first and possibly also the second meiotic division is abolished. Expression of Rec8-N in oocytes causes chromosome segregation to be asynchronous and delays its completion by 2-3 hours during anaphase I, probably due to inefficient proteolysis of Rec8-N by separase. Despite this effect, chromosome segregation must be quite accurate as Rec8-N does not greatly reduce female fertility. Our data is consistent with the notion that Rec8 cleavage is important and probably crucial for the resolution of chiasmata in males and females.

Supplementary material available online at
http://jcs.biologists.org/cgi/content/full/122/15/2686/DC1

Key words: Chromosome segregation, Cohesin, Meiosis, Oocyte maturation, Separase, Spermatogenesis

Introduction

Sister chromatid cohesion is mediated by a multi-subunit complex called cohesin (Nasmyth, 2005). During mitosis, cohesin resists the tendency of microtubules to pull sister chromatids apart and thereby generates the tension necessary to stabilize connections between the kinetochores and microtubules (Nicklas, 1997; Tanaka et al., 2005). Destruction of sister chromatid cohesion due to proteolytic cleavage of the α-kleisin subunit of cohesin Scc1 (also known as Rad21) by separase triggers the disjunction of sister chromatids (Uhlmann et al., 1999; Uhlmann et al., 2000; Waizenegger et al., 2000). Separase is inhibited through association with securin and cyclin B, which are destroyed by a ubiquitin protein ligase called the anaphase-promoting complex (APC/C) only when all chromosomes have come under tension on the metaphase plate (Gorr et al., 2005; Yanagida, 2005).

In meiosis, reciprocal recombination between homologous non-sister chromatids (crossing-over) creates bivalent chromosomes (bivalents) containing four chromatids that are joined together by sister chromatid cohesion (Petronczki et al., 2003). The cytological manifestation of crossovers is referred to as chiasma. The production of one (or more) chiasma per bivalent ensures that the two centromeres of the maternal chromosome are joined to those of the paternal homolog via cohesin distal to the chiasmata. This has a crucial consequence, namely that it is now possible to generate the tension necessary to stabilize the connections between kinetochores and microtubules by pulling maternal and paternal kinetochores in opposite directions. In mitotic cells, this tension can only be produced by pulling sister kinetochores in opposite directions, known as amphitelic attachment (Tanaka et al., 2005). In yeast, amphitelic attachment is actively prevented during the first meiotic division (meiosis I) by specific 'monopolin' proteins (Toth et al., 2000).

In budding yeast, cohesion of bivalents depends on a variant of the cohesin complex that contains a meiosis-specific α-kleisin subunit called Rec8 (Klein et al., 1999). Anaphase I is triggered by activation of separase, which cleaves Rec8 and thereby removes cohesin from chromosome arms (Buonomo et al., 2000). This resolves chiasmata, generating dyad chromosomes (dyads) containing two chromatids whose centromeres remain tied together by cohesin that has resisted separase at meiosis I. Cohesion between sister centromeres left intact facilitates amphitelic attachment of sister kinetochores on the meiosis II spindle, a process that largely resembles that of mitosis, with the key difference that centromeric cohesion in meiosis II had presumably been generated prior to meiosis I and not by a fresh round of DNA replication. Expression of Rec8 variants that cannot be cleaved by separase blocks meiosis

I chromosome segregation but has little or no effect on meiotic progression per se (Buonomo et al., 2000; Kitajima et al., 2003).

The discovery that cleavage of the α-kleisin subunits of cohesin by separase triggers meiotic as well as mitotic divisions in yeast suggested that the chemistry of chromosome segregation might be universal in all eukaryotic cells. However, this has been questioned by two findings. The first is the discovery that animal cells possess a second mechanism for removing cohesin from chromosomes during mitosis, one that involves phosphorylation of its Scc3-like subunits (SA1 and SA2) and does not require cleavage of α-kleisin subunits by separase (Hauf et al., 2005). This process precedes separase activation, commencing during prophase. It removes most but not all cohesin from chromosome arms by the time they have aligned on the metaphase plate. Cohesin residing at centromeres is protected from this 'prophase pathway' by Mei-S332-like proteins (also known as Shugoshins) (Kitajima et al., 2005; McGuinness et al., 2005). The second finding is the claim that meiosis I in *Xenopus* oocytes does not require the APC/C-separase pathway (Peter et al., 2001; Taieb et al., 2001). It has been suggested that the first meiotic division in animal cells might be triggered by removal of cohesin from chromosome arms either by the prophase pathway itself or by a process analogous to it. To address rigorously the role of separase during meiosis I, we recently developed a method to deplete separase specifically from mouse oocytes and to replace it by mutated versions (Kudo et al., 2006). This proved that the proteolytic activity of separase is essential for removing cohesin containing Rec8 from bivalents and for resolving chiasmata; a conclusion that is consistent with the finding that a non-degradable version of the separase inhibitor securin blocks chiasmata resolution in oocytes (Herbert et al., 2003; Terret et al., 2003). The chemistry of chiasma resolution might after all be similar in fungi and mammals.

The above studies have left unanswered the issue of whether cohesin containing Scc1 or Rec8 or both mediates cohesion between sister chromatids during meiosis I in animal cells and whether cleavage of either of these α-kleisins is the mechanism by which separase transforms bivalents into dyads. Mouse Rec8, like its fungal namesake, is expressed in meiotic cells, decorates the axial/lateral element (AE/LE) of the synaptonemal complex (SC) during prophase, localizes at the inter-chromatid regions of bivalents, disappears from chromosome arms at the onset of anaphase I in a manner dependent on the protease activity of separase, and persists at centromeres until metaphase II (Eijpe et al., 2003; Lee et al., 2003; Kudo et al., 2006). These features are consistent with the notion that Rec8 confers meiotic sister chromatid cohesion, but do not prove it. The phenotype of mutant mice lacking functional Rec8 has not settled this question because their oocytes or spermatocytes only develop to prophase, and their sister chromatids are at least partially kept in the vicinity of each other until this point (Bannister et al., 2004; Xu et al., 2005). It is therefore still possible that Scc1 or some hitherto-unidentified protein mediates cohesion and its cleavage resolves chiasmata. Such a situation might pertain in *Drosophila* where the only meiosis-specific α-kleisin-like protein, called C(2)M, does not appear to confer sister chromatid cohesion during alignment of bivalents on meiosis I spindles and might function solely in the double-strand-break repair leading to recombination (Heidmann et al., 2004). In summary, the evidence that Rec8 confers sister chromatid cohesion at the time of the first meiotic division is largely cytological and therefore indirect. There is no direct evidence that Rec8 actually confers sister chromatid cohesion in mammals.

The identity of the key target of separase is not merely of academic interest, as deregulated cleavage could contribute to the chromosome missegregation at meiosis I that causes aneuploidy in humans (Hassold and Hunt, 2001). We therefore set out to identify separase cleavage sites in the mouse meiosis-specific α-kleisin Rec8 and studied in vivo phenotypes caused by the expression of a mutant version (Rec8-N) that cannot be cleaved (at least in vitro).

Results

Identification of separase cleavage sites within Rec8

Fragments of α-kleisins cleaved by separase are highly unstable in vivo and are best detected in cells that undergo anaphase synchronously (Uhlmann et al., 1999; Buonomo et al., 2000; Tomonaga et al., 2000; Waizenegger et al., 2000; Kitajima et al., 2003). This largely precludes their detection in mammalian meiotic cells, because it is not possible to obtain homogenous populations of oocytes or spermatocytes at an appropriate stage in sufficient quantities. We therefore used an in vitro system to investigate whether Rec8 possesses separase cleavage sites. [^{35}S]Methionine-labeled human SCC1 tagged at its C-terminus with nine Myc epitopes and mouse Rec8 were synthesized using an in vitro transcription-translation system (IVT) and incubated with active and inactive versions of separase. The former could not be phosphorylated at residues serine 1126 or threonine 1346 whereas the latter contained serine in the place of a crucial catalytic cysteine (Stemmann et al., 2001). Active separase induced Scc1 but not Rec8 cleavage (lanes marked A, Fig. 1A). We detected four of the five SCC1 fragments expected from cleavage at the two known sites (Hauf et al., 2001).

Phosphorylation by the Polo-like kinase Cdc5 has been implicated in regulating Scc1 cleavage in yeast (Alexandru et al., 2001; Hornig and Uhlmann, 2004). Furthermore, yeast Rec8 phosphorylation depends on Cdc5 in vivo (Clyne et al., 2003; Brar et al., 2006). We therefore investigated whether mouse Rec8 can be phosphorylated by human Plk1 and, if so, whether this alters the susceptibility of Rec8 to separase. The electrophoretic mobility of Rec8 in SDS-PAGE was greatly reduced in the presence of Plk1 in a dosage-dependent manner (lanes marked i, Fig. 1B), presumably due to extensive phosphorylation (compare lanes marked i). Remarkably, this was accompanied by the appearance of two prominent cleavage fragments (red asterisks) in the presence of active separase (lanes marked A, Fig. 1B). We obtained a similar result with human Rec8 (data not shown). This suggests that phosphorylation by Plk1 of either Rec8 or separase, or both, promotes Rec8 cleavage, at least in vitro.

Proven separase substrates include Scc1 and separase itself in humans (Hauf et al., 2001; Waizenegger et al., 2002; Zou et al., 2002) and Scc1, Rec8 and Slk19 in yeast (Uhlmann et al., 1999; Buonomo et al., 2000; Tomonaga et al., 2000; Sullivan et al., 2001; Kitajima et al., 2003). The consensus recognition sequence is ExxR (the peptide bond after the Arg being cleaved) (Fig. 1D) and mutations of the conserved Arg alone, or both Arg and Glu, greatly reduce cleavage at that position (Sullivan et al., 2004). To locate the mouse Rec8 cleavage sites, we first tested the effect of mutations M1, M2 and M3 (Fig. 1C,E), which abolished three of its ten ExxR sites. M1 and M3 had no effect on the pattern of cleavage fragments but M2 caused the disappearance of the original fragments and the appearance of two new ones. The simplest explanation for this is that Rec8 has at least two cleavage sites. Separase prefers to cleave at R454, but mutation of this site (M2) revealed a cryptic secondary site elsewhere in the protein. Co-migration of aa 1-454 and aa 455-591 polypeptides

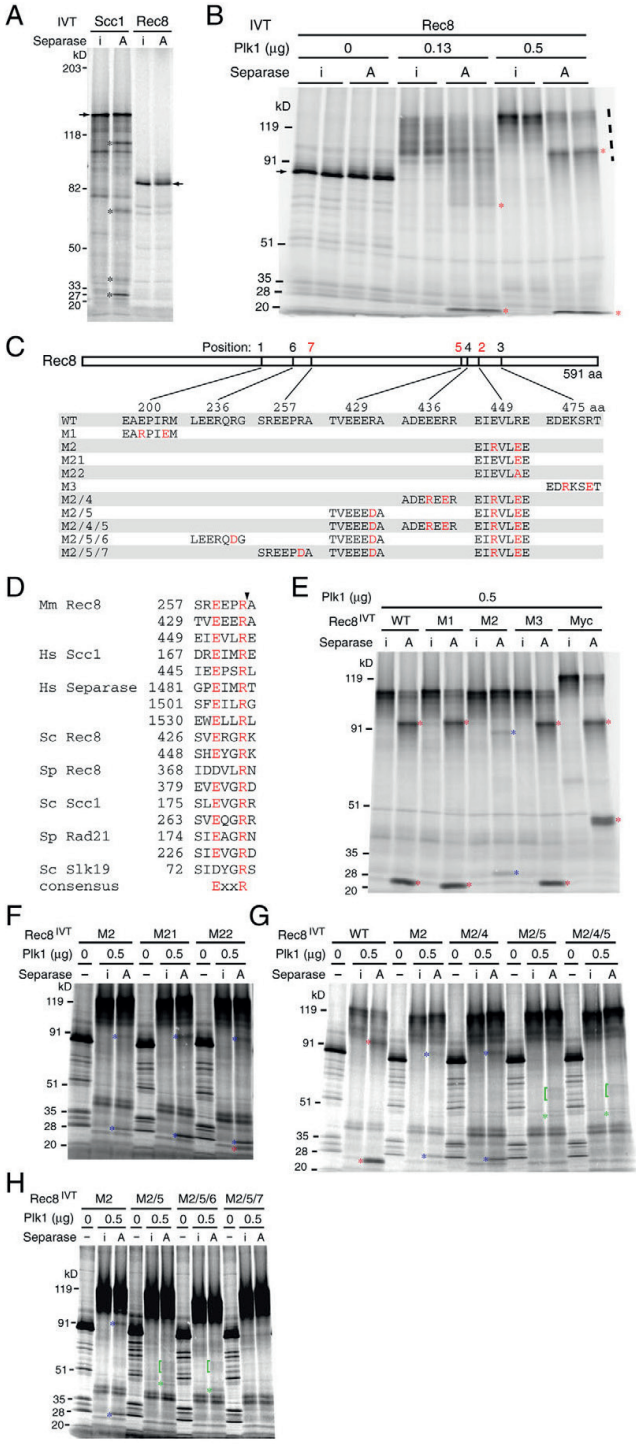

Fig. 1. Identification of separase cleavage sites within Rec8 in vitro. [^{35}S]Methionine-labeled mouse wild-type and mutant Rec8 and human SCC1-Myc were prepared in an in vitro transcription-translation system (IVT) and subjected to an in vitro separase cleavage assay using recombinant active separase (lanes marked A) or its inactive mutant (lanes marked i) in the presence or absence of recombinant polo-like kinase 1 (Plk1) as indicated. Autoradiographs of SDS-PAGE gels on which incubated samples were run are shown. Fragments resulting from cleavage at the primary, secondary and tertiary sites are indicated by asterisks and brackets in red, blue and green, respectively. (**A**) Cleavage assay of mouse Rec8 and C-terminally 9× Myc-tagged human SCC1. Arrows indicate full-length proteins. Cleavage fragments (asterisks) are the bands uniquely seen in A. (**B**) Cleavage assay in the presence of Plk1. Duplicated samples were run side by side. The amount (μg) of purified Plk1 added to each reaction is indicated. Dashed line (right) shows positions of phosphorylated Rec8. (**C**) Identities of mouse Rec8 mutants. (**D**) Alignment of experimentally proven separase target sites (Uhlmann et al., 1999; Buonomo et al., 2000; Tomonaga et al., 2000; Hauf et al., 2001; Sullivan et al., 2001; Waizenegger et al., 2002; Zou et al., 2002; Kitajima et al., 2003). The arrowhead indicates positions of cleavage. Mm, *Mus musculus*; Hs, *Homo sapiens*; Sc, *Saccharomyces cerevisiae*; Sp, *Schizosaccharomyces pombe*. (**E**) Cleavage assay of wild-type (WT), M1, M2, M3 and C-terminally 9× Myc-tagged wild-type Rec8 (Myc). (**F**) Cleavage assay of M2, M21 and M22. (**G**) Cleavage assay of WT, M2, M2/4, M2/5 and M2/4/5. (**H**) Cleavage assay of M2, M2/5, M2/5/6 and M2/5/7.

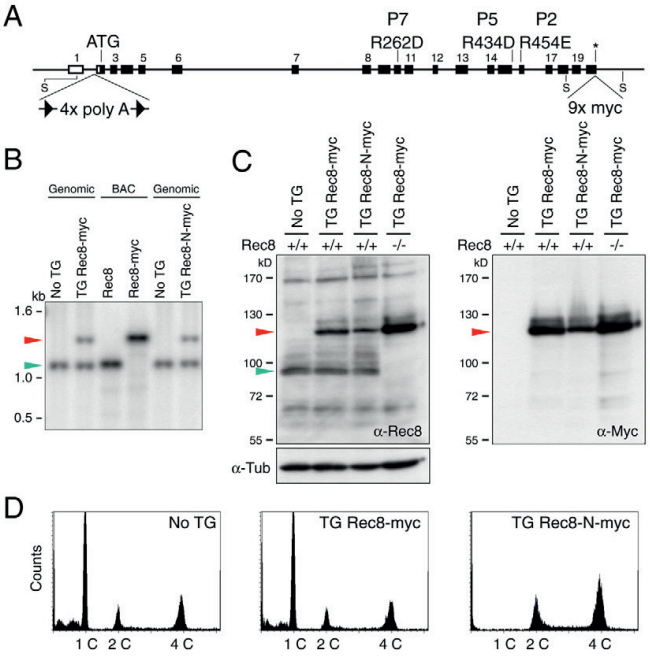

Fig. 2. Male transgenic mice expressing Rec8-N-Myc fail to produce haploid cells. (A) A schematic representation of the mouse *Rec8* genomic locus showing the mutagenized loci for generating BAC-mediated transgene constructs. A DNA fragment encoding 9× Myc epitopes (9× Myc) was inserted at the termination codon (asterisk) to make the Rec8-Myc expression construct (for *TG Rec8-Myc* mice). This construct was further modified to obtain the Rec8-N-Myc expression construct (for *TG Rec8-N-Myc* mice) by replacing the following residues: 262nd Arg to Asp (R262D), 434th Arg to Asp (R434D) and 454th Arg to Glu (R454E). For a conditional construct (for *TG Stop/Rec8-N-Myc* mice), a *loxP*-flanked stop cassette was inserted at the intron 1 (4× polyA). Boxes represent exons. ATG, initiation codon; S, *Stu* I site; The P represents the position of cleavage sites in Fig. 1C. (B) Southern blot analysis of genomic DNA from transgenic mice and littermates without transgene (No TG) digested by *Stu I*. The BACs encoding *Rec8* or *Rec8-Myc* were examined as controls (BAC). The 1089 bp *Stu* I fragment was used as a probe. Expected sizes of fragments encoding the C-termini of Rec8 and Rec8-Myc are 1089 (green arrowhead) and 1478 bp (red arrowhead), respectively. (C) Western blot analysis testing the expression of Rec8-Myc and Rec8-N-Myc in total testicular cell extracts. Genotypes of endogenous *Rec8* are indicated. One blot was used for three examinations by anti-Rec8, anti-Myc and anti-tubulin (loading control). Green arrowhead, endogenous Rec8; red arrowhead, Rec8-Myc or Rec8-N-Myc. (D) FACS analysis of testicular cells for the DNA content. Histogram peaks indicated as 1C, 2C and 4C correspond to cells having one, two or four copies of the genome, respectively.

produced by IVT and Plk1 treatment with the larger and smaller cleavage fragments produced by separase confirmed that cleavage had occurred close to or at R454 (see supplementary material Fig. S1A). This assignment is consistent with the observation that the mobility of the smaller but not the larger cleavage fragment is reduced by Myc epitopes added to the C-terminus of Rec8 (Fig. 1E). R454E mutation (M21) also abolished Rec8 cleavage at this site, but M22 containing R454A was partially cleaved (Fig. 1F).

We used a similar approach to map the secondary separase cleavage site to R434. Thus, the M2/5 and M2/4/5 mutations abolished the fainter secondary fragments (blue asterisks) produced by M2 Rec8 protein but M2/4 had no effect (Fig. 1G). Co-migration of phosphorylated aa 1-434 and aa 435-591 polypeptides produced by IVT with the larger and smaller secondary cleavage fragments (supplementary material Fig. S1B) confirmed that cleavage had indeed occurred close to or at R434. We noticed that Rec8 protein lacking both primary and secondary sites (M2/5) still gave rise to a cluster of very faint bands (green asterisks and brackets, seen in M2/5 and M2/4/5) when incubated with active but not with inactive separase, which suggests that Rec8 contains a third cleavage site (Fig. 1G). The tertiary cleavage products were still detectable when M2/5/6 but not when M2/5/7 was used as a substrate, suggesting that separase cleaves Rec8 after R262 when R454 and R434 have been mutated (Fig. 1H). We conclude that separase cleaves mouse Rec8 at three positions in vitro (Fig. 1C,D). Rec8 protein with R262D, R434D and R454E mutations will be referred to as Rec8-N.

Generation of transgenic mice expressing Rec8-Myc and Rec8-N-Myc

In yeast, non-cleavable Rec8 protein blocks chiasma resolution even when coexpressed with endogenous wild-type Rec8 (Buonomo et al., 2000). We therefore investigated the effect of expressing Rec8-N at physiological levels from a transgene containing the entire *Rec8* locus plus neighboring genes on a bacterial artificial chromosome (BAC). Because it was possible that the *Rec8-N* transgene might cause infertility in both sexes, we also created lines in which expression of Rec8-N from the BAC was prevented by a transcription-terminator cassette flanked by *loxP* recombination sites (conditional stop cassette) inserted into the first intron. Homologous recombination in *Escherichia coli* was used first to insert nine Myc epitopes at the C-terminus of Rec8, then to introduce the R262D, R434D and R454E mutations, and finally to insert the conditional stop cassette (Fig. 2A). Transgenes for expression of Rec8-Myc (*TG Rec8-Myc*) or for silenced Rec8-N-Myc (*TG Stop/Rec8-N-Myc*) had no effect on the fertility of males or females. The former fully suppressed the infertility of offspring homozygous for a *Rec8* deletion (Kudo et al., 2006). Surprisingly, the transgene expressing *Rec8-N-Myc* (*TG Rec8-N-Myc*) caused male but not female sterility, as did *TG Stop/Rec8-N-Myc* when combined with a transgene that expressed Cre recombinase ubiquitously, which caused efficient deletion of the stop cassette (data not shown). Because Rec8-N-Myc females were fertile, all subsequent analyses were performed with mice that expressed Rec8-N unconditionally. Southern blots using a probe that detects a genomic DNA fragment encoding the C-terminus of Rec8 (whose size is altered by the Myc tags) revealed that the *TG Rec8-Myc* and *TG Rec8-N-Myc* transgenes were present as single or at most two copies per haploid genome (Fig. 2B).

Rec8-N-Myc prevents production of haploid spermatids

Mice heterozygous for *TG Rec8-N-Myc* developed normally and had unaltered life spans. However, their testes were approximately half as large (in weight) as those of non-transgenic littermates or males heterozygous for *TG Rec8-Myc* (data not shown). Western blots using antibodies specific for Rec8 or the Myc epitope showed

that Rec8-Myc was expressed at a level similar to endogenous Rec8 whereas Rec8-N-Myc was if anything slightly less abundant (Fig. 2C). FACS analysis revealed that the testes of *TG Rec8-N-Myc* mice lacked any cells with a 1 C DNA content, which constituted the majority of cells in testes of wild-type or *TG Rec8-Myc* mice (Fig. 2D). About two thirds of the cells in *TG Rec8-N-Myc* testes had a 4 C DNA content, suggesting that meiotic DNA replication had occurred but was not followed by the nuclear divisions that usually reduce chromatid numbers.

The spermatogenic failure caused by Rec8-N was then histologically studied by comparing cross-sections of seminiferous tubules within the testes from *TG Rec8-N-Myc* mice, *TG Rec8-Myc* mice and non-transgenic littermates. Mitotic spermatogonia are situated at the basal lamina of the tubules. As the germ cells differentiate, they migrate toward the lumen. Each cross-section contains a defined combination of cell types at different spermatogenic stages, which facilitates assessment of the developmental process (Russell et al., 1990). Spermatogonia were found at the cortex of *TG Rec8-N-Myc* tubules at frequencies similar to those found in tubules of non-transgenic littermates or *TG Rec8-Myc* tubules (Fig. 3A,B), suggesting that mitotic proliferation within spermatogonia is unaffected by Rec8-N expression. Likewise, no abnormalities were detected within populations of primary spermatocytes in meiotic prophase (e.g. pachytene and zygotene in Fig. 3A,B, respectively, and other stages, not shown). Spermatogenic development during meiotic prophase appears therefore to be unaffected by *TG Rec8-N-Myc*. By contrast, spermatids, either round or elongating types, which are abundant at the luminal region of the tubules at all stages of wild-type and *TG Rec8-Myc* testes, were absent in *TG Rec8-N-Myc* tubules. Instead, large numbers of large and densely stained nuclei occupied the luminal part of stage V (Fig. 3A) and other stage tubules (not shown). At the innermost surface of *TG Rec8-N-Myc* tubules, densely stained irregularly shaped nuclei that resemble elongating spermatids with oversized nuclei and sperm tails were observed (Fig. 3A,B).

In wild-type mice, spermatocytes undergoing the first and second meiotic divisions are exclusively seen in stage XII tubules (Russell et al., 1990). Such tubules from *TG Rec8-N-Myc* testes contained metaphase I spermatocytes (Fig. 3B), suggesting that Rec8-N does not block progression from pachytene to metaphase I. Wild-type and *TG Rec8-Myc* stage XII tubules also contain secondary spermatocytes at interkinesis (interphase between meiosis I and II). *TG Rec8-N-Myc* tubules at this stage contained spermatocytes whose nuclei were morphologically similar but notably larger (Fig. 3B). To determine the identity of these abnormally large interkinesis-like spermatocytes, we examined stage XII tubule sections using immunofluorescence to detect Sycp3, a major component of the AE/LE. Sycp3 persists in the vicinity of centromeres until the early stages of round spermatid development but there are striking differences in its distribution before and after meiosis I. Sycp3 associated with metaphase I chromosomes is globular and abundant. It is less abundant and adopts the shape of a short bar in post-meiosis I interkinesis nuclei (see Fig. 4). The Sycp3 pattern within the enlarged irregular nuclei of stage XII sections of *TG Rec8-N-Myc* tubules was similar if not identical to that seen in normal interkinesis nuclei. Because step 1 round spermatids (haploid cells immediately after meiosis II) are not present in stage XII sections (Russell et al., 1990), we suggest that the enlarged irregular nuclei (seen in Fig. 3B) are interkinesis nuclei that are generated by a failure of the first meiotic division but otherwise normal chromosome development. These observations suggest that earlier stages of

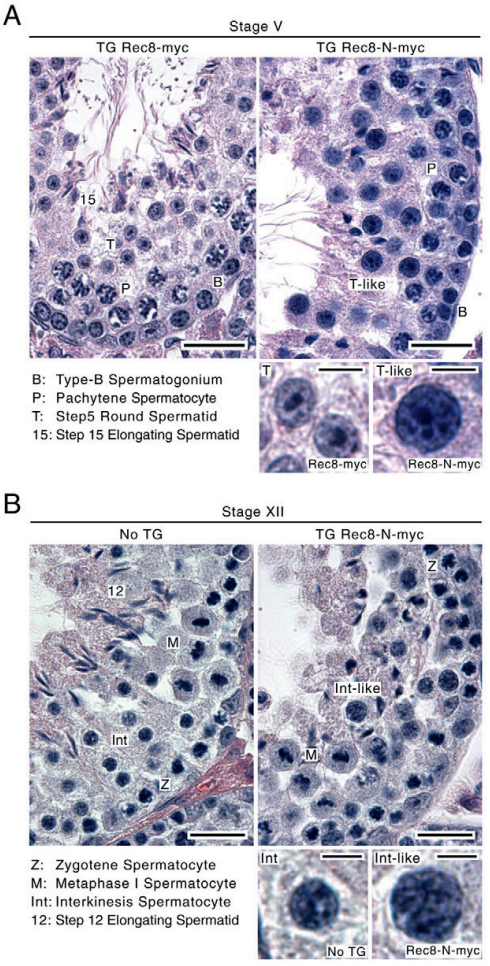

Fig. 3. Spermatogenic failure of *TG Rec8-N-Myc* males. Hematoxylin and eosin staining of seminiferous tubule sections from transgenic mice (TG) and a non-transgene littermate (No TG). Representative sections of stage V (A) and XII (B) are shown. Representative nuclei for each cell type present in the sections are shown at higher magnification. Scale bars: 20 and 5 μm for low and high magnification images, respectively.

spermatogenesis up to metaphase I are unaffected in *TG Rec8-N-Myc* cells and that the first abnormality appears between metaphase I and the interkinesis stages. The large interkinesis and spermatid nuclei and the accumulation of cells with a 4C DNA content suggest that Rec8-N-Myc interferes with nuclear division at the first or possibly both meiotic divisions.

Normal chromosome development until metaphase I in spermatocytes expressing Rec8-N-Myc

Immunofluorescence staining of Sycp3 and Myc-tagged Rec8 in testicular chromosome spreads revealed that synapsis during pachytene was unaltered in *TG Rec8-N-Myc* spermatocytes. Typical examples of 19 fully synapsed autosomes together with a pair of

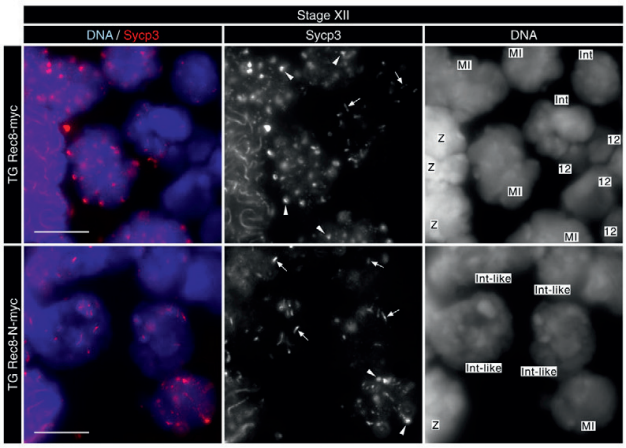

Fig. 4. Morphological change of Sycp3 after meiosis I is unaffected in *TG Rec8-N-Myc* spermatocytes. Immunofluorescence images of stage XII tubule sections stained by DAPI (for DNA) and anti-Sycp3 antibody. Arrowheads and arrows indicate typical patterns of Sycp3 signals in metaphase I and post-metaphase I, respectively. Stages are: Z, zygotene; MI, metaphase I; Int, interkinesis; 12, step 12 elongating spermatid. Scale bars: 10 μm.

sex chromosomes synapsed solely at the pseudo-autosomal region (PAR) from *TG Rec8-Myc* and *TG Rec8-N-Myc* testes are shown in Fig. 5A. Importantly, Rec8-N-Myc and Rec8-Myc colocalized with Sycp3 along the AE/LE of pachytene bivalents. The chromosomal distribution of Sycp3 and Myc-tagged Rec8 also appeared normal at preleptotene, leptotene, zygotene and diplotene (data not shown). This contrasts with the phenotype of *Rec8*- or *Smc1*β-deficient spermatocytes that enter apoptosis in pachytene (Bannister et al., 2004; Revenkova et al., 2004; Xu et al., 2005). Both Rec8-Myc and Rec8-N-Myc localized to the inter-chromatid axes of metaphase I bivalents, both proximal and distal to chiasmata (Fig. 5B). The presence of chiasmata and the lack of precocious homolog disjunction confirm that crossover formation is normal in *TG Rec8-N-Myc* spermatocytes. Finally, we observed that metaphase I bivalents contained the normal two sets of doublet foci of centromeres associated with Sycp3 (Fig. 6A). We conclude that Rec8-N has no adverse effect on meiotic chromosome development up to metaphase I.

No nuclear division in spermatocytes expressing Rec8-N-Myc

If Rec8-N blocks the first meiotic division without halting meiotic chromosome development, then it should be possible to detect nuclei containing four chromatids of each chromosome with morphologies characteristic of meiosis II chromosomes. To address this, we examined DNA staining (using DAPI), kinetochores (using a CREST serum) and the distribution of Sycp3 in chromosome spreads from *TG Rec8-Myc* and *TG Rec8-N-Myc* testes. This revealed three types of abnormal nuclei in *TG Rec8-N-Myc* testes: those with short bars of Sycp3 and pronounced CREST foci associated with centromeric heterochromatin (Fig. 6A, 'Interkinesis'); nuclei with bar-like Sycp3 at chromocenters but lacking CREST foci (not shown); and nuclei without either Sycp3 or pronounced CREST foci (not shown). The CREST and Sycp3 signals (compared with those of wild type) suggest that these three types represent nuclei at interkinesis and at an early and late stage of round spermatid development, respectively. DAPI staining revealed that all three types of nuclei [which would have undergone one (interkinesis) or two (spermatids) meiotic divisions in wild type] were abnormally large, being similar in size or even somewhat larger than those from pachytene or diplotene (see Fig. 6C). Interkinesis nuclei from wild-type or *TG Rec8-Myc* secondary spermatocytes contained 20 sets of doublet CREST foci associated with Sycp3 signals, which reflects the fact that they have 20 dyads, each containing two chromatids (Fig. 6A,B). By striking contrast, the enlarged interkinesis-like nuclei of *TG Rec8-N-Myc* spermatocytes contained 40 sets of doublet CREST foci, which implies that they contain 40 dyads. Together, these data suggest that *TG Rec8-N-Myc* prevents the first meiotic division, and thereby generates 4 C instead of 2 C interkinesis nuclei.

This conclusion was confirmed using chromosome painting to detect the X and Y sex chromosomes. These synapse partially during meiotic prophase (Fig. 5A, Fig. 6C) and segregate at the first meiotic division, which produces secondary spermatocytes with either an X or a Y dyad chromosome. As expected, the interkinesis nuclei from wild-type or *TG Rec8-Myc* secondary spermatocytes contained either X or Y chromosomes and the ratio of nuclei with X chromosomes to those with Y chromosomes was 1:1 (Fig. 6C,D). By contrast, almost all interkinesis-like nuclei from *TG Rec8-N-Myc* spermatocytes contained both X and Y chromosomes. We conclude that *TG Rec8-N-Myc* prevents the first meiotic division at which X and Y chromosomes segregate to 'sister' secondary spermatocytes.

The chromosome spreads from wild-type and *TG Rec8-Myc* spermatocytes contained three kinds of condensed chromosome sets: those containing 20 bivalents (metaphase I), 20 open arm dyads (metaphase II), and 40 closed arm chromosomes (mitotic metaphase). *TG Rec8-N-Myc* spermatocytes contained nuclei with mitotic metaphase and metaphase I chromosomes but lacked any containing the 20 open arm dyads characteristic of metaphase II. Notably, they contained nuclei with 40 instead of 20 open arm dyads (Fig. 6A,B). We presume that these abnormal nuclei have entered metaphase II without having undergone the first meiotic division. To confirm this, we prepared chromosome spreads fixed with methanol and acetic acid and measured the fraction of chromosome spreads with four different categories (Fig. 7A) of condensed chromosomes: mitotic metaphase, 20 bivalents (metaphase I), 20 dyads (metaphase II) and 40 dyads (irregular metaphase II). This revealed that *TG Rec8-N-Myc* testes had few if any chromosome sets containing 20 dyads. However, they contained chromosome sets with 40 dyads with a frequency similar to that of chromosome sets with 20 dyads in wild-type or *TG Rec8-Myc* testes (Fig. 7B).

Our data are consistent with the notion that Rec8-N blocks the first meiotic division. Does it also block the second? To address

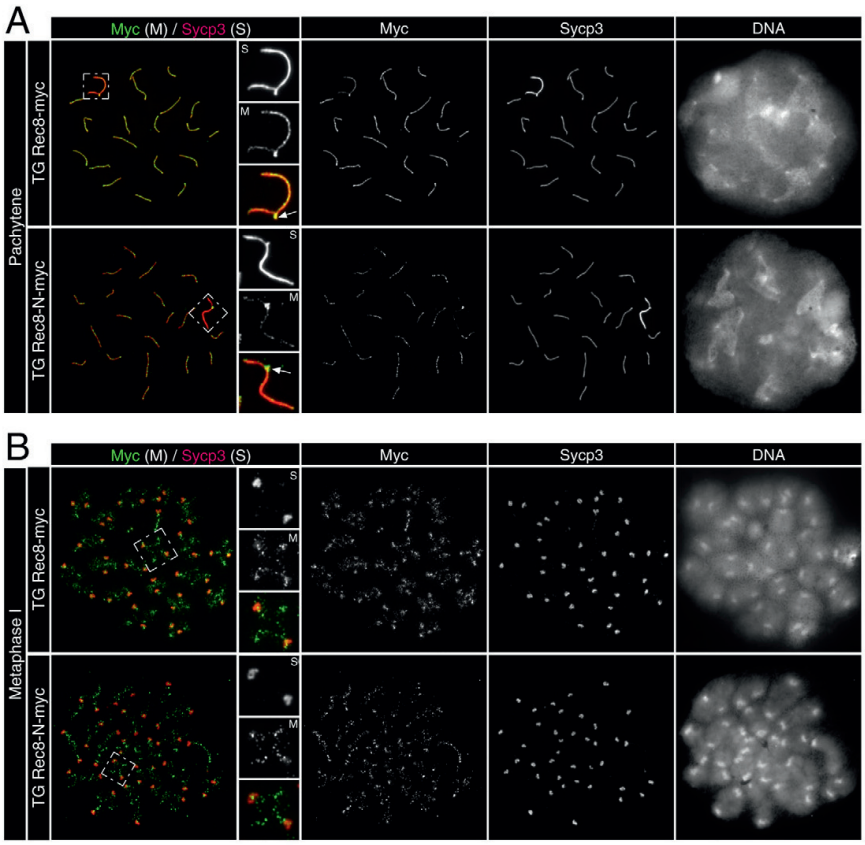

Fig. 5. Normal chromosome development until metaphase I in *TG Rec8-N-Myc* spermatocytes. Immunofluorescence images of chromosome spreads stained with anti-Myc and anti-Sycp3 antibodies. (A) Pachytene nuclei and magnified sex chromosomes synapsed at the PAR (arrow) are shown. (B) Metaphase I chromosomes and magnified images of representative bivalents are shown.

this, we examined the distribution of sex chromosomes in enlarged spermatid-like nuclei contained in *TG Rec8-N-Myc* testes and found that all of them contained both X and Y chromosomes (Fig. 6C,D). Importantly, we frequently observed two separate X or two separate Y chromatids within the same nucleus and sometimes two separate X and two separate Y chromatids within the same nucleus. This suggests that many if not all abnormally large spermatid-like nuclei have a 4 C DNA content and that *TG Rec8-N-Myc* prevents chromosome segregation during meiosis II as well as meiosis I.

Some but not all Rec8-N-Myc persists on chromatin after meiosis I and II

To ascertain whether Rec8-N-Myc persists on chromosomes after anaphase I and II, we compared the distribution of Sycp3 and Myc-tagged Rec8 proteins in chromosome spreads from *TG Rec8-Myc* and *TG Rec8-N-Myc* testes. Rec8-Myc was present (along with Sycp3) only at centromeres in interkinesis nuclei (Fig. 8A) but was completely absent from early stage round spermatids that still possessed Sycp3 signals (Fig. 8B). Very faint amounts of Rec8-Myc were detected throughout chromatin, and in particular at chromocenters in later stage round spermatids that lack Sycp3 signals (not shown). By contrast, modest amounts of Rec8-N-Myc protein were present throughout the chromatids of interkinesis-like and early stage of round spermatid nuclei (Fig. 8A,B). These results imply that some but not all Rec8-N-Myc persists on chromatin after the time by which both meiotic divisions should have taken place.

Rec8-N delays but does not block chiasma resolution at meiosis I in oocytes

TG Rec8-N-Myc females were fertile with slightly smaller litter size (average 7.8, 11 deliveries of six females) than *TG Rec8-Myc* females (average 9.6, five deliveries of three females). Oocytes from *TG Rec8-N-Myc* females extruded the first polar body (PB) with similar timing and efficiency as those from non-transgenic littermates in in vitro culture (Fig. 9A). Importantly, by 20 hours after the germinal vesicle breakdown (GVBD) most oocytes contained 20 dyads, implying that chiasmata had been resolved by metaphase II (Fig. 9B). The lack of any obvious block to meiosis I chromosome segregation or PB formation was not due to a lack of Rec8-N expression, as it was detected along interchromatid axes, both proximal and distal to chiasmata, of metaphase I bivalents. Like Rec8-Myc (Kudo et al., 2006), Rec8-N-Myc was detected in

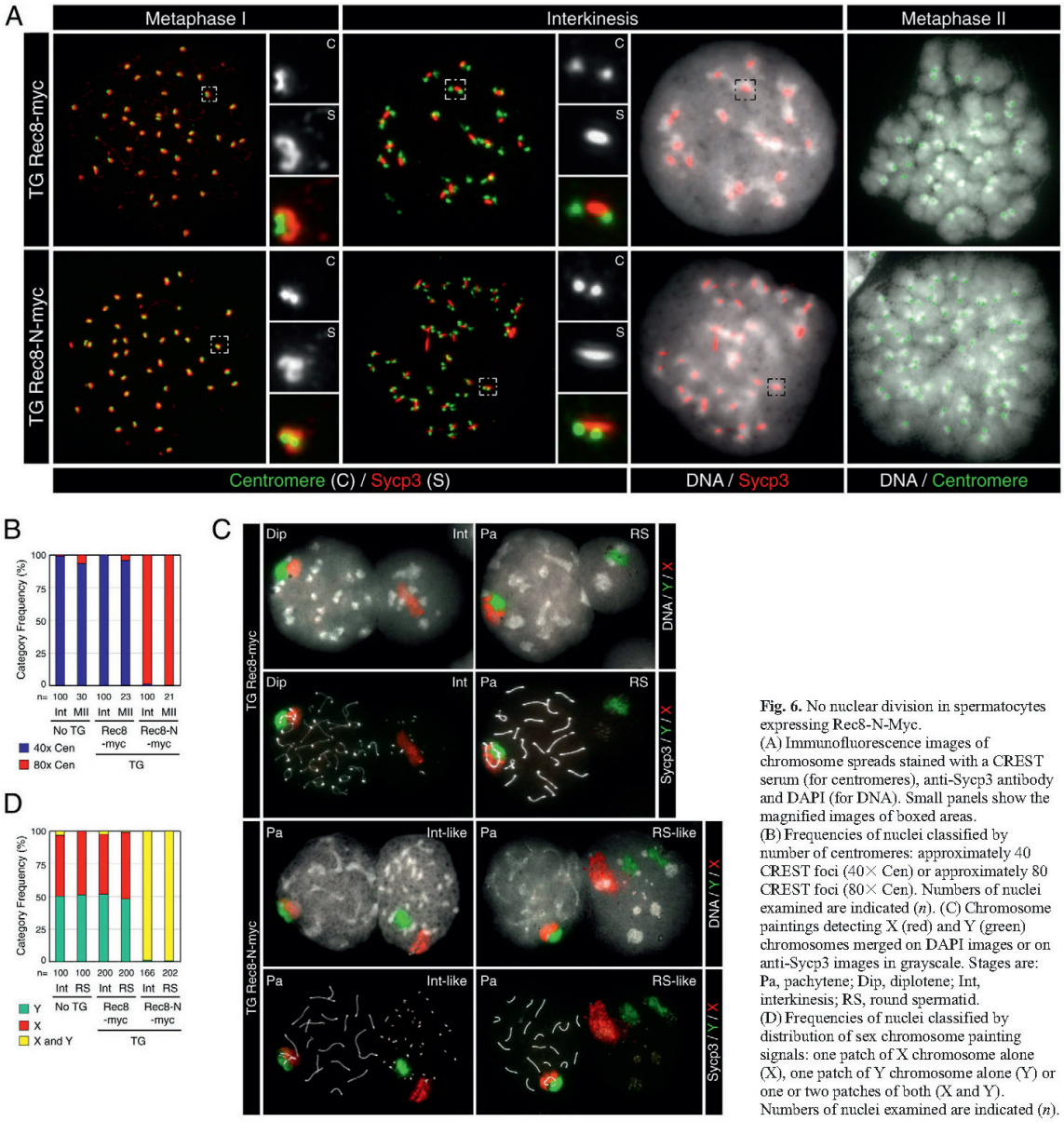

Fig. 6. No nuclear division in spermatocytes expressing Rec8-N-Myc.
(A) Immunofluorescence images of chromosome spreads stained with a CREST serum (for centromeres), anti-Sycp3 antibody and DAPI (for DNA). Small panels show the magnified images of boxed areas.
(B) Frequencies of nuclei classified by number of centromeres: approximately 40 CREST foci (40× Cen) or approximately 80 CREST foci (80× Cen). Numbers of nuclei examined are indicated (*n*). (C) Chromosome paintings detecting X (red) and Y (green) chromosomes merged on DAPI images or on anti-Sycp3 images in grayscale. Stages are: Pa, pachytene; Dip, diplotene; Int, interkinesis; RS, round spermatid.
(D) Frequencies of nuclei classified by distribution of sex chromosome painting signals: one patch of X chromosome alone (X), one patch of Y chromosome alone (Y) or one or two patches of both (X and Y). Numbers of nuclei examined are indicated (*n*).

the vicinity of sister centromeres of dyads at metaphase II (Fig. 9B). This contrasts with the situation in oocytes lacking separase activity, in which the persistence of Rec8 along inter-chromatid axes accompanies a complete absence of chiasma resolution (Kudo et al., 2006).

These data do not, however, exclude a role for Rec8 cleavage in chiasma resolution. If Rec8-N contained cryptic separase cleavage sites that permitted its eventual removal from the arms of bivalents, then it might merely slow down cleavage and chiasma resolution but not actually block either process. To address this, we used live microscopy to measure the timing of chromosome segregation relative to other anaphase hallmarks, namely PB extrusion (PBE) and securin degradation. Germinal vesicle-stage oocytes injected with mRNAs encoding H2B-mCherry and securin-EGFP were recorded using a confocal microscope either at 16 minutes (experiment A; supplementary material Movie 1) or 5-7 minutes intervals (experiment B, movies not shown). In control oocytes (females with the *TG Rec8-Myc* or no transgene), chromosome

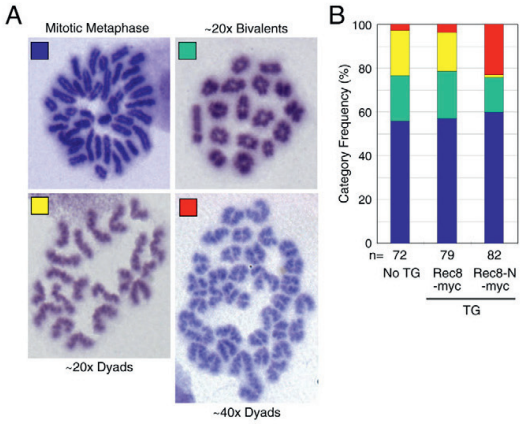

Fig. 7. Double number of dyad chromosomes in metaphase II *TG Rec8-N-Myc* spermatocytes. (A) Condensed chromosomes found in Giemsa-stained spread preparations: 40 chromosomes with arm closed (Mitotic Metaphase); approximately 20 bivalents; approximately 20 dyads; approximately 40 dyads. (B) Frequencies of different classes of condensed chromosomes shown in A. Numbers of nuclei examined are indicated (*n*).

segregation occurred soon after PBE (experiment A, 0.31±0.39 hours, *n*=7; experiment B, 0.20±0.04 hours, *n*=3) (Fig. 9C-E; supplementary material Movie 1) (Kudo et al., 2006; McGuinness et al., 2009). By contrast, chromosomes in *TG Rec8-N-Myc* oocytes linger for about two hours around the oocyte-PB junction before eventually segregating in an asynchronous manner to oocytes and PBs (Fig. 9C; supplementary material Movie 1). The intervals from PBE to the completion of chromosome segregation were 3.15±0.86 hours (experiment A, *n*=4) and 1.81±0.84 hours (experiment B, *n*=13) (Fig. 9D,E). The difference between *TG Rec8-N-Myc* and control oocytes was highly significant (experiment A, P=0.00003; experiment B, P=0.006, Student's *t*-test). The interval between chromosome segregation and securin destruction, namely the point by which securin sinks to 5% of its maximum, was also significantly greater in *TG Rec8-N-Myc* oocytes than in controls (experiment B: control, 0.55±0.13 hours, *n*=3; *TG Rec8-N-Myc* oocytes, 2.45±1.04 hours, *n*=13; P=0.011, Student's *t*-test) (Fig. 9F,G). These results are consistent with the notion that Rec8-N-Myc is cleaved more slowly than wild-type protein in vivo and that this delays chiasma resolution. The fertility of *TG Rec8-N-Myc* oocytes suggests that abscission between the PB and the oocyte is delayed until chiasmata have been completely resolved.

Discussion

The recent finding that proteolytic activity of separase is essential for the resolution of chiasmata during meiosis I in mouse oocytes (Kudo et al., 2006) is consistent with the notion that they are resolved by cleavage of α-kleisin proteins, as is the case in yeast (Buonomo et al., 2000). To test this, we set out to identify separase cleavage sites in the mouse meiosis-specific α-kleisin Rec8 and then expressed at physiological levels a version (Rec8-N) that is poorly if at all cleaved in vitro. The BAC transgene expressing Rec8-N causes sterility in males, but not in females. Spermatocytes expressing Rec8-N reach metaphase I with bivalents containing a normal complement of chiasmata, but thereafter fail to produce secondary spermatocytes containing the normal complement of 20 dyad chromosomes or to produce haploid gametes. They instead produce cells with 80 chromatids, suggesting that Rec8-N blocks chromosome segregation at the first meiotic division and possibly also at the second. The lack of divisions does not appear to be due to a block of meiotic development because changes in the distribution of Sycp3 and kinetochore proteins normally associated with progression from meiosis I to II appear to take place in the presence of Rec8-N, despite the lack of nuclear division. These observations suggest that cleavage of Rec8 by separase is essential for the first and possibly also for the second meiotic division of mouse spermatocytes. By contrast, Rec8-N has only a modest adverse effect on the fertility of females, blocking neither oocyte divisions. Importantly, chromosome spreads indicate that Rec8-N does not block chiasma resolution in either males or females.

On their own, these results imply that Rec8 cleavage might not be necessary for chiasmata resolution. Might the yeast model therefore apply to mammals? Two key findings indicate otherwise. First, it is clear that in oocytes the amount of Rec8-N persisting on chromosomes after separase activation is far less than the amount of Rec8 persisting on chromosomes in oocytes lacking separase activity. The implication is that Rec8-N does not in fact abolish cleavage in vivo. Rec8 must possess additional separase cleavage sites that we have not been able to detect in vitro. Our detection of modest amounts of Rec8-N associated with post-meiosis I chromosomes suggests that mutation of the three sites cleaved by separase in vitro does indeed slow down cleavage in vivo; it does not abolish it. Second, despite the incomplete penetrance of the Rec8-N phenotype, this allele has nevertheless proved a useful reagent for evaluating the role of Rec8 cleavage. In oocytes, where it is possible to film cells undergoing the first meiotic division and thereby obtain kinetic data, we observed that the chiasma resolution occurs asynchronously and is delayed by about two hours following separase activation (as detected by destruction of securin-EGFP). Such data imply that chiasma resolution is normally mediated by Rec8 cleavage. The data do not address directly the mechanism by which chiasmata are eventually resolved in oocytes expressing Rec8-N, but the eventual disappearance of Rec8-N from chromosomes suggests that resolution also arises from cleavage, albeit slower than in wild-type oocytes.

We suggest that the asynchrony of chromosome segregation arises from differences between bivalents in the position of their chiasmata. Bivalents with chiasmata proximal to centromeres will be held together by more cohesin than those with more distal chiasmata and might therefore take longer to be resolved by an inefficient cleavage process. It seems likely that chiasma resolution is also slowed by Rec8-N in spermatocytes (though catching this on film will be a formidable undertaking) and we suggest that this, as opposed to some other unknown role for cohesin cleavage in cell division, is the underlying cause of their meiotic division defect.

According to the above scenario, the differential effects of Rec8-N on male and female gametogenesis (preventing it in males but not females) arises not so much from more rapid cleavage of Rec8-N in oocytes than spermatocytes but rather in the manner in which these two types of cells respond to delayed chiasmata resolution. It is remarkable that Rec8-N delays chromosome segregation by about two hours in oocytes without greatly affecting their inheritance of a complete set of dyads; that is, slower chiasma resolution leads neither to chromosome gain or loss. There are two explanations for this: either abscission of oocytes from the first PB normally does not take place for two or more hours after PBE, providing sufficient

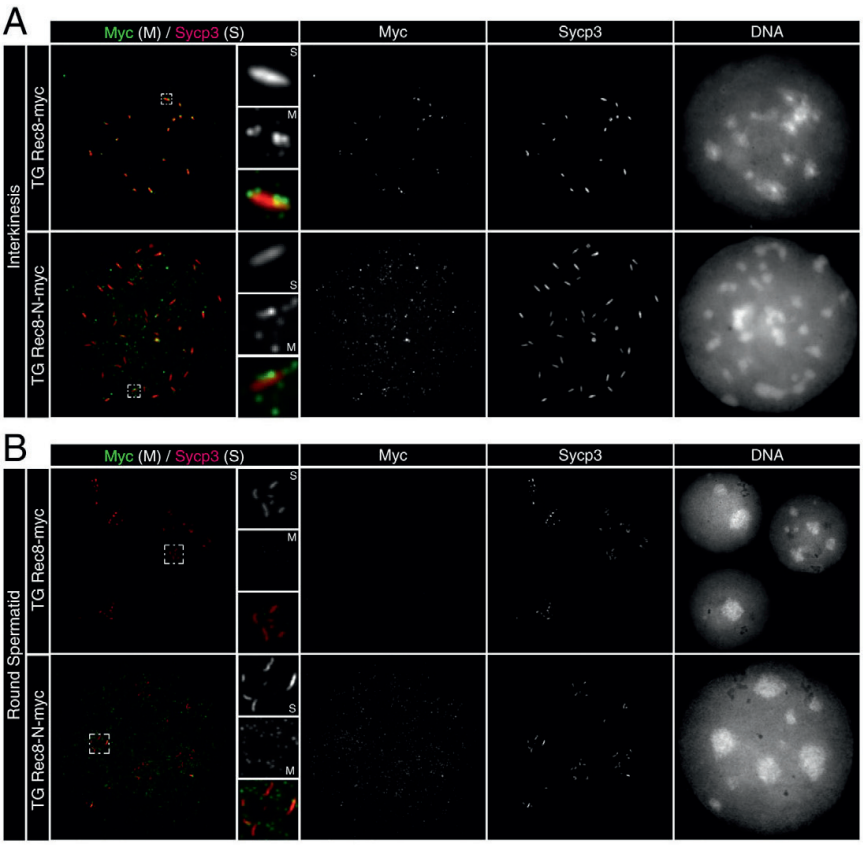

Fig. 8. Persistence of Rec8-N-Myc on chromatin after meiosis I and II. Immunofluorescence images of chromosome spreads stained with anti-Myc and anti-Sycp3 antibodies. (A) Interkinesis nuclei and representative areas in higher magnification that contain centromeric Rec8 foci are shown. (B) Spermatid nuclei and representative chromocenters in higher magnification that possess Sycp3 signals are shown.

time to segregate a complete set of dyads to both oocytes and PB; or the presence of unresolved bivalents in the cleavage furrow actively delays abscission, possibly by delaying inactivation of Aurora B (as recently found in HeLa cells), a process called the abscission checkpoint (Steigemann et al., 2009).

We suggest that a difference in the way that spermatocytes respond to the persistence of bivalents at the cleavage furrow is responsible for the male sterility caused by Rec8-N. It has been suggested that abscission in the presence of chromosome bridges induces furrow regression and formation of tetraploid cells in HeLa cells (Steigemann et al., 2009). Assuming that spermatocytes with delayed chiasma resolution proceed with furrow formation with normal kinetics (as clearly occurs in oocytes), they might then attempt abscission and then regress their furrows in response to the presence of chromatin or regress their furrows without even attempting abscission. Either response could account for the formation of cells with all 80 chromatids and the resulting sterility.

A key aspect of sister chromatid cohesion during meiosis is its persistence at centromeres after meiosis I. Recent work in yeast has shown that recruitment of phosphatase PP2A to centromeres by proteins of the Mei-S332 family is essential for the resistance of centromeric Rec8 to separase at meiosis I (Riedel et al., 2006). To explain this, it has been suggested that phosphorylation of cohesin or even of separase itself might be essential for Rec8 cleavage and that PP2A reverses such phosphorylation in the vicinity of centromeres. The finding that Rec8 but not Scc1 is subject to protection by Mei-S332–PP2A in vivo in yeast is most easily explained if Rec8 were crucial target of PP2A. Hyper-phosphorylation of yeast Rec8 at multiple serine and threonine residues during meiosis I has been reported, but their replacement by alanine appears to have little direct effect on the resolution of chiasmata (Brar et al., 2006). It is therefore still unclear whether Rec8 phosphorylation has a crucial role in promoting its cleavage by separase either in vivo or in vitro. Our finding that cleavage of mouse Rec8 by separase is completely dependent on Plk1 in vitro might be germane to this issue, particularly as Scc1 cleavage is far less dependent on Plk1 under the same conditions (Fig. 1). Plk1 is necessary for hyper-phosphorylation of Rec8 in yeast and has a role in promoting Scc1 cleavage during mitotic divisions (Alexandru et al., 2001; Clyne et al., 2003; Hornig and Uhlmann, 2004; Brar et al., 2006). Our in vitro cleavage data are consistent with the notion that Rec8 phosphorylation might indeed be essential for its cleavage and that PP2A protects sister chromatid cohesion at centromeres by de-phosphorylating Rec8.

In summary, our work suggests that chiasma resolution in mammals is mediated by Rec8 cleavage, as it is in yeast. Rec8 must therefore confer much of the sister chromatid cohesion (though we

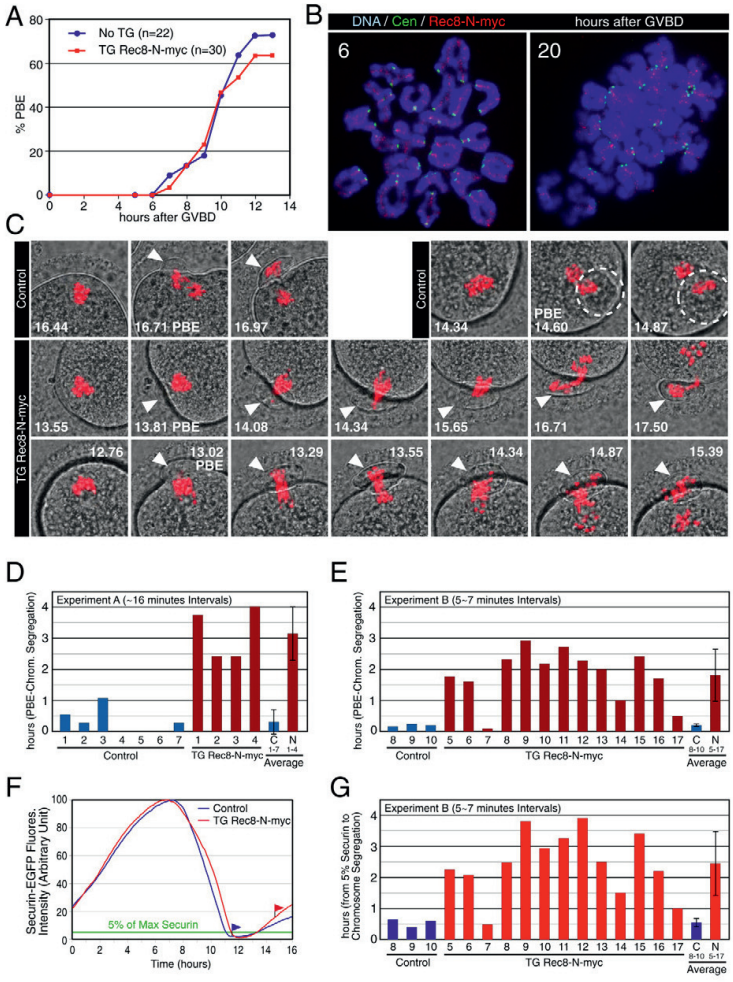

Fig. 9. Rec8-N delays but does not block chiasma resolution at meiosis I in oocytes. (A) Kinetics of the first polar body extrusion (PBE) of oocytes cultured in vitro. The numbers of oocytes examined are indicated (*n*). (B) Localization of Rec8-N-Myc on chromosomes in *TG Rec8-N-Myc* oocytes. Chromosome spreads prepared from oocytes in culture for the indicated time after germinal vesicle breakdown (GVBD) were stained with anti-Myc antibody (red), CREST antiserum (green) and DAPI (blue). (C) Live confocal microscopy of oocytes expressing H2B-mCherry. DIC images (gray) were merged with images of the mCherry channel (red). Frames at indicated time (hours after beginning of filming) were selected from the original time series (supplementary material Movie 1). PBs are indicated by arrowheads or circles (when extruded vertically). (D) Intervals from PBE to the completion of chromosome segregation analyzed by ~16-minute filming intervals (experiment A, supplementary material Movie 1). Error bar, s.d. (E) As in (D), analyzed by 5-7 minute intervals (experiment B, movies not shown). (F) Representative fluorescence quantifications of securin-EGFP signal in individual oocytes. The maximum value of the signal in each oocyte was set to 100 and relative intensity was plotted. Flags indicate time of the completion of chromosome segregation. Green line indicates the 5% level of the EGFP signal. (G) Intervals from 5% of the EGFP signal to the completion of chromosome segregation analyzed by 5-7 minute filming intervals (experiment B, movies not shown). Error bar, s.d.

cannot conclude all) that holds bivalents together. We propose that the chemistry of chiasma resolution is fundamentally the same in fungi and mammals and possibly universal amongst eukaryotes. Given that precocious loss of sister chromatid cohesion could have a role in the chromosome non-disjunction at meiosis I (Hodges et al., 2005), which gives rise to human aneuploidy, it is clearly important to understand better the mechanisms that confer and protect sister chromatid cohesion during meiosis. Further scrutiny of the relative roles of Rec8 and Scc1 in conferring meiotic sister chromatid cohesion as well as the role of their cleavage by separase will be essential for understanding the potential regulation of this process by Mei-S332 and PP2A.

Materials and Methods

In vitro Rec8 cleavage assay

cDNAs encoding mouse Rec8 (GenBank/EMBL/DDBJ accession number AF262055) and human Scc1-Myc (Hauf et al., 2001) were kindly provided by Michael McKay (Peter MacCallum Cancer Research Centre, Melbourne, Australia) and J.-M. Peters (Research Institute of Molecular Pathology, Vienna, Austria), respectively. [^{35}S]Methionine-labeled wild-type or mutant forms of Rec8 and Scc1-Myc proteins were produced using rabbit reticulocyte lysate-based in vitro coupled transcription-translation systems (Promega). The active (PM-2/4 which has S1126A and T1346A) and the inactive (C1129S) separase mutants were coexpressed in 293T cells with human securin, purified and activated as described (Stemmann et al., 2001). GST-human Plk1 was expressed in insect cells and purified as described (Sumara et al., 2002). A pre-incubation mixture composed of 2 µl reticulocyte lysate containing [^{35}S]methionine-labeled protein, 1 µl GST-Plk1 at 0.5 or 0.13 µg/µl and 6 µl cleavage buffer (20 mM HEPES/KOH pH 7.7, 100 mM KCl, 11 mM $MgCl_2$, 0.1 mM $CaCl_2$, 1 mM DTT, 1 mM ATP, 10 mM NaF, 0.5 µM microcystin-LR, 1 mM PMSF) was incubated at 37°C for 30 minutes. One microliter of active or inactive separase was added and the mixture was incubated for an additional 90 minutes at 37°C. The reactions were separated on gradient (8.5-15%) SDS-polyacrylamide gels and the radioactive signal was detected by the PhosphorImager system (Molecular Dynamics).

Mutagenesis and BAC modification

Site-directed mutagenesis of Rec8 cDNA was performed using the QuickChange kit (Stratagene). A BAC clone 546A10 encoding the Rec8 locus from the CT7 library (male CJ7/129SV genomic fragments on pBeloBAC11) was purchased from Invitrogen. Modification of BACs was performed as described (Yang et al., 1997). For each modification, a ~2 kb genomic fragment that works as ~1 kb homology arms for both sides was first cloned into pBluescript. For the Myc tagging construct, restriction sites were created at the termination codon and a nucleotide sequence encoding 9×Myc epitope (GEQKLISEEDLN) was inserted. For amino acid replacement, site-directed mutagenesis was performed using the QuickChange kit.

For conditional constructs, a loxP flanked transcription silencer cassette consisted of four polyA signal repeats and puroMycin-resistant gene provided by David Tuveson (Cancer Research UK Cambridge Research Institute, Cambridge, UK) (Tuveson et al., 2004), was inserted. After sequencing, the entire insert was cloned into pSV1.*RecA* and it was electroporated into bacteria harboring the BAC. Induction of homologous recombination and screening of the modified BAC clone was performed according to a previously described method (Yang et al., 1997). Modifications were confirmed by sequencing of the mutagenized regions and the integrity of the BACs was confirmed by restriction enzyme digestions. PCR primer sequences are available upon request.

Mouse strains and generation of transgenic mice

BAC DNA purified by CsCl-EtBr gradient centrifugation and prepared at 1 μg/ml was microinjected into pronuclei of *Mus musculus* B6CBAF2 zygotes. Transgenic founders confirmed by Southern blot and PCR analysis were bred to B6CBAF1 mice. Offspring that inherited the transgene through the germ line were further bred to B6CBAF1 mice, and 6- to 8-week-old mice were studied. For Southern blots, genomic DNA preparations were digested by *Stu* I, run on an agarose gel, transferred to a nylon membrane and hybridized with a ^{32}P-labeled 1089 bp *Stu* I genomic fragment encoding the C-terminus of Rec8.

Western blot and FACS analyses

For western blot analysis, a testicular cell suspension was made by physical disaggregation of seminiferous tubules with forceps in PBS and precipitated extracellular matrices were removed. Cells were collected by centrifugation, suspended in SDS-PAGE sample buffer and boiled. DNA was sheared by sonication and passed through a 27-gauge needle. Total extracts were run on a SDS-PAGE gel and transferred to a PVDF membrane. For detecting proteins, anti-Rec8 [RαN from rabbit (Eijpe et al., 2003)], anti-human c-*Myc* epitope [clone 4A6 from mouse (Upstate)] and anti-alpha-tubulin [clone YOL1/34 from rat (Serotec, Oxford, UK)] antibodies were used as primary antibodies, and appropriate secondary antibodies conjugated with HRP (GE Healthcare) were used. FACS analysis for the DNA content of testicular cells was performed by a method previously described (Malkov et al., 1998).

Histological analysis

Histological preparation of testes and staining for hematoxylin and eosine were as described (Peters et al., 2001). Testis cryosections were fixed by 4% PFA in PBS and stained by anti-Sycp3 antibody [clone 10G11 from mouse (Abcam, Cambridge, MA)] and anti-mouse IgG conjugated with Alexa Fluor 488 (Molecular Probes). DNA was counterstained with DAPI. Microscopic examination was performed as described (Kudo et al., 2006).

Preparation and examination of chromosome spreads

Chromosome spreads of testicular cells for immunofluorescence staining were prepared as described (Peters et al., 1997). Anti-human c-*Myc* epitope antibodies [clone 4A6 and CM-100 from rabbit (Gramsch, Schwabhausen, Germany)], anti-Sycp3 antibodies [clone 10G11 and Knuf from rabbit (Lammers et al., 1994)] and a CREST serum (gift of Arno Kromminga, IPM Biotech, Hamburg, Germany) were used as primary antibodies, and appropriate secondary antibodies conjugated with Alexa Fluor 488 or 568 (Molecular Probes) or Cy5 (Jackson ImmunoResearch) were used. DNA was counterstained with DAPI. Chromosome painting of spermatocyte spreads initially stained for Sycp3 was performed with biotin- and Cy3-labelled mouse X and Y chromosome painting probes (Cambio, Cambridge, UK), respectively. Sycp3 and Y chromosome were visualized by Alexa-Fluor-488 conjugated secondary antibody and Alexa-Fluor-633 conjugated streptavidin, respectively. The experimental procedure was described (Xu et al., 2005). Microscopic examination was performed as described (Kudo et al., 2006). Preparation and Giemsa staining of Metaphase spreads of testicular cells were as described (Peters et al., 2001).

Oocyte studies

Experiments involving oocytes were performed according to our methods described previously (Kudo et al., 2006; McGuinness et al., 2009). Germinal vesicle-stage oocytes were microinjected with mRNAs encoding histone H2B-mCherry and securin-EGFP in M2 media containing IBMX inhibitor. Transferring oocytes to the media without inhibitor after 1-2 hours triggered the meiotic maturation. Live confocal microscopy was performed using a Zeiss LSM510 META microscope equipped with C-Apochromat 40× 1.2 water objective (experiment A, supplementary material Movie 1) and Plan-Neofluor 20× 0.5 dry objective (experiment B). PeCon (Erbach, Germany) environmental microscope incubator was used to maintain 5% CO_2 atmosphere, temperature and humidity. Excitation wavelengths were 405, 488, 514 and 561 nm, and LP 420, BP 505-550, BP 530-600 and LP 575 filters were used for detection of Cascade-Blue dextran and EGFP and mCherry fluorescent proteins. During experiment A, AutofocusScreen macro [51] was used to track chromosomes labeled with H2B-mCherry. Five to seven (experiment A) or 20-25 (experiment B) z-stacks were captured every 16 minutes (experiment A) or 5-7 minutes (experiment B) for ~20 hours. Quantification of the signal was performed with ImageJ software (http://rsb.info.nih.gov/ij/). To measure securin-EGFP signal, individual frames were defined manually for each oocyte and values were normalized to the value measured at the time of GVBD.

We are grateful to Karin Wirth, Alexander Schleiffer, Marina Pasca di Magliano, Pawel Pasierbek and the IMP service and animal house staff for technical assistance, Jan-Michael Peters, Michael McKay, Nathaniel Heintz, David Tuveson and Arno Kromminga for materials, and Marc Kirschner for support. We also thank members of the Nasmyth laboratory for helpful discussion. The Research Institute of Molecular Pathology is funded by Boehringer Ingelheim. This work was partly supported by grants from the Austrian Science Fund (K.N. and N.R.K.), the European Community (contact number: QLG1-CT-2001-02026, shared costs action U2P2) (K.N. and N.R.K.), the Wellcome Trust (K.N.), the Japanese Society for the Promotion of Science and the Institute of Obstetrics & Gynaecology Trust (N.R.K.) and the Deutsche Krebshilfe (O.S.). Deposited in PMC for release after 6 months.

References

Alexandru, G., Uhlmann, F., Mechtler, K., Poupart, M. A. and Nasmyth, K. (2001). Phosphorylation of the cohesin subunit Scc1 by Polo/Cdc5 kinase regulates sister chromatid separation in yeast. *Cell* **105**, 459-472.

Bannister, L. A., Reinholdt, L. G., Munroe, R. J. and Schimenti, J. C. (2004). Positional cloning and characterization of mouse mei8, a disrupted allelle of the meiotic cohesin Rec8. *Genesis* **40**, 184-194.

Brar, G. A., Kiburz, B. M., Zhang, Y., Kim, J. E., White, F. and Amon, A. (2006). Rec8 phosphorylation and recombination promote the step-wise loss of cohesins in meiosis. *Nature* **441**, 532-536.

Buonomo, S. B., Clyne, R. K., Fuchs, J., Loidl, J., Uhlmann, F. and Nasmyth, K. (2000). Disjunction of homologous chromosomes in meiosis I depends on proteolytic cleavage of the meiotic cohesin Rec8 by separin. *Cell* **103**, 387-398.

Clyne, R. K., Katis, V. L., Jessop, L., Benjamin, K. R., Herskowitz, I., Lichten, M. and Nasmyth, K. (2003). Polo-like kinase Cdc5 promotes chiasmata formation and cosegregation of sister centromeres at meiosis I. *Nat. Cell Biol.* **5**, 480-485.

Eijpe, M., Offenberg, H., Jessberger, R., Revenkova, E. and Heyting, C. (2003). Meiotic cohesin REC8 marks the axial elements of rat synaptonemal complexes before cohesins SMC1beta and SMC3. *J. Cell Biol.* **160**, 657-670.

Gorr, I. H., Boos, D. and Stemmann, O. (2005). Mutual inhibition of separase and Cdk1 by two-step complex formation. *Mol. Cell* **19**, 135-141.

Hassold, T. and Hunt, P. (2001). To err (meiotically) is human: the genesis of human aneuploidy. *Nat. Rev. Genet.* **2**, 280-291.

Hauf, S., Waizenegger, I. C. and Peters, J. M. (2001). Cohesin cleavage by separase required for anaphase and cytokinesis in human cells. *Science* **293**, 1320-1323.

Hauf, S., Roitinger, E., Koch, B., Dittrich, C. M., Mechtler, K. and Peters, J. M. (2005). Dissociation of cohesin from chromosome arms and loss of arm cohesion during early mitosis depends on phosphorylation of SA2. *PLoS Biol.* **3**, e69.

Heidmann, D., Horn, S., Heidmann, S., Schleiffer, A., Nasmyth, K. and Lehner, C. F. (2004). The Drosophila meiotic kleisin C(2)M functions before the meiotic divisions. *Chromosoma* **113**, 177-187.

Herbert, M., Levasseur, M., Homer, H., Yallop, K., Murdoch, A. and McDougall, A. (2003). Homologue disjunction in mouse oocytes requires proteolysis of securin and cyclin B1. *Nat. Cell Biol.* **5**, 1023-1025.

Hodges, C. A., Revenkova, E., Jessberger, R., Hassold, T. J. and Hunt, P. A. (2005). SMC1beta-deficient female mice provide evidence that cohesins are a missing link in age-related nondisjunction. *Nat. Genet.* **37**, 1351-1355.

Hornig, N. C. and Uhlmann, F. (2004). Preferential cleavage of chromatin-bound cohesin after targeted phosphorylation by Polo-like kinase. *EMBO J.* **23**, 3144-3153.

Kitajima, T. S., Miyazaki, Y., Yamamoto, M. and Watanabe, Y. (2003). Rec8 cleavage by separase is required for meiotic nuclear divisions in fission yeast. *EMBO J.* **22**, 5643-5653.

Kitajima, T. S., Hauf, S., Ohsugi, M., Yamamoto, T. and Watanabe, Y. (2005). Human Bub1 defines the persistent cohesion site along the mitotic chromosome by affecting Shugoshin localization. *Curr. Biol.* **15**, 353-359.

Klein, F., Mahr, P., Galova, M., Buonomo, S. B., Michaelis, C., Nairz, K. and Nasmyth, K. (1999). A central role for cohesins in sister chromatid cohesion, formation of axial elements, and recombination during yeast meiosis. *Cell* **98**, 91-103.

Kudo, N. R., Wassmann, K., Anger, M., Schuh, M., Wirth, K. G., Xu, H., Helmhart, W., Kudo, H., McKay, M., Maro, B. et al. (2006). Resolution of chiasmata in oocytes requires separase-mediated proteolysis. *Cell* **126**, 135-146.

Lammers, J. H., Offenberg, H. H., van Aalderen, M., Vink, A. C., Dietrich, A. J. and Heyting, C. (1994). The gene encoding a major component of the lateral elements of synaptonemal complexes of the rat is related to X-linked lymphocyte-regulated genes. *Mol. Cell. Biol.* **14**, 1137-1146.

Lee, J., Iwai, T., Yokota, T. and Yamashita, M. (2003). Temporally and spatially selective loss of Rec8 protein from meiotic chromosomes during mammalian meiosis. *J. Cell Sci.* **116**, 2781-2790.

Malkov, M., Fisher, Y. and Don, J. (1998). Developmental schedule of the postnatal rat testis determined by flow cytometry. *Biol. Reprod.* **59**, 84-92.

McGuinness, B. E., Hirota, T., Kudo, N. R., Peters, J. M. and Nasmyth, K. (2005). Shugoshin prevents dissociation of cohesin from centromeres during mitosis in vertebrate cells. *PLoS Biol.* **3**, e86.

McGuinness, B. E., Anger, M., Kouznetsova, A., Gil-Bernabe, A. M., Helmhart, W., Kudo, N. R., Wuensche, A., Taylor, S., Hoog, C., Novak, B. et al. (2009). Regulation of APC/C activity in oocytes by a Bub1-dependent spindle assembly checkpoint. *Curr. Biol.* **19**, 369-380.

Nasmyth, K. (2005). How might cohesin hold sister chromatids together? *Philos. Trans. R. Soc. Lond. B Biol. Sci.* **360**, 483-496.

Nicklas, R. B. (1997). How cells get the right chromosomes. *Science* **275**, 632-637.

Peter, M., Castro, A., Lorca, T., Le Peuch, C., Magnaghi-Jaulin, L., Doree, M. and Labbe, J. C. (2001). The APC is dispensable for first meiotic anaphase in Xenopus oocytes. *Nat. Cell Biol.* **3**, 83-87.

Peters, A. H., Plug, A. W., van Vugt, M. J. and de Boer, P. (1997). A drying-down technique for the spreading of mammalian meiocytes from the male and female germline. *Chromosome Res.* **5**, 66-68.

Peters, A. H., O'Carroll, D., Scherthan, H., Mechtler, K., Sauer, S., Schofer, C., Weipoltshammer, K., Pagani, M., Lachner, M., Kohlmaier, A. et al. (2001). Loss of the Suv39h histone methyltransferases impairs mammalian heterochromatin and genome stability. *Cell* **107**, 323-337.

Petronczki, M., Siomos, M. F. and Nasmyth, K. (2003). Un menage a quatre: the molecular biology of chromosome segregation in meiosis. *Cell* **112**, 423-440.

Revenkova, E., Eijpe, M., Heyting, C., Hodges, C. A., Hunt, P. A., Liebe, B., Scherthan, H. and Jessberger, R. (2004). Cohesin SMC1 beta is required for meiotic chromosome dynamics, sister chromatid cohesion and DNA recombination. *Nat. Cell Biol.* **6**, 555-562.

Riedel, C. G., Katis, V. L., Katou, Y., Mori, S., Itoh, T., Helmhart, W., Galova, M., Petronczki, M., Gregan, J., Cetin, B. et al. (2006). Protein phosphatase 2A protects centromeric sister chromatid cohesion during meiosis I. *Nature* **441**, 53-61.

Russell, L. D., Ettlin, R. A., Sinha Hikim, A. P. and Clegg, E. D. (1990). Histological and histopathological evaluation of the testis. Clearwater, FL: Cache River Press.

Steigemann, P., Wurzenberger, C., Schmitz, M. H., Held, M., Guizetti, J., Maar, S. and Gerlich, D. W. (2009). Aurora B-mediated abscission checkpoint protects against tetraploidization. *Cell* **136**, 473-484.

Stemmann, O., Zou, H., Gerber, S. A., Gygi, S. P. and Kirschner, M. W. (2001). Dual inhibition of sister chromatid separation at metaphase. *Cell* **107**, 715-726.

Sullivan, M., Lehane, C. and Uhlmann, F. (2001). Orchestrating anaphase and mitotic exit: separase cleavage and localization of Slk19. *Nat. Cell Biol.* **3**, 771-777.

Sullivan, M., Hornig, N. C., Porstmann, T. and Uhlmann, F. (2004). Studies on substrate recognition by the budding yeast separase. *J. Biol. Chem.* **279**, 1191-1196.

Sumara, I., Vorlaufer, E., Stukenberg, P. T., Kelm, O., Redemann, N., Nigg, E. A. and Peters, J. M. (2002). The dissociation of cohesin from chromosomes in prophase is regulated by Polo-like kinase. *Mol. Cell* **9**, 515-525.

Taieb, F. E., Gross, S. D., Lewellyn, A. L. and Maller, J. L. (2001). Activation of the anaphase-promoting complex and degradation of cyclin B is not required for progression from Meiosis I to II in Xenopus oocytes. *Curr. Biol.* **11**, 508-513.

Tanaka, T. U., Stark, M. J. and Tanaka, K. (2005). Kinetochore capture and bi-orientation on the mitotic spindle. *Nat. Rev. Mol. Cell Biol.* **6**, 929-942.

Terret, M. E., Wassmann, K., Waizenegger, I., Maro, B., Peters, J. M. and Verlhac, M. H. (2003). The meiosis I-to-meiosis II transition in mouse oocytes requires separase activity. *Curr. Biol.* **13**, 1797-1802.

Tomonaga, T., Nagao, K., Kawasaki, Y., Furuya, K., Murakami, A., Morishita, J., Yuasa, T., Sutani, T., Kearsey, S. E., Uhlmann, F. et al. (2000). Characterization of fission yeast cohesin: essential anaphase proteolysis of Rad21 phosphorylated in the S phase. *Genes Dev.* **14**, 2757-2770.

Toth, A., Rabitsch, K. P., Galova, M., Schleiffer, A., Buonomo, S. B. and Nasmyth, K. (2000). Functional genomics identifies monopolin: a kinetochore protein required for segregation of homologs during meiosis I. *Cell* **103**, 1155-1168.

Tuveson, D. A., Shaw, A. T., Willis, N. A., Silver, D. P., Jackson, E. L., Chang, S., Mercer, K. L., Grochow, R., Hock, H., Crowley, D. et al. (2004). Endogenous oncogenic K-ras(G12D) stimulates proliferation and widespread neoplastic and developmental defects. *Cancer Cell* **5**, 375-387.

Uhlmann, F., Lottspeich, F. and Nasmyth, K. (1999). Sister-chromatid separation at anaphase onset is promoted by cleavage of the cohesin subunit Scc1. *Nature* **400**, 37-42.

Uhlmann, F., Wernic, D., Poupart, M. A., Koonin, E. V. and Nasmyth, K. (2000). Cleavage of cohesin by the CD clan protease separin triggers anaphase in yeast. *Cell* **103**, 375-386.

Waizenegger, I., Gimenez-Abian, J. F., Wernic, D. and Peters, J. M. (2002). Regulation of human separase by securin binding and autocleavage. *Curr. Biol.* **12**, 1368-1378.

Waizenegger, I. C., Hauf, S., Meinke, A. and Peters, J. M. (2000). Two distinct pathways remove mammalian cohesin from chromosome arms in prophase and from centromeres in anaphase. *Cell* **103**, 399-410.

Xu, H., Beasley, M. D., Warren, W. D., van der Horst, G. T. and McKay, M. J. (2005). Absence of mouse REC8 cohesin promotes synapsis of sister chromatids in meiosis. *Dev. Cell* **8**, 949-961.

Yanagida, M. (2005). Basic mechanism of eukaryotic chromosome segregation. *Philos. Trans. R. Soc. Lond. B Biol. Sci.* **360**, 609-621.

Yang, X. W., Model, P. and Heintz, N. (1997). Homologous recombination based modification in Escherichia coli and germline transmission in transgenic mice of a bacterial artificial chromosome. *Nat. Biotechnol.* **15**, 859-865.

Zou, H., Stemman, O., Anderson, J. S., Mann, M. and Kirschner, M. W. (2002). Anaphase specific auto-cleavage of separase. *FEBS Lett.* **528**, 246-250.

Xu Z, Cetin B, Anger M, Cho US, Helmhart W, Nasmyth K, et al. Structure and function of the PP2A-shugoshin interaction. Mol Cell. 2009;35: 426–441.

Impact Factor/Quartile: 14.902/Q2
Times cited (Wos May 2019): 116
Significance: The first mapping of reaction interface between Sgo I and PP2A
Contribution of the author: Microinjection experiments, testing mutants of both molecules in oocyte system

Molecular Cell
Article

Structure and Function of the PP2A-Shugoshin Interaction

Zheng Xu,[1,3] Bulent Cetin,[2,3] Martin Anger,[2,4,5] Uhn Soo Cho,[1,6] Wolfgang Helmhart,[2] Kim Nasmyth,[2,*] and Wenqing Xu[1,*]
[1]Department of Biological Structure, University of Washington, Seattle, WA 98195, USA
[2]Department of Biochemistry, University of Oxford, Oxford OX1 3QU, UK
[3]These authors contributed equally to this work
[4]Present address: Institute of Animal Physiology and Genetics, Libechov 277 21, Czech Republic
[5]Present address: Veterinary Research Institute, Brno 621 00, Czech Republic
[6]Present address: BCMP, Harvard Medical School, Boston, MA 02115, USA
*Correspondence: kim.nasmyth@bioch.ox.ac.uk (K.N.), wxu@u.washington.edu (W.X.)
DOI 10.1016/j.molcel.2009.06.031

SUMMARY

Accurate chromosome segregation during mitosis and meiosis depends on shugoshin proteins that prevent precocious dissociation of cohesin from centromeres. Shugoshins associate with PP2A, which is thought to dephosphorylate cohesin and thereby prevent cleavage by separase during meiosis I. A crystal structure of a complex between a fragment of human Sgo1 and an AB′C PP2A holoenzyme reveals that Sgo1 forms a homodimeric parallel coiled coil that docks simultaneously onto PP2A's C and B′ subunits. Sgo1 homodimerization is a prerequisite for PP2A binding. While hSgo1 interacts only with the AB′C holoenzymes, its relative, Sgo2, interacts with all PP2A forms and may thus lead to dephosphorylation of distinct substrates. Mutant shugoshin proteins defective in the binding of PP2A cannot protect centromeric cohesin from separase during meiosis I or support the spindle assembly checkpoint in yeast. Finally, we provide evidence that PP2A's recruitment to chromosomes may be sufficient to protect cohesin from separase in mammalian oocytes.

INTRODUCTION

The chromatids of bivalent chromosomes, like their mitotic counterparts, are held together by a multisubunit complex called cohesin, whose α-kleisin (Rec8), Smc1, and Smc3 subunits form a tripartite ring within which sister DNAs are thought to be trapped (Haering et al., 2008; Nasmyth and Haering, 2005). The first meiotic division is triggered by destruction of sister chromatid cohesion by a thiol protease called separase, which opens the cohesin ring by cleaving its α-kleisin subunit (Buonomo et al., 2000). This splits the bivalent into a pair of dyad chromosomes that are segregated to opposite poles at the first meiotic division. Crucially, the two chromatids of each dyad remain associated with each other both during and after anaphase I, because cohesin holding sister centromeres together is protected from cleavage by separase by a class of proteins called shugoshins (Goldstein, 1980; Kerrebrock et al., 1995; Kitajima et al., 2004; Rabitsch et al., 2004). The persistence of centromeric cohesion is essential to ensure that sister kinetochores and hence individual chromatids are pulled to opposite poles at the second meiotic division. A failure to protect centromeric cohesin from separase might contribute to the human aneuploidy caused by chromosome missegregation during meiosis I in oocytes, especially in older women (Vogt et al., 2008).

How do shugoshins protect sister chromatid cohesion at centromeres? Recent work indicates that shugoshins protect centromeric cohesin by interacting with protein phosphatase 2A (PP2A) (Kitajima et al., 2006; Riedel et al., 2006). PP2A holoenzymes are composed of a catalytic C subunit, a structural or scaffold A subunit, and a regulatory B subunit. The A and C subunits bind directly to each other, forming a core enzyme. The B subunits, in contrast, are much more varied, and mammals possess at least 18 types, which belong to four subfamilies: PR55/B, PR61/B′, PR72/B″, and PR110/B‴ (Janssens and Goris, 2001; Lechward et al., 2001; Sontag, 2001; Yu, 2007). During meiosis in both fission and budding yeast, a shugoshin, namely Sgo1, is found stably associated with AB′C PP2A holoenzyme (Riedel et al., 2006). This led to the suggestion that phosphorylation of cohesin's Rec8 subunit may be required for its cleavage by separase (Brar et al., 2006; Riedel et al., 2006), as is at least partly the case for its Scc1 mitotic counterpart (Alexandru et al., 2001), and that by recruiting PP2A, Sgo1 prevents cleavage of centromeric Rec8 by inducing its dephosphorylation. Consistent with this hypothesis, yeast mutants lacking PP2A's B′ subunits fail to prevent Rec8's removal from centromeres at the first meiotic division, which is accompanied by their precocious disjunction soon after the first meiotic division (Riedel et al., 2006).

However, inactivation of PP2A causes highly pleiotropic phenotypes, because the enzyme has a wide variety of functions and substrates, and the effect on chromosome segregation of mutating PP2A could conceivably be due to indirect effects. To address whether recruitment of PP2A really is a crucial part of the mechanism by which shugoshins protect centromeric cohesin, it is necessary to understand how PP2A actually binds to shugoshin and to use this information to investigate the phenotype of mutant proteins that are defective in their ability to bind

the phosphatase. This sort of approach is equally important for disentangling the role of PP2A-shugoshin interactions during mitotic chromosome segregation in mammals, where hSgo1 has a crucial role in preventing dissociation of cohesin from centromeres (Kitajima et al., 2005; McGuinness et al., 2005; Salic et al., 2004), and it is unclear whether Sgo1's role is to recruit PP2A to centromeres or the converse (Kitajima et al., 2006; Tang et al., 2006).

PP2A binds to an hSgo1 fragment containing its N-terminal 176 amino acids, and the interaction is abolished by mutation of a highly conserved asparagine (N61I) within a region predicted to form a coiled coil (Tang et al., 1998, 2006). The N61I mutation abolishes persistence of sister centromere cohesion during meiosis in *Drosophila* (Kerrebrock et al., 1995), but it might have rather pleiotropic consequences, as it supposedly also affects the ability of hSgo1/ MEI-S332 to bind chromosomes (Tang et al., 1998, 2006) and possibly disrupts Sgo1's putative coiled coil.

A crystal structure of a complex formed between a fragment of hSgo1 and an AαB56γCα PP2A holoenzyme (from now on referred to as AB′C PP2A or PP2A) reveals that Sgo1 forms a parallel coiled coil whose N- and C-terminal ends bind to C and B′ PP2A subunits, respectively. Analysis of phenotypes of shugoshin mutants defective in PP2A binding demonstrates that recruitment of PP2A by Sgo1 is essential for the protection of sister chromatid cohesion at centromeres at meiosis I and for the spindle assembly checkpoint (SAC) during mitosis in yeast and that recruitment of PP2A to chromosome arms may be sufficient to block the resolution of chiasmata in mouse oocytes. Another important implication of our findings is that PP2A's specificity is not determined solely by its regulatory B subunits.

RESULTS

Shugoshin's Putative Coiled Coil Is Responsible for PP2A Binding

Recombinant hSgo1 fragments containing hSgo1's N-terminal 176 residues (Figure 1A) aggregate, but MBP-Sgo1 fusion proteins are soluble and interact with PP2A. Binding studies with a variety of MBP-Sgo1 fusion proteins reveal that the putative coiled coil (residues 47–105) confers interaction with AB′C PP2A holoenzyme (Figure 1B). A slightly shorter fragment (51–96) also confers binding, but with much lower affinity (Figures 1B and S1).

Two Shugoshin Molecules Interact with a Single PP2A Holoenzyme in Solution

Because the coiled-coil region is predicted to form a homodimer, we determined the molecular stoichiometry of the PP2A-Sgo1 complex. Both size-exclusion chromatography and dynamic light scattering indicate that the complex formed between PP2A and MBP-Sgo1(51–105) has a molecular weight of ~250 kDa, while that formed with Sgo1(51–105) after MBP had been removed by cleavage has a molecular weight of ~148–160 kDa (Figures 1C and S1). Because the molecular weights of the AB′C PP2A holoenzyme, Sgo1(51–105), and MBP are 146 kDa, 6 kDa, and 45 kDa, respectively, the molecular stoichiometry of the PP2A-Sgo1 complex in solution is likely 1:2. This molar ratio is consistent with MBP-Sgo1 bands having twice the intensity of PP2A subunits with an equivalent molecular weight in Coomassie blue-stained SDS gels of purified PP2A-Sgo1 complexes purified using either the GST tag on the PP2A A subunit or the MBP moiety of MBP-Sgo1 and/or by gel filtration (Figures 1B, 1D, 1E, and S1A). To show that there is only a single PP2A holoenzyme in the complex, we incubated GST-tagged PP2A A subunit (GST-A) with excessive untagged A, B, and C subunits and MBP-Sgo1. If there were two or more PP2A holoenzymes, then GST-A should pull down untagged PP2A A subunits, which we do not observe (Figure 1D). The complexes contain at least two Sgo1 molecules, because after mixing Sgo1 fragments with different lengths and tags (one was fused to MBP and the other to MBP and a FLAG epitope), addition of PP2A holoenzyme enabled FLAG affinity beads to pull down both MBP-Sgo1 proteins (Figure 1E). Dimerization of Sgo1 fragments within PP2A complexes is not caused by their fusion to MBP, because copurification occurs even when the latter is removed (Figure 1F, Supplemental Data).

Crystal Structure of the PP2A-Sgo1 Complex: Overall Architecture

We failed to obtain useful crystals with complexes containing Sgo1(51–105) or longer fragments, but eventually obtained a crystal structure with Sgo1(51–96), which lacks a complete coiled-coil region (Figures S1B and S1C). Despite not forming stable homodimers in solution (data not shown), MBP-Sgo1(51–96) does pull down PP2A holoenzyme (Figure 1B), though the complex dissociates partially during gel filtration, producing a peak fraction containing a mixture of the PP2A-Sgo1 complex and unbound PP2A holoenzyme (Figures S1B and S1C). It is this mixture that forms useful crystals, presumably because "free" PP2A holoenzymes shield the hydrophobic surface of Sgo1's coiled coil not covered by the binding of the first PP2A holoenzyme (see below).

The crystal structure was determined at 2.7 Å resolution (Table 1). Each asymmetric unit within the crystal lattice contains one human PP2A AB′C holoenzyme, one Sgo1(51–96) peptide, and one microcystin PP2A inhibitor molecule. The Sgo1(51–96) peptide forms a single long helix. Two Sgo1 peptides, related by a two-fold crystallographic symmetry, form a parallel coiled-coil homodimer and interact with both B and C subunits of two PP2A holoenzymes (Figure S2). In this way, two symmetry-related PP2A holoenzymes interact with symmetrical surfaces of the Sgo1 coiled-coil dimer. Because only a single PP2A holoenzyme interacts with the Sgo1 dimer in solution, the two surfaces of the Sgo1 coiled-coil homodimer must be slightly different, though this is not apparent in the crystal structure. We imagine that the two surfaces of Sgo1's coiled coil have different affinities for PP2A, with the lower affinity surface binding PP2A only under crystallization conditions, when protein concentrations are much higher. Structure-based mutagenesis (see below) confirmed that the PP2A-Sgo1 interface observed in our crystal structure is physiologically relevant. For the rest of this work, we will discuss the interaction of one PP2A AB′C complex with two Sgo1(51–96) peptides and, for simplicity, refer to them as Sgo1a and Sgo1b, respectively (Figure 2).

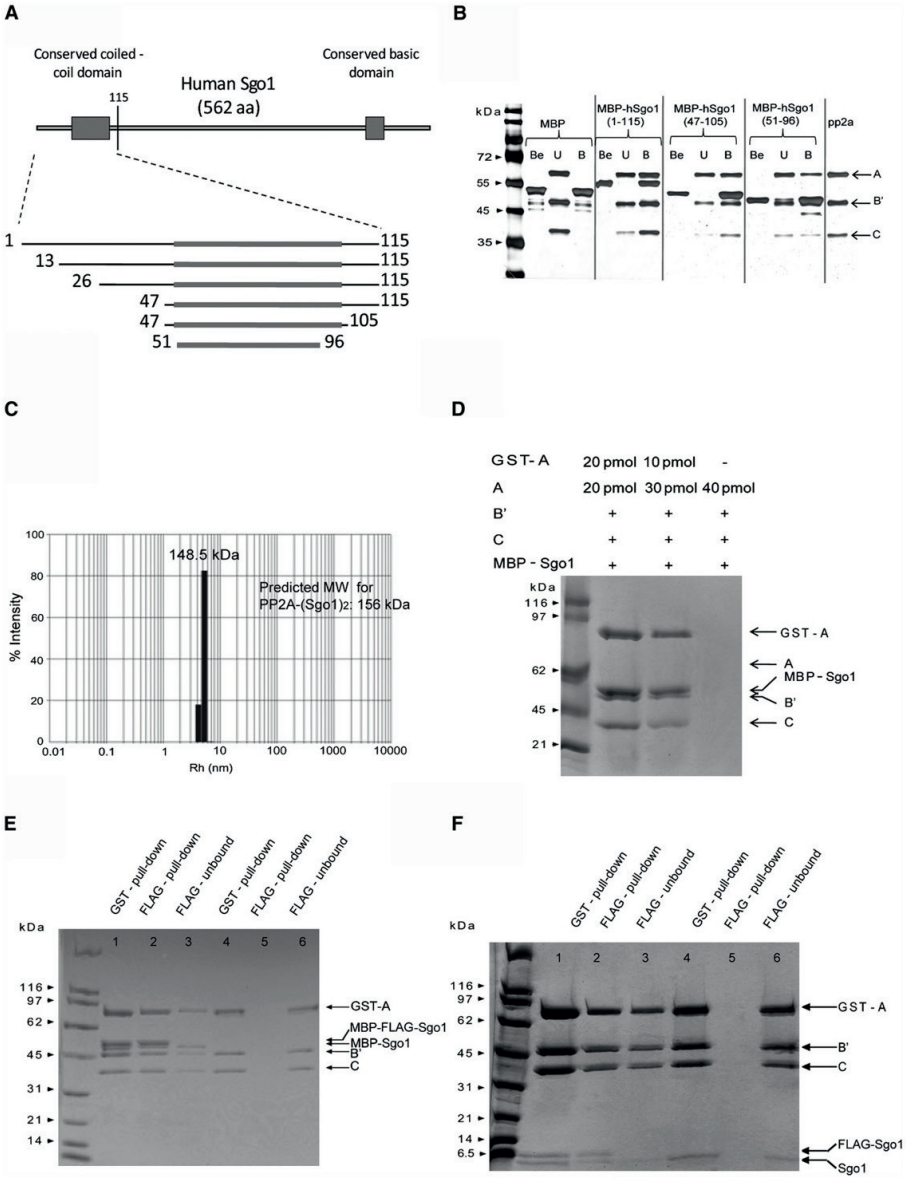

Figure 1. One AB′C PP2A Holoenzyme Binds with Two Sgo1 Molecules in the Solution

(A) Domain structure of Sgo1. MBP fusions of the indicated fragments tested positive for binding to AB′C PP2A (data not shown except in B).

(B) The coiled-coil domain of Sgo1 is sufficient for binding to AB′C PP2A holoenzyme. Purified AB′C PP2A holoenzyme was pulled down by corresponding MBP-Sgo1 fragments. The SDS-PAGE gel was silver stained. Be, U, and B represent the MBP-Sgo1 sample before PP2A binding, unbound PP2A, and total proteins bound to the amyloid beads, respectively.

(C) Size distribution of the PP2A-Sgo1(51–105) complex measured by dynamic light scattering.

(D) There is one PP2A holoenzyme in each PP2A-Sgo1 complex. Indicated amounts of GST-A and A subunits were incubated with MBP-Sgo1(51–105), as well as the B′ and C subunits of PP2A, prior to GST affinity pull-down. Bead-bound proteins were eluted in a buffer containing glutathione and resolved on an SDS-PAGE gel.

Table 1. Statistics of Crystallographic Analysis of the PP2A-Sgo1 Complex

Data collection	
Space group	C2221
Cell dimensions: a, b, c (Å)	104.94, 145.86, 294.15
Resolution (Å)	50.0–2.7 (2.8–2.7)
[a]Rsym	0.135 (0.494)
I/σI	12.2 (1.6)
Completeness (%)	92.0 (51.3)
Redundancy	6.2 (2.8)
Refinement	
Resolution (Å)	50.0–2.7
No. reflections	54,842
[b]Rwork/Rfree	22.6%/27.7%
No. atoms	
Proteins	10,802
Ions	2
B factor	
Proteins	47.5
Ions	37.2
Rmsd	
Bond lengths (Å)	0.011
Bond angles (°)	1.52
[c]Ramachandran plot (core, disallowed, %)	91.5%, 0%

Values in the parentheses refer to the outer-shell bin.
[a] Rsym = $\Sigma_i||(I_i(j) - I(j)|/\Sigma_i I_i(j)$, where $I_i(j)$ is the intensity of the i–th observation of reflection j. I(j) is the weighted mean of all measurements of j.
[b] $R = \Sigma_i||F_{obs}(j)| - |F_{calc}(j)||/\Sigma_i|F_{obs}(j)|$. R_{work} and R_{free} were calculated with the working and test reflection sets, respectively.
[c] As defined in PROCHECK.

The structure of PP2A holoenzyme in the complex is similar to the lower-resolution structures containing PP2A alone (Cho and Xu, 2007; Xu et al., 2006). Briefly, the 15 HEAT repeats of the A subunit form a horseshoe-shaped scaffold that holds B and C subunits using the ridge formed by intrarepeat loops. The only significant structural difference concerns the C-terminal region of the B′ subunit's conserved domain, which was mostly invisible in previous PP2A structures. It forms a long helix and interacts with the A subunit's most N-terminal HEAT repeat. This suggests that the divergent C-terminal domain of B′ subunits resides "below" or inside the horseshoe scaffold and has a role in PP2A localization (Figure S3).

Both Sgo1a and Sgo1b interact with both B′ and C subunits of PP2A. The N- and C-terminal ends of Sgo1's coiled coil form discrete interfaces with C and B′ subunits, respectively. Each binding interface contains a hydrophobic core as well as peripheral hydrogen bonds and salt bridges. The contact area between the C subunit and the N-terminal half of the Sgo1 homodimer (1328 Å^2) is larger than that between the B′ subunit and its C-terminal half (1046 Å^2). Several highly conserved hydrophobic Sgo1 residues (L64, L68, V75, I81, I82, L85, and L92) as well as two other residues (L53 and L54) found in Sgo1 but not Sgo2 appear to stabilize the Sgo1a-Sgo1b dimerization (Figure S4).

The PP2A-Sgo1 Interface: Hydrophobic Interactions Buttressed by Hydrophilic Interactions

The N-terminal region of Sgo1's coiled coil interacts directly with residues in two loops (between α9 and α10 and between β6 and α8) of the PP2A C subunit. Hydrophobic interactions involve Sgo1a's L64 and Sgo1b's L68, which stack on each other and are surrounded by the aliphatic parts of P172, W209, I211, and Y218 of the C subunit (Figure 3A). Hydrogen bonds involve Y57 and N60 from Sgo1a and E69 and K62 from Sgo1b (Figures 3A, 3C, and S5). The hydroxyl group of the conserved Sgo1a Y57 side chain interacts with the carbonyl of G207 on the longer of the two loops and D223 on α10. The side chain of Sgo1a's conserved N60 is nestled in a surface groove and forms multiple hydrogen bonds with C subunit residues 206–209. Oδ from N60 forms a hydrogen bond with Nε and Nη of R206, while Nδ of N60 interacts with the carbonyls of R206 and W209. On Sgo1b, Nζ of K62 forms a hydrogen bond with the carbonyl of P172 and a salt bridge with D175, residues situated on the shorter loop. In addition, Sgo1b E69 docks into a surface groove and thereby interacts with the main-chain amide nitrogen of G193 and with Oη of Y218, which is also on the longer loop. Surprisingly, Sgo1 residue N61, previously found to be critical for interaction with PP2A, does not participate directly in the PP2A-Sgo1 interface. N61 residues from Sgo1a and Sgo1b instead form a pair of strong hydrogen bonds (2.48 Å) in the middle of the coiled-coil interface (Figure S4).

The PP2A holoenzyme contains 1 of 4 types of B subunit (PR55/B, PR61/B′, PR72/B″, and PR110/B‴). Importantly, only PR61/B′ was found associated with Sgo1 from meiotic yeast cells (Riedel et al., 2006) or mitotic mammalian cells (Kitajima et al., 2006; Riedel et al., 2006). The crystal structure reveals that the C-terminal end of Sgo1's coiled-coil region (residues 80–94) interacts with the last pseudo HEAT repeat of the conserved domain of PP2A's B′ subunit (Figures 3B, 3C, and S5). The hydrophobic parts of the side chains from Sgo1b's L83, K87, Y90, and C94 interact with Y365, H377, Y381, L384, and M388 on the last pair of pseudo-HEAT repeats of PP2A's B′ subunit. This interaction is strengthened by two salt bridges between K374 and K385, which are conserved within the B′ subfamily, and Sgo1b's D80 and Sgo1a's E88, respectively. Structural superposition of the AB′C-Sgo1 complex and the ABC family PP2A holoenzyme (Xu et al., 2008) indicates that Sgo1 cannot interact with both the C subunit and the PP2A B subunit, which explains why Sgo1 does not interact with the ABC family PP2A holoenzymes (Figure S6).

(E and F) There are at least two Sgo1 molecules in each PP2A-Sgo1 complex. MBP-Sgo1(51–105) was incubated either with equal amounts of (lanes 1, 2, and 3) or without (lanes 4, 5, and 6) MBP-FLAG-Sgo1(51–105) and with PP2A GST-A, -B′, and -C subunits prior to GST affinity pull-down. Bead-bound proteins were eluted in a buffer containing glutathione. Eluted proteins were incubated with FLAG affinity beads before elution in a buffer containing FLAG peptide. Eluates and unbound fractions were resolved on an SDS-PAGE gel (E). This experiment was repeated using Sgo1(51–105) and FLAG-Sgo1(51–105) peptides instead of MBP fusions of these peptides (F).

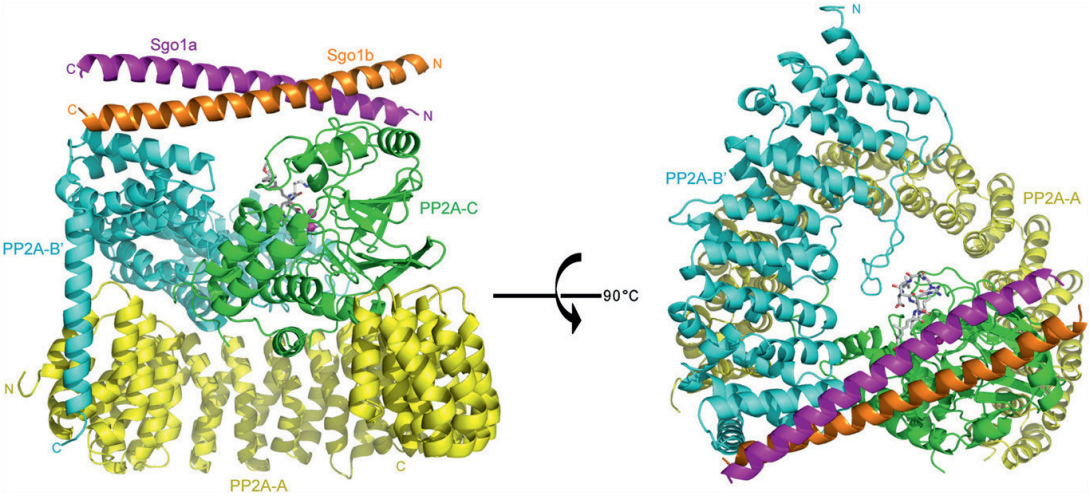

Figure 2. Overall Structure of PP2A-Sgo1 Complex

A, B′, and C subunits of PP2A, Sgo1a, and Sgo1b are shown and labeled in yellow, cyan, green, orange, and purple, respectively. The PP2A inhibitor microcystеine is represented by stick mode, and two manganese atoms binding with PP2A are shown in pink and sphere mode. The orthogonal view of PP2A-Sgo1 complex is shown on the right. All structural images were prepared using the PyMOL Molecular Graphics System (DeLano Scientific; Palo Alto, CA).

The Effect of Mutations on PP2A Binding and Sgo1 Dimerization

To assess the contribution of key residues to Sgo1 dimerization and its interaction with PP2A, we measured the effects of mutating them, mainly to alanine. Substitution of Sgo1's N61 by either alanine or isoleucine, which causes precocious loss of sister centromere cohesion in *Drosophila* (Tang et al., 1998), abolishes binding to PP2A (Figure 3D and data not shown). Substitutions at L64 and L68, which participate in dimer formation as well as hydrophobic interactions with PP2A's C subunit, have a similar effect. L64A reduces PP2A binding while L68A abolishes it (Figure 3D). Substitution by alanine of a conserved leucine within the Sgo1 dimer interface (L85) has a moderate effect. Mutations of individual residues specifically involved in PP2A binding, including Y57A, N60A, and K62A, have little effect on PP2A binding, though Y57A causes a modest reduction. In contrast, several double substitutions, namely Y57A/N60A, Y57A/E69A, and N60A/K62A, greatly reduce PP2A binding under our experimental conditions (Figure 3D).

To test the effects on Sgo1 dimerization, we purified mutant proteins with or without a FLAG tag. To distinguish them in SDS-PAGE gels, the tagged and untagged proteins contained different amounts of Sgo1 sequence, namely 47–105 and 51–105, respectively. Equal amounts of tagged and untagged proteins containing the same mutation were mixed, the tagged protein was pulled down using anti-FLAG beads, and the abundance of tagged and untagged protein was compared using SDS-PAGE. The Y57A/N60A, Y57A/K62A, and N60A/K62A double mutations, which should only affect interaction with PP2A, have no effect on dimer formation using this assay. According to the crystal structure, L68 is involved in Sgo1a-Sgo1b interaction and has little direct involvement in PP2A interaction. Its substitution by alanine (L68A) abolishes dimer formation as well as interaction with PP2A. This result, together with our observation that both Sgo1 helices interact extensively with the same PP2A complex, imply that Sgo1 homodimerization is a prerequisite for binding to PP2A. Surprisingly, N61I forms dimers as efficiently as wild-type. N61 side chains pack tightly at the center of the coiled-coil interface, and introduction of a larger side chain (as occurs after substitution by isoleucine) might have been expected to disrupt dimer formation. Remaining interactions between the Sgo1a and Sgo1b helices must therefore be sufficient for dimerization. Why, if N61 side chains are not required for dimer formation and make no direct contacts with PP2A, does N61I disrupt binding of PP2A and cause a dramatic phenotype in flies? Introduction of a larger side chain (as in substitution by isoleucine) or simply loss of key hydrogen bonds (as in substitution by alanine) presumably disrupts the coiled coil's conformation, affecting the interaction with PP2A of neighboring residues such as Y57, N60, and K62. In summary, our mutagenesis is consistent with the crystal structure and with amino acid conservation. Crucially, we realized one of our primary goals, namely to design mutant shugoshins defective in PP2A interaction without changing other properties of the protein (that we know about).

Sgo2 Interacts as a Dimer with All PP2A Forms

Mammalian cells express two major types of shugoshin, called Sgo1 and Sgo2. The finding that mice lacking Sgo2 are viable (Llano et al., 2008) is inconsistent with the claims that this protein has an important role during mitosis (Huang et al., 2007; Kitajima et al., 2006), and it is likely that Sgo1 alone is necessary to protect centromere cohesion during mitosis (McGuinness et al., 2005; Salic et al., 2004). What about meiosis? RNA

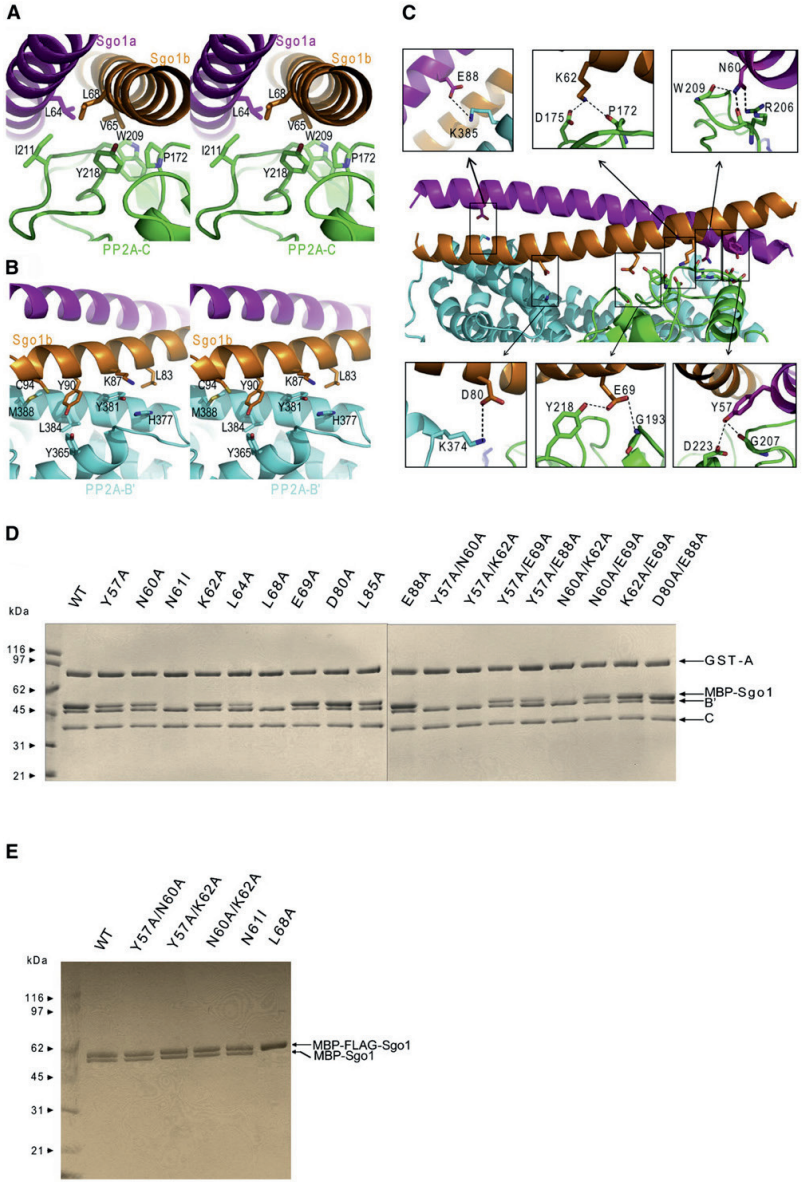

Figure 3. The Specific Interactions between PP2A and Sgo1 and the Effect of Sgo1 Mutations on the Interaction

(A) Stereo views of hydrophobic interactions between PP2A-C and Sgo1. The residues involved in the hydrophobic core are indicated and represented in the stick mode.

(B) Stereo views of hydrophobic interactions between PP2A-B′ and Sgo1.

(C) Hydrophilic interactions between PP2A and Sgo1. The residues (Y57, N60, K62, E69, D80, and E88, as indicated) from both Sgo1 molecules form hydrogen bonds or salt bridges with PP2A B′ and C subunits, as indicated by dashed lines.

(D) The binding assay of PP2A with various Sgo1 mutants. Wild-type (WT) and various single or double mutant Sgo1s, as indicated, were tested to bind with PP2A.

(E) Dimerization assay of several selected mutant Sgo1s. The mutant Sgo1s that cannot bind with PP2A were selected to test the dimerization. The mutant Sgo1 (MBP-tagged) was pulled down by the same mutant Sgo1 (FLAG-tagged), followed by elution (100 ng/ml FLAG peptide solution), and detected by SDS-PAGE analysis.

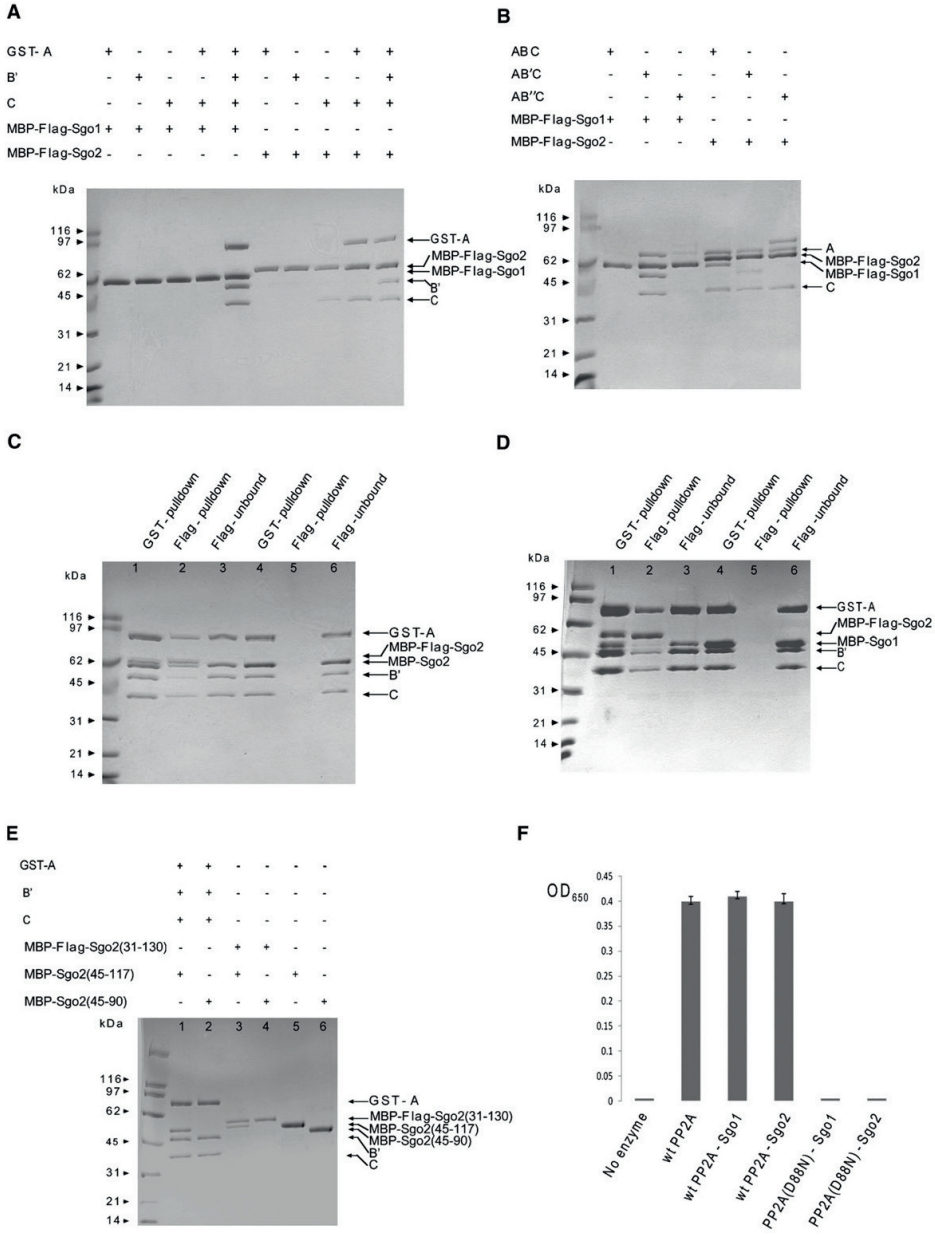

Figure 4. Comparison and Characterization of Sgo1 and Sgo2 Binding with PP2A

(A) PP2A C subunit is sufficient for Sgo2 but not for Sgo1 binding. PP2A A, B′, and C individual subunits, the AC core enzyme, and the AB′C holoenzyme were incubated with MBP-FLAG-Sgo1(51–105) or MBP-FLAG-Sgo2(45–117) for 1 hr followed by FLAG affinity pull-down. Bead-bound proteins were eluted in a buffer containing FLAG peptide and were resolved on an SDS-PAGE gel.

(B) Interaction of Sgo1 or Sgo2 with PP2A holoenzyme containing different B-type regulatory subunits. MBP-FLAG-Sgo1(51–105) or MBP-FLAG-Sgo2(45–107) was incubated with ABC, AB′C, or AB″C for 1 hr followed by FLAG affinity pull-down. Bead-bound proteins were eluted and resolved on an SDS-PAGE gel. Sgo1 interacts specifically with the AB′C PP2A only, whereas Sgo2 can interact with all PP2A isoforms.

interference studies have come to conflicting conclusions as to Sgo1's role (Lee et al., 2008; Yin et al., 2008). What is clear is that *sgo2Δ/sgo2Δ* mice are infertile and defective in retaining cohesin at centromeres after meiosis I (Llano et al., 2008). This suggests that mammalian Sgo2 and possibly not Sgo1 fulfills the function performed by proteins called Sgo1 or MEI-S332 in yeast and flies, respectively. Does hSgo2 also bind PP2A? Like hSgo1, it contains an N-terminal coiled-coil region (residues 31–130), which we found to be sufficient for PP2A interaction. In contrast to hSgo1, which interacts with the AB′C holoenzyme in vivo (Kitajima et al., 2006; Riedel et al., 2006; Tang et al., 2006) and in vitro (Figure 1) but not with individual PP2A A, B, and C subunits or the AC core complex, mouse Sgo2 forms a stable complex with the PP2A's C subunit (Figure 4A). It interacts with all three types of PP2A holoenzyme as well as with core PP2A AC complex. This demonstrates that mammalian Sgo1 and Sgo2 form distinct shugoshin-PP2A complexes and may therefore have distinct substrate specificities at centromeres.

In the presence of PP2A, FLAG-tagged Sgo2 pulls down untagged Sgo2, implying that PP2A-Sgo2 complexes contain two Sgo2 molecules and a single PP2A (Figure 4C). Sgo2's dimerization differs, however, from that of Sgo1. Thus, FLAG-Sgo2(31–130) pulls down Sgo2(45–117), but not Sgo2(45–90) (Figure 4E). Indeed, a failure to form dimers explains why MBP-Sgo1(51–96) pulls down PP2A (Figure 1B) while the corresponding fragment of Sgo2 (residues 45–90) cannot do so (data not shown). Sequence alignments show that L53, L54, I81, and I82 of Sgo1, which are involved in dimer formation, are replaced by small or hydrophilic residues in Sgo2, which would explain why Sgo2 dimer formation requires a longer coiled coil. Indeed, Sgo2's predicted coiled coil containing periodic L/I residues extends further in a C-terminal direction than that of Sgo1. Sgo2's tight interaction with PP2A's C subunit might nevertheless involve only the N-terminal part of this extended coiled coil. Finally, we found that MBP-Sgo1 forms a stable heterodimer with MBP-Sgo2 (data not shown) that binds PP2A, albeit less efficiently than homodimers (Figure 4D).

Sgo1 Does Not Alter PP2A's Catalytic Activity

We measured phosphatase activities of wild-type and catalytically inactive (D88N) PP2A in the presence and absence of purified MBP-Sgo1 or MBP-Sgo2 proteins. While the PP2A-C(D88N) mutation abolishes activity, neither Sgo1 nor Sgo2 has an effect on the dephosphorylation of peptide substrate (Figure 4F), which fits with the finding that Sgo1 does not induce a change in the conformation of PP2A's active site. Shugoshins might nevertheless affect substrate recruitment in vivo.

The Shugoshin-PP2A Interaction Protects Centromeric Cohesin in Yeast

To address the physiological significance of shugoshin's interaction with PP2A, we turned to the budding yeast *S. cerevisiae*, whose sole shugoshin, scSgo1, is essential for protecting centromeric cohesin from separase at meiosis I (Katis et al., 2004; Marston et al., 2004). scSgo1 possesses the conserved N-terminal coiled coil within which scN51 corresponds to hN61 (Figure S8). Mutation to alanine of three surface residues expected to contact PP2A, namely Y47, Q50, and S52 (equivalent to Y57, N60, and K62 in hSgo1), abolishes colocalization of PP2A's B′ subunit Rts1 with centromeric Ndc10 in chromosome spreads from pachytene cells (Figure 5A). Replacement of N51 to isoleucine (N51I) has a similar effect (data not shown). Importantly, these mutations have no effect either on Sgo1's steady-state levels (i.e., stability; data not shown) or on its recruitment to centromeres (Figures 5B and S9). These findings both validate the Sgo1:PP2A crystal structure and demonstrate that interaction between PP2A and shugoshin is essential for the PP2A's centromere localization, at least during yeast meiosis.

Like *sgo1Δ* (Katis et al., 2004), *sgo1 N51I* and *sgo1Y47A/Q50A/S52A* (*sgo1-3A*) diploids produce inviable haploid spores, while *Y47A/S52A*, *Y47A*, *S52A*, and *Q50A* diploids produce spores whose viability is 8.3%, 15.8%, 90.8%, and 91.3%, respectively (Figure S10). To address whether the mutations cause nondisjunction of sister centromeres at meiosis II, we scored segregation within tetrads of a single chromosome V marked by Tet repressor fused to GFP bound to a tandem array of operators at the *URA3* locus 35 kb away from the centromere (Michaelis et al., 1997). Y47A, N51I, Y47A/S52A, and Y47A/Q50A/S52A mutations cause high rates of sister centromere (*URA3*) nondisjunction (Figure 5C), which presumably arise from precocious loss of sister centromere cohesion, because Y47A/Q50A/S52A causes 70% of sister *URA3* sequences to disjoin by the end of anaphase I (Figure 5D), unlike wild-type, where they only disjoin at anaphase II. None of the mutations alter the kinetics of meiosis I (data not shown) or cosegregation of sister *URA3* sequences to the same pole at anaphase I (Figure 5D), implying that interaction between PP2A and scSgo1 is not required for meiosis I mono-orientation of sister

(C) At least two Sgo2 molecules bind to the same PP2A complex simultaneously. MBP-Sgo2(45–117) was incubated either with equal amounts of (lanes 1, 2, and 3) or without (lanes 4, 5, and 6) MBP-FLAG-Sgo2(45–117) and PP2A GST-A, -B, and -C subunits prior to GST affinity pull-down. Bead-bound proteins were eluted in a buffer containing glutathione. Eluted proteins were incubated with FLAG affinity beads before elution in a buffer containing FLAG peptide. Eluates and unbound fractions were resolved on an SDS-PAGE gel.

(D) Sgo1 and Sgo2 peptides can form stable heterodimers (data not shown), but they cannot bind to PP2A as stably as the homodimers. MBP-Sgo1(51–105) was incubated either with equal amounts of (lanes 1, 2, and 3) or without (lanes 4, 5, and 6) MBP-FLAG-Sgo2(45–117) and PP2A GST-A, -B, and -C subunits prior to GST affinity pull-down. Bead-bound proteins were eluted in a buffer containing glutathione. Eluted proteins were incubated with FLAG affinity beads before elution in a buffer containing FLAG peptide. Eluates and unbound fractions were resolved on an SDS-PAGE gel.

(E) Sgo2 requires a coiled-coil region longer than that of Sgo1 for dimer formation and PP2A binding. MBP-Sgo2(45–90) and MBP-Sgo2(45–117) were tested for binding to PP2A as described in (B) (lanes 1 and 2). Dimerization abilities of these fragments were determined by testing their binding to the longer MBP-FLAG-Sgo2(31–130). After FLAG affinity pull-down, bead-bound proteins were eluted in a buffer containing FLAG peptide, and the eluates were resolved on the SDS-PAGE gel (lanes 3 and 4). Individual MBP-Sgo2(45–117) and MBP-Sgo2(45–90) samples were loaded on lanes 5 and 6, respectively.

(F) Sgo1 binding does not change PP2A enzymatic activity. Phosphatase activities of wild-type PP2A, PP2A-Sgo1, PP2A-Sgo2, PP2A(D88N)-Sgo1, and PP2A(D88N)-Sgo2 were analyzed by a standard Ser/Thr Phosphatase Assay Kit. The reaction without PP2A was used as a negative control.

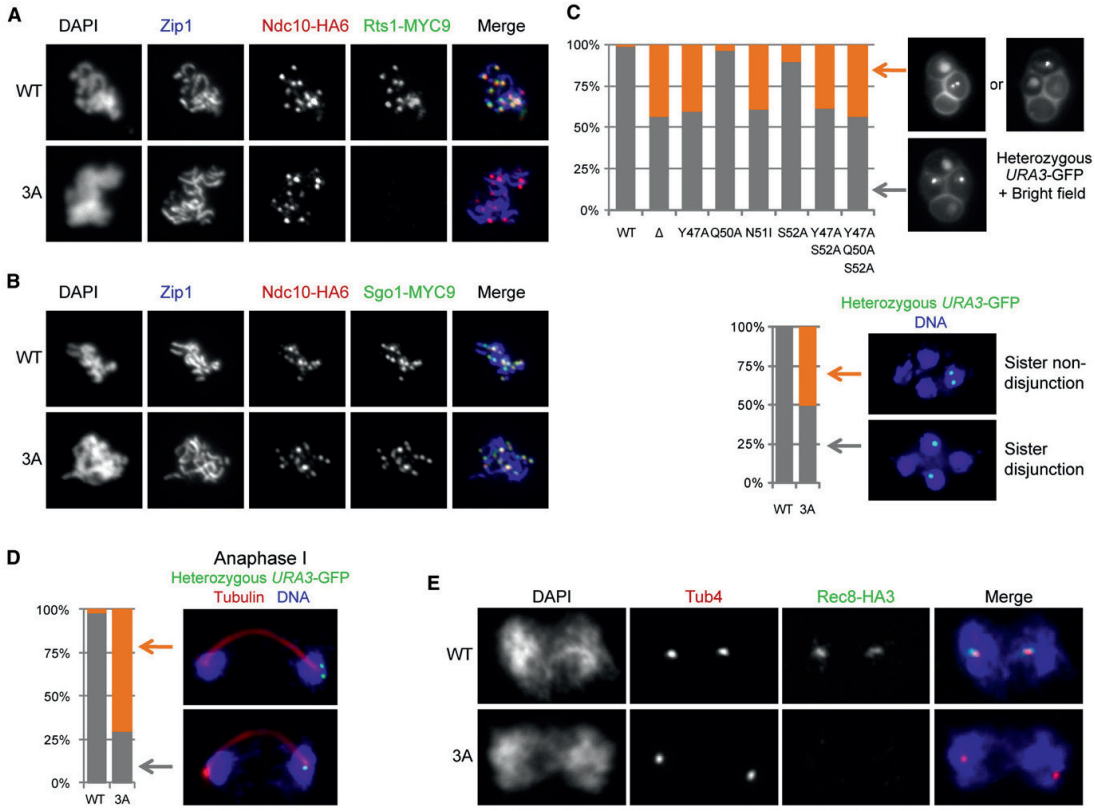

Figure 5. Sgo1-PP2A Interaction Is Necessary for Protecting Centromeric Cohesin

(A) Colocalization of 9× MYC epitope-tagged PP2A-B′ subunit Rts1 with 6× HA epitope-tagged kinetochore protein Ndc10 on pachytene-stage nuclear spreads of wild-type (WT; K16140) or *sgo1-3A* (3A; K16139) cells. Pachytene stage was identified by the Zip1 staining that lines the axis of synapsed chromosomes. At least 30 pachytene nuclei were scored for both strains.

(B) Colocalization of 9× MYC epitope-tagged wild-type (WT; K12113) or Y47A/Q50A/S52A mutant form (3A; K16235) of scSgo1 with 6× HA epitope-tagged kinetochore protein Ndc10 on pachytene-stage nuclear spreads. At least 30 pachytene nuclei were scored for both strains.

(C) Diploid wild-type (WT; K16213) or mutant strains carrying the scSgo1 mutations *sgo1*Δ (Δ; K16214), Y47A (K16226), Q50A (K16259), N51I (K16216), S52A (K16227), Y47A/S52A (K16228), Y47A/Q50A/S52A (K16215), and heterozygous GFP-marked chromosome V at *URA3* locus (*URA3*-GFP) were sporulated on plates, and 100 tetrads produced from each strain were scored for the segregation of *URA3*-GFP to asci using fluorescence microscopy with brightfield illumination (upper panel). Wild-type (WT; K16213) and *sgo1-3A* (3A; K16215) cells were also scored after sporulation in liquid culture, formaldehyde fixation, spheroplasting, and DAPI staining (lower panel).

(D) Diploid wild-type (WT; K16213) and *sgo1-3A* (3A; K16215) cells containing heterozygous *URA3*-GFP as well as Pds1-myc18 and Rec8-HA3 epitope-tagged proteins were sporulated in synchronous liquid cultures, and samples were taken for in situ staining. For each strain, 100 anaphase I-stage cells, identified by two DNA masses connected with elongated spindles and low levels of Pds1 (data not shown), were scored for the reductional and equational (never observed) segregation of *URA3*-GFP dots. Reductional segregation was further scored for precocious sister splitting.

(E) Immunostaining of anaphase I-stage nuclear spreads from wild-type (WT; K16213) and *sgo1-3A* (3A; K16215) cells expressing Rec8-HA3 epitope-tagged protein. Tub4 staining marks the spindle pole bodies. Bilobed DNA mass around two Tub4 foci is an indication for anaphase I. At least 20 anaphase I spreads were scored for both strains.

kinetochores (Tóth et al., 2000). To address whether the interaction is required to protect centromeric cohesin, we compared the distribution of cohesin's Rec8 protein in chromosome spreads from wild-type and triple mutant (*sgo1-3A*) cells. Rec8's association with pachytene chromosomes (Figure S11) was unaffected by the mutation, but its persistence at centromeres between meiotic divisions was abolished by the *sgo1-3A* triple mutation (Figure 5E). We conclude that protection of centromeric cohesin from separase at meiosis I depends on Sgo1's ability to bind PP2A, a function that is possibly conserved in animal cells given the precocious loss of sister chromatid cohesion in *Drosophila* caused by N61I (Tang et al., 1998). Our findings extend in an important way the previous demonstration that PP2A's Rts1 B′ subunit is required for centromeric cohesin protection (Riedel

et al., 2006). PP2A has many functions during mitosis and meiosis, and the effect of Rts1 inactivation on cohesin protection may have been indirect. The current data demonstrate that it is only the small pool of PP2A molecules associated with Sgo1 that is essential for cohesin protection.

Recruitment of PP2A to Chromatin by Sgo1 Blocks Cohesin Cleavage in Oocytes

If recruitment of PP2A to centromeres were the mechanism by which shugoshins protect cohesin, then deposition of PP2A onto the arms of meiosis I bivalents should prevent their conversion to dyads. To address this, we investigated the effects of overexpressing Sgo1 in mouse oocytes. mSgo1-GFP fusion protein concentrates at centromeres after injection of modest amounts of mRNA into oocytes at the GV stage (data not shown), but decorates the arms of bivalent chromosomes after injection of larger amounts (Figure 6A). This is accompanied by a similar redistribution of PP2A (Figure 6A), which is normally found only at centromeres (data not shown). PP2A's artificial recruitment to the arms of bivalents is largely abolished by N61I (Figure 6A) and reduced by Y57A/N60A/R62A mutations (data not shown). Remarkably, the redistribution of PP2A caused by mSgo1 overexpression is accompanied by a block to meiosis I chromosome segregation. The failure to segregate chromosomes is not caused by a failure to activate separase, because destruction of securin-GFP protein (produced by an mRNA injected along with that of untagged mSgo1) (Figures 6B and 6C) takes place on schedule. Oocytes overexpressing mSgo1 also extrude polar bodies with normal kinetics, but these are subsequently retracted (Figures 6B and 6C).

Chromosome spreads from metaphase II oocytes reveal that Sgo1 overexpression blocks resolution of chiasmata and removal of cohesin's Rec8 subunit from chromosome arms (Figures 6D and 6E). Crucially, N61I and Y57A/N60A/R62A mutations largely abolish mSgo1's ability to block the chiasmata resolution (Figures 6E and 6F). These data suggest that recruitment of PP2A to chromosome arms may be sufficient to block Rec8 cleavage. It is likely that centromeric Rec8 in mouse oocytes is normally protected from separase not by mSgo1, but by mSgo2 (Llano et al., 2008). We suggest that mSgo2 performs this function, like scSgo1, by recruiting PP2A. If this proves to be case, then our experiments imply that PP2A recruitment would be sufficient to protect centromeric cohesin. No other function might be required.

The Spindle Assembly Checkpoint in Yeast Requires Binding of PP2A to Shugoshin

In budding yeast, which expresses only a single shugoshin, scSgo1 also has important functions in mitotic cells, one of which is to delay activation of the anaphase-promoting complex/cyclosome (APC/C) when there is a lack of tension at the interconnection between microtubules and kinetochores (Indjeian et al., 2005). When cells with a temperature-sensitive *cdc15-2* mutation are released from G1 arrest at the restrictive temperature, they undergo DNA replication, securin (Pds1) destruction, and chromosome segregation, but fail to exit mitosis due to a defect in the mitotic exit network (MEN) (Bardin et al., 2003). Securin destruction and stable spindle elongation do not take place in *scc1-73 cdc15-2* double mutant cells, which cannot form sister chromatid cohesion (Figures 7A–7C) (Severin et al., 2001). Both phenotypes are presumably due to a spindle assembly checkpoint (SAC)-induced APC/C activation block, as they are suppressed by deleting *MAD2* (Figures 7A–7C). Importantly, *sgo1-3A*, as well as *sgo1Δ* (Figures 7A–7C), also suppresses the spindle instability and the lack of securin destruction in *scc1-73 cdc15-2* cells. Binding of PP2A to Sgo1 is therefore required for inhibition of the APC/C by the SAC in response to a lack of cohesion. Consistent with this finding, *sgo1-3A* and *RTS1* deletion cells are hypersensitive to the microtubule-destabilizing drug benomyl (Figure 7D).

DISCUSSION

The myriad functions performed by PP2A, or any other phosphatase, for that matter, pose a major problem: how to regulate its activity against particular substrates? Protein phosphorylation is determined by a delicate balance between kinases and phosphatases, and changes in substrate phosphorylation cannot be regulated merely by raising or lowering activity of kinases and phosphatases throughout the cell. A capacity to regulate differentially specific phosphatase subpopulations that target specific substrates in specific locations would therefore be a desirable property. It was hitherto thought that this sort of specificity was conferred largely by PP2A's regulatory B subunits, of which there are several types (B, B′, B″, B‴). However, the finding that a fraction of AB′C PP2A holoenzymes associate with Shugoshin/Mei-S332-type proteins that are concentrated mainly at centromeres (and centrosomes) raises the prospect of far greater specificity. Our structural and biochemical data show that shugoshin is an adaptor protein, which does not affect PP2A enzymatic activity, but instead determines the specific PP2A form(s) to be recruited and thus determines the PP2A substrate specificity at centromeres. In contrast to the conventional view that the targeting/regulatory B subunit is responsible for PP2A localization, the catalytic C subunit of PP2A is the primary docking site for shugoshin. Our work therefore provides a paradigm according to which PP2A targets substrates via an adaptor protein that concentrates the enzyme at a particular location in the cell.

Structural Basis of the PP2A-Shugoshin Interaction: The Importance of Sgo Dimerization

A key feature of the Sgo1-PP2A interaction is that the both strands of Sgo1's coiled coil interact with both catalytic C and regulatory B subunits of the same PP2A holoenzyme. This means that formation of Sgo1's coiled-coil homodimer is essential for its interaction with PP2A, a conclusion confirmed by the effects of the L68A mutation, which disrupts formation of the coiled-coil dimer and abolishes the PP2A-Sgo1 interaction (Figures 3A, 3D, and 3E). Indeed, the dramatic difference between the PP2A binding affinities of hSgo1(51–96) and hSgo1(51–103) (Figure S1) can be explained not by differences in the number of their contacts with PP2A, but rather by the fact that the latter is predicted to form two extra helical turns, thereby creating a more stable Sgo1 homodimer. Likewise, mSgo2(45–107) forms a stable homodimer that interacts with PP2A, while mSgo2(45–90), which shares the identical N-terminal half that is most likely responsible for interacting with PP2A's C subunit,

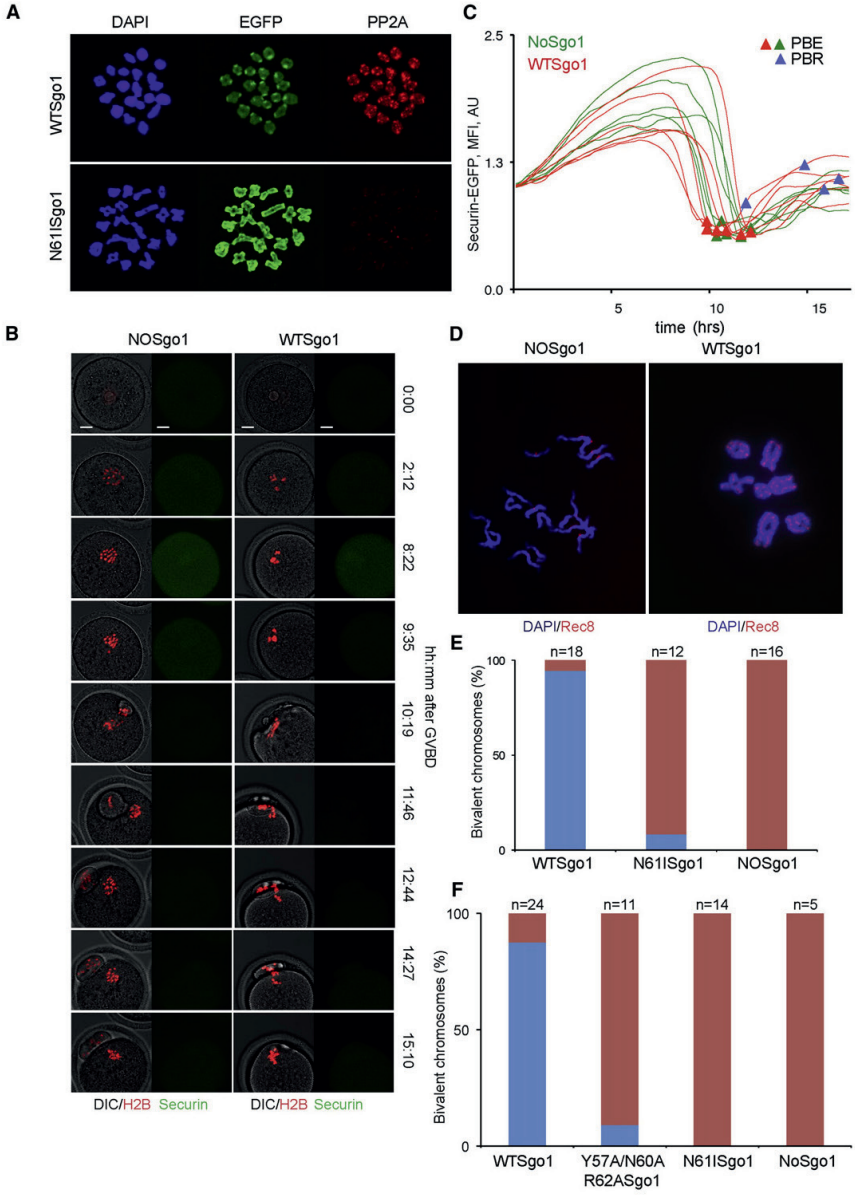

Figure 6. PP2A Recruitment to Bivalent Arms Blocks Chiasmata Resolution in Mouse Oocytes

(A) GV-stage CD1 oocytes were injected with wild-type Sgo1-EGFP and N61ISgo1-EGFP mRNAs and matured for approximately 6 hr. Chromosome spreads were prepared from individual oocytes and stained with DAPI (blue), PP2A was detected with PP19 antibody (red), and mSgo1 was detected with EGFP (green).

(B) Images from movies with CD1-strain oocytes injected with H2B-mCherry, securin-EGFP, and wild-type Sgo1 mRNAs as indicated. The merged DIC/H2B-mCherry (left) and securin-EGFP (right) channels are shown. Bar = 10 μm.

(C) Securin-EGFP levels in oocytes injected with H2B-mCherry and securin-EGFP (green) or with H2B-mCherry and securin-EGFP together with wild-type Sgo1 (red) were measured at each time point. Values were normalized relative to that at GVBD (0 hr) and plotted, in arbitrary units (AU), against time. The timing of polar body extrusion (PBE, green or red triangles) or retraction (PBR, blue triangles) is indicated.

cannot form a homodimer and does not, therefore, interact with PP2A.

mSgo2 Forms Complexes with Multiple Types of PP2A Holoenzyme

mSgo2 also interacts with PP2A using its coiled-coil domain. That it does so in a manner similar to hSgo1 is suggested by sequence conservation and the finding that hSgo1 and mSgo2 form heterodimers capable of interacting with PP2A, at least in vitro. In contrast to hSgo1, which only interacts with the AB′C family trimeric holoenzymes, hSgo2 can form stable complexes with PP2A's catalytic C subunit in the absence of A and B subunits. As a consequence, hSgo2 interacts with AC core complexes and with trimeric holoenzymes containing a variety of B subunits. Indeed, hSgo2's coiled coil appears to bind more tightly with ABC and AB″C holoenzymes than with the AB′C holoenzymes. Because regulatory B subunits have an important role in substrate specificity (Cho and Xu, 2007; Janssens and Goris, 2001; Lechward et al., 2001; Sontag, 2001; Xu et al., 2006; Yu, 2007), it is therefore conceivable that PP2A recruited to centromeres by hSgo2 might regulate phosphorylation of a different set of substrates from those regulated by hSgo1. This could explain how different types of shugoshin have different functions despite having similar cellular locations. In mitotic mammalian cells, for example, Sgo1 and Sgo2 are both concentrated at centromeres, but only the former is necessary to protect cohesin from the prophase dissociation pathway (Llano et al., 2008; McGuinness et al., 2005). Likewise, in fission yeast, both spSgo1 and spSgo2 are associated with centromeres during meiosis I, but only the former is required to protect cohesin from separase at the onset of anaphase I (Rabitsch et al., 2004; Riedel et al., 2006; Vanoosthuyse et al., 2007; Vaur et al., 2005). Thus, the finding that PP2A is still present at centromeres after depletion of hSgo1 in HeLa cells (Lee et al., 2008) does not necessarily imply that hSgo1 does not protect centromeric cohesin by recruiting PP2A, because the PP2A remaining at centromeres in the depleted cells may have different properties to PP2A putatively associated with hSgo1. Whether or not binding of PP2A to hSgo1 is necessary to protect centromeric cohesin from the prophase pathway therefore remains an open question. Importantly, our crystal structure enables this to be addressed in a rigorous manner by testing the phenotype of mutations that abolish, specifically, PP2A binding. The sequences flanking the coiled-coil regions of hSgo1 and hSgo2 are predicted to be unstructured (Figure S7). This potentially flexible region is considerably larger in hSgo2, which might therefore bind to a different set of centromeric proteins, further differentiating its activity from that of hSgo1.

Recruitment of PP2A to Centromeres by Shugoshin Protects Cohesin from Separase

A key finding made possible by the crystal structure of the hSgo1-PP2A complex is that mutation (within yeast Sgo1) of key residues involved in PP2A binding abolishes recruitment of the Rts1 AB′C holoenzyme to centromeres and causes the precocious loss of cohesin from this location at the onset of anaphase I and massive nondisjunction at meiosis II. Mutation of the highly conserved asparagine (equivalent to N61 in humans) has a similar phenotype in yeast and in flies (Tang et al., 1998). In this case, however, the mutation may affect more than just PP2A binding, as it probably alters the coiled coil's conformation. Our observations extend the previous finding that inactivation of Rts1 causes precocious loss of sister centromere cohesion (Riedel et al., 2006). Crucially, we now know that it is the small population of PP2A recruited to centromeres by scSgo1 that is responsible for protecting centromeric cohesin and not merely global AB′C holoenzyme activity.

How might PP2A associated with scSgo1 protect centromeric cohesin? More specifically, what is the process whose deregulation causes precocious centromeric cohesin loss when Sgo1 cannot bind PP2A? There are two possibilities: cleavage of Rec8 by separase or cleavage-independent dissociation. The finding that noncleavable Rec8 blocks both meiotic divisions (Buonomo et al., 2000; Kitajima et al., 2003) suggests that cleavage-independent mechanisms analogous to the mitotic prophase pathway are not capable of destroying cohesion. PP2A must therefore regulate Rec8 cleavage. It could do this by regulating either separase or its target, Rec8. The finding that cleavage of Rec8's mitotic counterpart Scc1 cannot be protected by Sgo1 when expressed in meiotic cells (Tóth et al., 2000), the recent identification of Rec8 phosphorylation sites essential for its cleavage along chromosome arms at meiosis I, and the finding that phosphomimicking Rec8 mutants cause precocious loss of sister centromere cohesion (V. Katis, J. Lipp, K. Mechtler, B. Novák, W. Zachariae, and K.N., unpublished data) suggest that PP2A targets Rec8 and not separase. We suggest that PP2A's preferential accumulation at centromeres leads to dephosphorylation of centromeric Rec8, which therefore cannot be cleaved by separase. Our finding that overexpression of hSgo1 induces the recruitment of PP2A to the arms of bivalent chromosomes in oocytes and that this is

(D) Oocytes carrying Rec8-myc transgene were injected with wild-type Sgo1-EGFP mRNA (WTSgo1) or uninjected (NoSgo1). Live imaging was used to monitor a meiotic progression for approximately 18 hr, and only oocytes, which extruded the polar body, were processed for DNA spreads. Chromosome spreads were stained with DAPI (blue) to visualize DNA and with anti-myc antibody (red) to detect Rec8.

(E) GV-stage CD1 oocytes were injected with H2B-mCherry and with wild-type Sgo1 and N61ISgo1 mRNAs and monitored by live imaging for 18 hr. Chromosome spreads were prepared only from oocytes, which extruded polar body. Spreads were stained with DAPI and CREST or PP2A and scored for the presence of bivalent chromosomes. Blue columns represent a percentage of cells containing at least one bivalent chromosome; red columns represent a percentage of cells containing only univalent chromosomes. Data were obtained from four independent experiments; numbers of cells in each group are indicated.

(F) CD1 oocytes were injected with H2B-mCherry mRNA and also with wild-type Sgo1-EGFP, N61ISgo1-EGFP, and Y57A/N60A/R62ASgo1-EGFP mRNAs. Meiotic maturation and chromosome segregation were monitored by live imaging, and after 18 hr, oocytes, which extruded polar bodies, were assayed by Z stacks covering the entire cell volume. After 3D reconstruction, cells were scored for presence of bivalent chromosomes. Blue columns represent a percentage of cells containing at least one bivalent chromosome; red columns represent a percentage of cells containing only univalent chromosomes. Data were collected from six experiments, and the numbers of cells are indicated.

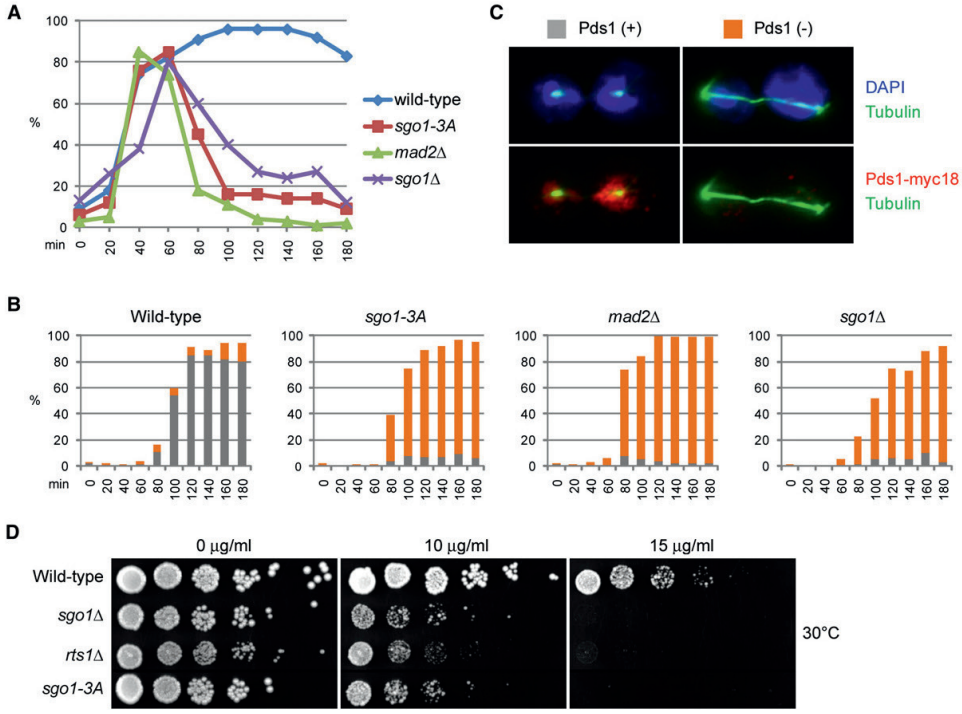

Figure 7. Sgo1-PP2A Interaction Is Required for Spindle Assembly Checkpoint Activation in Yeast

(A–C) Haploid *MATa* strains carrying mutations *cdc15-2*, *scc1-73* (wild-type; K16260), *cdc15-2*, *scc1-73*, *sgo1-3A* (*sgo1-3A*; K16261), *cdc15-2*, *scc1-73*, *mad2Δ* (*mad2Δ*; K16262), *cdc15-2*, *scc1-73*, *sgo1Δ* (*sgo1Δ*; K16315) were synchronized at G1 stage by α factor arrest at 24°C and released from the arrest at nonpermissive temperature, 35.5°C. Samples of the cultures were taken at indicated time points and analyzed by FACS for cellular DNA content (Figure S12) and by in situ immunostaining of α-tubulin and 18xMYC epitope-tagged Pds1. Shown are: fraction of Pds1-myc18-positive cells (A) and fraction of binucleates that are Pds1 positive (gray bar) or Pds1 negative (orange bar) (B). In (C), representative images for (B) are shown.

(D) Wild-type (K15785), *sgo1Δ* (K15784), *rts1Δ* (K14165), and *sgo1-3A* (K15789) cells were tested for growth at indicated concentrations of benomyl at 30°C.

accompanied by a block to chiasmata resolution indicate that the above model applies to meiosis in mammals as well as yeast.

Role of PP2A in the SAC

Our finding that *sgo1-3A* mutants are defective in blocking APC/C activation in cells lacking sister chromatid cohesion suggests that binding of PP2A to Sgo1 has a crucial role in the "tension-dependent" SAC. Previous work has implicated PP2A's B regulatory subunit (Cdc55) in the SAC (Wang and Burke, 1997; Tang and Wang, 2006). However, *cdc55* mutants in yeast have rather pleiotropic effects on the cell cycle, and it has never been clear how direct a role PP2A has in the SAC. Our finding that both *sgo1-3A* and *rts1* (PP2A B′) mutants are similarly sensitive to benomyl, together with the observation that Sgo1 has hitherto been copurified only with its B′ (Rts1) regulatory subunit (albeit so far only in meiotic yeast cells), indicates that Sgo1's SAC function is mediated by AB′C PP2A and not the ABC form. Nevertheless, it is conceivable that Sgo1 might also bind ABC PP2A in vivo in mitotic cells, a possibility strengthened by our finding that human Sgo2 binds the ABC as well as the AB′C form. PP2A's mechanistic role in the SAC remains enigmatic; that is, what are its substrates? Interestingly, orderly homolog disjunction during meiosis I, which is dependent on Mad2 (Shonn et al., 2003), is not affected by the *sgo1-3A* mutation. This implies that the SAC's mechanism differs between mitosis, where Sgo1's association with PP2A may be important, and meiosis I, where it is probably not.

Implications of the Structure for Shugoshin and PP2A Localization

Shugoshins recruit PP2A to chromosomes, both in yeast and in mouse oocytes. Might PP2A, in turn, facilitate the chromosomal association of shugoshins? We find no evidence that this is the case during yeast meiosis, where mutations that abolish PP2A binding have little or no effect on scSgo1's accumulation at centromeres. However, the finding that N61I abolishes hSgo1's accumulation at centromeres in HeLa cells raises the possibility that PP2A bound to Sgo1 might facilitate Sgo1's association with centromeres in mitotic cells (Tang et al., 2006). Discovering whether this is indeed the case will

require analysis of mutations that affect residues specifically involved in PP2A interaction. It is certainly not inconceivable, because at least two different mitotic kinases have been implicated in reducing hSgo1's association with chromatin. Phosphorylation of Mei-S332 by Polo kinase has been implicated in dissociation from centromeres during anaphase (Clarke et al., 2005), while inhibition of Aurora B leads to increased association of hSgo1 with chromosome arms (Kueng et al., 2006; Lipp et al., 2007). In *Drosophila*, the chromosome passenger complex and Aurora B phosphorylation are needed for proper localization of MEI-S332 to the centromere as opposed to the chromosome arms (Resnick et al., 2006). If phosphorylation of shugoshins does indeed reduce its affinity for chromatin, then hSgo1's interaction with PP2A would plausibly counteract this process, and if the dephosphorylation of hSgo1 were largely mediated by PP2A associated with a separate hSgo1 molecule, then the interaction between hSgo1 and PP2A would tend to "sharpen" differences between arms and centromeres in the concentration of hSgo1. Our discovery that shugoshins only bind to PP2A as dimers might contribute to such a sharpening process, because as hSgo1 levels drop along chromosome arms, dimer formation might decrease, leading to less PP2A binding and thereby to yet less hSgo1. In addition, if the two tails of shugoshin dimers bind to different but neighboring chromatin domains, then it is conceivable that stretching, either within or between chromatids, could lead to disruption of the coiled coil and thereby to dissociation of PP2A. Whether or not dynamical and mechanical processes of this nature contribute to the formation of shugoshin and PP2A concentration, gradients along chromosomes can now be tested using insights into the mechanism by which shugoshins bind PP2A.

Our work demonstrates that shugoshin's most conserved domain forms a coiled coil that is both necessary and sufficient for PP2A binding. Because disruption of this coiled-coil structure abolishes PP2A binding, it is conceivable that it might be used to convert mechanical tension on chromosomes (Indjeian et al., 2005) into a change in the local concentration of PP2A, thereby changing the susceptibility of cohesin to cleavage by separase and also turning off the SAC. Learning whether this is indeed the case, and if so, how, await future experiments.

EXPERIMENTAL PROCEDURES

Data Collection and Structure Determination

Details of protein preparation, crystallization, and the phosphatase assay are described in the Supplemental Data. There was one complex per asymmetric unit with a solvent content of approximately 65%. A 2.7 Å data set was collected at ALS beamline 5.0.2. These data sets were integrated and scaled using HKL2000 (Otwinowski and Minor, 1997). Statistics for the collected data are summarized in Table 1. The structure was solved by molecular replacement using a molecule of PP2A holoenzyme (PDB ID code 2IAE) (Cho and Xu, 2007) as a search model. After rigid-body refinement, model building and refinement were performed using COOT (Emsley and Cowtan, 2004) and Refmac-restrained refinement in CCP4 package (Murshudov et al., 1997), respectively. The electron density maps from $2F_o - F_c$ and $F_o - F_c$ calculations were used for model building. The final model contained residues 7–589 of the PP2A A subunit, 26–426 of the PP2A B′ subunit, 2–309 of the PP2A C subunit, and 51–96 of Sgo1, with a working R factor of 22.8% and a free R factor of 27.7%. In the Ramachandran plot, 91.5%, 8.5%, and 0% of all residues in PP2A-Sgo1 complex fall within most favored, allowed, and disallowed regions, respectively.

PP2A-Shugoshin In Vitro Binding Assay

In all in vitro binding experiments, highly purified PP2A and shugoshin proteins were used. To test the binding of PP2A to various Sgo1 mutants, 2 μg of GST-tagged PP2A A was incubated with extra amount of PP2A B′ and C subunits and MBP-Sgo1 fusion protein for 1 hr on ice. Following the incubation, GST affinity beads were added to the mixture for GST-A pull-down. Washed beads were boiled and subjected to SDS-PAGE analysis using Coomassie blue staining. To investigate whether more than one Sgo1 molecule binds to the same PP2A complex, GST-tagged PP2A-A was incubated with excess of PP2A B′ and C subunits and Sgo1 or Sgo2 peptides or MBP fusions with or without a FLAG tag. The protein mixture was incubated with GST affinity beads for 1 hr at 4°C. After washing three times with binding buffer (150 mM NaCl, 20 mM Tris [pH = 7.5]), proteins were eluted with the binding buffer containing 20 mM glutathione. Eluates were then incubated with FLAG affinity beads for 1 hr at 4°C. Afterward, bead-bound proteins were eluted using FLAG peptide (Sigma) and subjected to SDS-PAGE analysis using Coomassie blue staining. Other FLAG- or GST-tagged pull-down experiments were done using the same strategy.

Yeast Strains, Growth, and Sporulation Conditions

The yeast strains used in this study are listed in Table S1. Sgo1 mutant strains were generated by integrating PCR-based mutagenized *SGO1* ORFs cloned in pAG32 plasmids (Goldstein and McCusker, 1999) into endogenous *SGO1* loci in *sgo1*Δ strains that have been published previously (Katis et al., 2004). Sporulation was performed at 30°C as described before (Buonomo et al., 2000).

Immunofluorescence Staining of Yeast Cells and Nuclear Spreads

In situ immunofluorescence staining of whole cells and surface-spread nuclei was performed as described in Katis et al., 2004. DNA was visualized using 4′,6-diamidino-2-phenylindole (DAPI). Images were taken using the Zeiss Axio fluorescent microscope with appropriate filter sets that is attached to a CoolSNAP HQ2 CCD camera and analyzed using MetaMorph Software (Molecular Devices; Sunnyvale, CA).

Mouse Strains

GV oocytes used in this study were isolated from CD1 strain (Harlan; Bicester, UK). A transgenic line (C57BL/6J) that expresses Rec8 from a bacterial artificial chromosome (BAC), with nine tandem copies of the human c-*myc* epitope at its C terminus, was described previously (Kudo et al., 2006). Mice were housed in animal facilities at the University of Oxford, and all procedures were approved by local Ethical Review Committees and licensed by the Home Office under the Animal (Scientific Procedures) Act 1986.

Oocyte Culture, Microinjection, and Live Imaging

Techniques used for oocyte culture, micromanipulation, and microinjection were described previously (Kudo et al., 2006; McGuinness et al., 2009). Zeiss LSM510 META confocal microscope equipped with incubator, maintaining stable temperature and CO_2, and with Plan-Neofluor 20 × /0.5, C-Apochromat 40 × /1.2 NA W Corr, and C-Apochromat 63 × /1.2 NA W Corr lenses was used for live imaging. For detection of Cascade Blue dextran, EGFP, and mCherry signal, we used 405 nm, 488 nm, and 561 nm excitation and LP 420, BP 505–550, and LP 575 filters. Chromosomes were tracked using H2B-mCherry signal and EMBL-developed tracking software (Rabut and Ellenberg, 2004) adapted to our microscope by Annelie Wuensche (EMBL Heidelberg). Image stacks were captured every 5–15 min for 16–20 hr. Quantification was performed using ImageJ software (http://rsb.info.nih.gov/ij/). The area for measuring securin-EGFP signal was defined manually in each frame, and the mean fluorescence intensity of the signal was normalized to the value at the time of GVBD.

ACCESSION NUMBERS

Coordinates and structure factors have been deposited in the Protein Data Bank (http://www.rcsb.org/pdb) under ID code 3FGA.

SUPPLEMENTAL DATA

Supplemental Data include Supplemental Experimental Procedures, Supplemental References, 12 figures, and one table and can be found online at http://www.cell.com/molecular-cell/supplemental/S1097-2765(09)00472-9.

ACKNOWLEDGMENTS

We thank Zhiyi Wei for help with crystallographic computation, Julia Zhu for providing purified active PP2A samples, Vittorio L. Katis for his advice on yeast meiotic cultures, and Andrew Murray for his advice about using *cdc15* mutants. We also appreciate the support from the staff at ALS for beamlines 5.0.2 and 8.2.2. This work was supported by NIH grant CA 129509 to W.X.

Received: January 6, 2009
Revised: April 21, 2009
Accepted: June 30, 2009
Published: August 27, 2009

REFERENCES

Alexandru, G., Uhlmann, F., Mechtler, K., Poupart, M.A., and Nasmyth, K. (2001). Phosphorylation of the cohesin subunit Scc1 by Polo/Cdc5 kinase regulates sister chromatid separation in yeast. Cell *105*, 459–472.

Bardin, A.J., Boselli, M.G., and Amon, A. (2003). Mitotic exit regulation through distinct domains within the protein kinase Cdc15. Mol. Cell. Biol. *23*, 5018–5030.

Brar, G.A., Kiburz, B.M., Zhang, Y., Kim, J.E., White, F., and Amon, A. (2006). Rec8 phosphorylation and recombination promote the step-wise loss of cohesins in meiosis. Nature *441*, 532–536.

Buonomo, S.B., Clyne, R.K., Fuchs, J., Loidl, J., Uhlmann, F., and Nasmyth, K. (2000). Disjunction of homologous chromosomes in meiosis I depends on proteolytic cleavage of the meiotic cohesin Rec8 by separin. Cell *103*, 387–398.

Cho, U.S., and Xu, W. (2007). Crystal structure of a protein phosphatase 2A heterotrimeric holoenzyme. Nature *445*, 53–57.

Clarke, A.S., Tang, T.T., Ooi, D.L., and Orr-Weaver, T.L. (2005). POLO kinase regulates the Drosophila centromere cohesion protein MEI-S332. Dev. Cell *8*, 53–64.

Emsley, P., and Cowtan, K. (2004). Coot: model-building tools for molecular graphics. Acta Crystallogr. D Biol. Crystallogr. *60*, 2126–2132.

Goldstein, A.L., and McCusker, J.H. (1999). Three new dominant drug resistance cassettes for gene disruption in Saccharomyces cerevisiae. Yeast *15*, 1541–1553.

Goldstein, L.S. (1980). Mechanisms of chromosome orientation revealed by two meiotic mutants in Drosophila melanogaster. Chromosoma *78*, 79–111.

Haering, C.H., Farcas, A.M., Arumugam, P., Metson, J., and Nasmyth, K. (2008). The cohesin ring concatenates sister DNA molecules. Nature *454*, 297–301.

Huang, H., Feng, J., Famulski, J., Rattner, J.B., Liu, S.T., Kao, G.D., Muschel, R., Chan, G.K., and Yen, T.J. (2007). Tripin/hSgo2 recruits MCAK to the inner centromere to correct defective kinetochore attachments. J. Cell Biol. *177*, 413–424.

Indjeian, V.B., Stern, B.M., and Murray, A.W. (2005). The centromeric protein Sgo1 is required to sense lack of tension on mitotic chromosomes. Science *307*, 130–133.

Janssens, V., and Goris, J. (2001). Protein phosphatase 2A: a highly regulated family of serine/threonine phosphatases implicated in cell growth and signalling. Biochem. J. *353*, 417–439.

Katis, V.L., Galova, M., Rabitsch, K.P., Gregan, J., and Nasmyth, K. (2004). Maintenance of cohesin at centromeres after meiosis I in budding yeast requires a kinetochore-associated protein related to MEI-S332. Curr. Biol. *14*, 560–572.

Kerrebrock, A.W., Moore, D.P., Wu, J.S., and Orr-Weaver, T.L. (1995). Mei-S332, a Drosophila protein required for sister-chromatid cohesion, can localize to meiotic centromere regions. Cell *83*, 247–256.

Kitajima, T.S., Miyazaki, Y., Yamamoto, M., and Watanabe, Y. (2003). Rec8 cleavage by separase is required for meiotic nuclear divisions in fission yeast. EMBO J. *22*, 5643–5653.

Kitajima, T.S., Kawashima, S.A., and Watanabe, Y. (2004). The conserved kinetochore protein shugoshin protects centromeric cohesion during meiosis. Nature *427*, 510–517.

Kitajima, T.S., Hauf, S., Ohsugi, M., Yamamoto, T., and Watanabe, Y. (2005). Human Bub1 defines the persistent cohesion site along the mitotic chromosome by affecting Shugoshin localization. Curr. Biol. *15*, 353–359.

Kitajima, T.S., Sakuno, T., Ishiguro, K., Iemura, S., Natsume, T., Kawashima, S.A., and Watanabe, Y. (2006). Shugoshin collaborates with protein phosphatase 2A to protect cohesin. Nature *441*, 46–52.

Kudo, N.R., Wassmann, K., Anger, M., Schuh, M., Wirth, K.G., Xu, H., Helmhart, W., Kudo, H., McKay, M., Maro, B., et al. (2006). Resolution of chiasmata in oocytes requires separase-mediated proteolysis. Cell *126*, 135–146.

Kueng, S., Hegemann, B., Peters, B.H., Lipp, J.J., Schleiffer, A., Mechtler, K., and Peters, J.M. (2006). Wapl controls the dynamic association of cohesin with chromatin. Cell *127*, 955–967.

Lechward, K., Awotunde, O.S., Swiatek, W., and Muszyńska, G. (2001). Protein phosphatase 2A: variety of forms and diversity of functions. Acta Biochim. Pol. *48*, 921–933.

Lee, J., Kitajima, T.S., Tanno, Y., Yoshida, K., Morita, T., Miyano, T., Miyake, M., and Watanabe, Y. (2008). Unified mode of centromeric protection by shugoshin in mammalian oocytes and somatic cells. Nat. Cell Biol. *10*, 42–52.

Lipp, J.J., Hirota, T., Poser, I., and Peters, J.M. (2007). Aurora B controls the association of condensin I but not condensin II with mitotic chromosomes. J. Cell Sci. *120*, 1245–1255.

Llano, E., Gómez, R., Gutiérrez-Caballero, C., Herrán, Y., Sánchez-Martín, M., Vázquez-Quiñones, L., Hernández, T., de Álava, E., Cuadrado, A., Barbero, J.L., et al. (2008). Shugoshin-2 is essential for the completion of meiosis but not for mitotic cell division in mice. Genes Dev. *22*, 2400–2413.

Marston, A.L., Tham, W.H., Shah, H., and Amon, A. (2004). A genome-wide screen identifies genes required for centromeric cohesion. Science *303*, 1367–1370.

McGuinness, B.E., Hirota, T., Kudo, N.R., Peters, J.M., and Nasmyth, K. (2005). Shugoshin prevents dissociation of cohesin from centromeres during mitosis in vertebrate cells. PLoS Biol. *3*, e86.

McGuinness, B.E., Anger, M., Kouznetsova, A., Gil-Bernabe, A.M., Helmhart, W., Kudo, N.R., Wuensche, A., Taylor, S., Hoog, C., Novak, B., and Nasmyth, K. (2009). Regulation of APC/C activity in oocytes by a Bub1-dependent spindle assembly checkpoint. Curr. Biol. *19*, 369–380.

Michaelis, C., Ciosk, R., and Nasmyth, K. (1997). Cohesins: chromosomal proteins that prevent premature separation of sister chromatids. Cell *91*, 35–45.

Murshudov, G.N., Vagin, A.A., and Dodson, E.J. (1997). Refinement of macromolecular structures by the maximum-likelihood method. Acta Crystallogr. D Biol. Crystallogr. *53*, 240–255.

Nasmyth, K., and Haering, C.H. (2005). The structure and function of SMC and kleisin complexes. Annu. Rev. Biochem. *74*, 595–648.

Otwinowski, Z., and Minor, W. (1997). Processing of X-ray diffraction data collected in oscillation mode. In Methods in Enzymology, *Volume 276*, C.W. Carter, Jr. and R.M. Sweet, eds. (New York: Academic Press).

Rabitsch, K.P., Gregan, J., Schleiffer, A., Javerzat, J.P., Eisenhaber, F., and Nasmyth, K. (2004). Two fission yeast homologs of Drosophila Mei-S332 are required for chromosome segregation during meiosis I and II. Curr. Biol. *14*, 287–301.

Rabut, G., and Ellenberg, J. (2004). Automatic real-time three-dimensional cell tracking by fluorescence microscopy. J. Microsc. *216*, 131–137.

Resnick, T.D., Satinover, D.L., MacIsaac, F., Stukenberg, P.T., Earnshaw, W.C., Orr-Weaver, T.L., and Carmena, M. (2006). INCENP and Aurora B promote meiotic sister chromatid cohesion through localization of the Shugoshin MEI-S332 in Drosophila. Dev. Cell *11*, 57–68.

Riedel, C.G., Katis, V.L., Katou, Y., Mori, S., Itoh, T., Helmhart, W., Gálová, M., Petronczki, M., Gregan, J., Cetin, B., et al. (2006). Protein phosphatase 2A protects centromeric sister chromatid cohesion during meiosis I. Nature *441*, 53–61.

Salic, A., Waters, J.C., and Mitchison, T.J. (2004). Vertebrate shugoshin links sister centromere cohesion and kinetochore microtubule stability in mitosis. Cell *118*, 567–578.

Severin, F., Hyman, A.A., and Piatti, S. (2001). Correct spindle elongation at the metaphase/anaphase transition is an APC-dependent event in budding yeast. J. Cell Biol. *155*, 711–718.

Shonn, M.A., Murray, A.L., and Murray, A.W. (2003). Spindle checkpoint component Mad2 contributes to biorientation of homologous chromosomes. Curr. Biol. *13*, 1979–1984.

Sontag, E. (2001). Protein phosphatase 2A: the Trojan Horse of cellular signaling. Cell. Signal. *13*, 7–16.

Tang, T.T., Bickel, S.E., Young, L.M., and Orr-Weaver, T.L. (1998). Maintenance of sister-chromatid cohesion at the centromere by the Drosophila MEI-S332 protein. Genes Dev. *12*, 3843–3856.

Tang, X., and Wang, Y. (2006). Pds1/Esp1-dependent and -independent sister chromatid separation in mutants defective for protein phosphatase 2A. Proc. Natl. Acad. Sci. USA *103*, 16290–16295.

Tang, Z., Shu, H., Qi, W., Mahmood, N.A., Mumby, M.C., and Yu, H. (2006). PP2A is required for centromeric localization of Sgo1 and proper chromosome segregation. Dev. Cell *10*, 575–585.

Tóth, A., Rabitsch, K.P., Gálová, M., Schleiffer, A., Buonomo, S.B., and Nasmyth, K. (2000). Functional genomics identifies monopolin: a kinetochore protein required for segregation of homologs during meiosis i. Cell *103*, 1155–1168.

Vanoosthuyse, V., Prykhozhij, S., and Hardwick, K.G. (2007). Shugoshin 2 regulates localization of the chromosomal passenger proteins in fission yeast mitosis. Mol. Biol. Cell *18*, 1657–1669.

Vaur, S., Cubizolles, F., Plane, G., Genier, S., Rabitsch, P.K., Gregan, J., Nasmyth, K., Vanoosthuyse, V., Hardwick, K.G., and Javerzat, J.P. (2005). Control of Shugoshin function during fission-yeast meiosis. Curr. Biol. *15*, 2263–2270.

Vogt, E., Kirsch-Volders, M., Parry, J., and Eichenlaub-Ritter, U. (2008). Spindle formation, chromosome segregation and the spindle checkpoint in mammalian oocytes and susceptibility to meiotic error. Mutat. Res. *651*, 14–29.

Wang, Y., and Burke, D.J. (1997). Cdc55p, the B-type regulatory subunit of protein phosphatase 2A, has multiple functions in mitosis and is required for the kinetochore/spindle checkpoint in Saccharomyces cerevisiae. Mol. Cell. Biol. *17*, 620–626.

Xu, Y., Xing, Y., Chen, Y., Chao, Y., Lin, Z., Fan, E., Yu, J.W., Strack, S., Jeffrey, P.D., and Shi, Y. (2006). Structure of the protein phosphatase 2A holoenzyme. Cell *127*, 1239–1251.

Xu, Y., Chen, Y., Zhang, P., Jeffrey, P.D., and Shi, Y. (2008). Structure of a protein phosphatase 2A holoenzyme: insights into B55-mediated Tau dephosphorylation. Mol. Cell *31*, 873–885.

Yin, S., Ai, J.S., Shi, L.H., Wei, L., Yuan, J., Ouyang, Y.C., Hou, Y., Chen, D.Y., Schatten, H., and Sun, Q.Y. (2008). Shugoshin1 may play important roles in separation of homologous chromosomes and sister chromatids during mouse oocyte meiosis. PLoS ONE *3*, e3516.

Yu, H. (2007). PP2A as a mercenary for warring kinases in the egg. Proc. Natl. Acad. Sci. USA *104*, 17245–17246.

Kovacovicova K, Awadova T, Mikel P, Anger M. In Vitro Maturation of Mouse Oocytes Increases the Level of Kif11/Eg5 on Meiosis II Spindles. Biol Reprod. 2016

Impact Factor/Quartile: 3,184/Q1
Times cited (Wos May 2019): 3
Significance: Report demonstrates important functional differences between *in vitro* and *in vivo* cells.
Contribution of the author: Experimental design, interpretation of experiments manuscript preparation, securing funding

BIOLOGY OF REPRODUCTION (2016) 95(1):18, 1–9
Published online before print 4 May 2016.
DOI 10.1095/biolreprod.115.133900

In Vitro Maturation of Mouse Oocytes Increases the Level of Kif11/Eg5 on Meiosis II Spindles[1]

Kristina Kovacovicova,[3,4] Thuraya Awadova,[3] Pavel Mikel,[3] and Martin Anger[2,3,4]

[3]*Veterinary Research Institute, Brno, Czech Republic*
[4]*Faculty of Medicine, Department of Histology and Embryology, Masaryk University, Brno, Czech Republic*

ABSTRACT

Although in vitro maturation (IVM) of oocytes has been used for a relatively long time, during which the culture conditions have improved remarkably, the resulting germ cells are still not fully comparable to the cells obtained from the ovary in many important aspects, namely in fertilization rate and subsequent embryonic development. Some of the differences between IVM and in vivo maturation (IVV) oocytes were already discovered, including variability in spindle assembly and morphology. In this study we focused on a role of molecular motor Kif11 (hereafter referred to as Eg5) in maintaining bipolar spindle structure in IVM and IVV oocytes. Our experiments revealed that in IVM oocytes, Eg5 is abundant on meiosis II spindle, which makes these cells more sensitive to Eg5 inhibition than IVV oocytes. We further demonstrate that this sensitivity is acquired gradually with exposure to the in vitro conditions. This is a remarkable difference in function of spindle apparatus between IVM and IVV oocytes, and we believe our results are important not only for understanding of the chromosome segregation in mammalian oocytes but also because they indicate cells are using alternative pathways to achieve the same function when exposed to different conditions.

Eg5, germ cells, in vitro maturation, Kif11, meiosis, oocyte maturation, spindle

INTRODUCTION

Fully grown, mitotically competent mammalian oocytes are capable of resuming and completing both meiotic divisions in vitro [1]. However, the data from several species demonstrate that the fertilization rate and the developmental capacity of in vitro maturation (IVM) oocytes are lower than those of in vivo maturation (IVV) oocytes [2–5]. It seems that the impact of IVM on the quality of female gametes is quite complex, affecting multiple processes and events, including gene expression and epigenetic profile [5–8], distribution of cortical granules [9], size of the polar body [10, 11], structure of the zona pellucida [12], polarity of granulosa cells [13], and position of the spindle [14]. A typical example of the subcellular structure that seems to be particularly sensitive to the IVM conditions is the spindle. Thanks to the effort of several laboratories, we already know that the morphological parameters of the spindle, including its dimensions and volume, are affected in IVM oocytes [10, 11, 15–18]. Moreover, from the same experiments, we also know that the important molecular characteristics, including level of acetylation of the microtubules, distribution of γ-tubulin, and the number of microtubule organizing centers are also changed in IVM oocytes in comparison to those in cells obtained from the ovary.

In our study, we focused on functional characterization of meiosis II (MII) spindles in IVM and IVV oocytes. Our data uncovered functional changes introduced by IVM, namely the higher demand for Eg5 in maintaining bipolar spindles in IVM oocytes, which are not only very important for our understanding of chromosome segregation in mammalian female germ cells but have crucial implications for in vitro manipulation of germ cells used in human and animal reproduction.

MATERIALS AND METHODS

Animals

CD-1 mice were purchased from Animal Breeding and Experimental Facility, Faculty of Medicine, Masaryk University, Czech Republic. Bl/6 and MF1 mice were purchased from Anlab (Czech Republic). CD-1/BDF1 female mice were obtained from crossing CD1 females and BDF1 males (Anlab, Czech Republic). All animal work was conducted according to Act number 246/1992 Coll., under the protection of animals against cruelty under supervision of Central Commission for Animal Welfare, approval IDs 1285/2011, 1504/2013, and 1566/2014.

Mouse Stimulation, Oocyte Collection, and Maturation

All experiments were performed using 9- to 20-wk-old animals. Germinal vesicle (GV) stage oocytes were collected from ovaries in M2 medium (Sigma-Aldrich) containing 100 μM 3-isobutyl-1methylxantine (IBMX; Sigma-Aldrich). Cells were cultured in M16 medium (Sigma-Aldrich) supplemented with IBMX and covered with mineral oil (Sigma-Aldrich) for 1 h at 37°C in the presence of 5% CO_2. Only oocytes, which achieved GV breakdown (GVBD) within 90 min after removal of IBMX from the medium, were used for experiments. All experiments were performed using MI and MII stage oocytes, which were obtained from mice previously stimulated with 5 IU of gonadotropin from equine chorionic gonadotropin (eCG; Sigma-Aldrich), followed 44–48 h later by stimulation with 5 IU of human chorionic gonadotropin (hCG, Sigma-Aldrich). Oocytes were collected by manual rupturing of Graafian follicles in M2 medium at 6 h (MI stage) or from the ampulla at 12, 14, 16, or 18 h post-hCG administration (MII stage). The cumulus cells were removed by gentle pipetting in M2 medium with hyaluronidase (150 IU/ml; Sigma-Aldrich). Cells were subsequently cultured in M16 medium and covered with mineral oil under the standard conditions.

Microinjection

GV stage and MII stage oocytes were cultured in M16 medium (Merck Millipore) prior to microinjection. Microinjection was performed in M2 medium supplemented with IBMX (GV stage) or without inhibitors (MII stage)

[1]Supported by Czech Science Foundation project P502/12/2201 and Ministry of Education, Youth and Sports of the Czech Republic projects CEITEC 2020 (LQ1601) and LH 13072–Kontakt II.
[2]Correspondence: Martin Anger, Veterinary Research Institute, Hudcova 70, 621 00 Brno, Czech Republic. E-mail: anger@vri.cz

Received: 29 July 2015.
First decision: 3 September 2015.
Accepted: 2 May 2016.

eISSN: 1529-7268 http://www.biolreprod.org
ISSN: 0006-3363

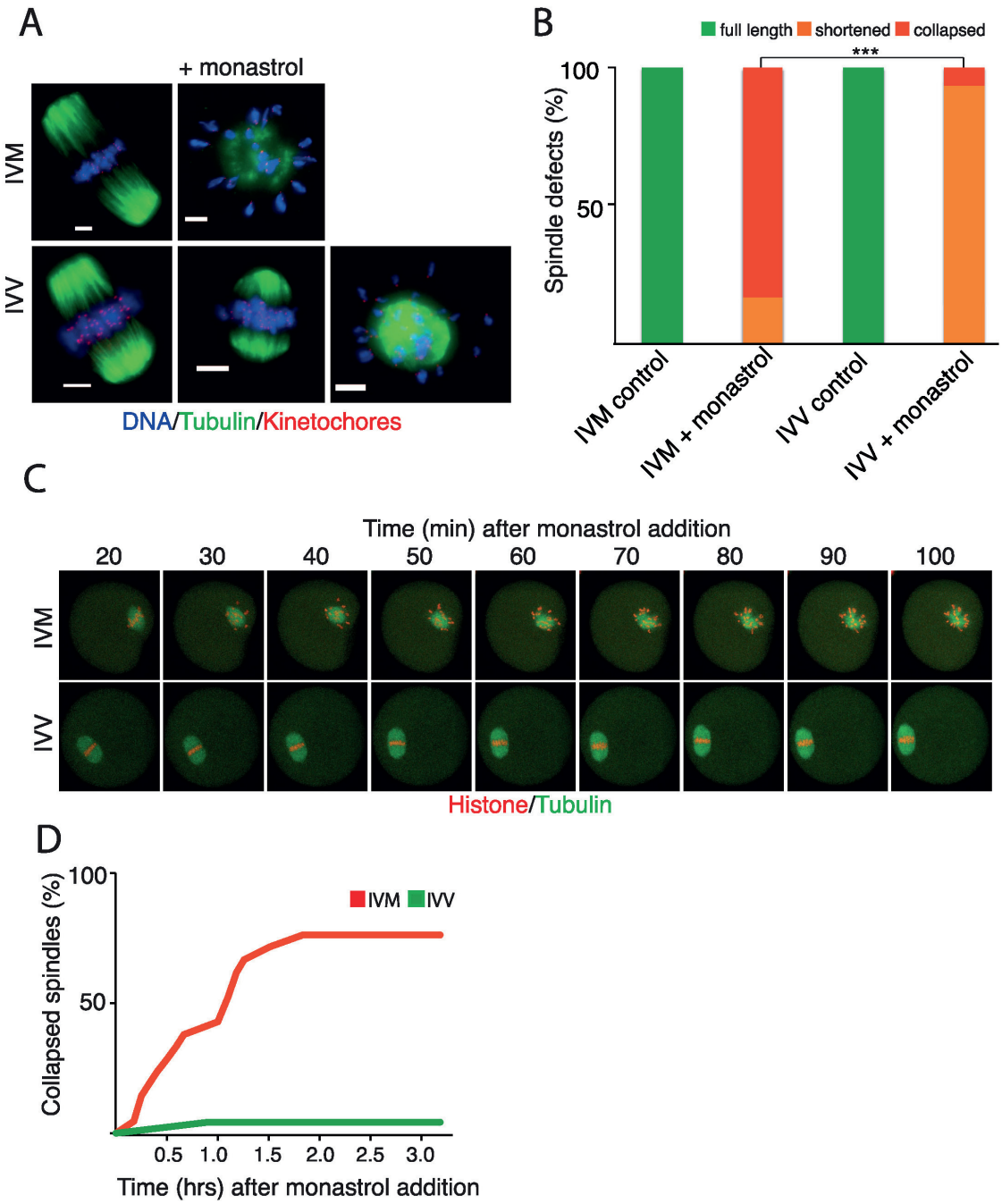

FIG. 1. The effect of monastrol on IVM and IVV oocytes. **A**) Spindles of IVM (upper panel) and IVV (lower panel) oocytes stained for DNA (blue [DAPI]), microtubules (green [α-tubulin-specific antibody]) and kinetochores (red [CREST]). Left and right panels show meiosis II spindles of IVM and IVV oocytes before and after exposure, respectively, to 100 μM monastrol for 2 h. The scale represents 5 μm. **B**) Quantification of spindle defects (from three independent experiments) in control IVM oocytes (n = 62), in IVM oocytes exposed for 2 h to 100 μM monastrol (n = 86), in control IVV oocytes (n = 63), and in IVV oocytes exposed for 2 h to 100 μM monastrol (n = 79). Spindles were scored as full length (green bars), shortened (orange bars), or collapsed (red bars). Differences between the number of collapsed spindles between IVM and IVV oocytes exposed to monastrol are statistically significant (***$P <$

by using an I10 microinjector (Narishige) on a model DM IL inverted microscope (Leica). Complementary RNAs for microinjection encoding open reading frames (ORF) of mouse kinesin 5, β-tubulin, and H2B fused with the fluorescent proteins CFP, Venus, and mCherry were prepared by in vitro transcription and polyadenylation, using an mMESSAGE mMACHINE T3 transcription kit and poly(A) tailing kit (Life Technologies). After microinjection, oocytes were cultured at 37°C in the presence of 5% CO_2. In the rescue experiments, cells were microinjected in the presence of 100 μM monastrol (Sigma-Aldrich).

Live-Cell Imaging

Two hours after microinjection, oocytes were transferred to an SP5 confocal microscope (Leica), equipped with an incubator (EMBL), allowing time-lapse documentation of experiments in the presence of 5% CO_2 at 37°C. Settings of excitation wavelengths 415, 488, and 561 nm; an HCX plan apochromat ×40/1.1 water, numerical aperture 1.1 objective; and hybrid detectors were used for detection of CFP, Venus, and mCherry signals. Typically, the pixel size of acquired images was 191.3 μm, and the *z*-resolution was 2.01 μm. For all live-cell imaging experiments, 200 μM monastrol was used.

Kinetochore-Counting Assay and Immunofluorescence Staining

The immunofluorescence protocol and kinetochore-counting assay were modified from Duncan et al. [19] and Sebestova et al. [20]. At 20 h after GVBD, MII stage oocytes were selected and incubated in M16 medium with 100 μM monastrol (Sigma-Aldrich) for 2 h at 37°C and 5% CO_2. For analysis of cold-stable microtubules, the protocol from Lane et al. [21] was adopted. In certain experiments, 100 μM nocodazole (Sigma-Aldrich) was used to disrupt spindles for 30 min.

For immunostaining, cells were fixed with 2% paraformaldehyde (Sigma-Aldrich) in phosphate-buffered saline (PBS; 0.140 M NaCl, 0.005 M KCl, 0.010 M Na_2HPO_4, and 0.002 M KH_2PO_4) for 20 min; permeabilized with 0.5% Triton X-100 (Sigma-Aldrich) in PBS for 20 min; and blocked for 30 min at room temperature. The following antibodies were used: human anticentromere antibody (1:500 dilution; ImmunoVision), mouse antiacetylated α-tubulin (1:500 dilution; Sigma-Aldrich), rabbit anti-Eg5 (1:250 dilution; Novus Biologicals), Alexa Fluor 488 or 568 goat anti-mouse secondary antibody (1:500 dilution; Invitrogen, Life Technologies), Alexa Fluor 488 goat anti-rabbit secondary antibody (1:500 dilution; Invitrogen Life Technologies), and Alexa Flour 555 or 647 goat anti-human secondary antibody (1:500 dilution; Invitrogen Life Technologies). Vectashield with 4′,6-diamidino-2-phenylindole (DAPI; Vector Laboratories) was used for mounting. The oocytes were scanned using an AF6000 inverted fluorescence microscope with HCX plan apochromat ×100 1.4-0.7 oil objective with numerical aperture of 1.4 and Microsystems camera model DFC365FX (Leica). Filter cubes A (excitation filter BP 360/40), green fluorescent protein (GFP; excitation filter BP 470/40), and dsRed ET (excitation filter BP 546/11) were used for detection of DAPI, Alexa Fluor 488, and Alexa Fluor 555. The *x*–*y* resolution of images was 92 nm, and LAS AF software was used to achieve optimal *z*-resolution. For measurement of interkinetochore distances, the chromosomes were stained by DAPI in PBS, and cells were scanned using an SP5 confocal microscope equipped with HCX plan apochromat ×40/1.1 water objective with numerical aperture of 1.1 (Leica), in drops of PBS covered with mineral oil. For detection of DAPI and antibodies labeled with Alexa Fluore 488, 555, 568, or 647 excitation, wavelengths of 405, 488, 561, and 631 nm were used. The pixel size ranged from 50.3 to 113.3 nm, and the *z*-resolution was set to 0.2 μm to obtain proper resolution for three-dimensional (3D) reconstruction. For this measurement, only the cells with spindle axis parallel to the scanning plane were scanned to avoid the changes introduced by rotation of the spindle and chromosomes.

Image Analysis

Data analysis was performed using ImageJ (ImageJ, U.S. National Institutes of Health, http://imagej.nih.gov/ij), LAS AF (http://www.leica-microsystems.com), and Imaris software (www.bitplane.com). The interkinetochore distance was measured in 3D as the distance between the central mass of two sister kinetochores signals. For counting of kinetochores, measurement of spindle length and quantification of tubulin density, the same software tools were used.

Isolation of RNA and mRNA Quantification

Total RNA was extracted from 50 oocytes per group using Trizol (Life Technologies) and standard protocol. Prior to RNA isolation, in vitro transcribed EGFP cRNA was added (0.25 ng) to each group, which was later used as an external control for RNA recovery and normalization of the quantitative PCR (qPCR) data. Complementary DNA (cDNA) synthesis was performed using random hexamers and Supescript III first-strand synthesis SuperMix (Life Technologies). qPCR was performed using Kapa SYBR Fast MasterMix (Kapa Biosystems) in a LightCycler model 480 unit (Roche). Each reaction was performed in triplicate and repeated twice. The following primers were used for detection of EGFP, TTCAAGATCCGCCACAACATCG and GACTGGGTGCTCAGGTAGTGG; and Eg5 was detected using primers ACCTCCAAGAAAACATACACGTT and CGAAGATGGTGCAATTA TAGCCC.

Statistical Analysis

Statistical analysis was performed using Prism version 5.00 software (GraphPad Software) for Macintosh (Apple). The statistical significance of the difference between control and experimental group was tested using Mann-Whitney *U*-test, one-way ANOVA, and chi-square test for categorical data, respectively.

RESULTS

Different Effect of Eg5 Inhibition on MII Spindles in IVM and IVV Oocytes

In order to study the effect of IVM on the MII spindle, IVM and IVV oocytes were exposed to monastrol, an inhibitor of the molecular motor Eg5, which is essential for bipolar spindle maintenance in oocytes [22]. Monastrol was frequently used for the purpose of disruption of bipolar spindles in oocytes [19, 23, 24]. For this experiment, we used IVM cells matured for 20 h in the incubator, whereas the IVV oocytes were isolated for 18 h after hCG stimulation from the oviduct. The reason for this time difference is the accelerated MI in IVV oocytes (Supplemental Fig. S1A; all supplemental data are available online at www.biolreprod.org). Scoring GVBD in oocytes in the ovary following hCG stimulation showed that the resumption of meiosis starts between 2 and 3 h after hormonal stimulation, and most cells extrude their polar bodies (PBE) between 9.5 and 11.5 h after hCG stimulation. A majority of IVM oocytes resumed meiosis within 90 min after IBMX removal from the medium and achieved PBE between 8 and 11 h. Aligning IVM and IVV oocytes to the time of GVBD showed that PBE in IVV oocytes is accelerated in comparison to that in IVM oocytes by 2–3 h, and therefore, for our experiments we used 20-h IVM oocytes and 18-h IVV oocytes. Both groups of cells were exposed to 100 μM monastrol for 2 h. To our surprise, we noticed that the sensitivity to monastrol depended on whether oocytes matured in vitro or in vivo (Fig. 1, A–D, Supplemental Movies S1 and S2). Upon exposure to the same levels of the inhibitor in the maturation media, spindles in 83.15% of the IVM oocytes collapsed and remained bipolar in 16.85% of oocytes, although their length was clearly shorter (Fig. 1, A, upper panel, and B). In contrast, 93.42% of the spindles in IVV oocytes were shorter than the controls, and

0.0001). **C**) Movie frames represent IVM (upper panels) and IVV (lower panels) oocytes after exposure to monastrol. Frames show times from 20 to 100 min after exposure to the inhibitor. Oocytes were injected with cRNAs encoding histone H2B (red) and tubulin (green) fused to fluorescent proteins prior to live-cell-imaging assay. **D**) Chart summarizing results from three independent experiments shows dynamics of the spindle collapse in IVM (red line [n = 21]) and IVV (green line [n = 24]) oocytes after exposure to 200 μM monastrol (time in h).

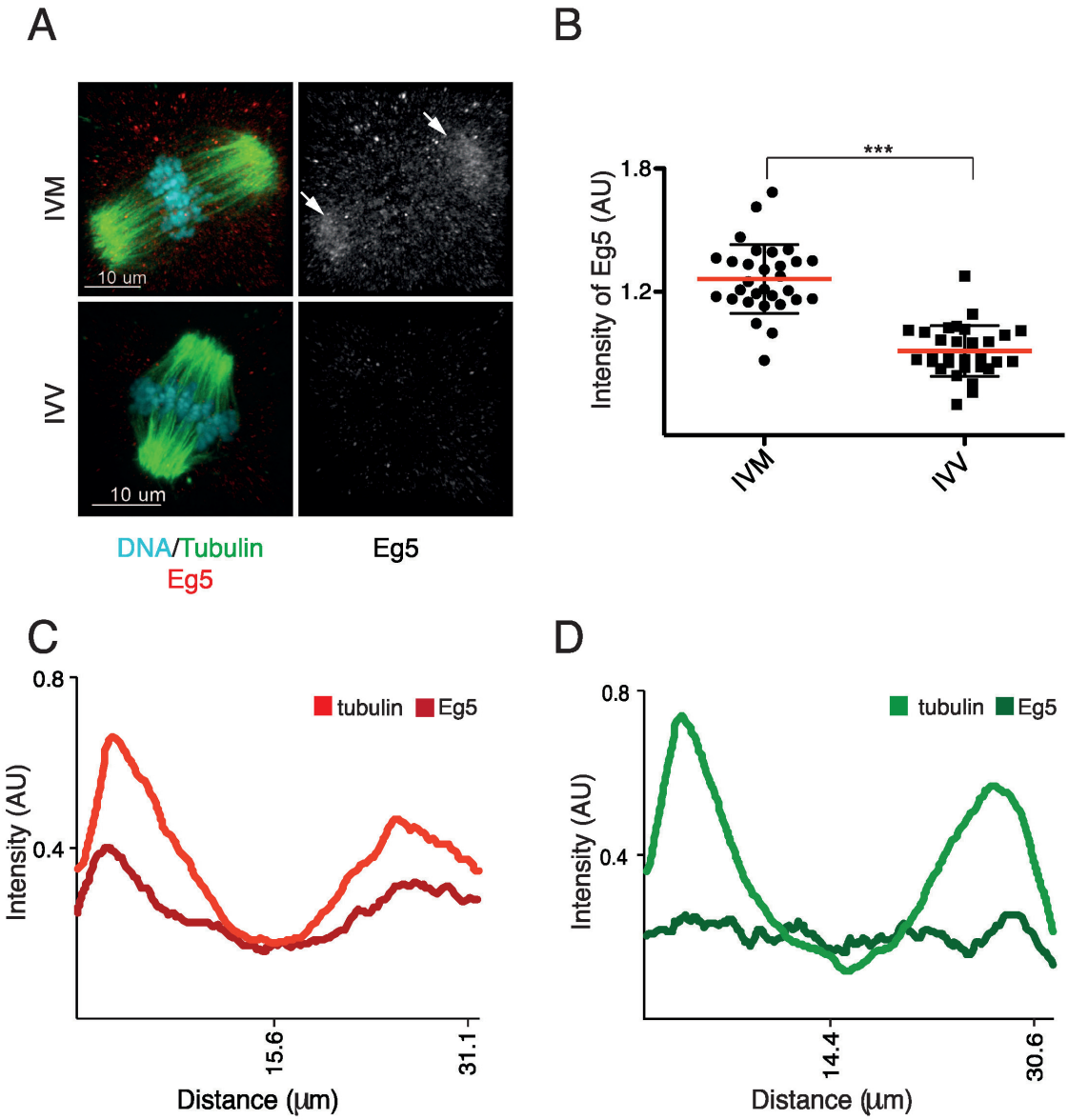

FIG. 2. The accumulation of Eg5 on meiosis II spindles in IVM oocytes. **A**) Representative images of IVM (upper panel) and IVV (lower panel) oocytes. Cells were fixed after 20 h of IVM or 18 h after hCG administration. The α-acetylated tubulin (green), Eg5 (red/gray [arrows in IVM oocyte]) and DNA (cyan) were stained. **B**) Relative level of Eg5 fluorescence signal in the area of the spindle in IVM (n = 30) and IVV (n = 30) oocytes. Differences between groups are significant (***$P < 0.0001$); data were collected from three independent experiments. **C**) The average profiles of tubulin (bright red) and Eg5 (dark red) in IVM meiosis II (n = 26) oocytes are shown. Lines represent average curves. Signal was measured in the middle slice of each spindle, which was parallel to the plane of observation. **D**) The average profiles of tubulin (bright green) and Eg5 (dark green) in IVV meiosis II oocytes (n = 19) were measured as in **C**. Experiments in **C** and **D** were repeated three times.

only 6.58% collapsed (Fig. 1, A, lower panel, and B). Importantly, in both groups, no cells whose spindle lengths were similar to those of control (full length spindles) were observed after the exposure to monastrol. In order to analyze the dynamics of the spindle collapse, metaphase II IVV and IVM oocytes were injected with cRNAs encoding histone H2B and tubulin fused to fluorescent proteins [20]. Cells were subsequently exposed to monastrol, and time-lapse images were recorded (Fig. 1C and Supplemental Movies S1 and S2). Stacks of images were acquired every 5 min, and image

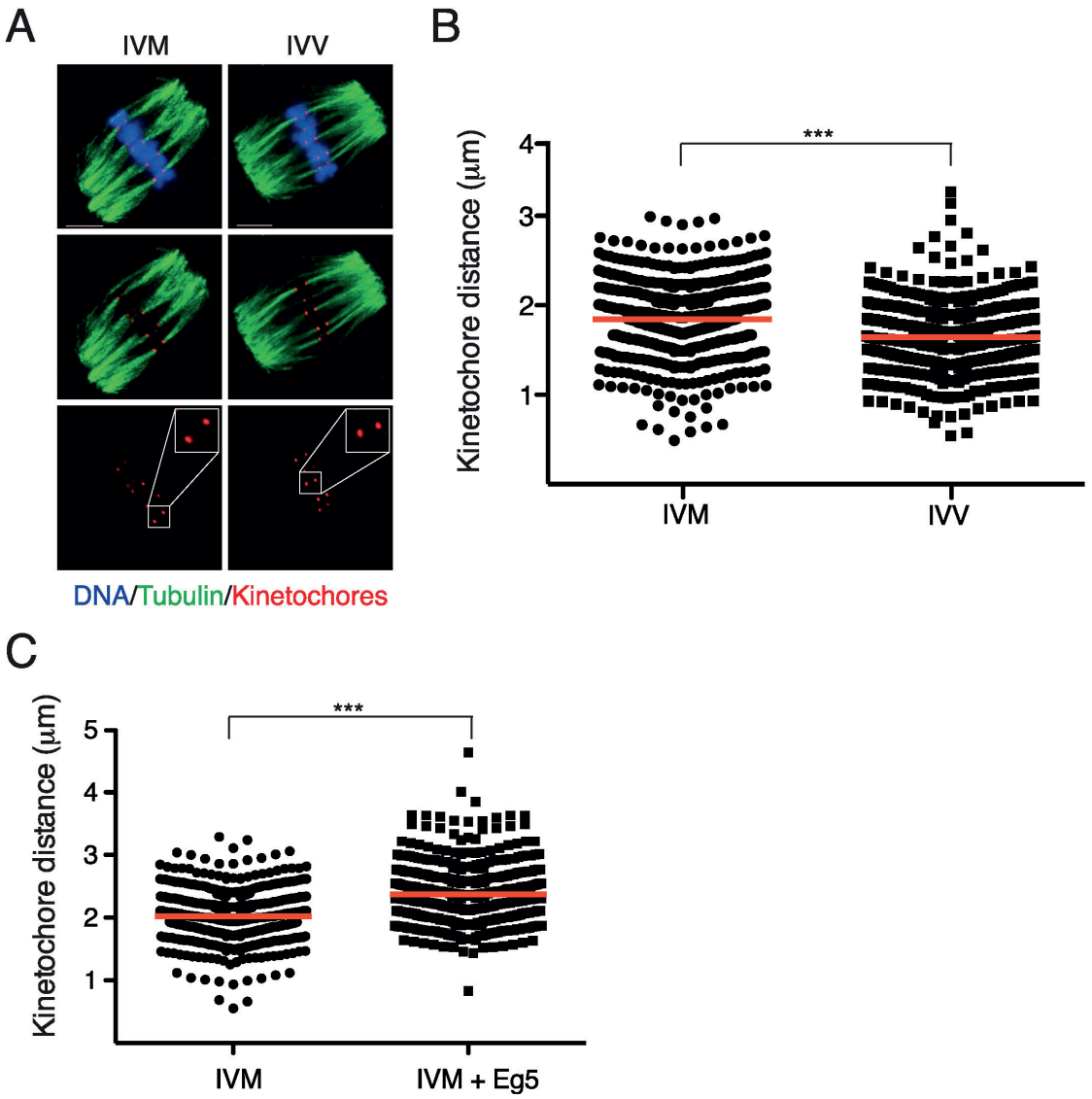

FIG. 3. In vitro maturation conditions and Eg5 overexpression affect the interkinetochore distances in oocytes. **A**) IVM (left panel) and IVV (right panel) oocytes were stained for DNA (blue [DAPI]), microtubules (green [α-tubulin-specific antibody]), and kinetochores (red [CREST]). Magnification of a typical pair of sister kinetochores in IVM and IVV oocytes (lower panel) is shown. **B**) Distances between sister kinetochores in IVM (1.83 μm [n = 300]) and IVV (1.57 μm [n = 300]) oocytes are plotted. Measurements represent distances between the centers of maximal density of kinetochore signals, and the differences between groups are significant ($P < 0.0001$). Data were collected from three independent experiments. **C**) The effect of Eg5 overexpression on the distances between sister kinetochores in IVM oocytes (2.023 ± 0.3848 μm [n = 240]) and in IVM oocytes microinjected with Eg5 cRNA (IVM+Eg5) (2.371 ± 0.4577 μm [n = 220]) are shown. Data were obtained from three independent experiments, and the differences between groups are significant (***$P < 0.0001$).

analysis showed a quite rapid effect on the spindle (Fig. 1, C and D). The differences between IVV and IVM oocytes were significant ($P < 0.0001$), and, although the effect of monastrol was visible almost instantly in some cells, the proportion between shortened and collapsed spindles in IVM oocytes stabilized within the first 2 h (Fig. 1D). To exclude the possibility that the resistance to monastrol in IVV oocytes was due to the hormonal stimulation, we compared the dynamics of the response to monastrol in IVM oocytes with and without eCG stimulation and found no effect (data not shown). We also tested earlier time intervals, 12, 14, and 16 h, in order to determine whether the sensitivity to monastrol in IVM oocytes

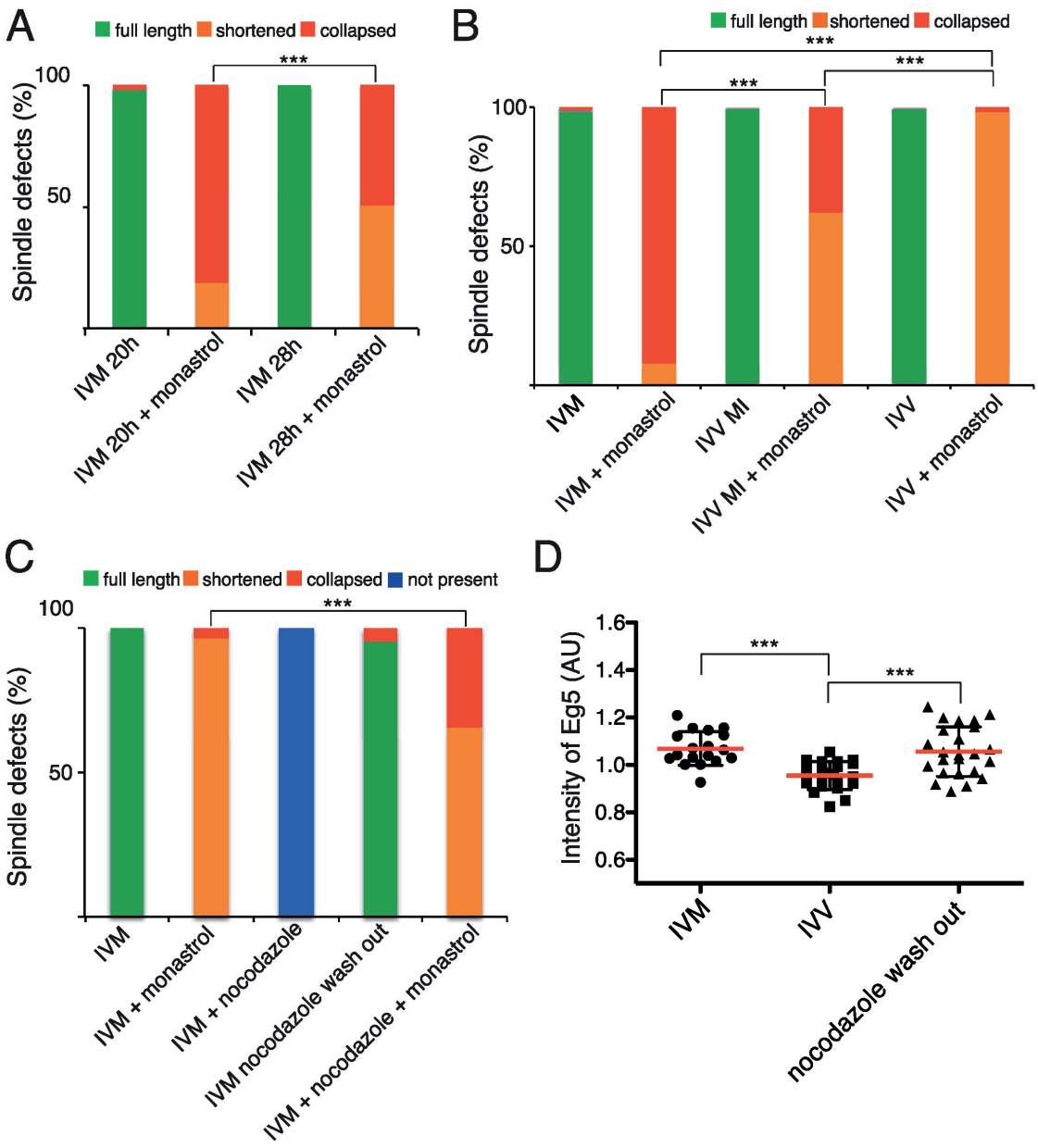

FIG. 4. Sensitivity to monastrol depends on duration of IVM and decreases with its duration. **A**) The following groups of IVM oocytes were processed for DNA α-acetylated tubulin and CREST staining and were subsequently scored for spindle defects: IVM oocytes for 20 h in maturation (n = 51); IVM oocytes for 20 h in maturation plus 2 h in 100 μM monastrol (n = 53); IVM oocytes 28 h in maturation (n = 57); and IVM oocytes for 28 h in maturation plus 2 h in 100 μM monastrol (n = 59). Full-length (green bars), shortened (orange bars), and collapsed (red bars) spindles were counted. The proportion of cells with collapsed spindles is significantly different between the eggs matured for 20 h and those matured for 28 h prior to monastrol exposure ($P = 0.0004$) in all three independent experiments. **B**) The following groups of IVM and IVV oocytes were processed for DNA, tubulin, and CREST staining and scored for spindle defects: IVM oocytes 20 h in maturation (n = 98); IVM oocytes for 20 h in maturation plus 2 h in 100 μM monastrol (n = 103); MI IVV oocytes isolated 6 h after hCG and then cultured for 12 h in vitro (n = 109); MI IVV oocytes isolated 6 h after hCG and cultured for 12 h in vitro and then for 2 h in 100 μM monastrol (n = 98); IVV oocytes isolated for 20 h after hCG (n = 101); and IVV oocytes isolated for 20 h after hCG and cultured for 2 h in 100 μM monastrol (n = 110). Full-length (green bars), shortened (orange bars), and collapsed (red bars) spindles were scored, results showed significant differences between groups ($P < 0.0001$), and data were collected from four independent experiments. **C**) The scoring of spindle defects in following groups: IVV control oocytes (n = 55); IVV oocytes exposed to 100 μM monastrol (n = 56); IVV oocytes treated with 100 μM nocodazole (n = 45); IVV oocytes treated with nocodazole for 30 min and then washed into M16 medium for 2 h (n = 44); and IVV oocytes treated with nocodazole, washed into clean medium for

at 20 h post-hCG was not a consequence of in vitro aging (Supplemental Fig. S1B). Our data also showed that, in these earlier intervals, the difference in sensitivity to monastrol between IVM and IVV oocytes was significant. Likewise, we tested two other mouse laboratory strains, MF1 and Bl6, and the results showed that the differences in sensitivity to monastrol between IVM and IVV oocytes was not restricted to CD-1 strain (Supplemental Fig. S1C).

Eg5 Accumulates on IVM Spindles

We aimed to determine whether the variability in sensitivity to monastrol between IVM and IVV oocytes was caused by different amounts of Eg5 on their spindles. IVM (20-h) and IVV (18-h) oocytes were obtained as described previously, and Eg5 was detected with specific antibody. The quantification of the total amount of the protein in the whole area of the spindle showed significantly higher levels of Eg5 in IVM oocytes than in IVV oocytes (Fig. 2, A and B) with distribution to the spindle poles in IVM oocytes (Fig. 2, C and D). We also analyzed the accumulation of the Eg5 protein on the spindle in oocytes in earlier time intervals, 12, 14, and 16 h (Supplemental Fig. S1D). The results were consistent with our previous results showing significant difference in Eg5 accumulation on MII spindles between IVM and IVV oocytes. To analyze whether the accumulation of Eg5 protein on spindles in IVM oocytes is caused by recruitment of this molecule from cytoplasm or whether the total level of this molecule is higher in IVM oocyte, we used qPCR and measured the level of Eg5 mRNA in both groups. Our results showed that the relative expression of Eg5 was similar between IVM and IVV oocytes at 12 h. Later, at 18 h, the level of Eg5 transcript was significantly higher in IVM oocytes than in IVV oocytes (Supplemental Fig. S1E).

Sister Kinetochores Are Farther Apart in IVM Oocytes

In order to capture subtle differences in morphology of the spindle, which might escape detection using standard procedures, we used modified immunofluorescence protocol and oocytes were scanned in drops of PBS without mounting and compressing them between glass slides. This allowed preservation of the unperturbed 3D structure of the spindle. For measurement, we used only cells in which the longitudinal spindle axis was parallel with the focal plane. Data obtained using this technique revealed that, although the length of the IVM and IVV MII spindles was similar (data not shown), the distances between sister kinetochores were extended in IVM oocytes (1.85 ± 0.37 μm) compared to those in IVV oocytes (1.64 ± 0.34 μm) (Fig. 3, A and B). In theory, forces pulling more strongly on spindle microtubules, conveyed to the kinetochore via kinetochore fibers [25], may generate this extension, and because the Eg5 is responsible for elongation of the spindle, we tested the effect of its overexpression on interkinetochore distances. IVM oocytes were matured for 18 h, and then half of them were injected with cRNA encoding Eg5. After 2 h of culture, cells were immunostained and scanned using confocal microscopy. The distances between sister kinetochores were measured as before. Our results showed that the overexpression of Eg5 increases distances between sister kinetochores (2.37 ± 0.46 μm) (Fig. 3C), which is consistent with the increased interkinetochore distances observed in IVM oocytes in our previous experiments, as these also have more Eg5 on the spindle than IVV oocytes do. It is, however, important to mention that the overexpression of Eg5 also increased the total length of the spindle (Supplemental Fig. S1F).

Sensitivity to Monastrol in IVM Oocytes Is Acquired Gradually and Decreases With Prolonged Culture

In order to establish whether the sensitivity to monastrol is changing with time of in vitro culture, IVM oocytes were exposed to monastrol at 20 and 28 h. At 20 h, 81.13% of IVM cells showed collapsed spindles, but 8 h later, this number was reduced to 49.15% (Fig. 4A). This demonstrated that, during prolonged in vitro culture, molecular composition of the MII spindle is changing and that the spindles became more resistant to monastrol. Next we aimed to determine when during meiosis the sensitivity to monastrol is acquired. We therefore compared usual groups of IVM and IVV oocytes with oocytes isolated from the ovaries 6 h after hCG administration at MI stage (IVV MI group). These oocytes were subsequently cultured in vitro for 12 h. All three groups were exposed to monastrol and scored for spindle phenotypes (Fig. 4B). Oocytes initially matured in vivo, and then isolated and cultured in vitro had spindles collapsed in 37.75% of cells, whereas 92.23% of IVM and 1.81% of IVV oocytes had spindles collapsed. The phenotype of IVV MI group was between IVV and IVM groups, indicating that the degree of monastrol sensitivity is dependent on duration of the exposure to the IVM conditions.

Forced Reassembly of the Meiosis II Spindle Renders IVV Oocytes Sensitive to Monastrol

To test whether a higher concentration of Eg5 protein on the spindle and increased sensitivity to monastrol is a direct consequence of assembly of the spindle in vitro, we used IVV oocytes isolated as described previously and forced them to rebuild the spindle in vitro by transiently depolymerizing spindle microtubules. In preliminary experiments, we determined that exposure of cells to 100 μM nocodazole for 30 min was sufficient to destabilize spindle microtubules (data not shown). After removal of the nocodazole from the medium, almost all oocytes reestablished their spindles within 2 h (data not shown). Oocytes with reassembled spindles were then exposed to 100 μM monastrol for 2 h and then fixed for scoring spindle defects. Some cells with reassembled spindles were used for the analysis of Eg5 protein levels without prior exposure to monastrol. Our results showed that IVV oocytes, which were forced to reassemble their spindles in vitro, are not only more sensitive to monastrol (Fig. 4C) but they also accumulate more Eg5 on their spindles, with levels similar to those of IVM oocytes (Fig. 4D).

DISCUSSION

Our results revealed an important difference in the molecular composition of the spindle between mouse oocytes matured in vitro and those which underwent first meiotic

2 h and subsequently exposed to 100 μM monastrol. Full-length (green), shortened (orange), collapsed (red), and not-present (blue) spindles were scored. The frequency of collapsed spindles in IVV oocytes and IVV oocytes after reestablishing the spindle in vitro conditions after monastrol treatment was significantly different ($P < 0.0001$); data were collected from three independent experiments. **D**) Relative quantification of Eg5 in the spindle area in IVM (n = 22) and IVV (n = 27) oocytes and in IVV oocytes after reestablishing the spindle (n = 28). Results were obtained from three independent experiments; the differences between groups (arrows) are statistically significant (***$P < 0.0001$).

division in the ovary. This difference, together with the data published by other laboratories, which demonstrated the differences in number and distribution of microtubule organizing centers between IVM and IVV oocytes [11, 15], emphasizes the profound changes in spindle assembly and maintenance caused by the exposure of oocytes to in vitro conditions. The currently accepted model describes the bipolar spindle as a result of equilibrium of various forces, including those produced by molecular motors [25, 26]. In respect to the formation of the bipolar spindle, the central role belongs to Eg5 molecular motor, which is capable of crosslinking and sliding antiparallel microtubules, thereby pushing the spindle poles outward [27]. Eg5 is an essential gene, and its disruption causes perturbation of the development with early embryonic lethality [28, 29]. It seems that in most model systems the role of Eg5 in the assembly of the spindle was firmly established; however, its further participation in the maintenance of the bipolar spindle appears to be more controversial [30–33]. In contrast, in mammalian oocytes, it was clearly shown that the Eg5 activity is required not only for assembling the spindle [23, 34, 35] but also for maintaining its bipolar character and poleward tubulin flux [22] and for spindle elongation during anaphase [22, 36]. The importance of Eg5 declines with the progression of the embryonic development, and cells in blastocysts are only partially sensitive to Eg5 inhibitors [22]. All this demonstrates that Eg5 plays a particularly important role in oocytes and early embryos. Our finding demonstrated that the spindles of IVM oocytes contain significantly more Eg5 and that they are also more sensitive to Eg5-specific inhibitor monastrol. Both of these results indicate that the IVM conditions are affecting an essential functional characteristic of the spindle and also that the bipolarity of the spindle in IVV oocytes must be achieved by a molecular mechanism less dependent on Eg5. However, the molecular components of this pathway remain to be elucidated. Quantification of *Eg5* mRNA showed elevated expression of *Eg5* mRNA in IVM oocytes at 18 h. This might be responsible for the differences in Eg5 protein levels on IVM and IVV spindles. However, we also showed that IVV oocytes forced by nocodazole to reassemble their spindles in vitro showed both characteristics of spindles assembled in IVM oocytes, namely elevated levels of Eg5 on the spindle and increased sensitivity to monastrol. Also, the Eg5 is accumulated at the spindle in IVM oocytes significantly more in 12 h, when, according to our qPCR results, the expression of mRNA is similar in both groups. Therefore, it needs to be determined whether the elevated Eg5 transcription or some other factors are responsible for the changes of pathways controlling spindle bipolarity in IVM oocytes. In conclusion, we revealed an important difference between IVM and IVV oocytes. The spindle apparatus controls the final distribution of the chromosomes between the egg and the polar body. Because the chromosome division in oocytes is frequently incorrect [37], it is also important to consider that the spindle assembly and maintenance in cells cultured in vitro are altered in comparison to in vivo cells. Major changes to the important pathways, such as the maintenance of spindle bipolarity, are likely to have an effect on the genetic integrity of gametes. It remains to be addressed whether similar differences between IVM and IVV oocytes could be also observed in other species, namely in human and other large mammals. It is quite important since in human assisted reproductive technologies (ART) as well as in techniques used in assisted animal reproduction IVM of gametes is frequently used.

ACKNOWLEDGMENT

We are thankful to all members of Martin Angers' laboratory staff for their comments and to Marie-Helene Verlhac, Keith Jones, and Greg Fitzharris for their stimulating discussion during presentation at the meeting.

REFERENCES

1. Edwards RG. Maturation in vitro of mouse, sheep, cow, pig, rhesus monkey and human ovarian oocytes. Nature 1965; 208:349–351.
2. Leibfried-Rutledge ML, Critser ES, Eyestone WH, Northey DL, First NL. Development potential of bovine oocytes matured in vitro or in vivo. Biol Reprod 1987; 36:376–383.
3. Laurincik J, Rath D, Niemann H. Differences in pronucleus formation and first cleavage following in vitro fertilization between pig oocytes matured in vivo and in vitro. J Reprod Fertil 1994; 102:277–284.
4. Trounson A, Anderiesz C, Jones G. Maturation of human oocytes in vitro and their developmental competence. Reproduction 2001; 121:51–75.
5. Kim DH, Ko DS, Lee HC, Lee HJ, Park WI, Kim SS, Park JK, Yang BC, Park SB, Chang WK, Lee HT. Comparison of maturation, fertilization, development, and gene expression of mouse oocytes grown in vitro and in vivo. J Assist Reprod Genet 2004; 21:233–240.
6. Jones GM, Cram DS, Song B, Magli MC, Gianaroli L, Lacham-Kaplan O, Findlay JK, Jenkin G, Trounson AO. Gene expression profiling of human oocytes following in vivo or in vitro maturation. Hum Reprod 2008; 23: 1138–1144.
7. Katz-Jaffe MG, McCallie BR, Preis KA, Filipovits J, Gardner DK. Transcriptome analysis of in vivo and in vitro matured bovine MII oocytes. Theriogenology 2009; 71:939–946.
8. Franciosi F, Lodde V, Goudet G, Duchamp G, Deleuze S, Douet C, Tessaro I, Luciano AM. Changes in histone H4 acetylation during in vivo versus in vitro maturation of equine oocytes. Mol Hum Reprod 2012; 18: 243–252.
9. Liu XY, Mal SF, Miao DQ, Liu DJ, Bao S, Tan JH. Cortical granules behave differently in mouse oocytes matured under different conditions. Hum Reprod 2005; 20:3402–3413.
10. Ibanez E, Sanfins A, Combelles CM, Overstrom EW, Albertini DF. Genetic strain variations in the metaphase-II phenotype of mouse oocytes matured in vivo or in vitro. Reproduction 2005; 130:845–855.
11. Barrett SL, Albertini DF. Allocation of gamma-tubulin between oocyte cortex and meiotic spindle influences asymmetric cytokinesis in the mouse oocyte. Biol Reprod 2007; 76:949–957.
12. Funahashi H, Ekwall H, Rodriguez-Martinez H. Zona reaction in porcine oocytes fertilized in vivo and in vitro as seen with scanning electron microscopy. Biol Reprod 2000; 63:1437–1442.
13. Plancha CE, Sanfins A, Rodrigues P, Albertini D. Cell polarity during folliculogenesis and oogenesis. Reprod Biomed Online 2005; 10:478–484.
14. Moon JH, Jee BC, Ku SY, Suh CS, Kim SH, Choi YM, Kim JG, Moon SY. Spindle positions and their distributions in in vivo and in vitro matured mouse oocytes. Hum Reprod 2005; 20:2207–2210.
15. Sanfins A, Lee GY, Plancha CE, Overstrom EW, Albertini DF. Distinctions in meiotic spindle structure and assembly during in vitro and in vivo maturation of mouse oocytes. Biol Reprod 2003; 69: 2059–2067.
16. Sanfins A, Plancha CE, Overstrom EW, Albertini DF. Meiotic spindle morphogenesis in in vivo and in vitro matured mouse oocytes: insights into the relationship between nuclear and cytoplasmic quality. Hum Reprod 2004; 19:2889–2899.
17. Coticchio G, Guglielmo MC, Canto Dal. M, Fadini R, Mignini Renzini M, De Ponti E, Brambillasca F, Albertini DF. Mechanistic foundations of the metaphase II spindle of human oocytes matured in vivo and in vitro. Hum Reprod 2013; 28:3271–3282.
18. Ueno S, Kurome M, Ueda H, Tomii R, Hiruma K, Nagashima H. Effects of maturation conditions on spindle morphology in porcine MII oocytes. J Reprod Dev 2005; 51:405–410.
19. Duncan FE, Chiang T, Schultz RM, Lampson MA. Evidence that a defective spindle assembly checkpoint is not the primary cause of maternal age-associated aneuploidy in mouse eggs. Biol Reprod 2009; 81:768–776.
20. Sebestova J, Danylevska A, Novakova L, Kubelka M, Anger M. Lack of response to unaligned chromosomes in mammalian female gametes. Cell Cycle 2012; 11:3011–3018.
21. Lane SI, Yun Y, Jones KT. Timing of anaphase-promoting complex activation in mouse oocytes is predicted by microtubule-kinetochore attachment but not by bivalent alignment or tension. Development 2012; 139:1947–1955.
22. Fitzharris G. A shift from kinesin 5-dependent metaphase spindle function

during preimplantation development in mouse. Development 2009; 136: 2111–2119.
23. Mailhes JB, Mastromatteo C, Fuseler JW. Transient exposure to the Eg5 kinesin inhibitor monastrol leads to syntelic orientation of chromosomes and aneuploidy in mouse oocytes. Mutat Res 2004; 559:153–167.
24. Danylevska A, Kovacovicova K, Awadova T, Anger M. The frequency of precocious segregation of sister chromatids in mouse female meiosis I is affected by genetic background. Chromosome Res 2014; 22:365–373.
25. Dumont S, Mitchison TJ. Force and length in the mitotic spindle. Curr Biol 2009; 19:R749–R761.
26. Goshima G, Scholey JM. Control of mitotic spindle length. Annu Rev Cell Dev Biol 2010; 26:21–57.
27. Kapitein LC, Peterman EJ, Kwok BH, Kim JH, Kapoor TM, Schmidt CF. The bipolar mitotic kinesin Eg5 moves on both microtubules that it crosslinks. Nature 2005; 435:114–118.
28. Chauviere M, Kress C, Kress M. Disruption of the mitotic kinesin Eg5 gene (Knsl1) results in early embryonic lethality. Biochem Biophys Res Commun 2008; 372:513–519.
29. Castillo A, Justice MJ. The kinesin related motor protein, Eg5, is essential for maintenance of pre-implantation embryogenesis. Biochem Biophys Res Commun 2007; 357:694–699.
30. Ferenz NP, Gable A, Wadsworth P. Mitotic functions of kinesin-5. Semin Cell Dev Biol 2010; 21:255–259.
31. Kapoor TM, Mayer TU, Coughlin ML, Mitchison TJ. Probing spindle assembly mechanisms with monastrol, a small molecule inhibitor of the mitotic kinesin, Eg5. J Cell Biol 2000; 150:975–988.
32. Blangy A, Lane HA, d'Herin P, Harper M, Kress M, Nigg EA. Phosphorylation by p34cdc2 regulates spindle association of human Eg5, a kinesin-related motor essential for bipolar spindle formation in vivo. Cell 1995; 83:1159–1169.
33. van Heesbeen RG, Tanenbaum ME, Medema RH. Balanced activity of three mitotic motors is required for bipolar spindle assembly and chromosome segregation. Cell Rep 2014; 8:948–956.
34. Schuh M, Ellenberg J. Self-organization of MTOCs replaces centrosome function during acentrosomal spindle assembly in live mouse oocytes. Cell 2007; 130:484–498.
35. Courtois A, Schuh M, Ellenberg J, Hiiragi T. The transition from meiotic to mitotic spindle assembly is gradual during early mammalian development. J Cell Biol 2012; 198:357–370.
36. Fitzharris G, Anaphase B. Precedes Anaphase A in the Mouse Egg. Curr Biol 2012; 22:437–444.
37. Nagaoka SI, Hassold TJ, Hunt PA. Human aneuploidy: mechanisms and new insights into an age-old problem. Nat Rev Genet 2012; 13:493–504.

Anger M, Stein P, Schultz RM. CDC6 requirement for spindle formation during maturation of mouse oocytes. Biol Reprod. 2005;72: 188–194.

Impact Factor/Quartile: 4,139/Q1
Times cited (Wos May 2019): 36
Significance: report showing a clear connection between pre-meiotic S phase and mitosis further demonstrating the importance of CDC6 for spindle assembly.
Contribution of the author: With Paula Stein and Richard Schultz experimental design, interpretation of experiments, manuscript preparation

BIOLOGY OF REPRODUCTION **72,** 188–194 (2005)
Published online before print 22 September 2004.
DOI 10.1095/biolreprod.104.035451

CDC6 Requirement for Spindle Formation During Maturation of Mouse Oocytes[1]

Martin Anger, Paula Stein, and Richard M. Schultz[2]

Department of Biology, University of Pennsylvania, Philadelphia, Pennsylvania 19104-6018

ABSTRACT

A master regulator of DNA replication, CDC6 also functions in the DNA-replication checkpoint by preventing DNA rereplication. Cyclin-dependent kinases (CDKs) regulate the amount and localization of CDC6 throughout the cell cycle; CDC6 phosphorylation after DNA replication initiation leads to its proteolysis in yeast or translocation to the cytoplasm in mammals. Overexpression of CDC6 during the late S phase prevents entry into the M phase by activating CHEK1 kinase that then inactivates CDK1/cyclin B, which is essential for the G_2/M-phase transition. We analyzed the role of CDC6 during resumption of meiosis in mouse oocytes, which are arrested in the first meiotic prophase with low CDK1/cyclin B activity; this is similar to somatic cells at the G_2/M-phase border. Overexpression of CDC6 in mouse oocytes does not prevent resumption of meiosis. The RNA interference-mediated knockdown of CDC6, however, reveals a new and unexpected function for CDC6; namely, it is essential for spindle formation in mouse oocytes.

gamete biology, kinases, meiosis, oocyte development

INTRODUCTION

During the relatively long period of oocyte growth and maturation, unscheduled DNA replication is prevented by repressing CDC6 (cell division cycle-6 homologue) function [1]. CDC6 plays an essential role in DNA replication, because it is required for loading prereplication complexes (pre-RC) during licensing of DNA for replication [2]. Assembly of pre-RCs on DNA during late mitosis and the early G_1 phase is initiated by loading origin-recognition complex (ORC) proteins followed by CDC6 and Cdt1, which are essential for recruiting minichromosome maintenance (MCM) proteins into the complex [3–5]. Once DNA replication is initiated, CDC6 is no longer required and is removed from pre-RCs. This step involves cyclin-dependent kinases (CDKs) phosphorylating consensus sites located in the amino terminal portion of CDC6 and results in changing its stability or localization. The nuclear concentration of CDC6 is highest during the G_1 phase, when CDK activity is low, whereas during the G_2 and early M phases, when CDK activity is high, CDC6 is inactivated by proteolysis in yeast or by translocation into the cytoplasm in mammals [6, 7]. This suggests that different strategies regulate the activity of pre-RCs in yeast and mammals [8–11].

Overexpression of CDC6 during the late S phase activates CHEK1 kinase. This prevents cyclin B/CDK1 activation and leads to cell-cycle arrest at the G_2/M-phase transition [12]. Detailed analysis of this phenomenon in *Xenopus laevis* has demonstrated that CDC6 activates CHEK1 directly and that MCM proteins as well as binding of CDC6 to chromatin are not required [13].

The difference in how the amount of CDC6 protein is regulated after the initiation of DNA replication in different eukaryotes raises the possibility that CDC6 has other functions during the late S phase and mitosis in mammals. To investigate this possibility in mammalian somatic cells, however, is difficult, both because a CDC6-specific inhibitor is lacking and because a *Cdc6* knockout or an RNA interference (RNAi)-mediated knockdown would be lethal. Mouse oocytes are a potentially suitable system to explore this possibility. Mouse oocytes are arrested in the first meiotic prophase after DNA replication; this is similar to being arrested at the G_2/M-phase transition. Cyclin B/CDK1 (i.e., M-phase promoting factor [MPF]) activity is low in these oocytes, which is similar to somatic cells at the G_2/M-phase transition. Resumption of meiosis entails an abrupt activation of MPF that leads to dissolution of the nuclear membrane (i.e., germinal vesicle breakdown [GVBD]), two rounds of chromosome segregation with no intervening DNA replication, and arrest at metaphase II [14].

We first analyzed whether overexpression of CDC6 inhibits GVBD. We found that in contrast to somatic cells, oocytes tolerate high levels of CDC6; that is, the oocytes mature normally and arrest at metaphase II. Reducing CDC6 by RNAi demonstrated that although GVBD occurred and chromosomes condensed, a spindle failed to form, suggesting a new function for CDC6 that is not related to DNA replication.

MATERIALS AND METHODS

Oocyte Collection, Culture, and Microinjection

Fully grown, germinal vesicle (GV)-intact oocytes were obtained from eCG-primed, 6-wk-old, female CF-1 mice (Harlan) and freed of attached cumulus cells as previously described [15]. The collection medium was bicarbonate-free minimal essential medium (Earle salt) supplemented with 3 mg/ml of polyvinylpyrrolidone (PVP) and 25 mM Hepes (pH 7.3). Germinal vesicle breakdown was inhibited by adding 0.2 mM 3-isobutyl-1-methyl-xanthine (IBMX) to the isolation or culture media. Oocytes were cultured in CZB medium [16] containing 0.2 mM IBMX and cultured in an atmosphere of 5% CO_2 in air at 37°C. Oocytes were microinjected in bicarbonate-free Whitten medium [17] supplemented with 10 mM Hepes (pH 7.3) and 0.2 mM IBMX with 5 pl of the RNA solution; the injections were performed as previously described [18]. Typically, greater than 70% of oocytes injected with either *Egfp* or *Cdc6* double-stranded (ds) RNA survived, and virtually all the surviving oocytes underwent GVBD. The dsRNA was diluted to 1–2 μg/μl and mRNAs to 0.5 μg/μl for injections. After microinjection, oocytes were cultured in CZB plus IBMX for 2 h when mRNA was injected and 24 h when dsRNA was injected. When required, the injected oocytes were matured by washing and culturing them in IBMX-free CZB medium for 18 h.

All animal experiments were approved by the Institutional Animal Use

[1]Supported by a grant from the National Institutes of Health (HD22681) to R.M.S. M.A. and P.S. contributed equally to this work.
[2]Correspondence: Richard Schultz, Department of Biology, University of Pennsylvania, 415 South University Avenue, Philadelphia, Pennsylvania 19104-6018. FAX: 215 898 8780; e-mail: rschultz@mail.sas.upenn.edu

Received: 18 August 2004.
First decision: 3 September 2004.
Accepted: 3 September 2004.

ISSN: 0006-3363. http://www.biolreprod.org

and Care Committee and were consistent with National Institutes of Health guidelines.

RNA Isolation and Quantification

Total RNA from 5 to 50 oocytes or eggs was isolated using the Absolutely RNA Microprep Kit (Stratagene, La Jolla, CA). The reverse transcription (RT) reaction, primed with random hexamers, was performed using Superscript II reverse transcriptase (Invitrogen, Carlsbad, CA) following the manufacturer's instructions. Total RNA isolated from 5 to 50 oocytes was reverse transcribed in 20-μl reactions. The resulting cDNA was quantified by real-time polymerase chain reaction (PCR) using SybrGreen and detecting the threshold cycle with an ABI Prism 7000 (Applied Biosystems, Foster City, CA). Histone $H1_{foo}$ was used as an internal standard. The following primers were used: histone $H1_{foo}$, 5′-GCGAAACCGAAAGAGGTCAGAA-3′ and 5′-TGGAGGAGGTCTTGGGAAGTAA-3,′; and CDC6, 5′-GTGCTGCGATCCAGTTCTGT-3′ and 5′-CTGCAAGTGCCATGAGTAAGA-3′.

Mutagenesis of Phosphorylation Sites

The QuikChange Multisite-Directed Mutagenesis Kit (Stratagene, La Jolla, CA) was used to produce mouse CDC6 with serine residues 55, 75, and 108 mutated to alanine or aspartic acid residues. The template for reaction was a pCMV-SPORT6 vector containing a mouse full-length *Cdc6* cDNA (clone 4946685, GenBank accession no. BG919477) that was purchased from Invitrogen. The mutated cDNA was completely sequenced and used as a template for in vitro transcription.

In Vitro Synthesis of dsRNA and Capped RNA

Two dsRNAs were used to target mouse *Cdc6* mRNA. The pT7T3D-PacI vector containing a full-length mouse *Cdc6* cDNA was purchased from Invitrogen (clone 477516, GenBank accession no. AI510027). The *Bgl*II/*Not*I fragment was excised from the plasmid to obtain a 1160-base pair (bp) fragment that was used as a template for in vitro transcription. The plasmid was linearized using *Xho*I and *Hin*dIII, purified by agarose gel electrophoresis, and used as the template for SP6 and T7 RNA polymerases (Promega, Madison, WI) to obtain sense and antisense RNAs. In vitro transcription and annealing were performed as described previously [19]. The second *Cdc6* dsRNA was obtained using MEGAscript® RNAi Kit (Ambion, Austin, TX). A PCR strategy in which the T7 sites were added on both sides of the template was used to generate template for in vitro transcription. The *Egfp* dsRNA also was prepared as a control dsRNA for injections. Primers for *Cdc6* were 5′-AGGATCCTAATACGACTCACTATAGGGAGAGCGATGACAACCTGTGCAA-3′ and 5′-ACTCGAGTAATACGACTCACTATAGGGAGACTGTCCGTGAGATCTAGGGTA-3′. Primers for *Egfp* were 5′-AGGATCCTAATACGACTAACTATAGGGAGAATGGTGAGCAAGGGCGAGGA-3′ and 5′-ACTCGAGTAATACGACTCACTATAGGGAGAGCGGCCGCTTTACTTGTACA-3′. The length of the dsRNA fragment was 780 bp for *Cdc6* and 712 bp for *Egfp*.

Polyadenylated capped mRNA for injections was obtained using mMESSAGE mMACHINE T7 Kit and Poly(A) Tailing Kit (Ambion). The template for in vitro transcription was a pCMV-SPORT6 plasmid containing full-length mouse *Cdc6* cDNA or point-mutated *Cdc6* cDNA, each digested with *Ban*II. The RNA was purified using RNeasy Mini Kit (Qiagen, Inc., Valencia, CA).

Antibodies

The CDC6 was detected using monoclonal antibody sc-9964 (Santa Cruz Biotechnology, Inc., Santa Cruz, CA); a dilution of 1:100 was used for Western blot analysis and 1:50 for immunofluorescence. β-Tubulin was detected with monoclonal antibody T4024 (Sigma-Aldrich, St Louis, MO) at a 1:500 dilution for immunofluorescence. Phosphoserine 10 in histone H3 was detected with 06-570 antibody from Upstate Biotechnology, Inc. (Lake Placid, NY) using a working dilution of 1:500 for immunofluorescence. Lamin A was detected with rabbit polyclonal antibody 2032 (Cell Signaling Technology, Inc., Beverly, MA) at a 1:100 dilution for immunofluorescence. Secondary antibodies (Jackson ImmunoResearch, West Grove, PA) were Cy5-conjugated anti-mouse or anti-rabbit immunoglobulin (Ig) G for immunofluorescence and an alkaline phosphatase-conjugated anti-mouse IgG for immunoblotting.

Immunocytochemistry

Zona pellucida-free oocytes, generated by a brief treatment with acid Tyrode solution, were washed in PBS containing 3 mg/ml of PVP (PBS/PVP) and fixed in 2% paraformaldehyde in PBS for 30 min at room temperature. All subsequent steps were carried out at room temperature in a humidified chamber. Oocytes were permeabilized in 0.1% Triton X-100 in PBS for 15 min, washed through three drops of PBS/PVP, and then blocked in PBS containing 0.1% BSA and 0.01% Tween-20 for 15 min. The oocytes were then incubated for 1 h in the presence of the primary antibody diluted in blocking solution. The cells were washed through three drops of blocking solution for 15 min each and then incubated for 60 min in the dark with a conjugated secondary antibody. The DNA was stained with 1 μM SYTOX Green (Molecular Probes, Eugene, OR). The cells were then washed and mounted under a coverslip with gentle compression in VectaShield antibleaching solution (Vector Labs). Fluorescence was detected on a Leica TCS SP laser-scanning confocal microscope.

Immunoblotting

Samples were separated in a 10% SDS-PAGE gel and transferred to a polyvinylidene fluoride (PVDF) membrane using semidry transfer. Membranes were blocked with 5% fetal calf serum or 5% teleostein gelatin (Sigma-Aldrich) dissolved in Tris-buffered saline containing 0.1% Tween 20 (TTBS) for 1 h at room temperature. Primary and secondary antibodies were diluted in TTBS, and the membrane was washed after each incubation. The signal was developed using ECF Western Blotting System (Amersham Biosciences, Piscataway, NY) and detected using a Storm 860 PhosphorImager and ImageQuant software (Molecular Dynamics, Sunnyvale, CA).

Kinase Assays

The activities of mitogen-activated protein kinase (MAPK) and MPF in single eggs were determined as previously described [19].

Statistical Analysis

One-way ANOVA or Student *t*-test was used to evaluate the difference between groups, and differences at $P < 0.05$ were considered to be significant. Prism software (Graph Pad Software Inc., San Diego, CA) was used to perform statistical analyses.

RESULTS

CDC6 protein and mRNA Expression During Maturation

Previous reports have shown that in various species, including mouse, CDC6 is not present in growing oocytes and is detected after resumption of meiosis [1, 20, 21]. We quantified the amount of *Cdc6* mRNA before meiotic maturation in GV-intact oocytes and after maturation in metaphase II-arrested eggs using real-time RT-PCR. We found that the amount of *Cdc6* mRNA decreases by approximately 50% following maturation (Fig. 1A). Immunoblot analysis revealed that CDC6 protein was not detected in GV-intact oocytes but was detected after GVBD (Fig. 1B). This maturation-associated increase was confirmed by immunocytochemistry. No detectable signal was observed in GV-intact oocytes, but a clear signal was localized to chromosomes of the metaphase II-arrested egg (Fig. 1C). Thus, degradation of *Cdc6* mRNA was apparently coupled with its translation.

CDC6 Overexpression During Resumption of Meiosis

Overexpression of CDC6 in somatic cells blocks the cell cycle at the G_2/M-phase transition by activating CHEK1 kinase, which in turn prevents activation of cyclin B/CDK1 complex that permits this transition [12]. As mentioned above, CDK1 activity is low in vertebrate oocytes arrested at the G_2/M-phase transition and in somatic cells at the G_2 phase. Activation of CDK1 is required for GVBD. We were

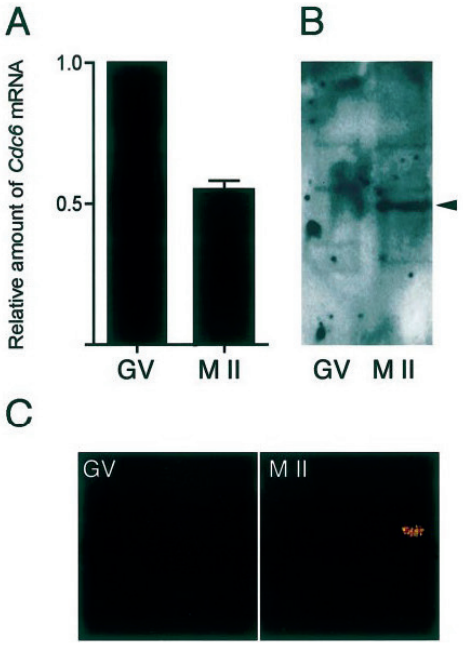

FIG. 1. Expression of *Cdc6* mRNA and protein in mouse oocytes and eggs. **A**) Real-time RT-PCR was used to quantify the level of *Cdc6* mRNA in GV-intact oocytes (GV) and metaphase II-arrested eggs (M II). The experiment was performed three times, and the data are expressed as the mean ± SEM. The decrease in the amount of *Cdc6* mRNA is significant ($P < 0.05$). **B**) Immunoblotting was used to detect CDC6 protein in GV-intact oocytes (GV) and metaphase II eggs (M II). The position of the CDC6 protein on the gel is indicated by the arrowhead. **C**) Immunocytochemical detection and localization of CDC6 in GV-intact (left) and metaphase II-arrested eggs (right). Original magnification ×300.

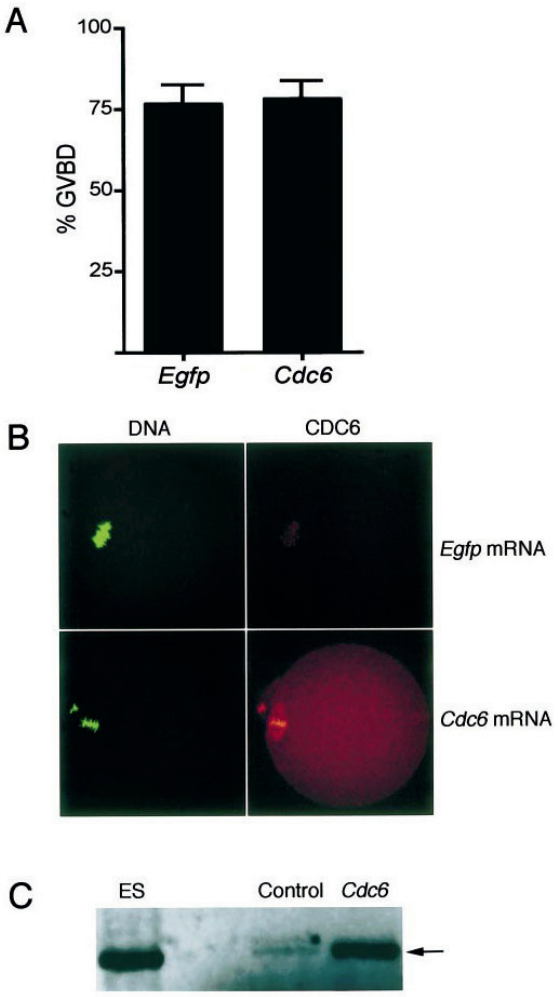

FIG. 2. Overexpression of *Cdc6* mRNA in mouse oocytes. **A**) Overexpression of CDC6 in GV-intact oocytes. Similar numbers of GV-intact oocytes were injected with *Egfp* or *Cdc6* mRNA. The results are expressed as the mean ± SEM of three independent experiments showing the percentage of oocytes resuming meiosis in each group. None of the differences is significant. **B**) Immunolocalization of CDC6 in injected oocytes. Mouse eggs injected with *Egfp* or *Cdc6* mRNA were stained with a monoclonal antibody that recognizes CDC6 (right) or SYTOX Green (left). The top represents CDC6, whereas the bottom, where the fluorescence intensity is much greater, demonstrates that overexpression was achieved. **C**) Representative immunoblot showing detection of CDC6 in approximately 50000 mouse embryonic stem cells (ES), 100 uninjected eggs (control), or 10 oocytes injected with *Cdc6* mRNA (*Cdc6*). The position of CDC6 on the gel is indicated by the arrow. Original magnification ×500.

interested in establishing if the overexpression of CDC6 in oocytes inhibits GVBD by inhibiting CDK1 activation. Full-length *Cdc6* mRNA without the 3′-untranslated region (UTR) regulatory sequences was prepared in vitro and microinjected into oocytes blocked at the GV stage with IBMX [18]. A control group was injected with in vitro-transcribed *Egfp* mRNA. Both groups of oocytes were arrested at the GV stage for additional 2 h after microinjection to allow expression and then matured for 18 h. Accumulation of the newly synthesized proteins was detected within 2 h following microinjection of the mRNAs (data not shown). Results of three independent experiments indicated no difference in the extent of resumption of meiosis following injection with either *Egfp* or *Cdc6* mRNA (Fig. 2A), and no difference was found in the kinetics of GVBD in both groups (data not shown). Thus, overexpression of CDC6 presumably did not inhibit CDK1 activation.

Immunolocalization of CDC6 in microinjected oocytes showed that ectopically expressed CDC6 was localized on chromatin and the spindle, which was similar to that of endogenous CDC6 (Figs. 1C and 2B). The higher level of fluorescence in the oocytes injected with *Cdc6* mRNA compared with that in controls was confirmed by immunoblot analysis (Fig. 2C). In summary, the results of these experiments indicate that overexpression of CDC6 by at least 30-fold (as determined by quantifying the signal intensity in Fig. 2C) when compared to the endogenous amount of CDC6 does not inhibit CDK1 activation.

Overexpression of Selected CDC6 Mutants

Previous work has shown that selected mutants of CDC6, including S74 converted to alanine and deletion of the Cy motif, are less efficient in arresting the cell cycle, whereas mutation of other serine sites (S54 and S107)

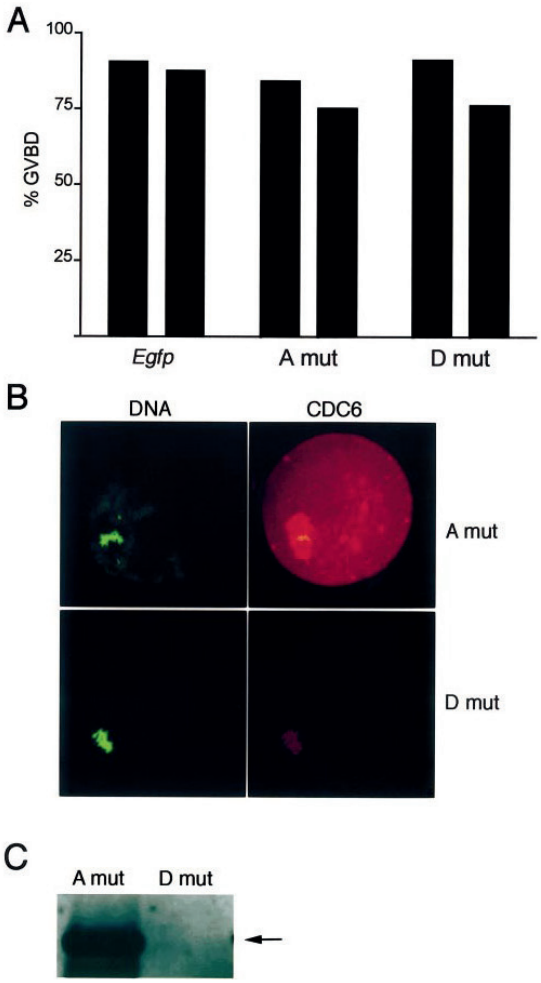

FIG. 3. Overexpression of selected mutated forms of mouse CDC6. **A**) A mutation (A mut) represents CDC6 with serines 55, 75, and 108 changed to alanine; D mutation (D mut) represents CDC6 with serines 55, 75, and 108 changed to aspartic acid. *Egfp* indicates oocytes injected with *Egfp* mRNA. The experiment was conducted twice, and the data are expressed as the percentage of oocytes that underwent GVBD. **B**) Eggs with overexpressed CDC6 were stained with anti-CDC6 monoclonal antibody (right) and with SYTOX Green (left). Because of the high abundance of the protein with the A mutation, different voltage settings at the confocal microscope were used to obtain images; therefore, the images cannot be compared directly. **C**) Immunoblotting with eggs (n = 10 per lane) injected with A mut and D mut showing the increased abundance of unphosphorylatable form (A mut). Original magnification ×475.

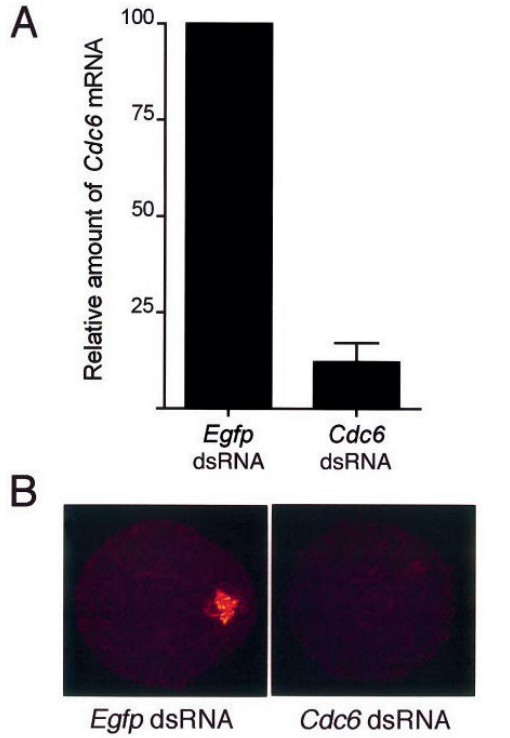

FIG. 4. RNAi knockdown of CDC6 in mouse oocytes. **A**) Targeting *Cdc6* mRNA in mouse oocytes. Oocytes injected with *Cdc6* dsRNA or with *Egfp* dsRNA as a control were cultured for 24 h in IBMX-containing medium. Total RNA was then isolated and used for real-time PCR. The experiment was conducted three times, and the data are expressed as the mean ± SEM. The decrease in the amount of *Cdc6* mRNA is significant ($P < 0.05$). **B**) Representative images showing localization of CDC6 in control eggs injected with *Egfp* dsRNA (left) and eggs injected with *Cdc6* dsRNA (right). Note the absence of CDC6 staining on the chromosomes in the *Cdc6* dsRNA-injected cells. Original magnification ×400.

showed the same efficiency as wild-type CDC6 [12]. To analyze whether the phosphorylation state of CDC6 is important for blocking meiotic progression, we generated *Cdc6* mRNAs with serines 55, 75, and 108 mutated into alanines (A mutation) or into aspartic acid (D mutation), and we injected mRNAs encoding these mutant forms into oocytes. Results of two independent experiments showed that both mutations did not increase the ability of CDC6 to prevent resumption of meiosis (Fig. 3A).

In mammals, CDC6 phosphorylation is responsible for its translocation to the cytoplasm; the unphosphorylated form is retained in the nucleus [22–24]. When we analyzed the localization of CDC6 mutants in oocytes before GVBD, we found that the A mutation was almost exclusively localized in the nucleus, which is consistent with previous results obtained in somatic cells (data not shown). Both immunolocalization (Fig. 3B) and immunoblotting (Fig. 3C) of eggs after maturation revealed a higher level of expression of the A form compared to the D form, even though similar amounts of the corresponding mRNAs were injected. The low level of expression of the D form precluded its localization in GV-intact oocytes.

CDC6 Is Essential for Spindle Formation During Oocyte Maturation

We used RNAi to assess the function of CDC6 in resumption of meiosis (i.e., to test whether CDC6 has additional functions beyond DNA replication). Two different dsRNAs (length, 1160 and 780 bp) were prepared to target *Cdc6* mRNA in GV-intact oocytes. After 24 h in culture medium containing IBMX to inhibit maturation, the amount of *Cdc6* mRNA was assayed by real-time PCR. As antici-

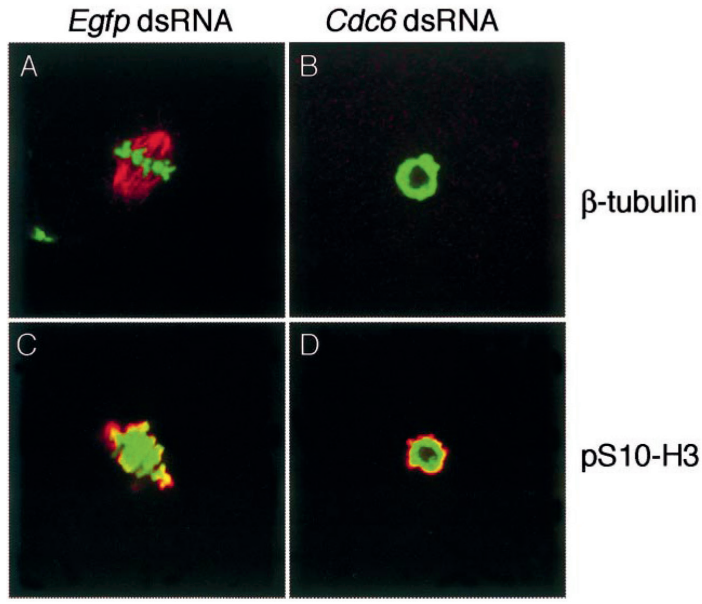

FIG. 5. Phenotype of CDC6 knockdown in mouse oocytes during meiotic maturation. Following injection, the oocytes were cultured for 24 h in IBMX-containing medium and then matured for 18 h in IBMX-free medium. Next, the cells were stained for DNA (green) and either β-tubulin (red, top) or histone H3 phosphorylated on S10 (red, bottom). **A** and **C**) Oocytes injected with *Egfp* dsRNA. **B** and **D**) Oocytes injected with *Cdc6* dsRNA. Of the 129 *Cdc6* dsRNA-injected oocytes, 89 (69%) displayed the shown phenotype. Original magnification ×600.

pated, the amount of *Cdc6* mRNA was dramatically reduced (Fig. 4A). When the oocytes were allowed to resume meiosis by transferring them to inhibitor-free medium, the maturation-associated increase in CDC6 protein was not observed, as evidenced by a decrease in the intensity of the fluorescent signal (Fig. 4B).

When these injected and matured oocytes were analyzed morphologically, it became apparent that although they underwent GVBD, they failed to reach metaphase I (MI); this effect was consistently observed in several experiments using long (1160-bp) or short (780-bp) dsRNA. Morphological analysis of the injected oocytes showed that the first polar body was not extruded and that DNA formed a hollow sphere, as revealed by optical sectioning, instead of a metaphase plate (Fig. 5B). We did not detect a spindle in oocytes injected with *Cdc6* dsRNA using a β-tubulin antibody; in contrast, a spindle was detected in oocytes injected with *Egfp* dsRNA (Fig. 5A). Although the chromosomes were condensed (a hallmark of cells undergoing mitosis/meiosis, because they stained for histone H3 phosphorylated on S10), they did not form visible bivalents (Fig. 5, C and D). In addition, the oocytes had undergone nuclear envelope breakdown, because lamin A was not detected (data not shown). Time-course studies revealed that the spindle never formed (data not shown).

In yeast and in mammals, CDC6 directly interacts with cyclin/CDK complexes, but the physiological importance of this interaction in mammals is not known [23, 25]. Activities of MPF and MAPK were measured in *Cdc6* dsRNA-injected oocytes to establish that the inhibitory effect on progression to MI was not because of the failure of these kinases to become fully activated. No apparent difference was noted in the activities of these kinases following maturation of oocytes injected with either *Cdc6* or *Egfp* dsRNA (Fig. 6).

DISCUSSION

We report that CDC6 protein is not detected in GV-intact oocytes and that the appearance and accumulation of CDC6 protein is coupled with a maturation-associated decrease in *Cdc6* mRNA. Recent results from mouse and other species indicate that this probably is a common mechanism to prevent unwanted DNA replication throughout oocyte growth and maturation [1]. This expression pattern (i.e., a maturation-associated increase in protein but decrease in mRNA) is reminiscent of that observed for dormant maternal mRNAs that are recruited during maturation. For example, *Mos* and cyclin B1 mRNAs contain a cytoplasmic polyadenylation element (CPE) located in their 3′-UTR, and recruitment of the mRNA leads to its translation and degradation [26]. Consistent with this proposal is that a

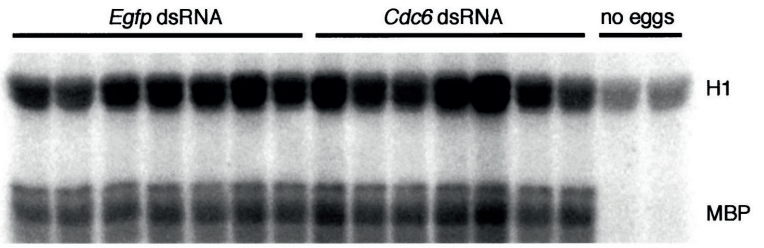

FIG. 6. Histone H1 and MAPK activities in single eggs injected with either *Cdc6* or *Egfp* dsRNA. The H1 and MAPK were measured by phosphorylation of histone H1 and myelin basic protein (MBP), respectively. The experiment was performed three times, and similar results were obtained in each case. A representative gel is shown.

CPE of the same sequence present in *Mos* and cyclin B1 mRNA also is present in the 3′-UTR of the mouse *Cdc6* mRNA. The appearance of CDC6 in the metaphase II-arrested egg aptly positions it to initiate DNA replication following egg activation.

As mentioned in *Results*, overexpression of CDC6 in somatic cells blocks the cell cycle at the G_2/M-phase transition via CHEK1 kinase [12]. Our results show that in contrast to somatic cells, resumption of meiosis (i.e., the G_2/M-phase transition) is not prevented by overexpression of CDC6. This difference could be explained by the requirements of different CDC25 isoforms for cyclin B/CDK1 activation in somatic cells and in mouse oocytes. CDC25B, which is essential for meiotic resumption in mouse oocytes, is dispensable in the somatic cell cycle [27]. In somatic cells, an activated DNA-replication checkpoint inhibits CDC25A and CDC25B, with MAPK being required for CDC25B inhibition [28, 29]. In mouse oocytes, however, MAPK is activated after MPF because of the recruitment of *Mos* mRNA after GVBD [30]. Thus, overexpression of CDC6 may not inhibit GVBD (i.e., the G_2/M-phase transition), because CDC25B is not inhibited by the low level of MAPK activity before GVBD.

We also observed that CDC6 with N-terminal serines mutated to aspartic acid is less stable in oocytes. This is reminiscent of yeast, in which CDC6 phosphorylation targets its destruction [31–34], and differs from mammals, in which phosphorylation promotes nuclear export of CDC6 [22–24]. However, the amount of CDC6 is relatively constant throughout cell cycle [9, 11]. Even so, it should be noted that data regarding the stability of exogenous CDC6 in mammalian cells are conflicting. For example, both mutations (CDK consensus serines into alanines or aspartic acid) are stably expressed from plasmids in HeLa cells [35], whereas using cell extracts, exogenous CDC6 is degraded in CDK-dependent fashion during the S phase [8].

In mammals, CDC6 is not destroyed after the initiation of DNA replication; rather, it persists bound to chromatin throughout the cell cycle, suggesting that it may have other functions during the late S phase or mitosis [35]. In support of this hypothesis, the present results show that CDC6 is critical for meiotic progression of mouse oocytes, because oocytes with a reduced amount of CDC6 fail to form a spindle.

An inactive form of CDC6 also can arrest yeast in mitosis [36]. Deleting both *Cdc6* alleles in yeast results in incomplete mitosis, with randomly distributed chromosomes and cells with a DNA content less than 1C. Mutation in the Walker A motif, which is essential for ATP binding and hydrolysis [36], results in expression of a nonfunctional CDC6, and the cells arrest in anaphase before chromosome segregation and have elongated spindles. This block, which is independent of a DNA-replication checkpoint and requires both an intact Cy box (mediating the binding of proteins to CDK cyclins in eukaryotes [36]) and CDK phosphorylation consensus sites, is overcome by increased CDK activity. Of interest is that in mouse oocytes with decreased CDC6 protein, CDK1 activity displays its normal maturation-associated increase in activity, yet the oocytes do not form a spindle and enter MI.

Other DNA replication proteins also are involved in chromosome condensation and distribution during mitosis. The ORC subunits 2, 5, and 6 and MCM10, which are all involved during the initial steps of DNA replication, also are required during mitosis, because decreasing the amount of these proteins leads to incorrect chromosome condensation and distribution or defects in cytokinesis [37–41]. In this regard, CDC6 also appears to be involved in chromosome condensation, because decreasing the amount of oocyte CDC6 results in abnormal chromosome condensation and failure to form bivalents.

The present results have unmasked a new function for CDC6 that apparently is unrelated to DNA replication—namely, that CDC6 is critical for meiotic progression of mouse oocytes, particularly formation of a meiotic spindle. The molecular mechanism underlying this new function and why the chromosomes are found condensed on the surface of a hollow sphere are the subject of future investigations.

REFERENCES

1. Lemaitre JM, Bocquet S, Terret ME, Namdar M, Ait-Ahmed O, Kearsey S, Verlhac MH, Mechali M. The regulation of competence to replicate in meiosis by Cdc6 is conserved during evolution. Mol Reprod Dev 2004; 69:94–100.
2. Bell SP, Dutta A. DNA replication in eukaryotic cells. Annu Rev Biochem 2002; 71:333–374.
3. Lei M, Tye BK. Initiating DNA synthesis: from recruiting to activating the MCM complex. J Cell Sci 2001; 114:1447–1454.
4. Coleman TR. The 3 Rs of Cdc6: recruitment, regulation, and replication. Curr Biol 2002; 12:R759.
5. Pelizon C. Down to the origin: Cdc6 protein and the competence to replicate. Trends Cell Biol 2003; 13:110–113.
6. Perkins G, Drury LS, Diffley JF. Separate SCF(CDC4) recognition elements target Cdc6 for proteolysis in S phase and mitosis. EMBO J 2001; 20:4836–4845.
7. Kearsey SE, Cotterill S. Enigmatic variations: divergent modes of regulating eukaryotic DNA replication. Mol Cell 2003; 12:1067–1075.
8. Coverley D, Pelizon C, Trewick S, Laskey RA. Chromatin-bound Cdc6 persists in S and G_2 phases in human cells, while soluble Cdc6 is destroyed in a cyclin A-cdk2 dependent process. J Cell Sci 2000; 113(Pt 11):1929–1938.
9. Mendez J, Stillman B. Chromatin association of human origin recognition complex, cdc6, and minichromosome maintenance proteins during the cell cycle: assembly of prereplication complexes in late mitosis. Mol Cell Biol 2000; 20:8602–8612.
10. Okuno Y, McNairn AJ, den Elzen N, Pines J, Gilbert DM. Stability, chromatin association, and functional activity of mammalian prereplication complex proteins during the cell cycle. EMBO J 2001; 20: 4263–4277.
11. Alexandrow MG, Hamlin JL. Cdc6 chromatin affinity is unaffected by serine-54 phosphorylation, S-phase progression, and overexpression of cyclin A. Mol Cell Biol 2004; 24:1614–1627.
12. Clay-Farrace L, Pelizon C, Santamaria D, Pines J, Laskey RA. Human replication protein Cdc6 prevents mitosis through a checkpoint mechanism that implicates Chk1. EMBO J 2003; 22:704–712.
13. Oehlmann M, Score AJ, Blow JJ. The role of Cdc6 in ensuring complete genome licensing and S phase checkpoint activation. J Cell Biol 2004; 165:181–190.
14. Jones KT. Turning it on and off: M-phase promoting factor during meiotic maturation and fertilization. Mol Hum Reprod 2004; 10:1–5.
15. Schultz RM, Montgomery RR, Belanoff JR. Regulation of mouse oocyte maturation: implication of a decrease in oocyte cAMP and protein dephosphorylation in commitment to resume meiosis. Dev Biol 1983; 97:264–273.
16. Chatot CL, Ziomek CA, Bavister BD, Lewis JL, Torres I. An improved culture medium supports development of random-bred 1-cell mouse embryos in vitro. J Reprod Fertil 1989; 86:679–688.
17. Whitten WK. Nutrient requirements for the culture of preimplantation mouse embryo in vitro. Adv Biosci 1971; 6:129–139.
18. Kurasawa S, Schultz RM, Kopf GS. Egg-induced modifications of the zona pellucida of mouse eggs: effects of microinjected inositol 1,4,5-trisphosphate. Dev Biol 1989; 133:295–304.
19. Svoboda P, Stein P, Hayashi H, Schultz RM. Selective reduction of dormant maternal mRNAs in mouse oocytes by RNA interference. Development 2000; 127:4147–4156.
20. Lemaitre JM, Bocquet S, Mechali M. Competence to replicate in the unfertilized egg is conferred by Cdc6 during meiotic maturation. Nature 2002; 419:718–722.

21. Whitmire E, Khan B, Coue M. Cdc6 synthesis regulates replication competence in *Xenopus* oocytes. Nature 2002; 419:722–725.
22. Jiang W, Wells NJ, Hunter T. Multistep regulation of DNA replication by Cdk phosphorylation of HsCdc6. Proc Natl Acad Sci U S A 1999; 96:6193–6198.
23. Petersen BO, Lukas J, Sorensen CS, Bartek J, Helin K. Phosphorylation of mammalian CDC6 by cyclin A/CDK2 regulates its subcellular localization. EMBO J 1999; 18:396–410.
24. Delmolino LM, Saha P, Dutta A. Multiple mechanisms regulate subcellular localization of human CDC6. J Biol Chem 2001; 276:26947–26954.
25. Calzada A, Sacristan M, Sanchez E, Bueno A. Cdc6 cooperates with Sic1 and Hct1 to inactivate mitotic cyclin-dependent kinases. Nature 2001; 412:355–358.
26. Mendez R, Richter JD. Translational control by CPEB: a means to the end. Nat Rev Mol Cell Biol 2001; 2:521–529.
27. Lincoln AJ, Wickramasinghe D, Stein P, Schultz RM, Palko ME, De Miguel MP, Tessarollo L, Donovan PJ. Cdc25b phosphatase is required for resumption of meiosis during oocyte maturation. Nat Genet 2002; 30:446–449.
28. Bulavin DV, Amundson SA, Fornace AJ. p38 and Chk1 kinases: different conductors for the G_2/M checkpoint symphony. Curr Opin Genet Dev 2002; 12:92–97.
29. Sancar A, Lindsey-Boltz LA, Unsal-Kacmaz K, Linn S. Molecular mechanisms of mammalian DNA repair and the DNA damage checkpoints. Annu Rev Biochem 2004; 73:39–85.
30. Gebauer F, Richter JD. Synthesis and function of Mos: the control switch of vertebrate oocyte meiosis. Bioessays 1997; 19:23–28.
31. Cocker JH, Piatti S, Santocanale C, Nasmyth K, Diffley JF. An essential role for the Cdc6 protein in forming the prereplicative complexes of budding yeast. Nature 1996; 379:180–182.
32. Piatti S, Böhm T, Cocker JH, Diffley JFX, Nasmyth K. Activation of S-phase-promoting CDKs in late G_1 defines a "point of no return" after which Cdc6 synthesis cannot promote DNA replication in yeast. Genes Dev 1996; 10:1516–1531.
33. Elsasser S, Chi Y, Yang P, Campbell JL. Phosphorylation controls timing of Cdc6p destruction: A biochemical analysis. Mol Biol Cell 1999; 10:3263–3277.
34. Drury LS, Perkins G, Diffley JF. The cyclin-dependent kinase Cdc28p regulates distinct modes of Cdc6p proteolysis during the budding yeast cell cycle. Curr Biol 2000; 10:231–240.
35. Petersen BO, Wagener C, Marinoni F, Kramer ER, Melixetian M, Denchi EL, Gieffers C, Matteucci C, Peters JM, Helin K. Cell cycle- and cell growth-regulated proteolysis of mammalian CDC6 is dependent on APC-CDH1. Genes Dev 2000; 14:2330–2343.
36. Weinreich M, Liang C, Chen HH, Stillman B. Binding of cyclin-dependent kinases to ORC and Cdc6p regulates the chromosome replication cycle. Proc Natl Acad Sci U S A 2001; 98:11211–11217.
37. Loupart ML, Krause SA, Heck MS. Aberrant replication timing induces defective chromosome condensation in *Drosophila* ORC2 mutants. Curr Biol 2000; 10:1547–1556.
38. Pflumm MF, Botchan MR. Orc mutants arrest in metaphase with abnormally condensed chromosomes. Development 2001; 128:1697–1707.
39. Prasanth SG, Prasanth KV, Stillman B. Orc6 involved in DNA replication, chromosome segregation, and cytokinesis. Science 2002; 297: 1026–1031.
40. Christensen TW, Tye BK. *Drosophila* mcm10 interacts with members of the prereplication complex and is required for proper chromosome condensation. Mol Biol Cell 2003; 14:2206–2215.
41. Chesnokov IN, Chesnokova ON, Botchan M. A cytokinetic function of *Drosophila* ORC6 protein resides in a domain distinct from its replication activity. Proc Natl Acad Sci U S A 2003; 100:9150–9155.

Novakova L, Kovacovicova K, Dang-Nguyen TQ, Sodek M, Skultety M, Anger M. A Balance between Nuclear and Cytoplasmic Volumes Controls Spindle Length. PLoS One. 2016;11: e0149535.

Impact Factor/Quartile: 3,540/Q1
Times cited (Wos May 2019): 6
Significance: Report showing for the first time in mammals that the length of the spindle increases with the cell volume and also that the length of the spindle is controlled by the proportion between cytoplasmic and nuclear volumes
Contribution of the author: Experimental design, interpretation of experiments manuscript preparation, securing funding

PLOS ONE

RESEARCH ARTICLE

A Balance between Nuclear and Cytoplasmic Volumes Controls Spindle Length

Lucia Novakova[1,2], Kristina Kovacovicova[1,2], Thanh Quang Dang-Nguyen[1¤], Martin Sodek[1,2], Michal Skultety[1], Martin Anger[1,2]*

1 Central European Institute of Technology - Veterinary Research Institute, Hudcova 70, 621 00 Brno, Czech Republic, **2** Institute of Animal Physiology and Genetics AS CR, Rumburska 89, 277 21 Libechov, Czech Republic

¤ Current address: National Institute of Agrobiological Sciences, 2-1-2 Kannondai, Tsukuba, Ibaraki 305–8062, Japan
* anger@vri.cz

Citation: Novakova L, Kovacovicova K, Dang-Nguyen TQ, Sodek M, Skultety M, Anger M (2016) A Balance between Nuclear and Cytoplasmic Volumes Controls Spindle Length. PLoS ONE 11(2): e0149535. doi:10.1371/journal.pone.0149535

Editor: Daniela Cimini, Virginia Tech, UNITED STATES

Received: August 17, 2015

Accepted: February 2, 2016

Published: February 17, 2016

Data Availability Statement: All relevant data are within the paper and its Supporting Information files.

Funding: This work was supported by Czech science foundation project P502/12/2201 and by Ministry of Education, Youth and Sports (MEYS) projects ED1.1.00/ 02.0068 – Central European Institute of Technology (CEITEC) and LH 13072 – Kontakt II.

Competing Interests: The authors have declared that no competing interests exist.

Abstract

Proper assembly of the spindle apparatus is crucially important for faithful chromosome segregation during anaphase. Thanks to the effort over the last decades, we have very detailed information about many events leading to spindle assembly and chromosome segregation, however we still do not understand certain aspects, including, for example, spindle length control. When tight regulation of spindle size is lost, chromosome segregation errors emerge. Currently, there are several hypotheses trying to explain the molecular mechanism of spindle length control. The number of kinetochores, activity of molecular rulers, intracellular gradients, cell size, limiting spindle components, and the balance of the spindle forces seem to contribute to spindle size regulation, however some of these mechanisms are likely specific to a particular cell type. In search for a general regulatory mechanism, in our study we focused on the role of cell size and nuclear to cytoplasmic ratio in this process. To this end, we used relatively large cells isolated from 2-cell mouse embryos. Our results showed that the spindle size upper limit is not reached in these cells and suggest that accurate control of spindle length requires balanced ratio between nuclear and cytoplasmic volumes.

Introduction

Faithful chromosome segregation is vital for transfer of intact genetic information into the daughter cells. A central role in this process is played by the spindle microtubule apparatus, which is involved in all crucial steps of chromosome division [1,2]. From engagement of the chromosomes into division by capturing kinetochores during the early stages of mitosis, through their alignment at the metaphase plate, up to the distribution of sister chromatids into daughter cells during the final stages of mitosis, all these functions are mechanistically carried out by the spindle. Although proper assembly of the spindle is required for accurate chromosome segregation, our understanding of the molecular mechanisms controlling this process is still incomplete. A clear example is the regulation of spindle length, which is important for faithful chromosome segregation [3], as well as for asymmetric cell division [4]. Although it

seems that in general spindle length is predetermined by the cell size, in certain cells, such as early mammalian embryos, it seems that the length of the spindle is regulated, to some extent, independent of cell size [5–8]. Similarly, in *Xenopus* embryos during initial cleavage cycles, the reduction in spindle size is not proportional to the decrease in cell size [9]. In these gigantic cells, spindle size is not proportional to the cell diameter and it is regulated by an upper limit, whereas when cells become smaller later in development, spindle size is more and more controlled by cell size [9–11]. Various mechanisms were shown to contribute to the regulation of spindle length. These include molecular gradients [12–14], density of kinetochore-microtubule attachments [15], a balance of the spindle forming forces [1], and limited availability of spindle building blocks in the cytoplasm [10,11]. In this study, we focused on a role of cell volume and nuclear to cytoplasmic ratio in the regulation of spindle length in mammalian blastomeres from 2-cell stage mouse embryos. By manipulating cell volume and nuclear to cytoplasmic ratio in combination with live cell imaging we discovered that cell size as well as the nuclear to cytoplasmic ratio have significant effect on spindle length. This indicates that the blastomeres of early cleavage cycles of mouse embryos regulate their spindle size by cell volume and by balanced equilibrium between nuclear and cytoplasmic volumes.

Materials and Methods

Animals

All animal work was conducted according to Act No 246/1992 Coll., on the protection of animals against cruelty and was approved by the Central Commission for Animal Welfare, approval ID 1505/2013 and 1566/2014 and supervised by the local institutional Expert committee for ensuring welfare of experimental animals of Veterinary Research Institute in Brno (*Odborná komise pro zajišťování dobrých životních podmínek pokusných zvířat*). All experiments were carried out following the rules of reduction of numbers of animals and minimizing their suffering during the experiments. BDF1 male mice were purchased from Anlab, Czech Republic. ICR/BDF1 female mice were obtained from crossing between ICR female (Animal Breeding and Experimental Facility, Faculty of Medicine, Masaryk University, Czech Republic) and BDF1 male (Anlab, Czech Republic). Experiments were performed using adult, 10–18 week old, animals.

Mouse stimulation, embryo handling

ICR/BDF1 mice were stimulated with pregnant mares serum gonadotropin (PMSG, 5 IU, Sigma Aldrich, Czech Republic) and human chorionic gonadotropin (hCG, 5 IU, Sigma Aldrich, Czech Republic) at a 44–48 hour interval. To collect embryos, mice were mated at the time of hCG administration. MII oocytes were collected 14–16 h after hCG administration from non-mated mice, 2-cell embryos were collected 40–44 h after hCG administration. MII oocytes and embryos were collect by manual rupturing of the ampulla. The cumulus cells were removed from MII oocytes by pipetting in M2 medium supplemented with hyaluronidase (150 IU/ml, Sigma Aldrich, Czech Republic). Cells were subsequently cultured in KSOM AA medium (Caisson, USA), covered with mineral oil at 37°C, 5% CO_2.

Microinjection and micromanipulations

Microinjection was performed in M2 medium (Sigma Aldrich, Czech Republic) with 1–10 microinjector (Narishige) on a Leica DM IL inverted microscope. Complementary RNAs for microinjection were prepared by *in vitro* transcription (mMESSAGE mMACHINE and Poly (A) Tailing kit, Lifetechnologies, Czech Republic) of plasmids containing ORFs of mouse β-

tubulin, TPX2, and H2B as transcription fusion with the sequence encoding fluorescent proteins EGFP, Venus, and mCherry, respectively. Enucleation was performed on a Leica DMI3000 B inverted microscope equipped with Eppendorf InjectMan® NI 2 Micromanipulator (Eppendorf, Czech Republic). 2-cell embryos were transferred into M2 medium supplemented by cytochalasin B (Sigma Aldrich, Czech Republic) for at least 15 minutes prior to micromanipulation. The nucleus was removed from one blastomere of the 2-cell embryo using a piezo drill-assisted micromanipulation system with a 12-μm-diameter pipette. The zona pellucida was removed from 2-cell embryos by treatment with 1% pronase (Sigma Aldrich, Czech Republic) dissolved in M2 medium. Blastomeres of 2-cell embryo were separated manually in M2 medium. 2-cell embryos or 3 separated blastomeres from 2-cell embryo were transferred into 0.3 mg/ml phytohemagglutinin (Sigma Aldrich, Czech Republic) in M2 medium for 30 minutes prior to fusion. The fusion of agglutinated cells was performed in 1mm fusion chamber with two direct current pulses of 75V for 50 μsec (2-cell embryo) or with 2 single pulse of 50V for 40 μsec (3 blastomeres) using Multiporator (Eppendorf, Czech Republic).

Parthenogenetic activation

MII oocytes were parthenogenetically activated by 4.5 min cultivation in 7% ethanol in M2 medium. After activation cells were transferred into KSOM AA medium (Caisson, USA), covered with mineral oil and cultured at 37°C, 5% CO_2 for 6–7 hours, after which cells were scored for pronuclei and microinjected. Embryos were transferred to microscope for live imaging at the 2-cell stage, approx. 47 hours after activation.

Live cell imaging

Embryos were transferred to a Leica SP5 confocal microscope, equipped with an EMBL incubator allowing time-lapse experiments in 5% CO2 at 37°C. 488, 514, and 561 nm excitation wavelengths, HCX PL APO 40 x /1.1 water objective, and hybrid detectors were used for detection of EGFP, Venus and mCherry fluorescent proteins. Z-stacks of 31 or 41, depending on the cell size, images were taken every 10 minutes.

Image analysis

Image analysis, spindle measurement, and nucleus and cytoplasm volume measurements were performed using Imaris software 7.6.5 (Bitplane AG, Switzerland, www.bitplane.com). Statistical analysis was performed using Prism software, version 5.00 for Mac (GraphPad Software, San Diego California USA, www.graphpad.com). Mean and SD values were calculated using MS Excel (Microsoft). The statistical significance of the difference between control and experimental group was tested using t-test or ANOVA.

Results

Spindle length scales with cell volume

In order to study the relationship between cell volume and spindle length, we employed a challenging procedure, during which two or three blastomeres from 2-cell embryos were electrofused, giving rise to cells with double or triple volume compared to an intact blastomere. The following cells were created and used in our experiments: intact blastomeres from 2-cell embryos (Intact), two fused blastomeres from 2-cell embryos (2 fused), and three fused blastomeres from 2-cell embryos (3 fused) (Fig 1A, left panel). Prior to the fusion, all cells were microinjected with cRNAs encoding Histone H2B and Tubulin tagged with fluorescent proteins; this was important for monitoring chromosome division and for measuring spindle size

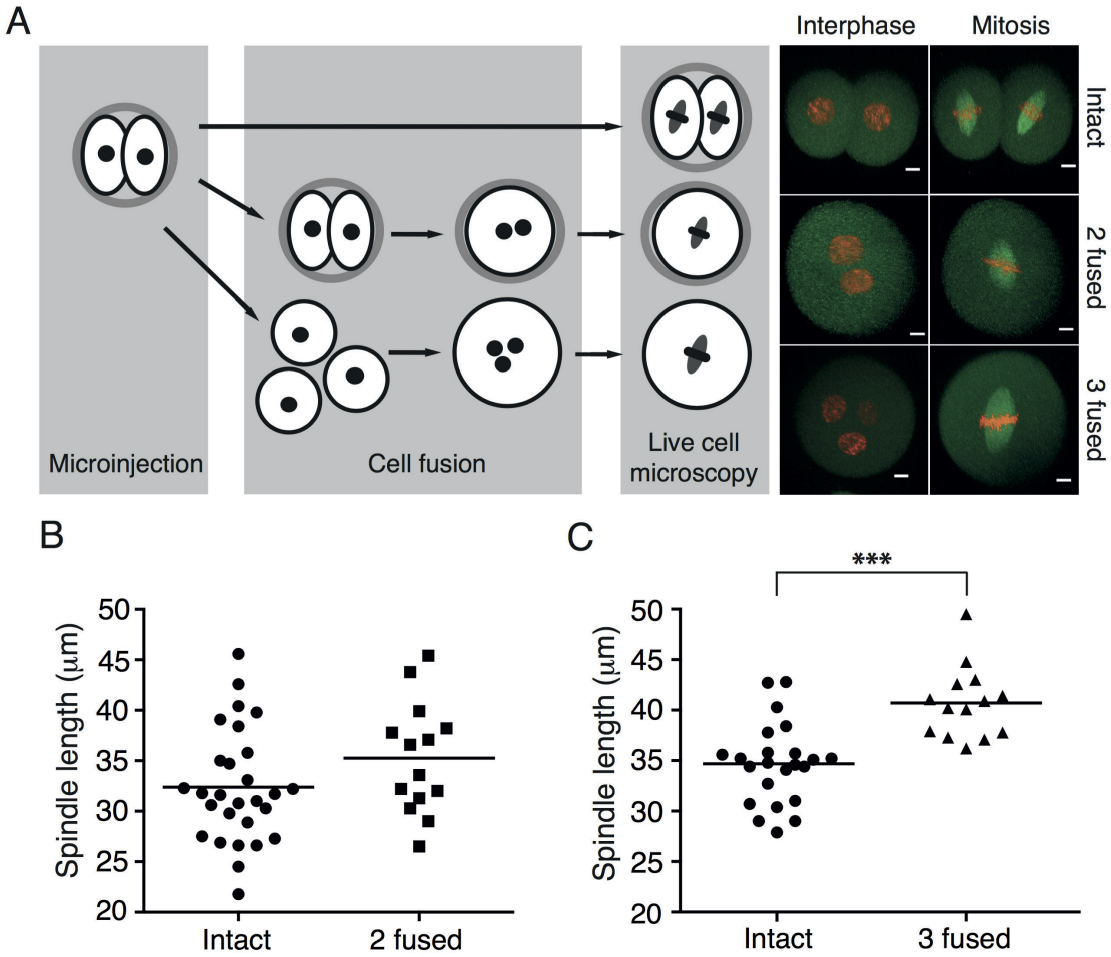

Fig 1. Spindle length increases proportionally with cell volume. (A) Left panel: Blastomeres of mouse 2-cell embryos were microinjected with cRNAs encoding Histone-H2B fused to mCherry and Tubulin fused to EGFP. The following cells were used for experiments: intact two cell embryos (Intact), cells with double volume obtained by fusion of two blastomeres (2 fused), and cells with triple volume obtained by fusion of three blastomeres (3 fused). Right panel shows representative movie frames from time lapse imaging of each cell type in interphase and in mitosis; chromosomes are in red, spindle is in green, scale bar represents 10 μm. (B) The length of the spindle in 2 fused cells (35.26 ± 5.52 μm, n = 14) was not significantly increased ($p = 0.1236$) in comparison to the length of the spindle in Intact cells (32.38 ± 5.63 μm, n = 28). (C) The length of the spindle in 3 fused cells (40.71 ± 3.57 μm, n = 14) was significantly increased ($p < 0.0001$) in comparison to the length of the spindle in Intact cells (34.68 ± 3.99 μm, n = 23).

doi:10.1371/journal.pone.0149535.g001

during the subsequent mitosis. It was shown previously that the duration of the second mitosis in mouse embryos is approximately 70 minutes [16]. We decided to avoid pharmacological synchronization in order to obtain spindles with unperturbed structure and function. However, under these conditions, the time interval during which cells are in metaphase is relatively narrow. To circumvent this, we used confocal live cell imaging and recorded the entire cell division. Cells were cultured on a confocal microscope equipped with temperature and CO_2

control and z-stacks of 31 or 41 images were taken every 10 minutes (Fig 1A, right panel). Our settings allowed good coverage of the whole cell volume and therefore morphological parameters of the spindles were possible to measure for each cell. The size of the spindle and the cell was measured using image stacks acquired during the last time interval before anaphase. Our results (Fig 1B) showed that the average spindle length in Intact cells was 32.38 ± 5.63 μm. The spindle size in 2 fused cells was increased, although not significantly, in comparison to the intact cells, on average it was 35.26 ± 5.52 μm. However, the spindles in 3 cells fused were significantly longer, measuring 40.71 ± 3.57 μm (Fig 1C). Although the spindle size difference between intact and 2 fused cells exists, only in 3 fused cells the difference in cell volume was sufficiently big to detect the variations in spindle size within a relatively narrow cohort of cells. In 3 fused cells the spindles were not only longer, but they were also significantly wider, which was probably due to a larger number of chromosomes occupying the equatorial plane (S1 Fig).

Metaphase spindle length is regulated by a balanced ratio between nuclear and cytoplasmic volumes

It was suggested that the number of chromosomes or kinetochores affects spindle length [15,17]. To test this, we compared spindle size in intact cells with 40 chromosomes (Intact) with spindle size in 2 fused cells with 80 chromosomes and two fused cells in which one of them was enucleated before fusion (2 fused enucleated) and therefore carried 40 chromosomes (Fig 2A). As in previous experiments, all cells were microinjected with cRNAs encoding Histone and Tubulin fusion proteins in order to follow chromosomes and spindles during cell division. The difference in spindle length between intact (32.83 ± 2.95 μm) and 2 fused cells (34.96 ± 3.37 μm) was not statistically significant, similarly to our previous experiments. However, the difference between these two groups and 2 fused enucleated cells was dramatic, with spindles measuring on average 42.91 ± 3.35 μm, in the latter group (Fig 2B). We also measured the width of the spindle in all three groups (S2 Fig). The spindle was wider in 2 fused than in intact cells or 2 fused enucleated cells. Since Intact and 2 fused enucleated cells harbor the same number of chromosomes, it seems that spindle width in this cell type is controlled by the number of chromosomes. Our results indicated that the number of chromosomes/kinetochores does not control spindle length since the Intact and 2 fused enucleated cells contain the same number of chromosomes/kinetochores although their spindle size differs significantly. To confirm this, we employed a different method for reducing chromosome numbers and prepared 2-cell blastomeres from parthenogenetically activated metaphase II eggs (Unfertilized) and compared them to intact blastomeres of 2-cell embryos (Fertilized) (Fig 2C). Spindle length in unfertilized haploid embryos was significantly increased (38.04 ± 4.06 μm) in comparison to intact control cells (31.18 ± 3.32 μm) (Fig 2D), whereas spindle width was greater in fertilized cells, which contained more chromosomes (S3 Fig). Therefore both cell types in which the number of chromosomes was reduced, namely 2 fused enucleated and Unfertilized cells, showed significant increase of mitotic spindle length. We were however puzzled by other cell types, which we created and in which the changes in chromosome numbers did not show this effect. Intact diploid blastomeres carrying 40 chromosomes with spindle length 32.65 ± 4.20 μm (average from all experiments), 2 fused cells carrying 80 chromosomes with spindle length 37.62 ± 6.49 μm, 3 fused cells with 120 chromosomes and spindle length 40.15 ± 2.61 μm, 2 fused enucleated cells with 40 chromosomes and spindles 41.54 ± 3.15 long, and finally parthenogenetically activated cells with 20 chromosomes and spindle length 38.04 ± 4.06 μm. From this comparison, it seems very likely, that the number of chromosomes may not be a major factor controlling spindle length. In order to search for other potential differences between these cells, we measured the nuclear to cytoplasmic (N:C) ratio in the last

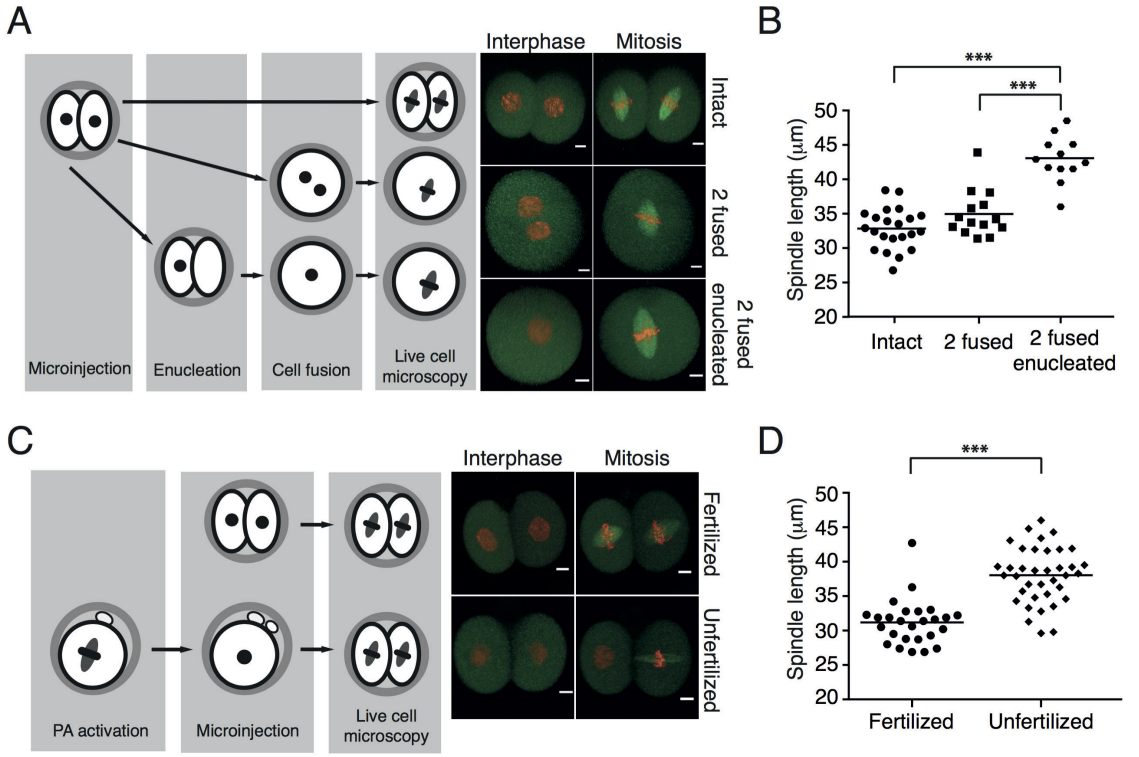

Fig 2. Changes in nuclear to cytoplasmic ratio have impact on spindle length. (A) Left panel: Blastomeres of mouse 2-cell embryos were microinjected with cRNAs encoding Histone-H2B fused to mCherry and Tubulin fused to EGFP. The following cells were used for experiments: intact two cell embryos (Intact), cells with double volume obtained by fusion of two blastomeres (2 fused), and cells with double volume of the cytoplasm and impaired nuclear to cytoplasmic ratio resulting from enucleation (2 fused enucleated). Right panel shows representative movie frames from time lapse imaging of each cell type in interphase and in mitosis; chromosomes are in red, spindle is in green, scale bar represents 10 µm. (B) The length of the spindle in 2 fused enucleated cells (42.91 ± 3.35 µm, n = 12) was significantly increased ($p < 0.0001$) in comparison to the length of the spindle in intact cells (32.83 ± 2.95 µm, n = 22) or 2 fused cells (34.96 ± 3.37 µm, n = 14). (C) Left panel: haploid embryos were produced by parthenogenetic activation of metaphase II eggs. Following activation, cells were microinjected with cRNAs encoding Histone-H2B fused to mCherry and Tubulin fused to EGFP together with blastomeres of 2-cell embryos. Right panel shows representative movie frames from time lapse imaging of each cell type in interphase and in mitosis; chromosomes are in red, spindle is in green, scale bar is 10 µm. (D) The length of the spindle in Unfertilized haploid cells (38.04 ± 4.06 µm, n = 37) was significantly increased ($p < 0.0001$) in comparison to the length of the spindle in intact cells (Fertilized) (31.18 ± 3.32 µm, n = 26).

doi:10.1371/journal.pone.0149535.g002

frame before NEBD (Fig 3A). It revealed that the two groups with significantly lower N:C ratio in comparison to intact cells are 2 fused enucleated and unfertilized cells. Further comparison of N:C ratio and spindle length showed that cells with significantly lower N:C ratio had longer spindles (Fig 3B). This correlation was specifically apparent in 2 fused enucleated cells, which had the lowest N:C ratio and also the longest spindles. We concluded that maintenance of a balanced ratio between cytoplasm and nucleus is important for accurate regulation of spindle length, whereas the number of chromosomes is important for spindle width. We believe that the simplest explanation of our experiments would envisage unknown component or components are lower in cells in which the nuclei are smaller compared to the cell volume. Several recent studies showed that the activity of spindle assembly factor TPX2 is important for the

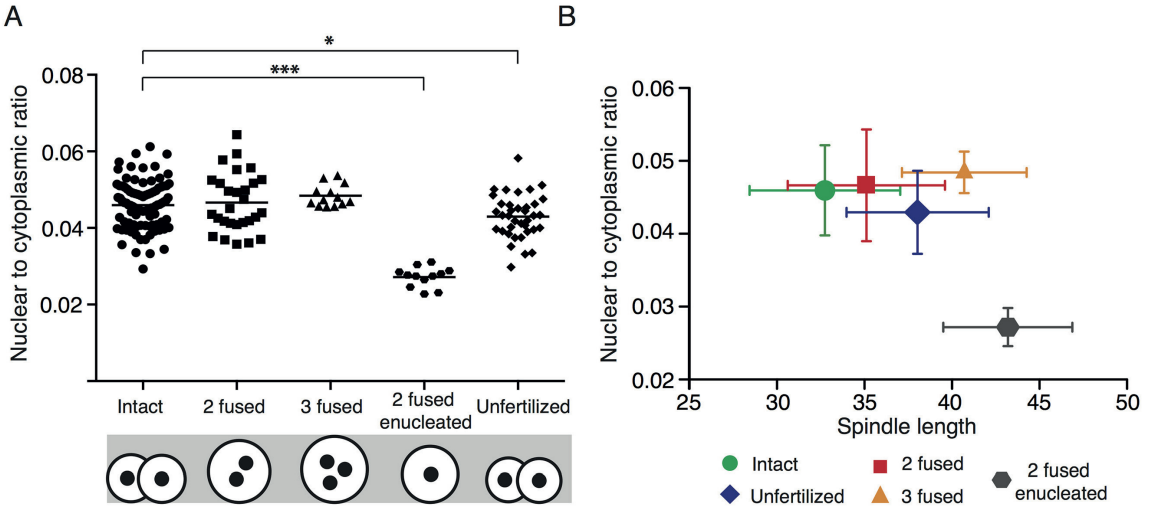

Fig 3. Nuclear to cytoplasmic ratio in cells created by fusion, enucleation, or parthenogenetic activation. Panel A: The chart shows nuclear to cytoplasmic ratio in all cells used in experiments described in Figs 1 and 2: Intact cells (0.046, n = 93), 2 fused cells (0.047, n = 28), 3 fused cells (0.048, n = 13), 2 fused enucleated cells (0.027, n = 12) and unfertilized cells (0.043, n = 40). N:C ratio of Intact cells is significantly different in comparison to 2 fused enucleated ($p < 0.0001$) and unfertilized cells ($p = 0.0116$). The diagram below the X-axis illustrates the proportional differences between cell and nuclear size of each cell type. Panel B: The plot shows a relationship between nuclear to cytoplasmic ratio and spindle length in all cells used in experiments described in Figs 1 and 2: Green dots represent intact cells (spindle length: 32.75 ± 4.30; NC ratio: 0.046 ± 0.006), red squares represent 2 fused cells (spindle length: 35.11 ± 4.49; NC ratio: 0.047 ± 0.008), orange triangles represent 3 fused cells (spindle length: 40.70 ± 3.56; NC ratio: 0.048 ± 0.003), blue rhombuses represent unfertilized cells (spindle length: 38.04 ± 4.06; NC ratio: 0.043 ± 0.006) and gray hexagons represent 2 fused enucleated cells (spindle length: 43.20 ± 3.69; NC ratio: 0.027 ± 0.003).

doi:10.1371/journal.pone.0149535.g003

regulation of spindle length [18–20]. Because of its exclusive nuclear localization before cell division, this was a good candidate as the decreased component caused by the relatively smaller nucleus vs. the volume of the cytoplasm. We tested the effect of TPX2 overexpression on spindle length using 2 fused enucleated cells, which displayed the longest spindles. Cells were microinjected with cRNAs encoding Histone and Tubulin fused to fluorescent proteins and half of the cells also with cRNA encoding TPX2 (Fig 4A). In some experiments the TPX2 was also fused to fluorescent protein in order to assess its localization during interphase and in mitosis. The localization of TPX2 in 2 fused enucleated cells was exclusively nuclear in interphase with transition to the whole cell volume as cells entered mitosis (Fig 4B).The overexpression of TPX2 in concentrations preserving intact spindles did not significantly affected spindle size (Fig 4C) and therefore we concluded that this factor is not crucial for the regulation of spindle length in this cell type.

Discussion

One set of fundamental questions in cell biology, which still remains to be elucidated, is how the size of organelles and intracellular structures is regulated [21]. Such regulation must be able to flexibly respond to dramatic changes, emerging for example during embryonic development, which is characterized by rapid sequential cell cycles with substantial decrease of the cell volume during every cleavage. In our study, we focused on general rules regulating spindle size, namely the role of cell size, nuclear to cytoplasmic ratio, and number of chromosomes in this process. We employed large cells of mouse 2-cell embryos because due to their size the changes

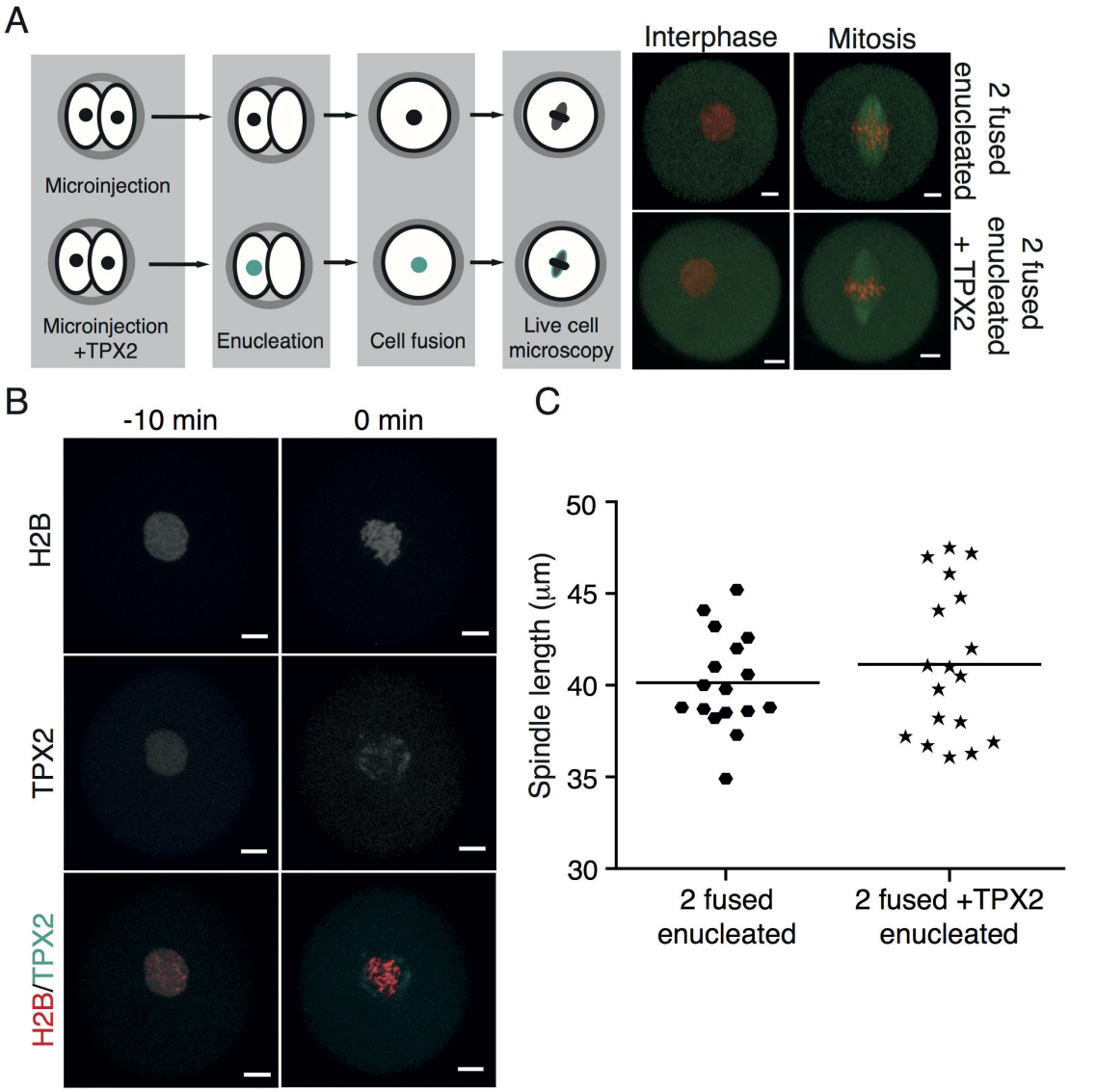

Fig 4. Overexpression of TPX2 has no effect on spindle length. (A) Left panel: Blastomeres of mouse 2-cell embryos were microinjected with cRNAs encoding Histone-H2B fused to mCherry and Tubulin fused to EGFP with (bottom) or without (top) cRNA encoding TPX2 protein. Following microinjection, one of the two blastomeres in each embryo was enucleated and then both fused together. Right panel shows representative movie frames from time lapse imaging of each cell type in interphase and in mitosis, chromosomes are in red, spindle is in green, scale bar represents 10 μm. (B) In some experiments, TXP2 was used with fluorescent tag. Representative images of cells before (left panels, 10 min) and during NEBD (right panel, 0 min) show the nuclear localization of exogenous TPX2 in interphase and its relocalization to the cytoplasm before spindle assembly. Chromosomes are in red, TPX2 in cyan, scale bar represents 10 μm. (C) The length of the spindle in 2 fused enucleated cells with overexpressed TPX2 (41.14 ± 4.07 μm, n = 18) was not significantly different (p = 0.3961) compared to the length of the spindle in 2 fused enucleated cells (40.14 ± 2.64 μm, n = 17).

doi:10.1371/journal.pone.0149535.g004

of the cell volume or nuclear to cytoplasmic ratio can be achieved. Our cell fusion experiments showed that the size of the spindle in early mammalian embryos is controlled by the cell size. This is in contrast with data obtained using *Xenopus* embryos, where the spindle size in initially extremely large embryonic cells has a maximum size limit [9]. Our cell fusion experiments suggested that the upper limit of the spindle is either not active in size regime of mouse embryo or was not reached in our experiments. It was shown that during mouse early embryonic cell cleavages spindle size decreases more slowly than cell size [5,8]. Also, removal of a substantial amount of the cytoplasm did not cause shortening of the spindle [5], suggesting that spindle size during this developmental period is at its lower limit. It was shown that the size of the organelles and subcellular structures is controlled by the pool of the available cytoplasmic components (reviewed in [22]). In *C. elegans* embryo for example, spindle length is regulated by centrosome size [13] and centrosome size is in turn regulated by limited amount of centrosome material in the cytoplasm [23]. Recently published work using *Xenopus* cell free extracts showed that in this system spindle size is controlled by the amount of cytoplasm [10,11]. To test this hypothesis using our model system, we compared cells which resulted from fusion of two equal 2-cell embryo blastomeres or one intact and one enucleated blastomere, therefore we obtained cells with different N:C ratio. If the size of the spindle is controlled by the availability of cytoplasmic components, in both groups the spindle should be equally increased. However, the spindles in 2 fused enucleated cells were significantly longer indicating that the cytoplasmic components are not limiting for the spindle size in these cells. Those results, in our opinion indicate that rather than by the amount of cytoplasm, spindle size is controlled by N:C ratio (Fig 3). The N:C ratio was shown to participate in regulation of zygotic gene activation at the midblastula transition in *Xenopus* [24]. The changes in this ratio influence a variety of cell behaviors [25,26] and it is conceivable that they could also have an effect on the regulation of spindle length. However, we need to keep in mind that our experimental procedure is not directly comparable to N:C changes during early development and the changes may not be limited to the N:C ratio. Indeed, it was recently shown that in Xenopus oocytes many proteins are exclusively located either in the nucleus or in the cytoplasm [27]. Therefore, during enucleation, proteins within nucleus are specifically depleted, which might change the stoichiometry of the system. In conclusion, our study brings some new insight into regulation of spindle length in early mouse embryo, namely the role of the nuclear to cytoplasmic ratio in this process. However, the molecular basis of this regulation needs to be revealed by future work. Obtaining more information about mechanisms controlling chromosome segregation, such as for example regulation of spindle length, is vital since mammalian early embryos are highly aneuploid [28] and it is conceivable that failure of the mechanisms controlling spindle size might contribute to the increased frequency of chromosome segregation errors.

Supporting Information

S1 Fig. The spindle of 3 fused embryos (21.27 ± 1.32 μm, n = 13) is significantly ($p < 0,0001$) wider in comparison to spindle of Intact cell (13.14 ± 0.72 μm, n = 21).
(TIFF)

S2 Fig. The spindle of 2 fused embryos (17.29 ± 1.01 μm, n = 14) is significantly wider ($p < 0.0001$) than the spindle of 2 fused embryos (15.28 ± 1.17 μm, n = 12) and intact embryos (13.17 ± 1.04 μm, n = 22).
(TIFF)

S3 Fig. The spindle of fertilized embryos (13.21 ± 1.14 μm, n = 26) is significantly wider ($p < 0,0001$) compared to the spindle of unfertilized embryos (9.42 ± 1.47 μm, n = 37). (TIFF)

Acknowledgments

We are thankful to all members of Martin Anger's laboratory for their comments. We would like to thank Prof. Daniela Cimini, Virginia Bioinformatics Institute, for support, guidance and encouragement during editorial process. We are also grateful for technical advice from Dr. Jason Knott, Michigan State University, USA.

Author Contributions

Conceived and designed the experiments: MA. Performed the experiments: LN KK TQDN M. Sodek. Analyzed the data: LN MA M. Sodek M. Skultety. Wrote the paper: LN MA.

References

1. Dumont S, Mitchison TJ. Force and length in the mitotic spindle. Curr Biol. 2009; 19: R749–61. doi: 10.1016/j.cub.2009.07.028 PMID: 19906577
2. Walczak CE, Cai S, Khodjakov A. Mechanisms of chromosome behaviour during mitosis. Nat Rev Mol Cell Biol. 2010; 11: 91–102. doi: 10.1038/nrm2832 PMID: 20068571
3. Choi SH, McCollum D. A role for metaphase spindle elongation forces in correction of merotelic kinetochore attachments. Curr Biol. 2012; 22: 225–230. doi: 10.1016/j.cub.2011.12.022 PMID: 22264609
4. Dumont J, Petri S, Pellegrin F, Terret ME, Bohnsack MT, Rassinier P, et al. A centriole- and RanGTP-independent spindle assembly pathway in meiosis I of vertebrate oocytes. J Cell Biol. 2007; 176: 295–305. PMID: 17261848
5. Courtois A, Schuh M, Ellenberg J, Hiiragi T. The transition from meiotic to mitotic spindle assembly is gradual during early mammalian development. J Cell Biol. 2012; 198: 357–370. doi: 10.1083/jcb.201202135 PMID: 22851319
6. Goshima G, Scholey JM. Control of mitotic spindle length. Annu Rev Cell Dev Biol. 2010; 26: 21–57. doi: 10.1146/annurev-cellbio-100109-104006 PMID: 20604709
7. Howe K, FitzHarris G. Recent insights into spindle function in mammalian oocytes and early embryos. Biol Reprod. 2013; 89: 71. doi: 10.1095/biolreprod.113.112151 PMID: 23966320
8. Yamagata K, FitzHarris G. 4D imaging reveals a shift in chromosome segregation dynamics during mouse pre-implantation development. Cell Cycle. 2013; 12: 157–165. doi: 10.4161/cc.23052 PMID: 23255117
9. Wühr M, Chen Y, Dumont S, Groen AC, Needleman DJ, Salic A, et al. Evidence for an upper limit to mitotic spindle length. Curr Biol. 2008; 18: 1256–1261. doi: 10.1016/j.cub.2008.07.092 PMID: 18718761
10. Good MC, Vahey MD, Skandarajah A, Fletcher DA, Heald R. Cytoplasmic volume modulates spindle size during embryogenesis. Science. 2013; 342: 856–860. doi: 10.1126/science.1243147 PMID: 24233724
11. Hazel J, Krutkramelis K, Mooney P, Tomschik M, Gerow K, Oakey J, et al. Changes in cytoplasmic volume are sufficient to drive spindle scaling. Science. 2013; 342: 853–856. doi: 10.1126/science.1243110 PMID: 24233723
12. Bastiaens P, Caudron M, Niethammer P, Karsenti E. Gradients in the self-organization of the mitotic spindle. Trends Cell Biol. 2006; 16: 125–134. PMID: 16478663
13. Greenan G, Brangwynne CP, Jaensch S, Gharakhani J, Jülicher F, Hyman AA. Centrosome size sets mitotic spindle length in Caenorhabditis elegans embryos. Curr Biol. 2010; 20: 353–358. doi: 10.1016/j.cub.2009.12.050 PMID: 20137951
14. Kalab P, Heald R. The RanGTP gradient—a GPS for the mitotic spindle. J Cell Sci. 2008; 121: 1577–1586. doi: 10.1242/jcs.005959 PMID: 18469014
15. Nannas NJ, O'Toole ET, Winey M, Murray AW. Chromosomal attachments set length and microtubule number in the Saccharomyces cerevisiae mitotic spindle. Mol Biol Cell. 2014; 25: 4034–4048. doi: 10.1091/mbc.E14-01-0016 PMID: 25318669

16. Ciemerych MA, Maro B, Kubiak JZ. Control of duration of the first two mitoses in a mouse embryo. Zygote. 1999; 7: 293–300. PMID: 10717947

17. Nicklas RB, Gordon GW. The total length of spindle microtubules depends on the number of chromosomes present. J Cell Biol. 1985; 100: 1–7. PMID: 4038398

18. Bird AW, Hyman AA. Building a spindle of the correct length in human cells requires the interaction between TPX2 and Aurora A. J Cell Biol. 2008; 182: 289–300. doi: 10.1083/jcb.200802005 PMID: 18663142

19. Fu J, Bian M, Xin G, Deng Z, Luo J, Guo X, et al. TPX2 phosphorylation maintains metaphase spindle length by regulating microtubule flux. J Cell Biol. 2015; 210: 373–383. doi: 10.1083/jcb.201412109 PMID: 26240182

20. Helmke KJ, Heald R. TPX2 levels modulate meiotic spindle size and architecture in Xenopus egg extracts. J Cell Biol. 2014; 206: 385–393. doi: 10.1083/jcb.201401014 PMID: 25070954

21. Chan YH, Marshall WF. How cells know the size of their organelles. Science. 2012; 337: 1186–1189. doi: 10.1126/science.1223539 PMID: 22955827

22. Goehring NW, Hyman AA. Organelle growth control through limiting pools of cytoplasmic components. Curr Biol. 2012; 22: R330–9. doi: 10.1016/j.cub.2012.03.046 PMID: 22575475

23. Kirkham M, Müller-Reichert T, Oegema K, Grill S, Hyman AA. SAS-4 is a C. elegans centriolar protein that controls centrosome size. Cell. 2003; 112: 575–587. PMID: 12600319

24. Jevtić P, Levy DL. Nuclear size scaling during Xenopus early development contributes to midblastula transition timing. Curr Biol. 2015; 25: 45–52. doi: 10.1016/j.cub.2014.10.051 PMID: 25484296

25. Edens LJ, White KH, Jevtic P, Li X, Levy DL. Nuclear size regulation: from single cells to development and disease. Trends Cell Biol. 2013; 23: 151–159. doi: 10.1016/j.tcb.2012.11.004 PMID: 23277088

26. Jevtić P, Edens LJ, Vuković LD, Levy DL. Sizing and shaping the nucleus: mechanisms and significance. Curr Opin Cell Biol. 2014; 28: 16–27. doi: 10.1016/j.ceb.2014.01.003 PMID: 24503411

27. Wühr M, Güttler T, Peshkin L, McAlister GC, Sonnett M, Ishihara K, et al. The Nuclear Proteome of a Vertebrate. Curr Biol. 2015; 25: 2663–2671. doi: 10.1016/j.cub.2015.08.047 PMID: 26441354

28. Fragouli E, Alfarawati S, Spath K, Jaroudi S, Sarasa J, Enciso M, et al. The origin and impact of embryonic aneuploidy. Hum Genet. 2013; 132: 1001–1013. doi: 10.1007/s00439-013-1309-0 PMID: 23620267

McGuinness BE, Anger M, Kouznetsova A, Gil-Bernabé AM, Helmhart W, Kudo NR, et al. Regulation of APC/C activity in oocytes by a Bub1-dependent spindle assembly checkpoint. Curr Biol. 2009;19: 369–380.

Impact Factor/Quartile: 10,445/Q1
Times cited (Wos May 2019): 123
Significance: Essential paper showing that SAC is crucial in oocytes by genetic tools
Contribution of the author: shared first author – microinjection experiments & time lapse imaging, data interpretation, design of some experiments

Current Biology 19, 369–380, March 10, 2009 ©2009 Elsevier Ltd All rights reserved DOI 10.1016/j.cub.2009.01.064

Article

Regulation of APC/C Activity in Oocytes by a Bub1-Dependent Spindle Assembly Checkpoint

Barry E. McGuinness,[1,7] Martin Anger,[1,2,7,8] Anna Kouznetsova,[3] Ana M. Gil-Bernabé,[4,9] Wolfgang Helmhart,[1] Nobuaki R. Kudo,[4,10] Annelie Wuensche,[5] Stephen Taylor,[6] Christer Hoog,[3] Bela Novak,[2] and Kim Nasmyth[1,*]

[1]Department of Biochemistry
[2]Oxford Centre for Integrative Systems Biology
University of Oxford
South Parks Road
Oxford, OX1 3QU
United Kingdom
[3]Department of Cell and Molecular Biology
Karolinska Institutet
S-171 77 Stockholm
Sweden
[4]Research Institute of Molecular Pathology
Dr. Bohr-Gasse 7
A-1030 Vienna
Austria
[5]EMBL Heidelberg
Meyerhofstraße 1
69117 Heidelberg
Germany
[6]Faculty of Life Sciences
Michael Smith Building
Oxford Road
Manchester M13 9PT
United Kingdom

Summary

Background: Missegregation of chromosomes during meiosis in human females causes aneuploidy, including trisomy 21, and is thought also to be the major cause of age-related infertility [1]. Most errors are thought to occur at the first meiotic division. The high frequency of errors raises questions as to whether the surveillance mechanism known as the spindle assembly checkpoint (SAC) that controls the anaphase-promoting complex or cyclosome (APC/C) operates effectively in oocytes. Experimental approaches hitherto used to inactivate the SAC in oocytes suffer from a number of drawbacks.
Results: Bub1 protein was depleted specifically in oocytes with a Zp3-Cre transgene to delete exons 7 and 8 from a floxed *BUB1*^{F} allele. Loss of Bub1 greatly accelerates resolution of chiasmata and extrusion of polar bodies. It also causes defective biorientation of bivalents, massive chromosome missegregation at meiosis I, and precocious loss of cohesion between sister centromeres. By using a quantitative assay for APC/C-mediated securin destruction, we show that the APC/C is activated in an exponential fashion, with activity peaking 12–13 hr after GVBD, and that this process is advanced by 5 hr in oocytes lacking Bub1. Importantly, premature chiasmata resolution does not occur in Bub1-deficient oocytes also lacking either the APC/C's Apc2 subunit or separase. Finally, we show that Bub1's kinase domain is not required to delay APC/C activation.
Conclusions: We conclude that far from being absent or ineffective, the SAC largely determines the timing of APC/C and hence separase activation in oocytes, delaying it for about 5 hr.

Introduction

Chromosome segregation in eukaryotic cells depends on attachment of sister kinetochores to microtubules emanating from opposite poles of the cell, a process known as amphitelic attachment or biorientation [2]. This is achieved at least partly because of a system that corrects errors. Connections between kinetochores and microtubules are selectively stabilized, or rather become refractory to the disrupting effect of the Aurora B kinase, by tension created when bioriented sister chromatids [3] are pulled in opposite directions while being held together by the cohesin complex [4]. Disjunction of sister chromatids at the onset of anaphase is eventually triggered by cleavage of cohesin's kleisin subunit at the hands of a highly regulated protease called separase [5, 6], which is kept inactive for most of the cell cycle through the binding of an inhibitory chaperone called securin and phosphorylation by cyclin B/Cdk1 kinase [7]. Separase is activated only through destruction of securin and cyclin B at the hands of an ubiquitin protein ligase called the anaphase-promoting complex or cyclosome (APC/C) when all chromosomes have bioriented [8].

Because it triggers the removal from centromeres of the Aurora B kinase [9] as well as the loss of sister-chromatid cohesion, the APC/C must not be activated until chromosome biorientation has been completed. The regulatory mechanism responsible for delaying anaphase in this manner, known as the spindle assembly checkpoint (SAC) [10], requires, among others, the Mad1, Mad2, Bub1, and BubR1 proteins. With the help of Bub1, Mad1 binds to unattached, mono-oriented, or syntelically attached kinetochores and catalyzes sequestration of the APC/C's Cdc20 activator protein by a protein called Mad2. The Cdc20/Mad2 complex, together with yet another SAC protein called BubR1, binds to the APC/C and blocks its ability to ubiquitinylate either securin or cyclin B. Production of inhibitory Cdc20/Mad2/BubR1 complexes only ceases when all chromosomes have bioriented, which triggers the ubiquitinylation and subsequent destruction of securin and cyclin B by the APC/C, which in turn activates separase and triggers sister-chromatid disjunction. In the cells of some organisms, such as yeast [11] and flies [12], the SAC is not essential for mitosis, though it greatly reduces rare missegregation events. Loss of the SAC in mammalian cells, on the other hand, causes premature sister-chromatid disjunction

*Correspondence: kim.nasmyth@bioch.ox.ac.uk
[7]These authors contributed equally to this work
[8]Present address: Institute of Animal Physiology and Genetics, AS CR, v.v.i., Rumburska 89, 277 21 Libechov, Czech Republic and Veterinary Research Institute, Hudcova 70, 621 00 Brno, Czech Republic
[9]Present address: Radiation Oncology and Biology, The Radiobiology Research Institute, Churchill Hospital, University of Oxford, Oxford OX3 7LJ, United Kingdom
[10]Present address: Institute of Reproductive and Developmental Biology (IRDB), Imperial College London, Hammersmith Hospital, Du Cane Road, London W12 0NN, United Kingdom

and as a consequence massive chromosome missegration and lethality [13, 14]. Presumably because of the SAC, a single misaligned chromosome delays the onset of anaphase in tissue-culture cells [15].

During the first meiotic division, biorientation of sister kinetochores is explicitly blocked and the tension necessary to ensure that kinetochores attach stably to microtubules is instead created by traction toward opposite poles of maternal and paternal kinetochores, whose disjunction is prevented by the chiasmata holding bivalent (tetrad) chromosomes together [16]. The first meiotic division is eventually triggered by destruction of sister-chromatid cohesion by separase along chromosome arms but not at centromeres. This resolves chiasmata, splitting the bivalent into two meiosis II (dyad) chromosomes, each containing a parental and a recombinant chromatid.

A suggestion that the SAC might be missing in vertebrate oocytes and that this could explain the high incidence of human aneuploidy comes from studies of XO mice, which carry only a single X chromosome but are phenotypically female. Despite not having a homologous X chromosome available for recombination, such females are fertile, albeit at a reduced level. In one-third of oocytes, sister chromatids disjoin precociously at anaphase I, producing eggs with individual X chromatids, but in the remaining two-thirds of oocytes, univalent X chromosomes segregate, without any major delay in the onset of anaphase, either to the egg or to the first polar body [17, 18]. If the SAC were effective in oocytes, it should surely detect mono-oriented univalent X chromosomes and block the first meiotic division, so the argument goes.

The notion that the SAC is ineffective in oocytes has been challenged by the finding that inhibitors such as nocodazole, which interfere with microtubule dynamics, clearly block polar body extrusion (PBE) [19, 20] and the onset of securin proteolysis [21–23]. Depletion of Mad2 through injection of morpholino antisense oligonucleotides alleviates, albeit only partially, the inhibition of securin destruction and permits a minor fraction of oocytes to undergo polar body extrusion (PBE) in the presence of nocodazole. It also induces modest chromosome missegregation at meiosis I in untreated oocytes, possibly by advancing the onset of securin destruction by about 60 min [21]. Meanwhile, injection into GV mouse oocytes of mRNAs that overexpress an N-terminal fragment of Bub1 (Bub1 dn, aa1–331), which binds to kinetochores and is thought to block activity of the endogenous protein, advances PBE by 3 hr [24]. However, the experimental approaches hitherto used to address the role of the SAC in oocytes suffer from a number of drawbacks. These include the likelihood of incomplete knockdown RNA interference, the certainty that at least half the Mad2 protein persists in the *Mad2*$^{+/-}$ oocytes [25], and the possibility that overexpressed Bub1 dn [24] and Mad2 dn [20] have unknown or unforeseen effects. To overcome these limitations, we created mice in which the *BUB1* gene is deleted specifically in oocytes.

Results

Deletion of *BUB1* in Oocytes Causes Sterility and Advances Polar Body Extrusion

To inactive Bub1 in oocytes, female mice with exons 7 and 8 of the *BUB1* gene flanked with *LoxP* sites (*BUB1*^{F}) [14] were crossed to males that express Cre recombinase under the control of the *Zona pellucida 3* promoter (*Zp3-Cre*) [26], which is expressed exclusively during the early stages of growing oocytes [27]. Genotyping of offspring from crosses of *BUB1*$^{F/+}$ *Zp3-Cre* females to wild-type males showed that 64 out of 64 *BUB1*^{F} alleles were converted to *bub1*$^{\Delta}$ in the female germline. *BUB1*$^{F/+}$*Zp3-Cre* and *BUB1*$^{F/F}$ females are fertile. In contrast, not a single pregnancy was observed after 10 weeks in any one of six *BUB1*$^{F/F}$ *Zp3-Cre* females crossed to wild-type males. The ovaries of *BUB1*$^{F/F}$ *Zp3-Cre* females contained normal numbers of germinal vesicle (GV)-stage oocytes surrounded by cumulus cells (40–60 oocytes per female; data not shown).

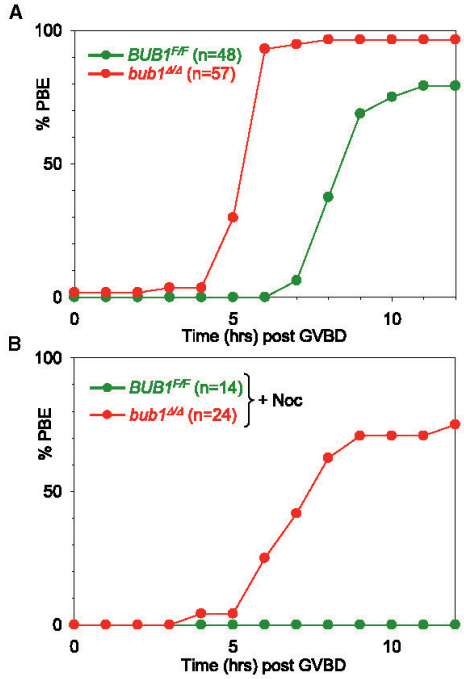

Figure 1. PBE Timing Is Advanced in *bub1*$^{\Delta/\Delta}$ Oocytes

(A) Kinetics of polar body extrusion (PBE). *BUB1*$^{F/F}$ and *bub1*$^{\Delta/\Delta}$ oocytes were harvested in M2 medium containing IBMX, which inhibits GVBD. Oocytes were released into inhibitor-free M16 medium. 90 min after release, those oocytes that had completed GVBD were selected for further analysis. This was set as time = 0 hr. Oocytes were monitored every hour and scored for completion of PBE.

(B) *bub1*$^{\Delta/\Delta}$ oocytes can escape a nocodazole-induced arrest. Oocytes were harvested and cultured as in (A) except nocodazole was added to the M16 medium at 5 μM from time = 0 hr until the end of the experiment.

To investigate Bub1's function during oocyte maturation, fully grown GV-stage mouse oocytes were harvested in the presence of IBMX from *BUB1*$^{F/F}$ females and *BUB1*$^{F/F}$ *Zp3-Cre* females (*bub1*$^{\Delta/\Delta}$). The two sets of oocytes underwent germinal vesicle breakdown (GVBD) with similar kinetics and efficiency upon removal of IBMX (data not shown). In contrast, the interval between GVBD and PBE was reduced from 08:30 ± 01:12 (n = 48) to 05:23 ± 01:04 hr (n = 57) by Bub1 depletion (Figure 1A). The fraction of cells that extruded a second polar body when cultured for 24 hr was equally low in *BUB1*$^{F/F}$ and *bub1*$^{\Delta/\Delta}$ oocytes (data not shown), which is consistent with the previous finding that CSF arrest was unaffected by a putatively dominant-negative Bub1 protein [24]. Strikingly, 75% of *bub1*$^{\Delta/\Delta}$ oocytes (n = 24) extruded the first polar body 07:20 ± 01:42 hr after GVBD (n = 18) in the presence of 5 μM nocodazole, a treatment that completely blocks PBE in *BUB1*$^{F/F}$ oocytes (n = 14) (Figure 1B).

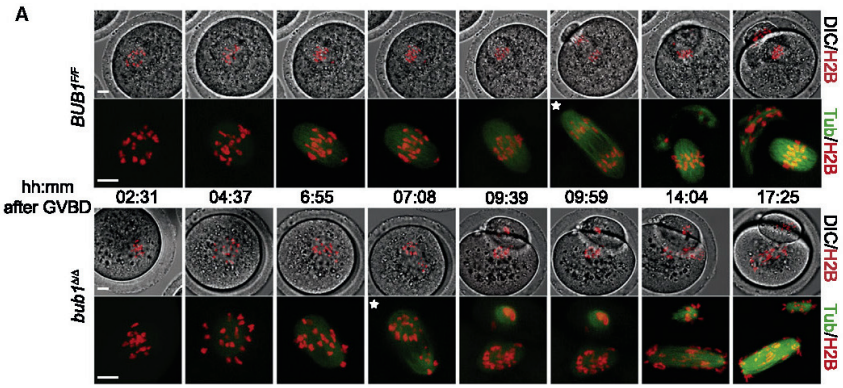

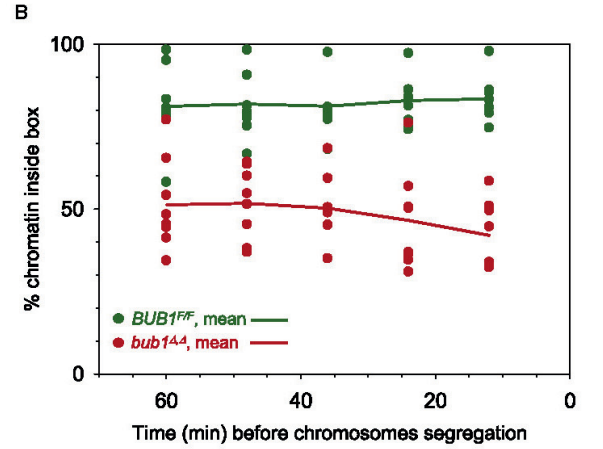

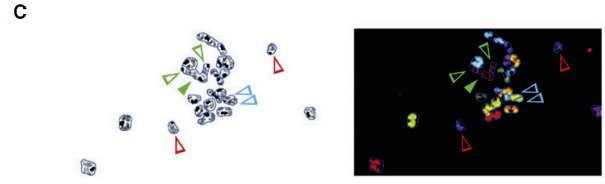

D

Chromosome	% cells in which chromosome was non-disjoined	% of separated chromatids as fraction of those observed
1	38.9	5.9
2	25.0	10.6
3	22.2	5.4
4	25.0	10.5
5	25.0	11.9
6	33.3	10.2
7	16.7	13.9
8	22.2	17.2
9	16.7	9.3
10	5.6	21.4
11	2.8	11.1
12	11.1	11.6
13	22.2	23.1
14	5.6	28.6
15	5.6	16.4
16	0.0	16.2
17	5.6	28.9
18	8.3	18.1
19	13.9	15.8
X	22.2	7.3

Figure 2. Chromosome Segregation in *bub1*$^{\Delta/\Delta}$ Oocytes Is Initiated prior to Congression to a Metaphase Plate

(A) Chromosome movements and microtubule spindle dynamics in *BUB1*$^{F/F}$ and *bub1*$^{\Delta/\Delta}$ oocytes expressing histone H2B-mCherry and β-Tubulin-EGFP were visualized by time-lapse confocal microscopy. Still images from a representative movie of each genotype are shown. The upper panels show DIC images merged with the H2B-mCherry channel pseudocolored in red. The lower panels show the H2B-mCherry and β-Tubulin-EGFP pseudocolored in red and green, respectively. The asterisks indicate the frame where chromosome segregation was first observed. Scale bars represent 10 μm.

(B) The extent of chromosome congression in movies similar to that shown in (A) was measured (see Figure S1) for the five frames prior to chromosome segregation and plotted against time. The oocytes were aligned relative to time of chromosome segregation. The solid lines show the mean values for each group of oocytes.

(C) *bub1*$^{\Delta/\Delta}$ MII oocytes were harvested 20 hr after hormonal stimulation. Chromosome spreads were prepared. An example of a chromosome spread stained with DAPI (left) and after hybridization with SKY probe (right) is shown. Chromosomes 7 (red arrows), 8 (blue arrows), and 11 (green arrows) with two single chromatids are indicated.

(D) Asymmetric distribution of chromosomes during meiosis I in *bub1*$^{\Delta/\Delta}$ oocytes. Frequency of segregation errors calculated for each chromosome. See text for details.

Chromosome Missegregation and Defective Congression in *bub1*$^{\Delta/\Delta}$ Oocytes

To investigate the effect of Bub1 ablation on chromosome segregation, we imaged oocytes that had been microinjected with mRNA for histone H2B-Cherry and β-Tubulin-EGFP (Figure 2A and Movie S2 available online). In *BUB1*$^{F/F}$ oocytes, chiasmata were only resolved and dyads segregated to the egg and first polar body after all bivalents had congressed,

forming a compact metaphase plate. Dyad chromosomes within the egg subsequently congressed to form metaphase plates on meiosis II spindles. In *bub1*$^{\Delta/\Delta}$ oocytes, chromosome segregation commenced before all chromosomes had congressed. Chromosome segregation was also invariably asymmetric in *bub1*$^{\Delta/\Delta}$ oocytes and often accompanied by the appearance of individual chromatids (monads). Meiosis II bipolar spindles formed (albeit longer than normal) despite the highly abnormal meiosis I chromosome segregation, but many of the egg's chromosomes failed to congress to the center of these spindles and instead moved back and forth between the poles in a highly dynamic fashion.

To measure the chromosome congression defects in *bub1*$^{\Delta/\Delta}$ oocytes, the chromosome segregation axis was determined for each individual cell (Figure S1). This was not always possible in *bub1*$^{\Delta/\Delta}$ oocytes and we therefore analyzed only oocytes whose axes could be determined unambiguously and were parallel to the imaging plane. A rectangular box (with a defined size) perpendicular to the segregation axis was positioned in each of the five frames prior to that in which chromosome segregation was first observed. This was done in a manner that maximized the amount of chromosomal DNA contained within the rectangular box. In *BUB1*$^{F/F}$ oocytes, the maximum amount of DNA contained within the box varied very little between 60 min (81.1% ± 12.4%, n = 8) and 12 min (83. 4% ± 6.9%) prior to anaphase I (Figure 2B). This figure is therefore a measure of maximum chromosome density, which is clearly enhanced by the process of chromosome congression. In *bub1*$^{\Delta/\Delta}$ oocytes, the equivalent maxima were merely 51.3% ± 13.9% (n = 8) at 60 min and 42.0% ± 10.1% at 12 min prior to anaphase ($p < 0.001$ at all time points).

To document chromosome missegregation in *bub1*$^{\Delta/\Delta}$ oocytes, we prepared chromosome spreads from *BUB1*$^{F/F}$ and *bub1*$^{\Delta/\Delta}$ oocytes before and after their first meiotic division. Oocytes used for preparing meiosis I spreads were matured in vitro for 2–3 hr after GVBD whereas MII oocytes were obtained directly from hormonally stimulated females. Spreads obtained from *BUB1*$^{F/F}$ (n = 20) and *bub1*$^{\Delta/\Delta}$ oocytes (n = 23) in meiosis I invariably contained 20 bivalent chromosomes. The abnormal chromosome missegregation within *bub1*$^{\Delta/\Delta}$ oocytes cannot therefore be caused by a lack of chiasmata before maturation. As expected, chromosome spreads from MII *BUB1*$^{F/F}$ oocytes (n = 28) invariably contained 20 dyad chromosomes. In contrast, spreads from MII *bub1*$^{\Delta/\Delta}$ oocytes (n = 36) revealed extensive aneuploidy, which was documented with spectral karyotyping (SKY) (Figures 2C and 2D; Table S1). We observed two types of numerical abnormality: cosegregation to the oocyte of both dyads produced by chiasmata resolution and the presence of single chromatids, indicating precocious loss of sister-chromatid cohesion at centromeres. The frequency with which dyads cosegregated varied between chromosomes, ranging from 5% to 30%, as did the fraction of chromatids present as single chromatids. Most of the latter were present as pairs, either two or four copies. These data imply that loss of Bub1 causes two independent types of aberration: first, nondisjunction of whole chromosomes at meiosis I, and second, a failure to hold sister centromeres together after the first meiotic division, which would cause missegregation at meiosis II but not at meiosis I. The finding that MII *bub1*$^{\Delta/\Delta}$ oocytes sometimes contain all four chromatids implies that individual chromosomes can simultaneously suffer both types of aberration. We conclude that Bub1 is important for congression of bivalents on the meiosis I spindle, disjunction of dyads at meiosis I, and persistence of sister-centromere cohesion until meiosis II.

APC/C Is Required for Meiosis I

To address whether the precocious PBE in *bub1*$^{\Delta/\Delta}$ oocytes is due to premature activation of the APC/C, we used mice in which exons 2 to 4 of the gene encoding the APC/C's Apc2 subunit were flanked by *LoxP* sites (*APC2*^{F}). *Zp3-Cre* converted ten out of ten *APC2*^{F} alleles to *apc2*$^{\Delta}$ in the female germline. Moreover, three out of three *APC2*$^{F/F}$ *Zp3-Cre* females failed to become pregnant when kept with wild-type males for 3 months or more. APC/C activity within oocytes is therefore essential. We observed in some but not all crosses that *APC2*$^{F/F}$ *Zp3-Cre* females possessed many fewer GV oocytes than did their *APC2*$^{F/F}$ littermates. The reason for this is that most oocytes had clearly already undergone GVBD in vivo. Ovary dissection revealed 9 GV and 28 GVBD oocytes from a *APC2*$^{F/F}$ *Zp3-Cre* female and 12 GV and 22 GVBD oocytes from a *BUB1*$^{F/F}$ *APC2*$^{F/F}$ *Zp3-Cre* female, even when dissection was performed in 5 times the normal concentration of IBMX. In contrast, a *BUB1*$^{F/F}$ *APC2*$^{F/F}$ littermate produced 41 GV and no GVBD oocytes. Importantly, of those *apc2*$^{\Delta/\Delta}$ GV oocytes that underwent GVBD only upon removal of IBMX, none underwent PBE (Figure 3A). The APC/C is therefore essential for the first meiotic division, as previously suggested [28]. It is very possibly also important for holding oocytes in prophase prior to GVBD [29].

A Quantitative Assay for APC/C Activity in Oocytes

One of the APC/C's key substrates is securin, whose destruction can be visualized in oocytes by injecting moderate amounts of mRNA encoding fluorescently tagged securin (securin-EGFP) [23, 30–32]. To test whether destruction is mediated by the APC/C, we used confocal microscopy to measure securin-EGFP fluorescence after injection of *apc2*$^{\Delta/\Delta}$ or *APC2*$^{F/F}$ GV oocytes. Neither the first meiotic division nor the rapid drop of securin-EGFP levels (Figure 3B) that precedes PBE in *APC2*$^{F/F}$ oocytes (Figure 3D) took place in *apc2*$^{\Delta/\Delta}$ oocytes. Instead, levels increased continuously for 24 hr, eventually approaching a plateau as the rate of increase gradually declined (Figure 3C). Bivalent chromosomes (marked with histone H2B-cherry) congressed to a metaphase plate but were not converted to dyads and no polar bodies were extruded (Figure 3B).

Because injection of securin-EGFP mRNA had no effect on the timing of PBE in wild-type oocytes, even at the highest levels (Figure S2), its destruction can be used as a marker for the proteolysis of endogenous securin. The rate of APC/C-dependent securin-EGFP proteolysis should be derivable from the first differential (slopes) of EGFP accumulation curves. The rate of change of securin mRNA (M) and protein (S) can be described by two differential equations (DE):

$$\frac{dM}{dt} = -k_d^m \cdot M$$

$$\frac{dS}{dt} = k_S \cdot M - \left(k_d' + k_d \cdot APC\right) \cdot S$$

Degradation of securin mRNA (M) is assumed to be first order, with rate constant k_d^m ($time^{-1}$). Securin synthesis (i.e., translation) is described by the first term in the securin DE ($k_S \cdot M$) whereas its degradation is described by APC/C-independent (k_d') and APC/C-dependent ($k_d \cdot APC$) terms. APC refers to active APC/C concentration and k_d to its specific activity or turnover rate. Because these cannot be estimated

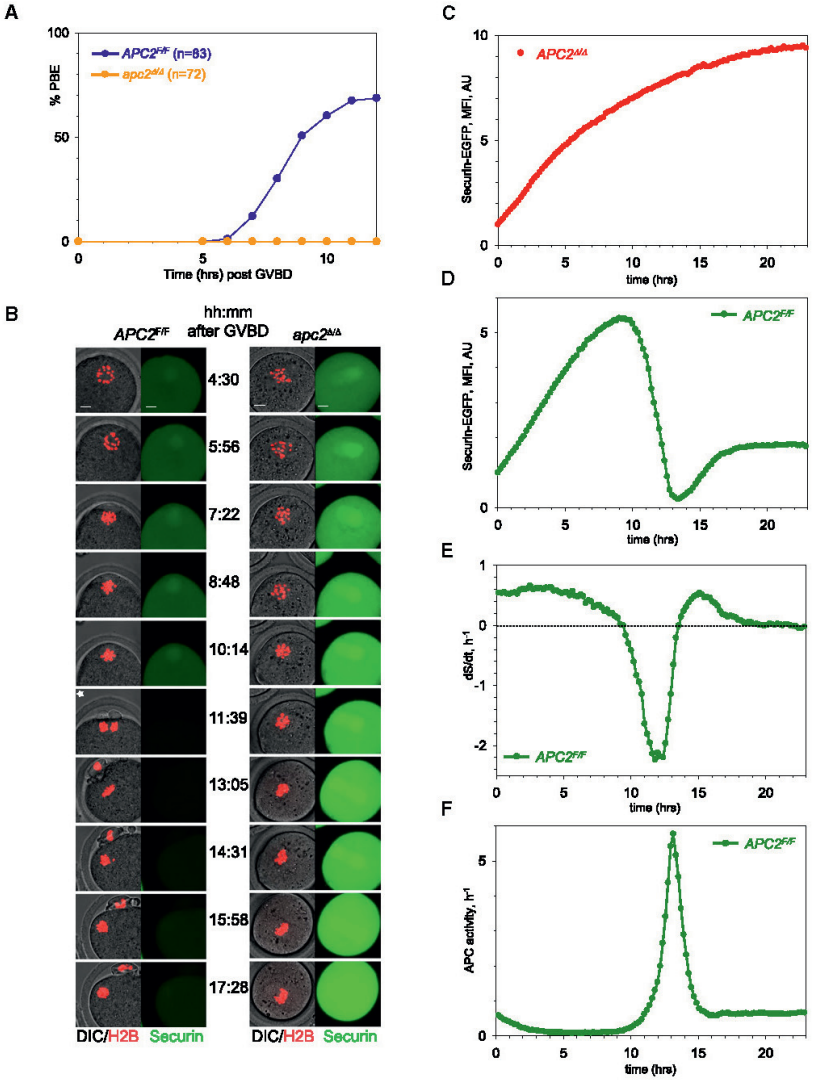

Figure 3. Calculation of APC/C Activity from Securin Level Changes in *APC2*$^{F/F}$ and *apc2*$^{\Delta/\Delta}$ Oocytes

(A) Kinetics of polar body extrusion (PBE) in *APC2*$^{F/F}$ and *apc2*$^{\Delta/\Delta}$ oocytes. *APC2*$^{F/F}$ and *apc2*$^{\Delta/\Delta}$ oocytes were harvested in M2 medium containing IBMX, which inhibits GVBD. Oocytes were released into inhibitor-free M16 medium. 90 min after release those oocytes that had completed GVBD were selected for further analysis. This was set as time = 0 hr. Oocytes were monitored every hour and scored for completion of PBE.

(B) Images from movies with *APC2*$^{F/F}$ and *apc2*$^{\Delta/\Delta}$ oocytes expressing H2B-mCherry and securin-EGFP. Observe that securin does not get degraded in the absence of Apc2.

(C and D) Securin-EGFP levels in *apc2*$^{\Delta/\Delta}$ (C) and in *APC2*$^{F/F}$ (D) oocytes were measured at each time point and background levels were subtracted. Values were normalized relative to that at GVBD (0 hr), and plotted, in arbitrary units (AU), against time.

(E) The first derivative (dS/dt) of the Securin level curve (Figure 2C) in *APC2*$^{F/F}$ oocytes.

(F) Changes in APC/C activity during meiotic maturation in *APC2*$^{F/F}$ oocytes. See details in the text.

separately, we simply refer to $k_d \cdot$ APC as APC/C activity. The key point is that this is not constant during oocyte maturation, with a large rise being responsible for the rapid drop in securin levels shortly before PBE. Importantly, $k_d \cdot$ APC can be calculated at each time point from the temporal pattern of its substrate (securin-EGFP) levels. Thus:

$$k_d \cdot APC = \frac{k_S \cdot M_0 \cdot e^{-k_d^m \cdot t} - \frac{dS}{dt}}{S} - k'_d$$

where M_0 is the level of injected securin mRNA and $k_S \cdot M_0$ is the maximal rate of securin mRNA translation. Calculation of

APC/C activity requires values for kinetic rate constants ($k_S \cdot M_0$, k_d', and k_d^m), the securin-EGFP level (S), and its rate of change (dS/dt, which is the slope of the securin curve).

The securin accumulation data in *apc2*$^{\Delta/\Delta}$ oocytes do not provide any information about the stability of securin mRNA (k_d^m), but it turns out that this can be estimated from changes in securin-EGFP levels in *APC2*$^{F/F}$ oocytes, where the time derivative of securin levels (dS/dt) becomes positive again (because of mRNA translation) after APC/C-dependent securin degradation during anaphase of MI (Figure 3E). Importantly, the maximal value of dS/dt is greater than 80% of its value at GVBD (15 hr previously), implying that the rate of mRNA degradation is negligible. We therefore assumed that $k_d^m = 0$.

The kinetic parameters, $k_S \cdot M_0 = 1.05\ h^{-1}$ and $k_d' = 0.1\ h^{-1}$, were estimated (see Figure S3) from the securin-EGFP data of *apc2*$^{\Delta/\Delta}$ oocytes (Figure 3C), where $k_d \cdot$APC is zero. With these kinetic parameters in hand, we can use values of S (Figure 3D) and dS/dt (Figure 3E) to calculate APC/C activity during meiotic progression (Figure 3F). Because the dominating terms are the securin levels (S) and its time derivative (dS/dt), the activities calculated are in fact quite insensitive to the precise kinetic parameter values. APC/C activity was also calculated assuming Michaelis-Menten rather than first-order degradation kinetics for securin (Figure S4).

These calculations reveal that APC/C activity relaxes rapidly to zero after GVBD, remains at this low level until about 10 hr after GVBD, increases dramatically shortly before the first meiotic division, and then drops back to a low but nonzero value (Figure 3F). Unlike peak levels during MI, resting APC/C activity during CSF arrest is sensitive to the value of k_d^m: the higher the rate of mRNA degradation, the lower the implied APC/C activity. Importantly, kinetic parameter combinations consistent with zero APC/C activity in MII are unrealistic because they predict negative APC/C activity during meiotic progression. We are therefore confident that APC/C activity against securin is not completely turned off during MII CSF arrest. Incomplete inhibition by Emi2 could be responsible for the gradual turn-over of cell cycle regulators at this stage of the meiotic process [33].

Premature APC/C Activation in *bub1*$^{\Delta/\Delta}$ Oocytes

To test whether APC/C activation precedes precocious chromosome segregation in oocytes lacking Bub1, we imaged oocytes from *BUB1*$^{F/F}$ *Zp3-Cre* and *BUB1*$^{F/F}$ females after their injection with securin-EGFP and histone H2B-cherry mRNAs (Figures 4A and 4B; Movie S1). In *BUB1*$^{F/F}$ oocytes, APC/C activity reaches a maximum at the time of chromosome segregation (Figure 4C, green arrowheads), about 12 hr after GVBD. The kinetics of the rise and fall of APC/C activity was similar in *bub1*$^{\Delta/\Delta}$ oocytes, but strikingly the burst of APC/C activity occurred 4–5 hr earlier. The implication is that Bub1 is necessary to inhibit APC/C activity for a large fraction of the period between GVBD and PBE. To our surprise, we found that Bub1 causes a similar delay in APC/C activity toward cyclin A-GFP (Figure S5).

Individual activity curves were aligned and an average activity curve calculated (Figure 4D). This reveals that there is little or no significant difference in maximal APC/C activity between *BUB1*$^{F/F}$ and *bub1*$^{\Delta/\Delta}$ oocytes, the only difference being the timing of the meiosis I burst of activity. It also shows that APC/C activity rises in an exponential fashion for 3–4 hr in *BUB1*$^{F/F}$ and *bub1*$^{\Delta/\Delta}$ oocytes (Figure 4E). There was a small difference in their exponents (−0.66 in the mutant versus −0.84 in the wild-type), implying a slightly more "explosive" activation in *BUB1*$^{F/F}$ than in *bub1*$^{\Delta/\Delta}$ oocytes. Interestingly, the period of exponential increase lasted nearly 4 hr in both sets of oocytes.

Premature Chiasmata Resolution in *bub1*$^{\Delta/\Delta}$ Oocytes Depends on APC/C and Separase

Many events are advanced by 4–5 hr in *bub1*$^{\Delta/\Delta}$ oocytes. Some are normally associated with the first meiotic division, namely securin destruction, chiasmata resolution, and PBE, whereas others such as loss of centromeric cohesion normally only take place at the second meiotic division. Temporal dislocation on this scale has hitherto not been documented in SAC mutants and it was therefore important to address whether premature activation of the APC/C (and thereby separase) was responsible. Because the tripeptide proteasome inhibitor MG132 was found to depress securin-EGFP synthesis (Figure S6), we addressed the APC/C's role by analyzing oocytes from *Bub1*$^{flox/flox}$*Apc2*$^{flox/flox}$ *Zp3-Cre* females, in which both Apc2 and Bub1 are depleted. The phenotype of such oocytes was similar, though not identical to those from *Apc2*$^{flox/flox}$ *Zp3-Cre* females. They did not extrude polar bodies and, after injection of securin-EGFP mRNAs, accumulated EGFP fluorescence in an asymptotic fashion over a 20 hr period (Figure 5A and data not shown). Congression of bivalents was, however, inefficient and they did not form compact metaphase plates (Figure 5B). Despite this, many if not most bivalents clearly came under tension, indicating biorientation of maternal and paternal kinetochores (Figure 5C). Importantly, chiasmata were not resolved (Figure 5C). Precocious APC/C activity must therefore be responsible for many of the phenotypes caused by Bub1 depletion. It is difficult to know whether the defective congression of bivalents in *apc2*$^{\Delta/\Delta}$ *bub1*$^{\Delta/\Delta}$ oocytes was exclusively due to depletion of Bub1 because congression also appeared somewhat abnormal in *apc2*$^{\Delta/\Delta}$ oocytes (Figure 5B).

To address whether the precocious resolution of chiasmata in *bub1*$^{\Delta/\Delta}$ oocytes is due to premature activation of separase as opposed to other activities capable of destroying sister-chromatid cohesion [34], we analyzed oocytes from *Bub1*$^{flox/flox}$ *separase*$^{flox/flox}$ *Zp3-Cre* females, in which both Bub1 and separase are depleted. Inactivation of separase did not alter precocious APC/C activation (Figure 5E) but it did hinder PBE (Figure 5D). 92.3% of *bub1*$^{\Delta/\Delta}$ oocytes (n = 36) extruded a polar body at an average time of 05:34 ± 01:53 hr post GVBD (n = 36) but only 14.9% of *sep*$^{\Delta/\Delta}$ *bub1*$^{\Delta/\Delta}$ oocytes did so, with an average time of 07:00 ± 04:44 hr (n = 46). Live imaging of *sep*$^{\Delta/\Delta}$*bub1*$^{\Delta/\Delta}$ oocytes injected with securin-EGFP and histone H2B-cherry showed that many bivalents came under tension, even after securin had been fully destroyed, presumably because chiasmata had not been resolved (data not shown). To confirm this, we prepared chromosome spreads from *bub1*$^{\Delta/\Delta}$ and *sep*$^{\Delta/\Delta}$ *bub1*$^{\Delta/\Delta}$ oocytes at various times after GVBD, starting from when at least 90% of *bub1*$^{\Delta/\Delta}$ oocytes had completed PBE. All bivalents had been converted to dyads or single chromatids in 100% (n = 66) of *bub1*$^{\Delta/\Delta}$ oocytes but never (n = 79) in *sep*$^{\Delta/\Delta}$ *bub1*$^{\Delta/\Delta}$ oocytes (Figure 5F), even long after APC/C activation.

The Oocyte SAC Does Not Require the Bub1 Kinase Domain

Injection of *bub1*$^{\Delta/\Delta}$ oocytes with wild-type Bub1 but not with a frame-shifted (NS-Bub1) mRNA delayed both APC/C activation (compare Figure 6A with Figure 4D) and PBE, causing both events to occur with a timing similar to that of *BUB1*$^{F/F}$

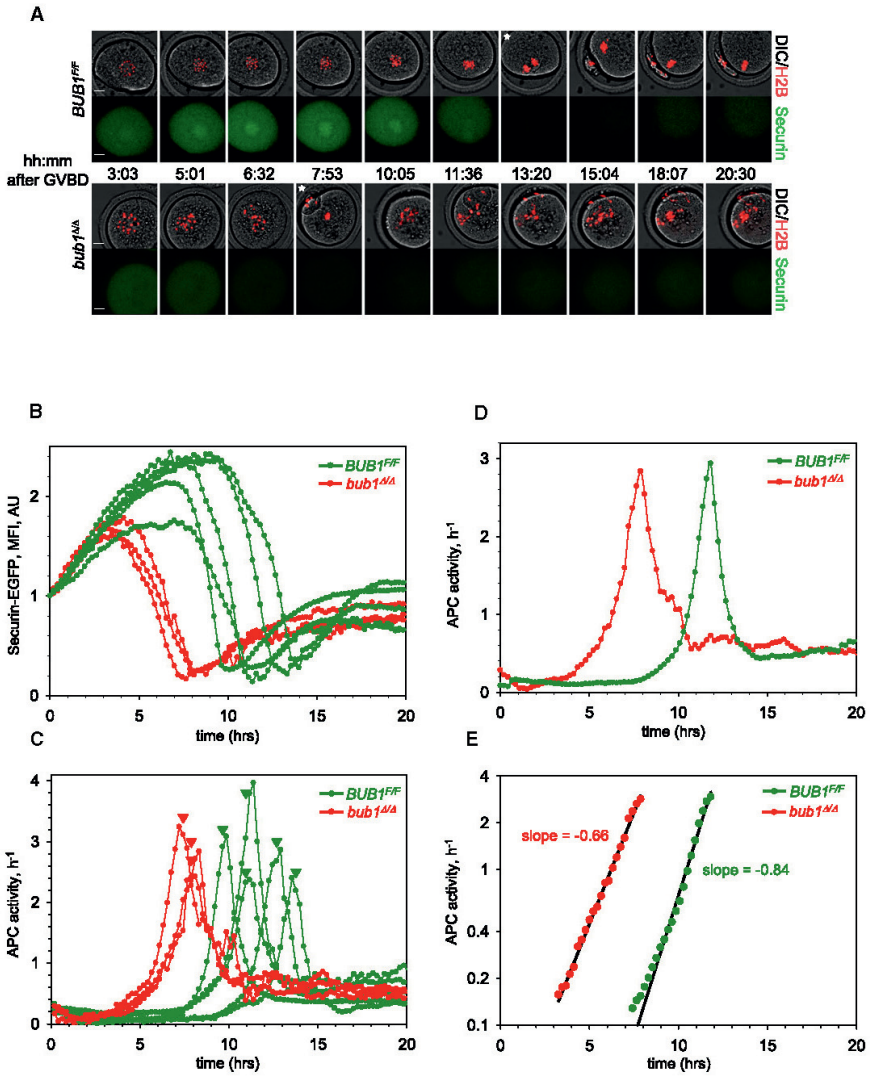

Figure 4. Premature Activation of the APC/C in *bub1*$^{\Delta/\Delta}$ Oocytes

Chromosome movements and securin levels in *BUB1*$^{F/F}$ and *bub1*$^{\Delta/\Delta}$ oocytes expressing H2B-mCherry and securin-EGFP were observed by time-lapse confocal microscopy.

(A) Still images from a representative movie of each genotype are shown. The upper panels show DIC images merged with the H2B-mCherry channel pseudocolored in red. The lower panels show the securin-EGFP channel pseudocolored in green. The asterisks indicate the frame where chromosome segregation was first observed. Scale bars represent 10 μm.

(B) Securin-EGFP levels in movies similar to those shown in (A) were measured at each time point and background levels were subtracted. Values were normalized relative to that at GVBD (0 hr), and plotted, in arbitrary units (AU), against time. Movies were aligned relative to time of GVBD.

(C) The securin-EGFP curves in (B) were transformed to produce a measure of APC/C activity over the course of the experiment (see text) and plotted against time.

(D) The APC/C-activity curves in (C) were aligned relative to the average time to peak APC/C activity for each genotype, and the average APC/C activity at each time point was calculated and plotted against time.

(E) The exponentially rising portions of the average APC/C-activity curves shown in (D) were plotted on a semilog plot, and a line of best fit was projected onto the data. The slopes of the lines are indicated on the graph.

oocytes (data not shown). To address the function of Bub1's conserved kinase domain, GV-stage *bub1*$^{\Delta/\Delta}$ oocytes were injected with mRNAs encoding H2B-cherry and securin-EGFP together with either wild-type Bub1 mRNA, NS-Bub1 mRNA, or an mRNA encoding a version of Bub1 lacking its C-terminal kinase domain (Bub1-KinΔ). Time-lapse confocal movies (data

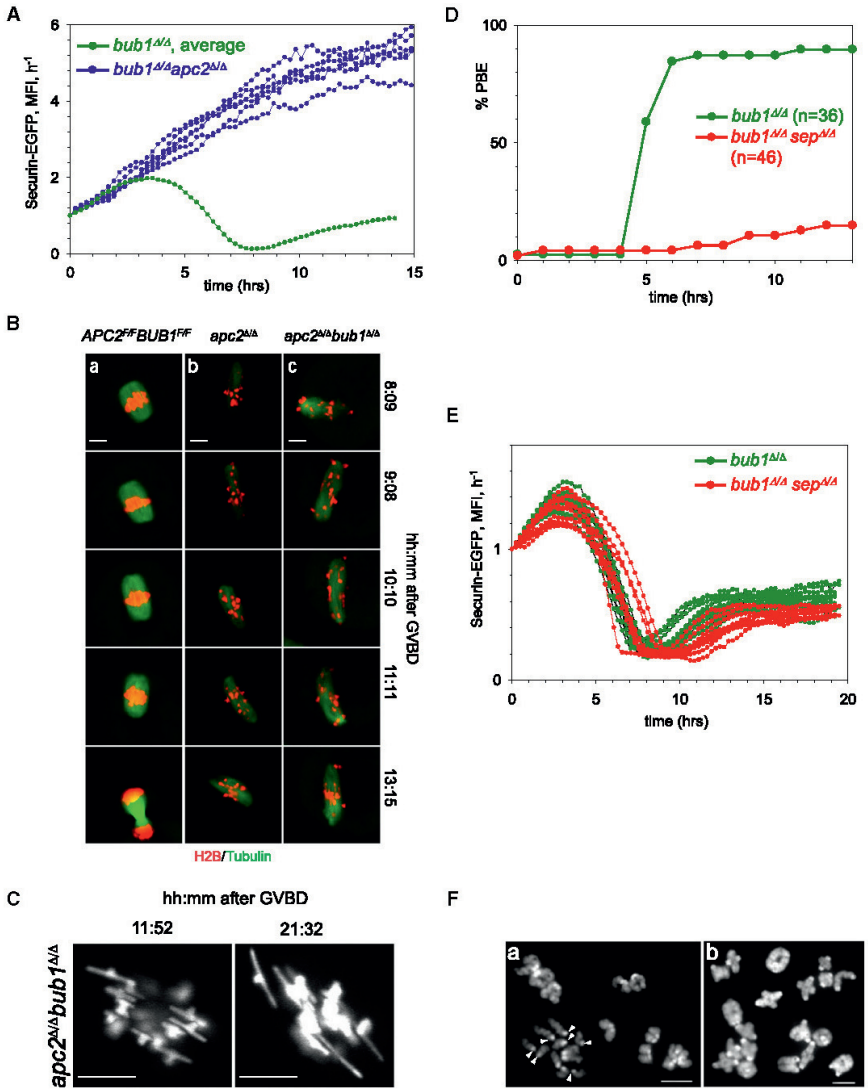

Figure 5. Separase and Apc2 Are Required for Precocious Chromosome Segregation and PBE in *bub1*$^{\Delta/\Delta}$ Oocytes

(A) Chromosome movements and securin levels in *bub1*$^{\Delta/\Delta}$ and *apc2*$^{\Delta/\Delta}$ *bub1*$^{\Delta/\Delta}$ oocytes expressing H2B-mCherry and securin-EGFP were observed by time-lapse confocal microscopy. Securin-EGFP levels were measured at each time point and plotted against time as previously. Movies were aligned relative to time of GVBD. Note the *bub1*$^{\Delta/\Delta}$ curve is the average of five individual oocytes.

(B) Chromosome movements and microtubule spindle dynamics were visualized by time-lapse confocal microscopy in three types of oocytes expressing histone H2B-mCherry and β-Tubulin-EGFP: (a) *APC2*$^{F/F}$ *BUB1*$^{F/F}$, (b) *apc2*$^{\Delta/\Delta}$, and (c) *apc2*$^{\Delta/\Delta}$ *bub1*$^{\Delta/\Delta}$. Still images from a representative movie of each genotype are shown. The merged H2B-mCherry and β-Tubulin-EGFP channels are shown pseudocolored in red and green, respectively. Scale bars represents 10 μm.

(C) Representative still images, taken at 11.87 hr and 21.54 hr after GVBD, from the chromatin (H2B-mCherry) channel shows highly stretched bivalents from an *apc2*$^{\Delta/\Delta}$ *bub1*$^{\Delta/\Delta}$ oocyte.

(D) Kinetics of polar body extrusion (PBE). *bub1*$^{\Delta/\Delta}$ and *bub1*$^{\Delta/\Delta}$ *separase*$^{\Delta/\Delta}$ oocytes were harvested in M2 medium containing IBMX, which inhibits GVBD. Oocytes were released into inhibitor-free M16 medium. 90 min after release, those oocytes that had completed GVBD were selected for further analysis. This was set as time = 0 hr. Oocytes were monitored every hour and scored for completion of PBE.

(E) Chromosome movements and securin levels in *bub1*$^{\Delta/\Delta}$ (n = 11) and *bub1*$^{\Delta/\Delta}$ *separase*$^{\Delta/\Delta}$ (n = 12) oocytes expressing H2B-mCherry and securin-EGFP were observed by time-lapse confocal microscopy. Securin-EGFP levels were measured at each time point and plotted against time as previously. Movies were aligned relative to time of GVBD.

(F) *bub1*$^{\Delta/\Delta}$ and *bub1*$^{\Delta/\Delta}$ *separase*$^{\Delta/\Delta}$ oocytes were harvested at GV stage and matured in vitro for up to 22 hr. Chromosome spreads were prepared when at least 90% of *bub1*$^{\Delta/\Delta}$ oocytes had completed MI, but not MII, as judged by extrusion of the first polar body. Only those *bub1*$^{\Delta/\Delta}$ oocytes that had completed

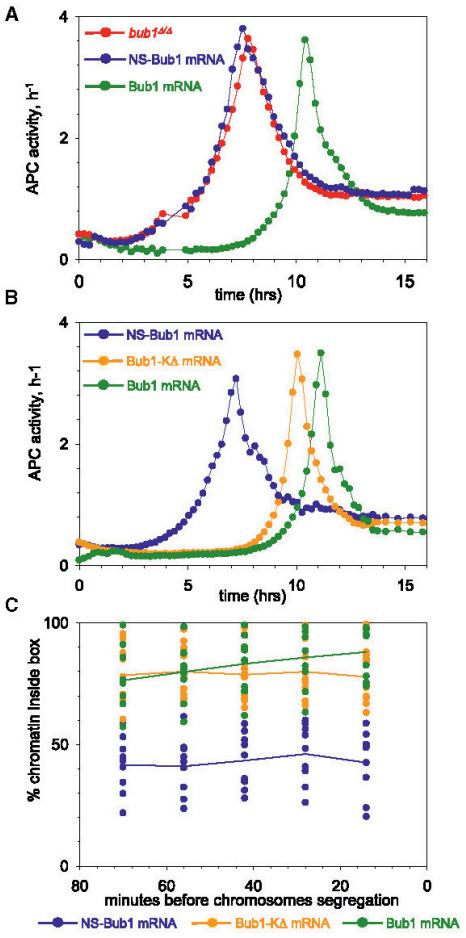

Figure 6. Bub1 Kinase Domain Is Largely Dispensable for the Spindle Assembly Checkpoint in Oocytes

(A) Chromosome movements and securin levels in *bub1*$^{\Delta/\Delta}$ oocytes expressing H2B-mCherry and securin-EGFP were observed by time-lapse confocal microscopy. A subset of the oocytes was also microinjected with Bub1 mRNA, a further subset was microinjected with NS-Bub1 mRNA, and the remainder were not microinjected with Bub1 mRNA. Securin-EGFP levels were measured at each time point and average APC/C activity curves for each group of oocytes were calculated and plotted against time as previously.

(B) As in (A) except the third group was also microinjected with mRNA for a Bub1 kinase-deletion mutant (Bub1-KΔ).

(C) The oocytes described in (A) and (B) were analyzed as in Figure 2B to measure the extent of chromosome congression.

not shown) demonstrated that the (average) interval between GVBD and PBE with wild-type Bub1 mRNA was 11:07 ± 01:08 hr (n = 10). It was 07:15 ± 00:38 hr (n = 9) with NS-Bub1 mRNA and 10:07 ± 01:02 hr (n = 14) with Bub1-KinΔ mRNA. The difference between NS-Bub1 and wild-type was statistically significant ($p < 0.001$) as was that between NS-Bub1 and Bub1-KinΔ ($p < 0.001$). Though the error bars overlap considerably, the small difference in timing between oocytes injected with wild-type and Bub1-KinΔ mRNA appears to be real, with $p = 0.041$.

Securin-EGFP levels were quantified and transformed into APC/C activity curves that were then aligned and averaged (Figure 6B). The average interval from GVBD to peak APC/C activity was 07:20 ± 00:43 hr with NS-Bub1 mRNA, 11:02 ± 01:03 hr with wild-type Bub1 mRNA, and 10:04 ± 01:04 hr with Bub1-KinΔ mRNA. The differences between Bub1-KinΔ and NS-Bub1 mRNA was highly significant ($p < 0.001$) whereas the difference between wild-type and Bub1-KinΔ was less so ($p = 0.039$). These data suggest that much of the delay in APC/C activation resulting from Bub1 can also be performed by a version completely lacking its kinase domain. Indeed, the shape of the APC/C activation curves is very similar with and without Bub1's kinase domain (Figure 6B). This domain is nevertheless highly conserved and appears from our data to enhance Bub1's ability to regulate (delay) APC/C activation and anaphase onset.

Wild-type Bub1 and Bub1-KinΔ but not NS-Bub1 mRNA ($p < 0.001$) restored chromosome congression in *bub1*$^{\Delta/\Delta}$ oocytes to wild-type levels (compare Figure 6C with Figure 2B). There was, however, a small statistically significant difference between wild-type and KinΔ mRNAs at the final time point, 14 min prior to segregation. The kinase activity of Bub1 can only have a minor function, if any, in regulating chromosome congression.

Discussion

The notion that the SAC may be unimportant or ineffective in oocytes still persists [35] despite evidence to the contrary [19, 21, 24, 25, 36]. We describe here the consequences of depleting a key SAC component, namely Bub1, by oocyte-specific deletion of a floxed allele of the *BUB1* gene. This adversely affects chromosome congression, advances chiasmata resolution and polar body extrusion by 4–5 hr, and causes precocious separation of sister centromeres. By using a quantitative assay for APC/C activity and analyzing the phenotypes of double mutants, we show that the precocious chiasmata resolution and PBE caused by loss of Bub1 is accompanied by and depends on premature activation of the APC/C and separase. Our data prove that the SAC has a fundamental role in regulating anaphase in oocytes and that it largely performs this function independently of Bub1's kinase domain.

Our measurements show that APC/C's activity toward securin remains very low from GVBD until 3 hr before PBE, at which point it rises at an exponential rate, peaking shortly before PBE, before declining to a low but significant level during CSF arrest. There are two possible explanations for the exponential APC/C activation (suggestive of an autocatalytic process). Given that the SAC depresses APC/C activity during the process of exponential activation in wild-type oocytes, it is

the first PBE were spread whereas all *bub1*$^{\Delta/\Delta}$ *separase*$^{\Delta/\Delta}$ oocytes were spread. Chromosome spreads were stained with DAPI to visualize DNA and resolution of chiasmata was scored as (a) positive or (b) negative. (a) shows a spread from a *bub1*$^{\Delta/\Delta}$ oocyte. Again, separated sister chromatids were observed (indicated by arrowheads). (b) shows a spread from a *bub1*$^{\Delta/\Delta}$ *separase*$^{\Delta/\Delta}$ oocyte. Note, chromosomes from *bub1*$^{\Delta/\Delta}$ oocytes were generally too widely dispersed on the slide to capture all chromosomes in a single image. The visible chromosomes from a single spread were photographed in a number of separate images at the same magnification; these images were subsequently arranged in proximity to one another to produce the images shown above. Scale bars represent 10 μm.

conceivable that APC/C activity inactivates a SAC component, such as Mad2 [37, 38] or Mps1 [39] and/or Aurora B [9] kinases. Alternatively, the exponential rise in the rate of securin destruction could come about because of competition with a competing APC/C substrate whose destruction must precede that of securin. Cyclin A might be such a protein. However, we found no major difference in the kinetics of securin and cyclin A destruction (see Figure S5).

If inactivation of the SAC drives APC/C activation in wild-type oocytes, what process does so in oocytes lacking Bub1? More precisely, what changes occur in $bub1^{\Delta/\Delta}$ oocytes during the 7 hr interval between GVBD, when cyclin B/Cdk1 is presumably activated, and the complete activation of the APC/C fully 7 hr later? Phosphorylation of several APC/C subunits accompanies its activation in mitotic cells [40, 41], though the physiological significance of this phosphorylation has not been addressed. It is conceivable that a battle between mitotic kinases and phosphatases takes place during this period, with the former finally triumphing. Our finding that the process of APC/C activation is exponential in $bub1^{\Delta/\Delta}$ oocytes potentially adds a new player, namely the APC/C itself, which might activate itself via a positive feedback loop. We note that the variation in time between GVBD and full APC/C activation in $bub1^{\Delta/\Delta}$ oocytes (38 min) was half that in wild-type ones (74 min). Presumably, the process activating the APC/C without a SAC is not subject to the vagaries of the stochastic process of kinetochore capture and biorientation. How might the APC/C promote its own activation? It has been suggested that inhibition of APC/C mediated ubiquitinylation of securin because its phosphorylation by Cdk1 makes the process more switch-like in yeast [42]. This model cannot account for the switch-like nature of securin destruction in oocytes because separase, a key part of the yeast autoactivation process, is not required for the exponential rise in APC/C activity in oocytes lacking both Bub1 and separase (data not shown).

Another function of the APC/C revealed by this work stems from our finding that oocytes whose Apc2 subunit has been depleted during their growing phase appear to re-enter the meiotic program precociously, apparently undergoing GVBD en masse within the ovary. This raises the possibility that the APC/C is at least partially active during the long prophase arrest in oocytes and that without it oocytes are more likely to re-enter the first meiotic division, possibly in the absence of the luteinizing hormone surge that normally induces this event. A related phenomenon, though one whose physiological significance is less clear, is the recent finding that antisense morpholinos directed against Cdh1 mRNA permit a fraction of GV oocytes to undergo GVBD in vitro in the presence of phosphodiesterase inhibitors that normally block this process [29]. The importance of molecular mechanisms controlling prophase I arrest in oocytes during folliculogenesis was recently demonstrated by disruption of PTEN, a regulator of phosphatidylinositol 3-kinase, which caused a reduction of the oocyte pool at an early age leading to premature ovarian failure (POF) [43]. In $apc2^{\Delta/\Delta}$ oocytes we have observed a similar effect and it is therefore conceivable that disruption of normal APC/C activity in growing oocytes might contribute to POF.

Our data suggest that Bub1 may have at least two other functions within oocytes besides delaying APC/C activation, namely to facilitate congression of bivalents on meiosis I spindles and prevent premature destruction of sister-centromere cohesion. It is important to point out that we cannot at this stage be certain that the congression and cohesion defects are not at least partly caused by the premature APC/C activation. It is easy to imagine that by giving cells less time to biorient bivalents, premature APC/C activation would by itself hinder their congression. It is less easy to imagine why it would hinder the mechanism that normally protects sister-chromatid cohesion at centromeres from separase during meiosis I. The precocious separation of sister centromeres in $bub1^{\Delta/\Delta}$ oocytes is reminiscent of the situation during meiosis I in yeast where Bub1 is necessary for the recruitment to centromeres of shugoshin proteins (e.g., Sgo1) that protect cohesin from separase [44–46]. Bub1 might act in a similar fashion in oocytes, helping to recruit Sgo1 or Sgo2 to centromeres. Because the precocious loss of sister-chromatid cohesion at centromeres in $bub1^{\Delta/\Delta}$ oocytes is not fully penetrant, afflicting less than one-third of all chromosomes, there must also exist a mechanism conferring protection that is Bub1 independent.

In the light of our finding that the SAC delays APC/C activation by 4 to 5 hr, the massive missegregation in aging human females cannot be attributed to an inherently ineffective SAC in oocytes. It is nevertheless conceivable that the SAC might work less effectively as oocytes ages and that this facilitates production of aneuploid gametes. It is also important to point out that our work does not address whether the delay in APC/C activation caused by Bub1 involves signaling from kinetochores that have not yet attached to microtubules. Indeed, it remains mysterious why univalent X chromosomes fail to block meiosis I in mouse oocytes. It seems implausible that oocytes would possess a SAC that cannot monitor the correct attachment of individual chromosomes and yet univalent X chromosomes apparently do not greatly delay APC/C activation. A recent study has shown that the sister kinetochores of univalent chromosomes in meiosis I oocytes can become bioriented on the meiosis I spindle, apparently satisfying the requirements of the SAC and contributing to chromosome missegregation [36]. Further insight into this process could be gained by monitoring activity of the APC/C and the actual movement of univalent chromosomes during meiosis I using the sort of techniques described in this paper.

Experimental Procedures

Mouse Strains

Generation of $BUB1^{F/F}$ [14], $SEPARASE^{F/F}$ [47], and $APC2^{F/F}$ [48] mice has been described previously. A transgenic mouse line that expresses Cre recombinase from the Zona pellucida 3 promoter (Zp3-cre) [26] was purchased from the Jackson Laboratory. Mouse strains used were of mixed C57BL/6J and 129/Sv backgrounds.

Oocyte Culture and Microinjection

Fully grown mouse GV-stage oocytes surrounded by cumulus cells were isolated by disaggregating ovaries in M2 medium (Specialty Media, Millipore, Watford, UK, or Sigma-Aldrich) supplemented with 200 mM 3-isobutyl-1-methylxanthine (IBMX, Sigma-Aldrich) at 37°C. Oocytes released from most of the surrounding cumulus cells were cultured in drops of medium (~50 μl) covered with mineral oil (Sigma-Aldrich). Oocytes were matured in M16 medium (Specialty Media) at 37°C in the presence of 5% CO_2. Only oocytes that had undergone GVBD (germinal vesicle breakdown) within 90 min after release into IBMX-free medium were selected (time 0 hr after GVBD) and cultured further for experiments. In experiments where oocytes were cultured in medium containing nocodazole at 5 μM or MG132 at 10 μM, controls were treated with an equivalent amount of ethanol or DMSO solvent, respectively. MII-arrested oocytes were obtained from females superovulated by intraperitoneal (i.p.) injection of PMSG (5 IU) followed 48 hr later by i.p. injection of human chorionic gonadotropin (hCG; 5 IU). Oocytes were isolated from oviducts approximately 16 hr after hCG and freed from cumulus cells by hyaluronidase (200 IU/ml, Sigma-Aldrich). GV oocytes were microinjected in M2 media supplemented with IBMX with a FemtoJet microinjector (Eppendorf) with 5–10 pl of mRNAs at a final

concentration of 0.1 μg/ml in RNase-free water (Ambion) into the cytoplasm. Up to two different mRNAs were mixed together prior to injection. Control and experimental oocytes for a single experiment were imaged simultaneously, distinguished by coinjection of 10 kDa Cascade-Blue-labeled dextran into one group. After approximately 1–2 hr to allow for protein expression, oocytes were matured.

Chromosome Spreads

Chromosome spreads from mouse oocytes were prepared as previously described [49, 50]. See Supplemental Data for further details.

SKY Analysis

BUB1$^{F/F}$ and *BUB1*$^{\Delta/\Delta}$ mice were primed with 5IU PMSG, then 48 hr later with 5IU hCG, and oviducts were isolated 16–18 hr after hCG. The cumulus-enclosed oocytes at the second meiotic division (MII) were released into M2 medium with 1% hyaluronidaze for 5–10 min. Cumulus-free oocytes were fixed in methanol-acetic acid solution (3:1). Slides were aged for 2–3 days at the room temperature and then hybridized with the SKY probe (Applied Spectral Imaging) according to the manufacturer's instructions. SKY image acquisition and analysis was performed on a Zeiss Axioscope 2 microscope equipped with SpectraCubeTM at 600× with Spectral Imaging Expo 2.6 software.

Live Imaging and Quantitative Analysis of Data

Oocytes were cultured in a PeCon (Erbach, Germany) environmental microscope incubator allowing the maintenance of a 5% CO_2 atmosphere with humidity at 37°C during time-lapse experiments. A customized Zeiss LSM510 META confocal microscope equipped with Plan-Neofluor 20×/0.5, C-Apochromat 40×/1.2 NA water immersion or C-Apochromat 40×/1.2 NA water immersion objective lenses was used for image acquisition. For detection of Cascade-Blue dextran, EGFP, YFP, and mCheery, we used 405 nm, 488 nm, 514 nm, and 561 nm excitation wavelengths and LP 420, BP 505-550, BP 530-600, and LP 575 filters. Chromosomes labeled with H2B-mCherry were tracked with an EMBL-developed tracking macro [51] adapted to our microscope. Image stacks were captured every 12–15 min for 16–20 hr. Quantitative analysis of the density of the fluorescence was performed with ImageJ software (http://rsb.info.nih.gov/ij/). To measure securin-EGFP signal, the area occupied by the oocyte in each individual frame was defined manually and the mean fluorescence intensity (MFI) of the signal within this area was measured. Values were corrected for background fluorescence by subtracting the MFI of the area surrounding the oocyte at each time point. To control for the apparent differences in MFI levels between individual oocytes caused by discrepancies in the amount of injected mRNA, background-corrected MFI values were normalized to the value measured at the time of GVBD. The changes in APC/C activity (kd.APC) during meiosis were calculated from the securin-EGFP signal with MS Excel. The time derivative of the Securin curve (dS/dt) was approximated by the ratio of differences ($\Delta S/\Delta t$) of subsequent time points. In order to reduce noise in the ratio of differences, the securin data were smoothed by calculating the average of three subsequent points (a three-point running mean).

DNA Constructs, Primers, mRNA Synthesis, and Statistical Analysis

See Supplemental Data.

Supplemental Data

Supplemental Data include Supplemental Experimental Procedures, six figures, one table, and two movies and can be found with this article online at http://www.current-biology.com/supplemental/S0960-9822(09)00685-X.

Acknowledgments

We are grateful to Jan Ellenberg and Melina Schuh for their help with live imaging of oocytes, Denise Jelfs for technical assistance, Katja Wassmann, Melina Schuh, and Nathalie Daigle for DNA plasmids, and all members of the Nasmyth lab for helpful discussions. M.A. was supported by EC Fellowship MEIF-CT-2005-024429 and by BBSRC through OCISB and GAAV no. IAA501620801.

Received: December 1, 2008
Revised: January 28, 2009
Accepted: January 29, 2009
Published online: February 26, 2009

References

1. Vogt, E., Kirsch-Volders, M., Parry, J., and Eichenlaub-Ritter, U. (2008). Spindle formation, chromosome segregation and the spindle checkpoint in mammalian oocytes and susceptibility to meiotic error. Mutat. Res. *651*, 14–29.
2. Mitchison, T.J., and Salmon, E.D. (2001). Mitosis: a history of division. Nat. Cell Biol. *3*, E17–E21.
3. Nicklas, R.B. (1967). Chromosome micromanipulation. II. Induced reorientation and the experimental control of segregation in meiosis. Chromosoma *21*, 17–50.
4. Nasmyth, K., and Haering, C.H. (2005). The structure and function of SMC and kleisin complexes. Annu. Rev. Biochem. *74*, 595–648.
5. Uhlmann, F., Wernic, D., Poupart, M.A., Koonin, E., and Nasmyth, K. (2000). Cleavage of cohesin by the CD clan protease separin triggers anaphase in yeast. Cell *103*, 375–386.
6. Waizenegger, I., Hauf, S., Meinke, A., and Peters, J.M. (2000). Two distinct pathways remove mammalian cohesin from chromosome arms in prophase and from centromeres in anaphase. Cell *103*, 399–410.
7. Stemmann, O., Zou, H., Gerber, S.A., Gygi, S.P., and Kirschner, M.W. (2001). Dual inhibition of sister chromatid separation at metaphase. Cell *107*, 715–726.
8. Peters, J.M. (2006). The anaphase promoting complex/cyclosome: a machine designed to destroy. Nat. Rev. Mol. Cell Biol. *7*, 644–656.
9. Taylor, S., and Peters, J.M. (2008). Polo and Aurora kinases: lessons derived from chemical biology. Curr. Opin. Cell Biol. *20*, 77–84.
10. Musacchio, A., and Salmon, E.D. (2007). The spindle-assembly checkpoint in space and time. Nat. Rev. Mol. Cell Biol. *8*, 379–393.
11. Li, R., and Murray, A.W. (1991). Feedback control of mitosis in budding yeast. Cell *66*, 519–531.
12. Buffin, E., Emre, D., and Karess, R.E. (2007). Flies without a spindle checkpoint. Nat. Cell Biol. *9*, 565–572.
13. Michel, L.S., Liberal, V., Chatterjee, A., Kirchwegger, R., Pasche, B., Gerald, W., Dobles, M., Sorger, P.K., Murty, V.V., and Benezra, R. (2001). MAD2 haplo-insufficiency causes premature anaphase and chromosome instability in mammalian cells. Nature *409*, 355–359.
14. Perera, D., Tilston, V., Hopwood, J.A., Barchi, M., Boot-Handford, R.P., and Taylor, S.S. (2007). Bub1 maintains centromeric cohesion by activation of the spindle checkpoint. Dev. Cell *13*, 566–579.
15. Rieder, C.L., Schultz, A., Cole, R., and Sluder, G. (1994). Anaphase onset in vertebrate somatic cells is controlled by a checkpoint that monitors sister kinetochore attachment to the spindle. J. Cell Biol. *127*, 1301–1310.
16. Petronczki, M., Siomos, M.F., and Nasmyth, K. (2003). Un menage a quatre: the molecular biology of chromosome segregation in meiosis. Cell *112*, 423–440.
17. Hunt, P., LeMaire, R., Embury, P., Sheean, L., and Mroz, K. (1995). Analysis of chromosome behavior in intact mammalian oocytes: monitoring the segregation of a univalent chromosome during female meiosis. Hum. Mol. Genet. *4*, 2007–2012.
18. LeMaire-Adkins, R., Radke, K., and Hunt, P.A. (1997). Lack of checkpoint control at the metaphase/anaphase transition: a mechanism of meiotic nondisjunction in mammalian females. J. Cell Biol. *139*, 1611–1619.
19. Brunet, S., Pahlavan, G., Taylor, S., and Maro, B. (2003). Functionality of the spindle checkpoint during the first meiotic division of mammalian oocytes. Reproduction *126*, 443–450.
20. Wassmann, K., Niault, T., and Maro, B. (2003). Metaphase I arrest upon activation of the Mad2-dependent spindle checkpoint in mouse oocytes. Curr. Biol. *13*, 1596–1608.
21. Homer, H.A., McDougall, A., Levasseur, M., Murdoch, A.P., and Herbert, M. (2005). Mad2 is required for inhibiting securin and cyclin B degradation following spindle depolymerisation in meiosis I mouse oocytes. Reproduction *130*, 829–843.
22. Homer, H.A., McDougall, A., Levasseur, M., Yallop, K., Murdoch, A.P., and Herbert, M. (2005). Mad2 prevents aneuploidy and premature proteolysis of cyclin B and securin during meiosis I in mouse oocytes. Genes Dev. *19*, 202–207.
23. Kudo, N.R., Wassmann, K., Anger, M., Schuh, M., Wirth, K.G., Xu, H., Helmhart, W., Kudo, H., Mckay, M., Maro, B., et al. (2006). Resolution of chiasmata in oocytes requires separase-mediated proteolysis. Cell *126*, 135–146.

24. Tsurumi, C., Hoffmann, S., Geley, S., Graeser, R., and Polanski, Z. (2004). The spindle assembly checkpoint is not essential for CSF arrest of mouse oocytes. J. Cell Biol. *167*, 1037–1050.
25. Niault, T., Hached, K., Sotillo, R., Sorger, P.K., Maro, B., Benezra, R., and Wassmann, K. (2007). Changing Mad2 levels affects chromosome segregation and spindle assembly checkpoint control in female mouse meiosis I. PLoS ONE *2*, e1165.
26. Lewandoski, M., Wassarman, K.M., and Martin, G.R. (1997). Zp3-cre, a transgenic mouse line for the activation or inactivation of loxP-flanked target genes specifically in the female germ line. Curr. Biol. *7*, 148–151.
27. Epifano, O., Liang, L.F., Familari, M., Moos, M.C., Jr., and Dean, J. (1995). Coordinate expression of the three zona pellucida genes during mouse oogenesis. Development *121*, 1947–1956.
28. Ledan, E., Polanski, Z., Terret, M.E., and Maro, B. (2001). Meiotic maturation of the mouse oocyte requires an equilibrium between cyclin B synthesis and degradation. Dev. Biol. *232*, 400–413.
29. Reis, A., Chang, H.Y., Levasseur, M., and Jones, K.T. (2006). APCcdh1 activity in mouse oocytes prevents entry into the first meiotic division. Nat. Cell Biol. *8*, 539–540.
30. Clute, P., and Pines, J. (1999). Temporal and spatial control of cyclin B1 destruction in metaphase. Nat. Cell Biol. *1*, 82–87.
31. Hagting, A., Den Elzen, N., Vodermaier, H.C., Waizenegger, I.C., Peters, J.M., and Pines, J. (2002). Human securin proteolysis is controlled by the spindle checkpoint and reveals when the APC/C switches from activation by Cdc20 to Cdh1. J. Cell Biol. *157*, 1125–1137.
32. Herbert, M., Levasseur, M., Homer, H., Yallop, K., Murdoch, A., and McDougall, A. (2003). Homologue disjunction in mouse oocytes requires proteolysis of securin and cyclin B1. Nat. Cell Biol. *5*, 1023–1025.
33. Wu, J.Q., Hansen, D.V., Guo, Y., Wang, M.Z., Tang, W., Freel, C.D., Tung, J.J., Jackson, P.K., and Kornbluth, S. (2007). Control of Emi2 activity and stability through Mos-mediated recruitment of PP2A. Proc. Natl. Acad. Sci. USA *104*, 16564–16569.
34. Kueng, S., Hegemann, B., Peters, B.H., Lipp, J.J., Schleiffer, A., Mechtler, K., and Peters, J.M. (2006). Wapl controls the dynamic association of cohesin with chromatin. Cell *127*, 955–967.
35. Reis, A., Madgwick, S., Chang, H.Y., Nabti, I., Levasseur, M., and Jones, K.T. (2007). Prometaphase APCcdh1 activity prevents non-disjunction in mammalian oocytes. Nat. Cell Biol. *9*, 1192–1198.
36. Kouznetsova, A., Lister, L., Nordenskjold, M., Herbert, M., and Hoog, C. (2007). Bi-orientation of achiasmatic chromosomes in meiosis I oocytes contributes to aneuploidy in mice. Nat. Genet. *39*, 966–968.
37. Stegmeier, F., Rape, M., Draviam, V.M., Nalepa, G., Sowa, M.E., Ang, X.L., McDonald, E.R., 3rd, Li, M.Z., Hannon, G.J., Sorger, P.K., et al. (2007). Anaphase initiation is regulated by antagonistic ubiquitination and deubiquitination activities. Nature *446*, 876–881.
38. Reddy, S.K., Rape, M., Margansky, W.A., and Kirschner, M.W. (2007). Ubiquitination by the anaphase-promoting complex drives spindle checkpoint inactivation. Nature *446*, 921–925.
39. Palframan, W.J., Meehl, J.B., Jaspersen, S.L., Winey, M., and Murray, A.W. (2006). Anaphase inactivation of the spindle checkpoint. Science *313*, 680–684.
40. Kraft, C., Herzog, F., Gieffers, C., Mechtler, K., Hagting, A., Pines, J., and Peters, J.M. (2003). Mitotic regulation of the human anaphase-promoting complex by phosphorylation. EMBO J. *22*, 6598–6609.
41. Herzog, F., Mechtler, K., and Peters, J.M. (2005). Identification of cell cycle-dependent phosphorylation sites on the anaphase-promoting complex/cyclosome by mass spectrometry. Methods Enzymol. *398*, 231–245.
42. Holt, L.J., Krutchinsky, A.N., and Morgan, D.O. (2008). Positive feedback sharpens the anaphase switch. Nature *454*, 353–357.
43. Reddy, P., Liu, L., Adhikari, D., Jagarlamudi, K., Rajareddy, S., Shen, Y., Du, C., Tang, W., Hamalainen, T., Peng, S.L., et al. (2008). Oocyte-specific deletion of Pten causes premature activation of the primordial follicle pool. Science *319*, 611–613.
44. Bernard, P., Maure, J.F., and Javerzat, J.P. (2001). Fission yeast Bub1 is essential in setting up the meiotic pattern of chromosome segregation. Nat. Cell Biol. *3*, 522–526.
45. Kitajima, T.S., Hauf, S., Ohsugi, M., Yamamoto, T., and Watanabe, Y. (2005). Human Bub1 defines the persistent cohesion site along the mitotic chromosome by affecting Shugoshin localization. Curr. Biol. *15*, 353–359.
46. Riedel, C.G., Katis, V.L., Katou, Y., Mori, S., Itoh, T., Helmhart, W., Galova, M., Petronczki, M., Gregan, J., Cetin, B., et al. (2006). Protein phosphatase 2A protects centromeric sister chromatid cohesion during meiosis I. Nature *441*, 53–61.
47. Wirth, K., Wutz, G., Kudo, N.R., Desdouets, C., Zetterberg, A., Taghybeeglu, S., Seznec, J., Ducos, G., Ricci, R., Firnberg, N., et al. (2006). Separase: a universal trigger for sister chromatid disjunction but not chromosome cycle progression. J. Cell Biol. *172*, 847–860.
48. Wirth, K.G., Ricci, R., Gimenez-Abian, J.F., Taghybeeglu, S., Kudo, N.R., Jochum, W., Vasseur-Cognet, M., and Nasmyth, K. (2004). Loss of the anaphase-promoting complex in quiescent cells causes unscheduled hepatocyte proliferation. Genes Dev. *18*, 88–98.
49. Hodges, C.A., and Hunt, P.A. (2002). Simultaneous analysis of chromosomes and chromosome-associated proteins in mammalian oocytes and embryos. Chromosoma *111*, 165–169.
50. Peters, A.H., Plug, A.W., van Vugt, M.J., and de Boer, P. (1997). A drying-down technique for the spreading of mammalian meiocytes from the male and female germline. Chromosome Res. *5*, 66–68.
51. Rabut, G., and Ellenberg, J. (2004). Automatic real-time three-dimensional cell tracking by fluorescence microscopy. J. Microsc. *216*, 131–137.

Sebestova J, Danylevska A, Novakova L, Kubelka M, Anger M. Lack of response to unaligned chromosomes in mammalian female gametes. Cell Cycle. 2012;11: 3011–3018.

Impact Factor/Quartile: 5,243/Q3
Times cited (Wos May 2019): 48
Significance: Important paper showing that the SAC in mouse oocytes is not able to prevent APC/C activation during errors of spindle assembly.
Contribution of the author: Experimental design, interpretation of experiments manuscript preparation, securing funding

Cell Cycle 11:16, 1-8; August 15, 2012; © 2012 Landes Bioscience

Lack of response to unaligned chromosomes in mammalian female gametes

Jaroslava Sebestova,[1,2] Anna Danylevska,[1,2] Lucia Novakova,[1,2] Michal Kubelka[1] and Martin Anger[1,2,*]

[1]Institute of Animal Physiology and Genetics; Libechov, Czech Republic; [2]CEITEC - Veterinary Research Institute; Brno, Czech Republic

Keywords: cell cycle, meiosis, chromosome segregation, anaphase, aneuploidy, oocytes

Chromosome segregation errors are highly frequent in mammalian female meiosis, and their incidence gradually increases with maternal age. The fate of aneuploid eggs is obviously dependent on the stringency of mechanisms for detecting unattached or repairing incorrectly attached kinetochores. In case of their failure, the newly formed embryo will inherit the impaired set of chromosomes, which will have severe consequences for its further development. Whether spindle assembly checkpoint (SAC) in oocytes is capable of arresting cell cycle progression in response to unaligned kinetochores was discussed for a long time. It is known that abolishing SAC increases frequency of chromosome segregation errors and causes precocious entry into anaphase; SAC, therefore, seems to be essential for normal chromosome segregation in meiosis I. However, it was also reported that for anaphase-promoting complex (APC) activation, which is a prerequisite for entering anaphase; alignment of only a critical mass of kinetochores on equatorial plane is sufficient. This indicates that the function of SAC and of cooperating chromosome attachment correction mechanisms in oocytes is different from somatic cells. To analyze this phenomenon, we used live cell confocal microscopy to monitor chromosome movements, spindle formation, APC activation and polar body extrusion (PBE) simultaneously in individual oocytes at various time points during first meiotic division. Our results, using oocytes from aged animals and interspecific crosses, demonstrate that multiple unaligned kinetochores and severe congression defects are tolerated at the metaphase to anaphase transition, although such cells retain sensitivity to nocodazole. This indicates that checkpoint mechanisms, operating in oocytes at this point, are essential for accurate timing of APC activation in meiosis I, but they are insufficient in detection or correction of unaligned chromosomes, preparing thus conditions for propagation of the aneuploidy to the embryo.

Introduction

Chromosome segregation errors during mammalian female meiosis frequently create gametes with aberrant number of chromosomes. After fertilization of such an egg, the incomplete chromosomal set is transferred to the newly formed embryo, which has devastating consequences for its further development, including embryonic lethality and severe developmental disorders.[1] The incidence of aneuploidy is usually higher in egg than in sperm, and a factor contributing highly to human and mouse oocyte aneuploidy is advanced maternal age.[2] It is, however, important to mention that not all mammalian species are suffering from the maternal age-related aneuploidy; for example, in porcine oocytes, this phenomenon was not established, which might reflect species specific differences in chromosome segregation mechanisms.[3] One of the factors contributing to such high occurrence of aneuploidy in aged egg is a weakening of centromeric cohesion,[4,5] arising due to the inability of the oocyte to replace cohesins during prolonged prophase arrest.[6,7] Reduced connection between sister chromatids is subsequently causing their precocious segregation in meiosis I. The propagation of meiosis I segregation defects to the embryo would, however, require also a failure of SAC controlling chromosome segregation in meiosis II. Although the function of SAC in oocytes was studied for quite some time,[8-10] it is still unresolved whether it is similar to somatic cells. So far we have clear evidence that SAC is required for precise timing of APC activity in meiosis I since depletion of its component Bub1 causes premature chromosome segregation, accompanied by extensive aneuploidy.[11] Also in mitosis, SAC components ensure proper timing of anaphase;[12] therefore, this function seems to be preserved. However, in contrast to mitosis, where the anaphase onset is blocked until last kinetochore is aligned on the metaphase plate,[13-15] it seems that oocytes are unable to respond to unaligned kinetochores by prolonging SAC activity.[16,17] To analyze this phenomenon more quantitatively, we used oocytes with extraordinarily high rate of aneuploidy, in which chromosome segregation errors are expected to be more frequent, and we monitored chromosome movements, spindle assembly, APC activity and polar body extrusion simultaneously in individual cells using confocal live imaging. Our data demonstrate that oocytes are not able to respond to multiple unaligned kinetochores and massive congression defects by delaying anaphase.

Results

The duration of meiosis I is not affected by presence of univalent chromosomes. For our study, we used oocytes isolated

*Correspondence to: Martin Anger; Email: anger@iapg.cas.cz
Submitted: 06/09/12; Revised: 07/03/12; Accepted: 07/06/12
http://dx.doi.org/

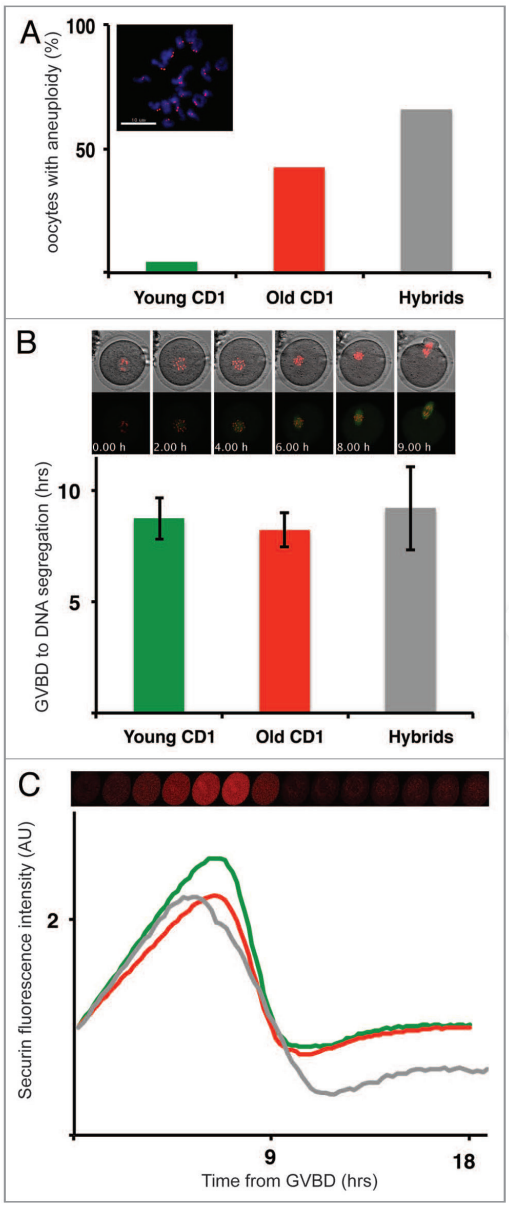

Figure 1. The duration of meiosis I is not affected by high frequency of aneuploidy. (A) Aneuploidy frequency in Young CD1 (green, n = 73), Old CD1 (red, n = 47) and Hybrid (gray, n = 33) was scored after monastrol treatment in meiosis II. Image represents typical staining of chromosomes with DAPI (blue), and kinetochores (red). (B) The length of meiosis I - oocytes were microinjected with fluorescently labeled histone H2B (red) and β-tubulin 2A (green) and analyzed by live imaging. Movie frames showing intervals from GVBD until DNA separation, time is indicated for each frame. Lower chart – the average length (hrs) of meiosis I in Young CD1 (green, n = 50), Old CD1 (red, n = 46) and Hybrid (green, n = 21) oocytes, error bars showing SD. (C) Dynamics of securin degradation during meiosis I. Average securin expression levels in Young CD1 (blue, n = 18), Old CD1 (red, n = 21) and Hybrid oocytes (n = 8) are shown, expression levels were normalized to the first frame.

from naturally aged CD1 outbred mice at age 19–25 mo ("old CD1") and oocytes isolated from *Mus musculus* x *Mus spretus* F1 hybrids ("hybrids"). These groups were selected based on previously reported high level of aneuploidy,[18,19] which would also increase probability of detecting chromosome segregation defects in vivo. Both groups were compared with the oocytes from CD1 animals 2–5 mo old ("young CD1"). To assess aneuploidy levels in all three groups, the oocytes were matured in vitro for 18 h, and subsequently the frequency of aneuploidy was measured by kinetochore-counting assay in monastrol-treated oocytes[19] (**Fig. 1A**). Our results showed that 4.1% of young CD1 (n = 73), 42.5% of old CD1 (n = 47) and 72.7% of hybrid oocytes (n = 33) had numerical chromosomal aberrations. Values obtained for both CD1 groups were similar to previously published figures,[19] and small variations were likely caused by age or strain differences. The aneuploidy observed in hybrid oocytes was, however, significantly higher compared with the previously published report.[18] Possible explanation for such high aneuploidy levels is the origin of mice. Whereas *Mus spretus* animals used for our interbreeding were derived from natural population, mice used in previous study were inbred. To address the question whether configuration of chromosomes in meiosis I is similar in all three groups, chromosome spreads were prepared from oocytes in meiosis I, matured for 7.5 h after IBMX removal. At this time, oocytes were still in meiosis I, verified by the absence of polar bodies. Chromosome spreads revealed that young CD1 (n = 46) and hybrids (n = 18) contained no univalents, whereas 19.2% of the old CD1 oocytes (n = 26) contained closely positioned univalents without visible chiasmata (data not shown). Single chromatids were not detected in any of the groups. Based on multiple evidence, including nocodazole treatment and measurement of meiosis I length, it was previously shown that SAC is intact in old oocytes.[19] Sixteen hour exposure of oocytes to a low level (0.04 μg/ml) of nocodazole, which was added to the media 4.5 h after germinal vesicle break down (GVBD), showed that 75% of young CD1 (n = 68), 71% of Old CD1 (n = 17) and 86% of hybrid oocytes (n = 21) remained arrested in meiosis I, indicating that in all three groups, the SAC was intact (data not shown). To analyze whether the presence of univalents in old CD1 group is affecting metaphase plate formation and timing of anaphase I, we used live-cell imaging. Oocytes were microinjected with mRNAs encoding histone H2B, β-tubulin 2a and securin fused to different fluorescent proteins and then matured on microscope. Images were taken every 10 to 15 min for period of 18 h. Such conditions allowed to simultaneously monitor various processes, including GVBD, chromosome movements, assembly of the meiotic spindle, polar body extrusion (PBE) and activity of APC in individual cells, representative movie frames are shown in **Figure 2**. Our results showed that the length of meiosis I, measured from GVBD to DNA masses segregation, was not significantly different in young CD1 oocytes (8.75 h ± 0.94, n = 50) and hybrid

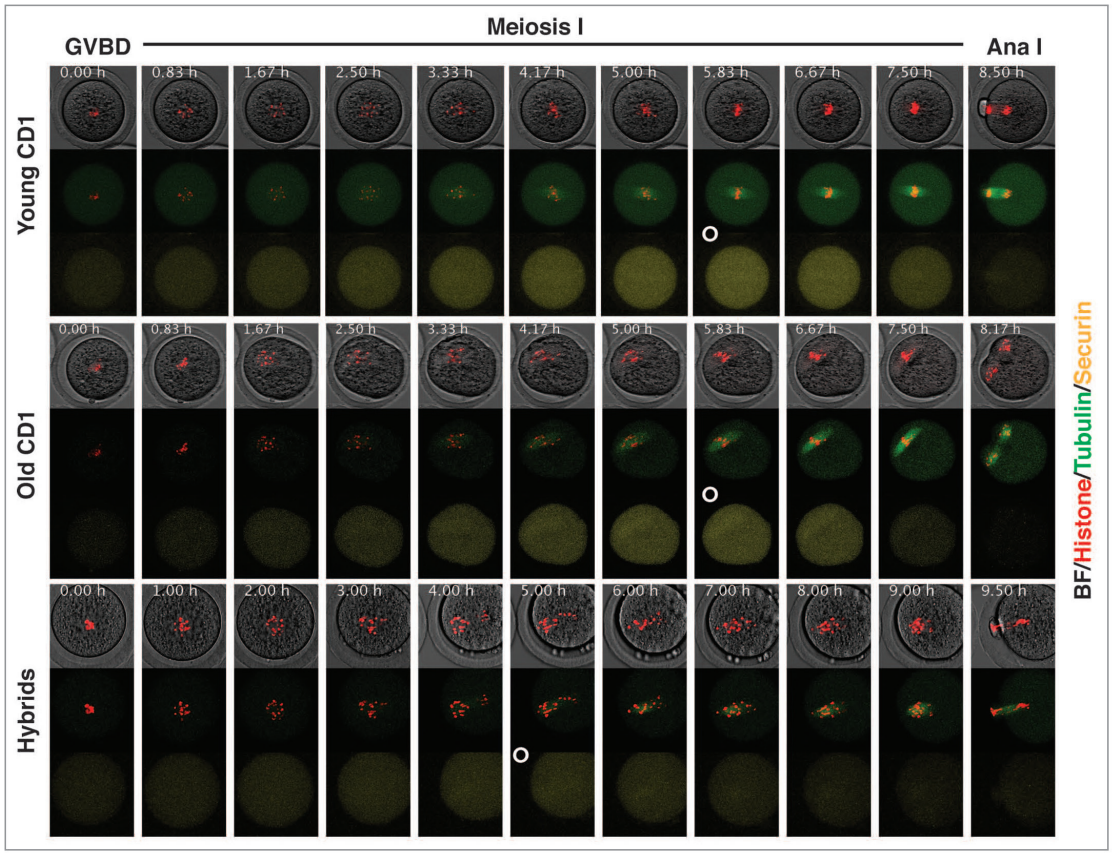

Figure 2. Time-lapse analysis of chromosome alignment and securin degradation. Oocytes were microinjected with fluorescently labeled histone H2B (red), β-tubulin 2A (green) and securin (yellow). Movie frames from representative Young CD1, Old CD1 and Hybrid oocyte are shown, the frame with maximal level of securin is marked with white circle.

oocytes (9.20 h ± 1.88, n = 21). It was slightly shorter in old CD1 (8.22 ± 0.78, n = 46) compared with young CD1 ($p = 0.037$) and hybrids ($p = 0.035$) (**Fig. 1B**), although the difference was minor. This indicates that the presence of univalent chromosomes in oocytes is not causing meiosis I extension by prolonging SAC activity, which might be consistent with the idea that univalent chromosomes are escaping SAC detection by bipolar attachment.[20-22] Securin levels measured during time-lapse experiments showed that APC was activated in all three groups with similar timing relative to GVBD (**Fig. 1C**).

Metaphase plate formation is compromised in oocytes with high aneuploidy. Analysis of the time-lapse movies also revealed that significant fraction of old CD1 oocytes and even more hybrid oocytes, contained unaligned chromosomes at the time of APC activation, assessed by measuring securin degradation (**Fig. 2**). In mitosis, alignment of all kinetochores on equatorial plane of the spindle is required for satisfying SAC, which, in turn, leads to activation of APC and subsequent destruction of multiple substrates, including securin and cyclin B.[15,23] Securin stability is therefore an excellent marker of initiation of metaphase to anaphase transition also in oocytes.[11] Quantification of securin levels and simultaneous detection of fluorescently labeled chromosomes in individual cells allowed to correlate dynamics of the metaphase plate formation with APC activation, which should coincide with SAC switching off (**Fig. 3**). We were interested in whether the metaphase plate formation, when all chromosomes congress on equatorial plane without a single chromosome visibly separated, is achieved in oocytes before initiation of securin destruction. For each cell, two time intervals were identified; the frame with the highest level of securin and then the frame with all chromosomes aligned on metaphase plate (**Fig. 3A**). Our results showed that 89% of young CD1 (n = 19) are able to form a metaphase plate before initiation of securin destruction; however, only 15% of old CD1 (n = 20) and 0% of hybrids (n = 13) achieved this. Following the same cells further as they were heading toward anaphase, showed that 55% of old CD1 and 92%

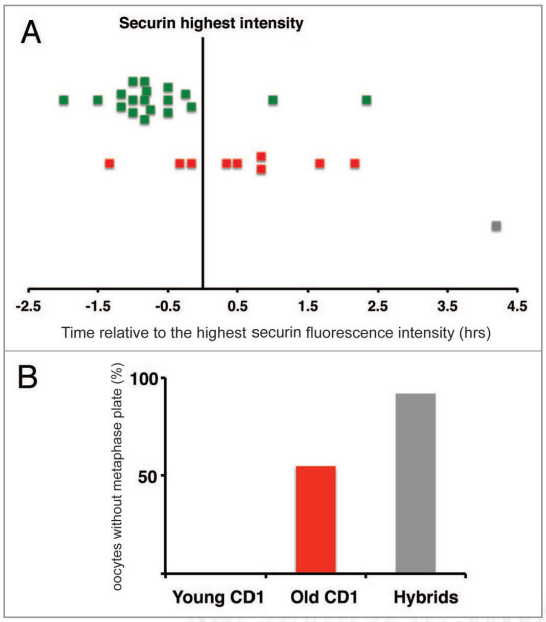

Figure 3. Metaphase plate formation vs. APC activation. (A) The highest level of securin is represented by vertical line. Squares are showing time of aligning of all chromosomes on equatorial plane in individual oocytes. Young CD1 (green, n = 19), Old CD1 (red, n = 20) and Hybrid (gray, n = 13). (B) Chart showing frequency of oocytes never forming metaphase plate before anaphase onset - Young CD1 (green, n = 19) 0%, Old CD1 (red, n = 20) 55% and Hybrid (gray, n = 13) 92%.

of hybrid oocytes were unable to form metaphase plate at any time interval before anaphase in contrast to young CD1 group, in which 100% formed the metaphase plate before reaching anaphase (**Fig. 3B**).

SAC inactivation in oocytes is independent on chromosome alignment. To study more quantitatively the correlation between chromosome alignment and APC activity, we used again oocytes injected with β-tubulin 2a, histone H2B and securin, all labeled with fluorescent proteins. Misaligned chromosomes, visibly separated from the metaphase plate, were scored in seven selected intervals: at 120 (-7), 90 (-6), 60 (-5) and 30 min (-4) before peak of securin, at highest securin level (-3), at half of the securin level after initiation of its destruction (-2) and finally at the last frame before anaphase (-1) (**Fig. 4A**). These intervals were selected to cover part of meiosis I with full SAC activity, APC activation during metaphase to anaphase transition and also time when cells were entering anaphase. Nineteen young CD1, 20 old CD1 and 13 hybrid oocytes in which the chromosomes were visible in each interval were used for this study. Our results (**Fig. 4B**) showed that all three groups contained unaligned chromosomes during two hours prior to the highest securin level, and therefore our observation is consistent with recently published data showing that SAC is turned off in the presence of unaligned chromosomes.[16,17] It is, however, important to mention that while young CD1 eventually organized their chromosomes on the metaphase plate before reaching anaphase, 50% of old CD1 and 85% of hybrid oocytes were entering anaphase with chromosomes separated from the metaphase plate. Further, we tested formation of metaphase II plate in all three groups of oocytes. In this analysis, the misaligned chromosomes were scored in 15 consecutive intervals throughout first 150 min after anaphase I (**Fig. 4C**) and also at 18 h after IBMX removal (**Fig. 4D**). Our results showed that 90% of young CD1 (n = 30) reached the stage, with all chromosomes aligned on metaphase plate within 150 min after anaphase I. In contrast to this, almost all old CD1 and hybrid oocytes, perhaps due to the aneuploidy resulting from separase activation in anaphase I, were unable to form metaphase plate within selected interval. This was confirmed by analysis of the chromosome alignment at 18 h (**Fig. 4C and D**), which indicated that the alignment defect in those cells might be permanent.

Severe alignment and congression defects are not preventing SAC inactivation in oocytes. Scoring cells with unaligned chromosomes does not fully reveal the severity of alignment defects in individual cells. To analyze this more quantitatively, we adapted method previously used to score congression defects.[11] In this experiment, we measured amount of DNA located inside a rectangle, which represented 25% of the spindle length (**Fig. 5A**). For this analysis we used only oocytes, in which the spindle axis was parallel with the focus plane. Cells were analyzed in five frames: at 90–96, 70–75, 45–50, 30–36 and 10–15 min prior to anaphase (**Fig. 5B**). Except for the last interval just before anaphase, young CD1 (n = 10) oocytes had significantly more ($p \leq 0.05$) DNA inside the rectangle compared with old CD1 oocytes (n = 6). In contrast to both CD1 groups, hybrid oocytes (n = 5) showed extensive chromosome alignment and congression defects, and except for the last frame before anaphase, less than 50% of the DNA were localized at the equatorial plane. This demonstrates that the oocytes were unable to detect or respond to unaligned chromosomes resulting in chromosomes scattered all over the spindle, when oocytes were entering anaphase.

Discussion

The data presented here are showing that mammalian oocytes are unable to respond to multiple unaligned kinetochores and to severe congression defects by prolonging SAC activity. Crucially, the anaphase in such oocytes is timely executed, despite the defects in chromosome alignment. Recent reports showed that a critical mass of chromosomes congressed on metaphase plate before anaphase onset is required.[16,17] At the time of APC activation, oocytes isolated from F1 hybrids of *Mus musculus* and *Mus spretus* have more than 50% of DNA positioned outside of the central quarter of the spindle, demonstrating that the required critical mass is either very low, or the alignment of the chromosomes is not prerequisite for APC activation. Importantly, in old and hybrid oocytes, which are both showing extensive spindle defects with no impact on timing of anaphase onset, their response to nocodazole depolymerizing the spindle microtubules is preserved, demonstrating that SAC is intact. Our data contribute to the recent discussion about the function of SAC in mammalian

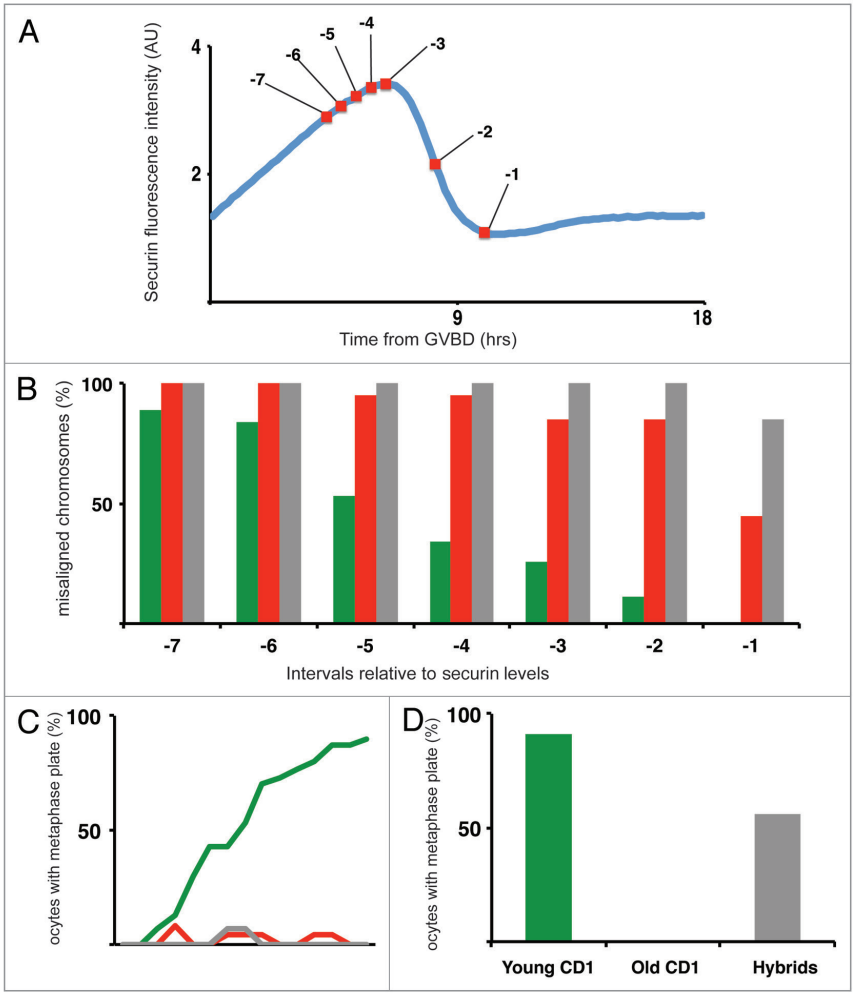

Figure 4. Correlation between chromosome alignment and securin levels. (A) Typical securin expression curve showing intervals for scoring chromosome alignment: -7 = 120, -6 = 90, -5 = 60, -4 = 30 min to highest securin, -3 = highest securin, -2 = half of the securin level, -1 = one frame before anaphase. (B) Scoring of unaligned chromosomes in meiosis I in intervals described in A – Young CD1 (green, n = 19), Old CD1 (red, n = 20) Hybrid (gray, n = 13). (C) Scoring oocytes with all chromosomes aligned on metaphase II plate during 150 min following anaphase I. Young CD1 (green, n = 30), Old CD1 (red, n = 24) Hybrid (gray, n = 15). (D) % of oocytes with metaphase plate at 18 h - Young CD1 (green, n = 22) 91%, Old CD1 (red, n = 20) 0% and Hybrid (gray, n = 13) 56%.

oocytes and its role in etiology of maternal age-related aneuploidy (reviewed in refs. 9, 16, 24 and 25). In mitosis, SAC was shown to be extremely efficient, delaying anaphase until all kinetochores are aligned on metaphase plate, and even one single unattached kinetochore is able to block the cell cycle progression.[13] Although it seems that the attachment of chromosomes to spindle microtubules is sufficient for switching SAC off and the kinetochore tension is sensed by attachment correcting mechanisms, it is likely that both mechanisms are linked by several key players participating in both processes.[15,26,27] From previous studies, we have strong evidence that SAC in mouse oocytes is essential for faithful chromosome segregation and its abolition, by depleting Bub1, has catastrophic consequences, including precocious APC activation and chromosome missegregation and resulting in extensive aneuploidy.[11] But we also know that unaligned chromosomes, both univalents and bivalents, in meiosis I are well tolerated (see refs. 16, 17, 28 and 29 and **Fig. 4B**). These data, together with our results, strongly suggest that attachment of the chromosomes to the spindle microtubules is sufficient for entering anaphase in mammalian oocytes. This is consistent with the hypothesis that

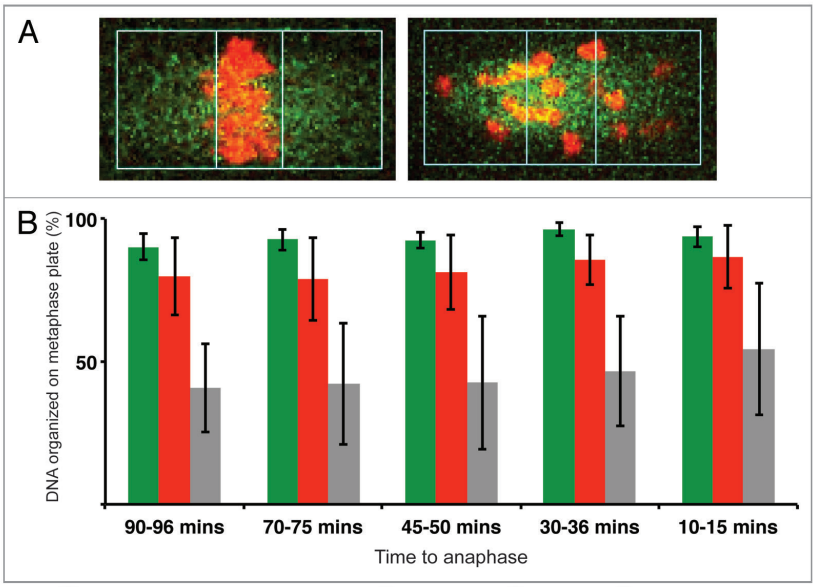

Figure 5. Severe congression defects in meiosis I in Old CD1 and Hybrid oocytes. (A) Oocytes were microinjected with fluorescently labeled histone H2B (red) and β-tubulin 2A (green). DNA was measured within a rectangle representing 25% of the spindle length. Typical images of oocytes with chromosomes aligned on equatorial plane (left panel) and unaligned (right panel). (B) Scoring of congression defects in meiosis I in Young CD1 (green, n = 10), Old CD1 (red, n = 6) Hybrid (gray, n = 5) oocytes, time of selected intervals relative to anaphase is indicated.

SAC is fully functional in mammalian oocytes, even in the situation when oocytes are isolated from aged animals or interspecific hybrids. We can speculate that in those cells, the high frequency of aneuploidy is due to the absence or failure of mechanisms correcting chromosome attachment errors, which are in somatic cells closely cooperating with SAC activity.

Materials and Methods

Mice strains. CD1 mice were purchased from Velaz, Czech Republic at the age of 6 weeks and then aged naturally. *Mus spretus* were obtained from Jaroslav Pialek, Institute of Vertebrate Biology, AS CR. F_1 hybrids resulted from mating *Mus musculus* C57BL/6 females (purchased from Anlab) and *Mus spretus* males. All animal work was conducted according to Act No 246/1992 Coll., on the protection of animals against cruelty under supervision of Central Commission for Animal Welfare, approval ID 018/2010.

Oocyte culture and microinjection. GV-stage oocytes were harvested from ovaries in M2 medium (Sigma-Aldrich) containing 200 mM 3-isobutyl-1-methylxanthine (IBMX, Sigma-Aldrich). After releasing from surrounding cumulus cells, oocytes were cultured in drops of M16 medium (Millipore) supplemented with IBMX and covered with mineral oil (Sigma-Aldrich) at 37°C in the presence of 5% CO_2. Microinjection was performed in M2 with IBMX. mRNAs for microinjection were prepared by in vitro transcription of plasmids containing ORFs of mouse histone H2B, β-tubulin 2a and securin. Oocytes were microinjected with I-10 microinjector (Narishige) with mixture of up to three different mRNAs into the cytoplasm. Microinjection was performed on Leica DM IL inverted microscope equipped with N PLAN 5 x /0.12 and HI PLAN I 20 x /0.3 objectives. Oocytes were matured in M16 medium without IBMX at 37°C in the presence of 5% CO_2. In some experiments, oocytes were cultured in the presence of 0.04 μg/ml nocodazole (Sigma-Aldrich) in the culture media.

Kinetochore counting assay. This method was adapted from reference 19. After 18 h of maturation, MII-stage oocytes were incubated in M16 containing 100 μM monastrol (Sigma-Aldrich) at 37°C and 5% CO_2. Zona pelucida and polar body were removed in Tyrode's solution (Sigma-Aldrich), fixation was performed using 2% paraformaldehyde (Sigma-Aldrich) for 20 min and cells were stained with human anti-centromere antibody (HCT-0100, 1:500, Immunovision) and Alexa Fluor 488 goat anti human secondary antibody (A11013, 1:500, Invitrogen, Life Technologies). Cells were mounted into Vectashield with Dapi (H-1200, Vector Laboratories) and finally scanned by Leica SP5 confocal microscope equipped with HCX PL APO 40 x /1.3 OIL CS objective. For detection of DAPI and Alexa Fluor 488 we used excitation wavelengths 405 nm and 488 nm and AOBS and AOTF filter system. By choosing appropriate Z resolution the optimal coverage of the whole cell volume was achieved.

Chromosome spreads. Chromosome spreads from MI-stage oocytes were prepared as described previously.[11,19] Oocytes were matured for 7.5 h. Only oocytes that achieved GVBD within 1.5 h after IBMX removal were used and matured subsequently for

additional 6 h. Spreads were stained with antibody against centromere (HCT-0100, 1:500, Immunovision). Primary antibodies were detected by Alexa Fluor 594 goat anti human (A11014, 1:500, Invitrogen, Life technologies). Slides were mounted into Vectashield containing DAPI (H-1200, Vector Laboratories) and scanned with Leica SP5 confocal microscope with AOBS equipped with HCX PL APO 40 x /1.3 OIL CS objective. For detection of DAPI and Alexa Fluor 594 excitation wavelengths 405 nm and 561 nm were used. Some of the spreads were scanned using Leica AF6000 inverted fluorescence microscope equipped with HC PL APO 20x/0.7 IMM CORR CS and HCX PL APO 100 x /1.4–0.7 OIL objectives.

Live imaging. 1–2 h after microinjection oocytes were transferred to Leica SP5 confocal microscope equipped with EMBL stage incubator and HCX PL APO 20 x /0.7 IMM CORR λ_{BL} and HCX PL APO 40 x /1.3 OIL CS objectives. For excitation 405, 488, 514 and 561 nm wavelengths were used. Fluorescently tagged proteins were detected with internal PMTs or HyDs. 9–13 Z-stacks were captured every 10–15 min for 18 h. Labeled chromosomes were tracked with Leica High Content Screening Automation software.

Analysis of data. Mean and standard deviation values were calculated using MS Excel, statistical significance of the differences between groups were tested using paired and unpaired Student's t-test (GraphPad Prism software for Macintosh). Time-lapse experiments were analyzed using ImageJ (http://rsbweb.nih.gov/ij), Imaris (www.bitplane.com) or Huygens (www.svi.nl/tiki-index.php?page=HomePage) software.

Disclosure of Potential Conflicts of Interest

No potential conflicts of interest were disclosed.

Acknowledgments

We are grateful to Jaroslav Pialek, Institute of Vertebrate Biology, A.S. C.R. for *Mus spretus* breading pairs, Prof. Jiri Rubes and to all members of Martin Anger's laboratory for helpful discussion and Dr. Frank Sieckmann (Leica Microsystems CMS GmbH) for optimizing High content Screening Software. M.A. was supported by Czech Science Foundation grant 523/09/0743, EMBO installation grant 1817 and Purkyne Fellowship. J.S., A.D. and L.N. were supported by above grants and also by Czech Science Foundation 204/09/H084. M.K. was supported by Czech Science Foundation grant P502–10–0944. Work in M.A. laboratory is supported by the project "CEITEC – Central European Institute of Technology" (CZ.1.05/1.1.00/02.0068) from European Regional Development Funds.

References

1. Hassold T, Hunt P. To err (meiotically) is human: the genesis of human aneuploidy. Nat Rev Genet 2001; 2:280-91; PMID:11283700; http://dx.doi.org/10.1038/35066065.
2. Hunt PA, Hassold TJ. Human female meiosis: what makes a good egg go bad? Trends Genet 2008; 24:86-93; PMID:18192063; http://dx.doi.org/10.1016/j.tig.2007.11.010.
3. Hornak M, Jeseta M, Musilova P, Pavlok A, Kubelka M, Motlik J, et al. Frequency of aneuploidy related to age in porcine oocytes. PLoS One 2011; 6:e18892; PMID:21556143; http://dx.doi.org/10.1371/journal.pone.0018892.
4. Chiang T, Duncan FE, Schindler K, Schultz RM, Lampson MA. Evidence that weakened centromere cohesion is a leading cause of age-related aneuploidy in oocytes. Curr Biol 2010; 20:1522-8; PMID:20817534; http://dx.doi.org/10.1016/j.cub.2010.06.069.
5. Lister LM, Kouznetsova A, Hyslop LA, Kalleas D, Pace SL, Barel JC, et al. Age-related meiotic segregation errors in mammalian oocytes are preceded by depletion of cohesin and Sgo2. Curr Biol 2010; 20:1511-21; PMID:20817533; http://dx.doi.org/10.1016/j.cub.2010.08.023.
6. Tachibana-Konwalski K, Godwin J, van der Weyden L, Champion L, Kudo NR, Adams DJ, et al. Rec8-containing cohesin maintains bivalents without turnover during the growing phase of mouse oocytes. Genes Dev 2010; 24:2505-16; PMID:20971813; http://dx.doi.org/10.1101/gad.605910.
7. Revenkova E, Herrmann K, Adelfalk C, Jessberger R. Oocyte cohesin expression restricted to predictyate stages provides full fertility and prevents aneuploidy. Curr Biol 2010; 20:1529-33; PMID:20817531; http://dx.doi.org/10.1016/j.cub.2010.08.024.
8. Holt JE, Jones KT. Control of homologous chromosome division in the mammalian oocyte. Mol Hum Reprod 2009; 15:139-47; PMID:19179408; http://dx.doi.org/10.1093/molehr/gap007.
9. Homer H. New insights into the genetic regulation of homologue disjunction in mammalian oocytes. Cytogenet Genome Res 2011; 133:209-22; PMID:21335952; http://dx.doi.org/10.1159/000324118.
10. Vogt E, Kirsch-Volders M, Parry J, Eichenlaub-Ritter U. Spindle formation, chromosome segregation and the spindle checkpoint in mammalian oocytes and susceptibility to meiotic error. Mutat Res 2008; 651:14-29; PMID:18096427; http://dx.doi.org/10.1016/j.mrgentox.2007.10.015.
11. McGuinness BE, Anger M, Kouznetsova A, Gil-Bernabé AM, Helmhart W, Kudo NR, et al. Regulation of APC/C activity in oocytes by a Bub1-dependent spindle assembly checkpoint. Curr Biol 2009; 19:369-80; PMID:19249208; http://dx.doi.org/10.1016/j.cub.2009.01.064.
12. Meraldi P, Draviam VM, Sorger PK. Timing and checkpoints in the regulation of mitotic progression. Dev Cell 2004; 7:45-60; PMID:15239953; http://dx.doi.org/10.1016/j.devcel.2004.06.006.
13. Rieder CL, Schultz A, Cole R, Sluder G. Anaphase onset in vertebrate somatic cells is controlled by a checkpoint that monitors sister kinetochore attachment to the spindle. J Cell Biol 1994; 127:1301-10; PMID:7962091; http://dx.doi.org/10.1083/jcb.127.5.1301.
14. Clute P, Pines J. Temporal and spatial control of cyclin B1 destruction in metaphase. Nat Cell Biol 1999; 1:82-7; PMID:10559878; http://dx.doi.org/10.1038/10049.
15. Musacchio A, Salmon ED. The spindle-assembly checkpoint in space and time. Nat Rev Mol Cell Biol 2007; 8:379-93; PMID:17426725; http://dx.doi.org/10.1038/nrm2163.
16. Lane SI, Yun Y, Jones KT. Timing of anaphase-promoting complex activation in mouse oocytes is predicted by microtubule-kinetochore attachment but not by bivalent alignment or tension. Development 2012; 139:1947-55; PMID:22513370; http://dx.doi.org/10.1242/dev.077040.
17. Nagaoka SI, Hodges CA, Albertini DF, Hunt PA. Oocyte-specific differences in cell-cycle control create an innate susceptibility to meiotic errors. Curr Biol 2011; 21:651-7; PMID:21497085; http://dx.doi.org/10.1016/j.cub.2011.03.003.
18. Koehler KE, Schrump SE, Cherry JP, Hassold TJ, Hunt PA. Near-human aneuploidy levels in female mice with homeologous chromosomes. Curr Biol 2006; 16:R579-80; PMID:16890511; http://dx.doi.org/10.1016/j.cub.2006.07.018.
19. Duncan FE, Chiang T, Schultz RM, Lampson MA. Evidence that a defective spindle assembly checkpoint is not the primary cause of maternal age-associated aneuploidy in mouse eggs. Biol Reprod 2009; 81:768-76; PMID:19553597; http://dx.doi.org/10.1095/biolreprod.109.077909.
20. Kouznetsova A, Lister L, Nordenskjöld M, Herbert M, Höög C. Bi-orientation of achiasmatic chromosomes in meiosis I oocytes contributes to aneuploidy in mice. Nat Genet 2007; 39:966-8; PMID:17618286; http://dx.doi.org/10.1038/ng2065.
21. Dudas A, Ahmad S, Gregan J. Sgo1 is required for cosegregation of sister chromatids during achiasmate meiosis I. Cell Cycle 2011; 10:951-5; PMID:21330786; http://dx.doi.org/10.4161/cc.10.6.15032.
22. Sakuno T, Tanaka K, Hauf S, Watanabe Y. Repositioning of aurora B promoted by chiasmata ensures sister chromatid mono-orientation in meiosis I. Dev Cell 2011; 21:534-45; PMID:21920317; http://dx.doi.org/10.1016/j.devcel.2011.08.012.
23. Peters JM. The anaphase-promoting complex: proteolysis in mitosis and beyond. Mol Cell 2002; 9:931-43; PMID:12049731; http://dx.doi.org/10.1016/S1097-2765(02)00540-3.
24. Jones KT, Lane SI. Chromosomal, metabolic, environmental, and hormonal origins of aneuploidy in mammalian oocytes. Exp Cell Res 2012; 318:1394-9; PMID:22394508; http://dx.doi.org/10.1016/j.yexcr.2012.02.012.
25. Wang ZB, Schatten H, Sun QY. Why is chromosome segregation error in oocytes increased with maternal aging? Physiology (Bethesda) 2011; 26:314-25; PMID:22013190; http://dx.doi.org/10.1152/physiol.00020.2011.

26. Khodjakov A, Pines J. Centromere tension: a divisive issue. Nat Cell Biol 2010; 12:919-23; PMID:20885417; http://dx.doi.org/10.1038/ncb1010-919.
27. Musacchio A. Spindle assembly checkpoint: the third decade. Philos Trans R Soc Lond B Biol Sci 2011; 366:3595-604; PMID:22084386; http://dx.doi.org/10.1098/rstb.2011.0072.
28. Hunt P, LeMaire R, Embury P, Sheean L, Mroz K. Analysis of chromosome behavior in intact mammalian oocytes: monitoring the segregation of a univalent chromosome during female meiosis. Hum Mol Genet 1995; 4:2007-12; PMID:8589675; http://dx.doi.org/10.1093/hmg/4.11.2007.
29. LeMaire-Adkins R, Radke K, Hunt PA. Lack of checkpoint control at the metaphase/anaphase transition: a mechanism of meiotic nondisjunction in mammalian females. J Cell Biol 1997; 139:1611-9; PMID:9412457; http://dx.doi.org/10.1083/jcb.139.7.1611.

Sodek M, Kovacovicova K, Anger M. True Nondisjunction of Whole Bivalents in Oocytes with Attachment and Congression Defects. Cytogenet Genome Res. 2017

Impact Factor/Quartile: 1,587/Q4
Times cited (Wos May 2019): 0
Significance: Report documenting the aetiology of nondisjunction and unresponsiveness of SAC to unattached kinetochores.
Contribution of the author: Experimental design, interpretation of experiments manuscript preparation, securing funding

Original Article

Cytogenetic and Genome Research

Cytogenet Genome Res
DOI: 10.1159/000458513

Accepted: October 6, 2016
by M. Schmid
Published online: March 10, 2017

True Nondisjunction of Whole Bivalents in Oocytes with Attachment and Congression Defects

Martin Sodek[a] Kristina Kovacovicova[a, b] Martin Anger[a, b]

[a]Veterinary Research Institute, and [b]Department of Histology and Embryology, Faculty of Medicine, Masaryk University, Brno, Czech Republic

Key Words
Aneuploidy · Bivalents · Chromosome congression · Chromosome segregation · Meiosis · Nondisjunction · Oocyte

Abstract
Chromosome segregation in mammalian oocytes is prone to errors causing aneuploidy with consequences such as precocious termination of development or severe developmental disorders. Aneuploidy also represents a serious problem in procedures utilizing mammalian gametes and early embryos in vitro. In our study, we focused on congression defects during meiosis I and observed whole nondisjoined bivalents in meiosis II as a direct consequence, together with a substantially delayed first polar body extrusion. We also show that the congression defects are accompanied by less stable attachments of the kinetochores. Our results describe a process by which congression defects directly contribute to aneuploidy.

Chromosome segregation in mammalian oocytes, more frequently than in somatic cells, is affected by errors leading to aneuploidy, premature termination of embryonic development, and severe developmental disorders [Hassold and Hunt, 2001]. The overall high aneuploidy rates are increasing further with maternal age, at least in human and mouse oocytes [Eichenlaub-Ritter, 2012; Nagaoka et al., 2012; Jones and Lane, 2013; Herbert et al., 2015], although for example porcine oocytes do not show a similar age-related increase in aneuploidy [Hornak et al., 2011]. Despite the fact that we can explain the increase of aneuploidy coincidently with maternal age by deterioration of cohesion between sister chromatids [Chiang et al., 2010; Lister et al., 2010] due to the absence of turnover of the cohesin complex during a prolonged prophase arrest [Revenkova et al., 2010; Tachibana-Konwalski et al., 2010], we are still uncertain why the aneuploidy is so high even in oocytes from young individuals in comparison to meiosis in yeast and *Drosophila* [Hassold and Hunt, 2001]. One of the mechanism, which likely contributes to this higher aneuploidy rate, is the spindle assembly checkpoint (SAC) and specifically changes to its function in oocytes compared to somatic cells [Mailhes, 2008; Jones and Lane, 2013; Touati and Wassmann, 2015; Collins and Jones, 2016].

In a previous study, we demonstrated that the SAC in oocytes is unable to detect extensive chromosome alignment and congression defects by using animals generated by crossbreeding of 2 different mouse species, *Mus mus-*

E-Mail karger@karger.com
www.karger.com/cgr

Martin Anger
Veterinary Research Institute
Hudcova 70
CZ–621 00 Brno (Czech Republic)
E-Mail anger@vri.cz

culus and *M. spretus* [Sebestova et al., 2012]. In this study we used the same interspecific hybrids and focused more closely on the consequences of these defects. We show that the congression defects are accompanied by less stable kinetochore-to-microtubule attachments. Both together then lead to nondisjunction and frequent co-segregation of whole bivalents. This situation is probably exacerbated by higher levels of cohesins on meiosis I chromosomes in hybrid oocytes. Our data show the process by which congression defects and improper kinetochore attachment are contributing to the overall oocyte aneuploidy.

Materials and Methods

Mice

Female CD-1 and C57/BL6 mice were purchased from Anlab (Czech Republic) or from the Animal Breeding and Experimental Facility, Faculty of Medicine, Masaryk University, Czech Republic. CD-1×B6D2F1 female mice were obtained from a cross between CD-1 female and B6D2F1 male (Anlab). *M. spretus* mice (SPRET) were obtained from the Jackson Laboratory, USA, and the hybrids were produced by crossing C57/BL6 females and SPRET males.

Oocytes Collection and Maturation

Female mice were sacrificed by cervical dislocation, and ovarian tissue was excised. The germinal vesicle stage (GV) oocytes were collected from ovaries in M2 medium (Sigma Aldrich) supplemented with 100 μM 3-isobutyl-1methylxantine (IBMX, Sigma Aldrich). Prior to maturation, cells were transferred into M16 medium (Sigma Aldrich) with IBMX and covered with mineral oil (Sigma Aldrich). Maturation at 37°C in the presence of 5% CO_2 was initiated by removing the IBMX. Oocytes which did not undergo germinal vesicle breakdown (GVBD) within 1.5 h were discarded.

Microinjection

Microinjection of GV oocytes was performed in M2 with IBMX, after which oocytes were cultured in colorless M16 (Merck Millipore) supplemented with IBMX. Microinjection was done using an IM-300 microinjector (Narishige) on a Leica DM IL inverted microscope as described previously [Kovacovicova et al., 2016]. cRNAs for microinjection were prepared by in vitro transcription (mMESSAGE mMACHINE T3 in vitro transcription kit, Life Technologies) of plasmids containing ORFs of mouse securin, β-tubulin, and histone 2B (H2B) in the transcription fusion with fluorescent proteins CFP, Venus, and mCherry, respectively. Oocytes were culture at 37°C in the presence of 5%CO_2 for 2–3 h prior to live cell imaging.

Live Cell Imaging

Oocytes were transferred to a Leica SP5 confocal microscope equipped with an EMBL incubator, allowing time-lapse experiments in 5% CO_2 at 37°C [Sebestova et al., 2012]. Excitation wavelengths 458, 514 and 561 nm, HCX PL APO 40×/1.1 water objective (NA 1.10), and hybrid detectors were used for the detection of CFP, Venus, and mCherry fluorescently tagged proteins.

Chromosomal Spreads and Immunofluorescence

If not stated otherwise, all chemicals were derived from Sigma Aldrich. For chromosomal spreads the oocytes were harvested at 6 or 18 h after GVBD. The zona pellucida was dissolved using pronase, and cells were lysed overnight in PBS containing 1.0% PFA, 0.15% Triton-X100, and 3mM DTT (pH 9.2). The chromosome spreads were immunostained with primary antibodies CREST (ImmunoVision) and Anti-Smc3 Antibody (Abcam) and with secondary antibodies Alexa Fluor 488 Goat anti-Rabbit IgG (Life Technologies) and Alexa Fluor 555 Goat anti-Human IgG (Life Technologies). Spreads were mounted inVectashield with DAPI (Vector Laboratories). Images were captured using a Leica AF 6000 inverted fluorescence microscope equipped with a HCX PL APO × 100/1.4 0.7 oil objective, Leica Microsystems DFC365FX camera, Leica A, GFP, and dsRed filter cubes.

Cold-Stable Microtubules

If not stated otherwise, all chemicals were derived from Sigma Aldrich, and protocols from Lane et al. [2012], Kovacovicova et al. [2016], and Chmátal et al. [2015] were adopted. Briefly, the oocytes were incubated in pre-cooled M2 medium (4–8°C) for 7 min before fixation with 2% paraformaldehyde. Cell were permeabilized by 0.5% Triton in PBS and then blocked in PBS. The following antibodies were used for immunostaining: human autoantibody against centromere (CREST, ImmunoVision), mouse anti acetylated α-tubulin, Alexa Fluor 488 Goat anti-Mouse IgG (Life Technologies), and Alexa Fluor 555 conjugate Goat anti-Human IgG (Life Technologies). For image acquisition, a Leica SP5 confocal microscope equipped with HCX PL APO 63×/1.4 oil objective, excitation wavelengths 405, 488, and 561 nm and hybrid detectors were used.

Image Analysis and Statistical Analysis

Data analysis was performed using ImageJ (http://rsb.info.nih.gov/ij/) and Leica LAS AF (http://www.leica-microsystems.com). Statistical analysis was performed using Prism software, version 5.00 for Mac (GraphPad Software, San Diego, CA, USA; www.graphpad.com). The statistical significance of the difference between the control and the experimental group was tested using unpaired *t* test or Mann Whitney test for quantitative data and χ^2 test for categorical data.

Results

Congression Defects in Meiosis I Are Transformed into a Struggle to Segregate Chromosomes during Anaphase

We previously reported that oocytes from *M. musculus* and *M. spretus* hybrids suffer from extensive congression defects and aneuploidy [Sebestova et al., 2012]. In this study we wanted to address the effect of congression defects on chromosome segregation in anaphase I. Hybrid GV oocytes, together with control CD-1 oocytes, were microinjected with cRNAs encoding histone 2B, securin, and β-tubulin fused to different fluorescent proteins. Oocytes were then matured, and the combination

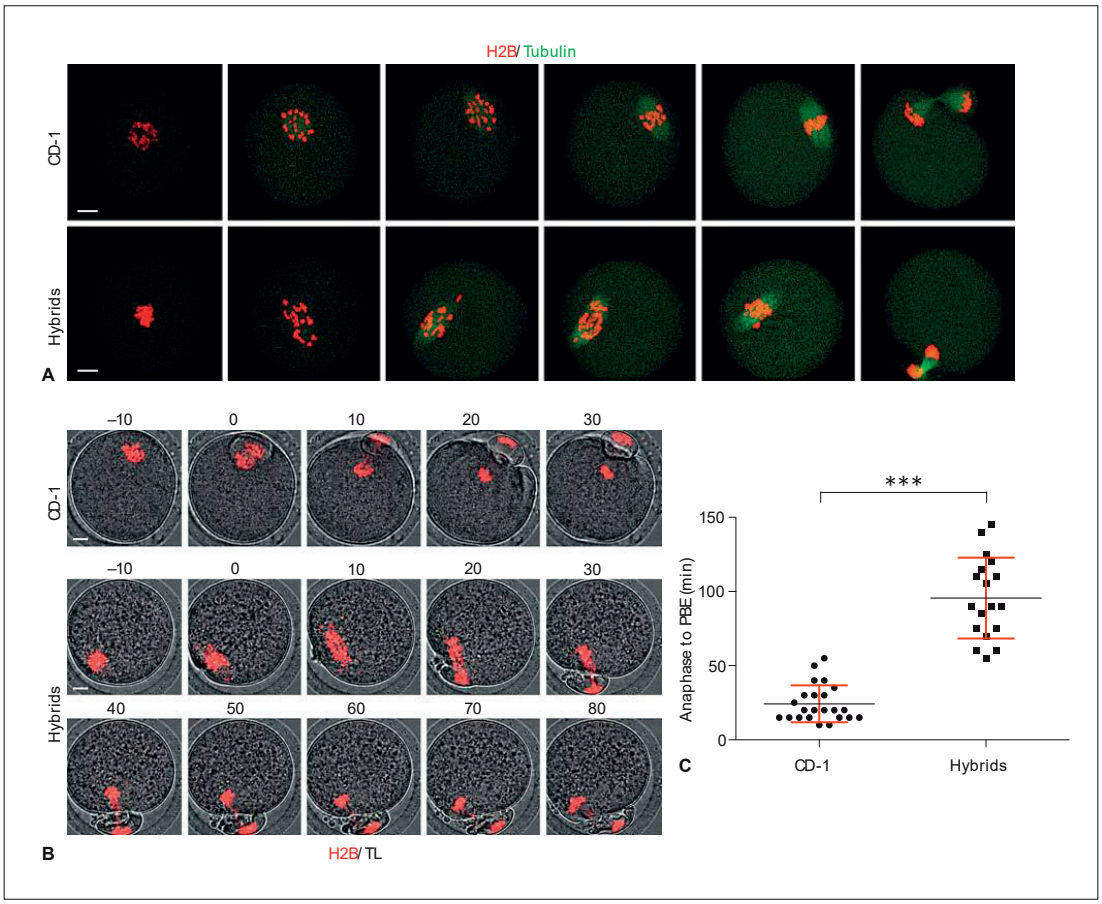

Fig. 1. Congression defects causing delays in polar body extrusion. **A** Pictures from the time-lapse experiment showing the first meiotic division in CD-1 and hybrid oocytes. Histone H2B is visualized by mCherry fluorescent tag and is presented in red, β-tubulin fused with Venus fluorescent tag is shown in green. Scale bars, 10 μm. **B** The separation of the chromosomal mass is delayed in hybrids. Time point zero represents the first frame in which the visible separation of chromosomal masses was observed. Histone H2B was visualized as in **A**. Scale bars, 10 μm. **C** The total time from anaphase to extrusion of the first polar body (PBE) is significantly ($p < 0.0001$) different in hybrids ($n = 19$) compared to CD-1 ($n = 23$) oocytes.

of fusion proteins allowed a simultaneous monitoring of chromosome movement, assembly, and movement of the spindle and activation of anaphase promoting complex (APC/C) in each cell individually. We confirmed our previous results [Sebestova et al., 2012] showing that the congression is significantly affected in hybrid oocytes (Fig. 1A). From the time-lapse imaging it was obvious that the actual chromosome segregation during anaphase and also the formation of the first polar body takes longer in hybrid oocytes compared to CD-1 oocytes (Fig. 1B). Whereas the control oocytes separate chromosomes into 2 resolved DNA masses with the spindle still located almost entirely inside the cell and extruding the polar body (PB), the hybrid oocytes struggle to complete division of their chromosomes. Subsequently, PB extrusion takes significantly longer, while chromosomes are being entrapped between the oocyte and the PB. Measuring the time interval between the initiation of chromosomal

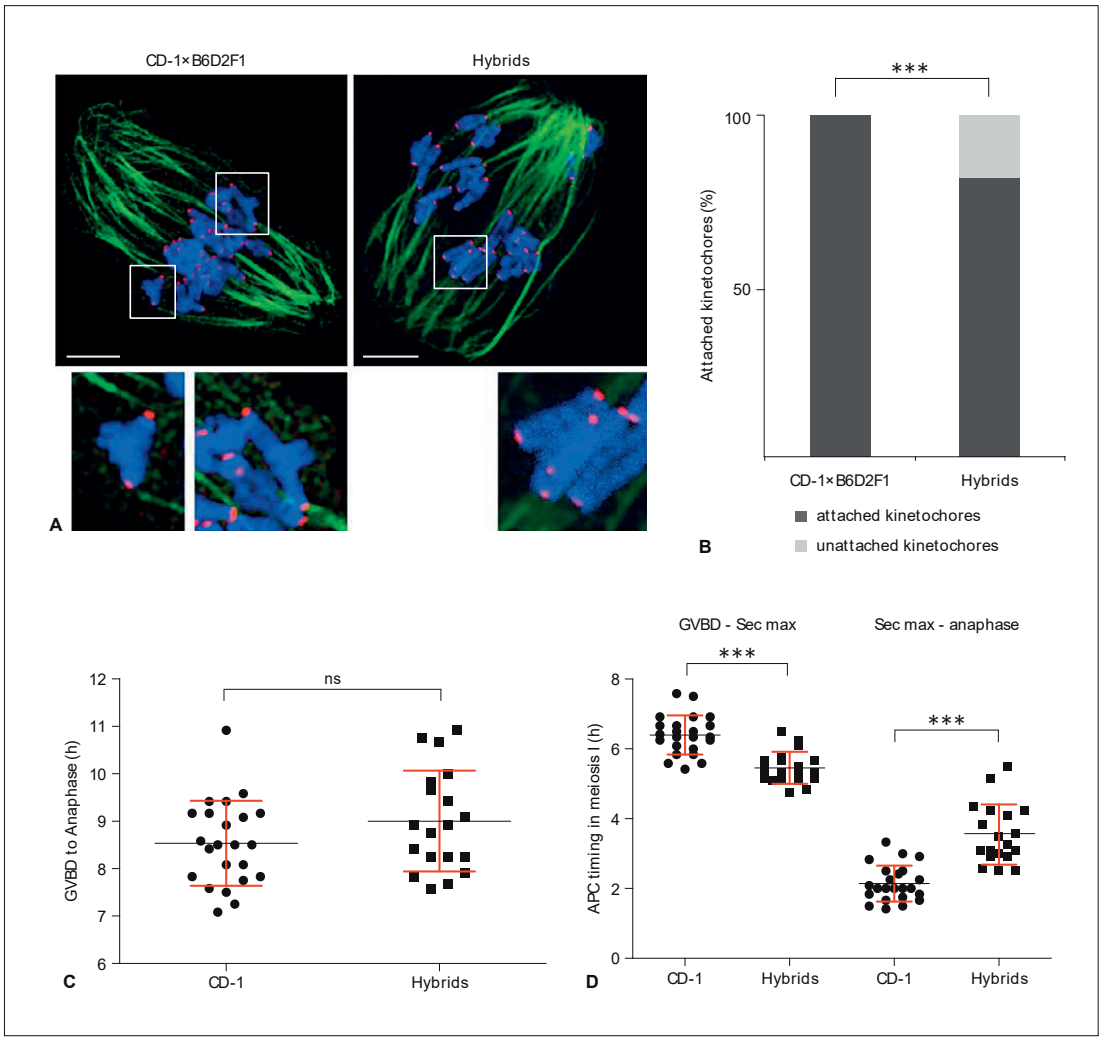

Fig. 2. Unattached kinetochores in hybrid oocytes. **A** Example of permanently attached and unattached kinetochores in CD-1 and hybrid oocytes 6.5 h post germinal vesicle breakdown (GVBD), when oocytes are in metaphase I and have fully developed a bipolar meiosis I spindle. DNA is shown in blue, α-tubulin in green, and kinetochores in red. Scale bars, 10 μm. **B** Scoring of attached (dark gray) and unattached (light gray) kinetochores in CD-1 (n = 160) and hybrid (n = 200) oocytes. Data are from 2 independent experiments, differences are significant ($p < 0.0001$). **C** Duration of the first meiotic division, measured as time from GVBD to anaphase onset in CD-1 (n = 23) and hybrid (n = 19) oocytes. Both intervals are similar ($p = 0.1291$). **D** The progression of meiosis I divided into 2 intervals – before and after APC/C activation. The onset of APC/C activity is marked by initiation of securin destruction, therefore we consider the interval with the highest securin signal (Sec max) as the time point when the APC/C becomes activated. The cells are the same as in **C**. The APC/C is activated significantly earlier in hybrids ($p < 0.0001$).

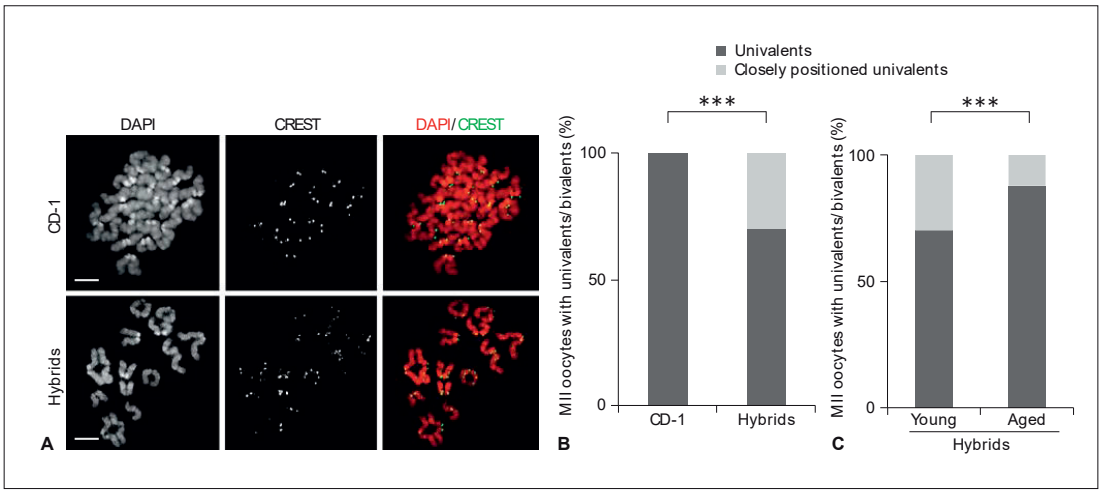

Fig. 3. Occurrence of closely positioned bivalents in meiosis II spreads in hybrid oocytes. **A** Chromosomal spreads from CD-1 (upper panel) and hybrid (lower panel) MII oocytes. DNA (red) is visualized by DAPI and kinetochores (green) by antibody staining against centromeres (CREST). Scale bars, 10 μm. **B** Scoring of presence of closely attached univalents in CD-1 (n = 92) and hybrid (n = 120) oocytes. Both groups contain univalents, and 30% of hybrid MII oocytes contain also at least 2 univalents positioned as bivalents. **C** Scoring of chromosomal spreads obtained from MII oocytes (cells are identical as in **A**) from young (n = 120) and old (n = 81) hybrids. The frequency of closely positioned univalents is significantly lower in eggs from elder animals than from young mice (***p = 0.035).

DNA separation and PB extrusion (Fig. 1C) showed that in CD-1 oocytes this process takes on average 24.35 min in contrast to hybrid oocytes where the same event takes significantly longer, on average 95.56 min.

Congression Defects in Hybrid Oocytes Are Accompanied with Unattached Kinetochores

Congression of chromosomes on the equatorial metaphase plate requires bipolar attachment of microtubule bundles to the sister kinetochores [Simunić and Tolić, 2016]. To analyze whether the kinetochores in hybrid oocytes that are characterized by congression defects are correctly attached to the spindle microtubules, we cultured oocytes for 6.5 h after GVBD and then used cold shock treatment for destabilizing microtubules, which are only temporarily attached. After cold shock, cells were fixed and subsequently chromosomes, kinetochores, and the spindle apparatus were labeled (Fig. 2A). Scanning of fixed cells using a confocal microscope allowed assessing which kinetochores are still attached to the microtubules. Our scoring showed that in control oocytes, which were in these experiments isolated from CD-1×B2D6F1 hybrid animals, virtually all kinetochores at 6.5 h were already permanently attached to the spindle microtubules. In oocytes from hybrid animals on the other hand, 18.5% of kinetochores lacked connection to the microtubules at the same interval (Fig. 2B). It is, however, important to mention that the vast majority of the bivalents lost the connection only unilaterally, and their attachment to the spindle by the remaining kinetochore pair was still preserved. The interval 6.5 h post GVBD was selected because we anticipated that at this time all kinetochores already acquired their permanent attachment and the SAC is silenced [Sebestova et al., 2012]. The APC/C activation could be monitored by measuring the destruction of its substrates. Since in these experiments we co-injected securin as an APC/C substrate, we were able to detect whether the interval we used for scoring attachment was after APC/C activation and therefore after silencing the SAC. Similarly to our previous results [Sebestova et al., 2012], the length of meiosis I between CD-1 and control oocytes was not different (Fig. 2C), and although we found that the activation of APC/C in hybrid oocytes was significantly advanced compared to CD-1 oocytes (Fig. 2D), the APC/C in both cases at 6.5 h was already active, indicating that the SAC was also silenced.

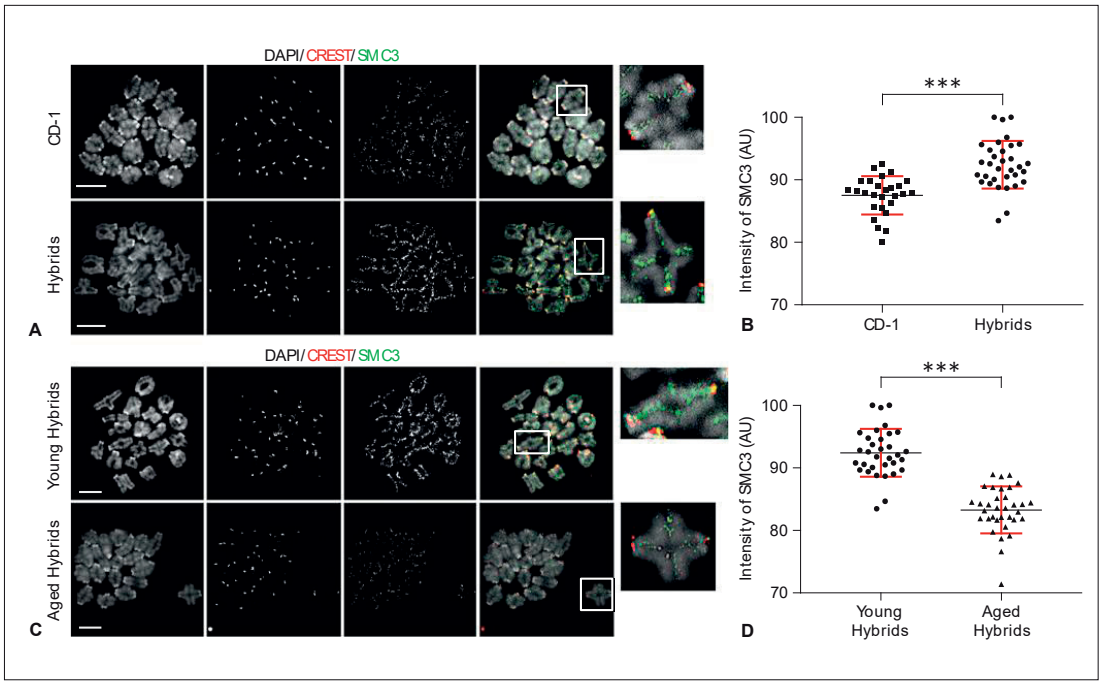

Fig. 4. SMC3 levels are higher on chromosomes from hybrid oocytes. **A** Chromosomal spreads from CD-1 and hybrid oocytes (both 12–22 weeks old) prepared 6 h post germinal vesicle breakdown stained for DNA (DAPI, gray) kinetochores (CREST, red), and cohesin (SMC3, green). Scale bars, 10 μm. **B** Quantification of SMC3 levels on chromosomal arms in CD-1 ($n = 27$) and hybrids ($n = 33$). The SMC3 level is significantly higher in hybrid MI oocytes ($p < 0.0001$). Data are collected from 2 independent experiments; each value is normalized to the background. **C** Representative chromosomal spreads from young (6–10 months) and old (14–20 months) hybrid mice. The staining is the same as in **A**. Scale bars, 10 μm. **D** The SMC3 level is reduced ($p < 0.0001$) in oocytes obtained from older animals ($n = 34$) in comparison to young hybrids ($n = 33$).

Hybrid Oocytes Frequently Harbor Nondisjoined Bivalents in Meiosis II

During anaphase I, activated separase destroys cohesins distal to chiasmata causing separation of homologous chromosomes which are then segregated between the oocyte and the first PB [Kudo et al., 2006]. In case of nondisjunction, both univalents co-segregate to the same cell; in most cases, however, the connection between homologous chromosomes is lost during anaphase. To our surprise, in hybrid oocytes we frequently observed closely positioned univalents resembling bivalents in meiosis I (Fig. 3A). Although we were unable to detect a SMC3 cohesin subunit on the arms of such chromosomes (data not shown), it seemed unlikely that their position was random. The spreads prepared from CD-1 oocytes did not contain such chromosomes whereas in hybrid oocytes 30% of cells had one or more univalent pair arranged as bivalents (Fig. 3B).

It is generally accepted that the frequency of chromosome segregation errors and aneuploidy in oocytes increases with maternal age [Eichenlaub-Ritter, 2012; Nagaoka et al., 2012; Jones and Lane, 2013; Herbert et al., 2015]. To test whether the occurrence of true nondisjoined chromosomes is dependent on maternal age, we compared hybrid oocytes from Figure 3B, obtained from 3- to 4.5-months-old animals, with hybrid oocytes isolated from 15- to 22-months-old animals (Fig. 3C). This comparison revealed that the true nondisjunction described here shows an opposite trend; the frequency of this phenomenon is reduced with maternal age (30% in oocytes from young animals versus 12% in oocytes from aged animals). We were not able to detect a SMC3

cohesin subunit on the arms of the true nondisjoined chromosomes in meiosis II (data not shown). Therefore, we measured cohesin on chromosomes prepared from meiosis I. Staining of SMC3 cohesin on spreads prepared at 6 h after GVBD (Fig. 4A) showed that oocytes from hybrids had significantly higher levels of this protein during meiosis I (Fig. 4B). The average SMC3 levels were about 11% higher in hybrid oocytes than on chromosomes in the CD-1 strain. During maternal aging, the increase of oocyte aneuploidy is accompanied with a general decrease of cohesin during meiosis I [Chiang et al., 2010; Lister et al., 2010; Tsutsumi et al., 2014]. The comparison of SMC3 levels on chromosomes in young (3–4.5 months old) and aged (15–22 months old) hybrid oocytes (Fig. 4C) showed that the levels of SMC3 are reduced during maternal aging to the levels similar to young CD-1 (Fig. 4D).

Discussion

Congression defects in oocytes play an important role in the etiology of oocyte aneuploidy [Holt et al., 2012; Sebestova et al., 2012; Danadova et al., 2016]. In this study, we used oocytes isolated from hybrids between the 2 mouse species *M. musculus* and *M. spretus* to explore the causes and consequences of chromosome congression defects. Our results showed that the congression defects are translated into a struggle to resolve chromosomes during anaphase. We also showed that kinetochores with less stable attachment to the spindle microtubule apparatus are accompanying congression defects in hybrid oocytes. However, we were unable to distinguish whether the congression defects were caused by the lack of permanent attachment or vice versa. Since we used oocytes from interspecific hybrids, it is conceivable that the kinetochore pairs of bivalents are unbalanced in the strength of their connection to the spindle poles [Chmátal et al., 2014] and that a correction mechanisms involving Aurora A might be responsible for the lack of permanent attachments. However, it is important to emphasize that neither congression defects nor the lack of cold-stable microtubules in hybrid oocytes were able to prevent APC/C activation and anaphase.

Chromosome segregation during meiosis is a highly orchestrated process that requires precise coordination of various events. The first meiotic division is characterized by separation of homologous chromosomes, which are organized as bivalents when oocytes are resuming meiosis after prolonged arrest in prophase of the first meiotic division. The success of this division largely depends on coordination between the removal of the cohesin protein complex from chromosome arms and its preservation at the centromere [Petronczki et al., 2003]. Removal of cohesins prematurely from both sites already during meiosis I leads to a precocious segregation of sister chromatids. We can only speculate that the opposite situation, when cohesin links between homologue chromosomes are preserved beyond anaphase I, might lead into true whole chromosome nondisjunction. The observed struggle to separate chromosomes in hybrid oocytes resembled the situation when non-cleavable Rec8 caused delays during polar body extrusion in oocytes [Kudo et al., 2009]. It was shown previously in both budding and fission yeast that incomplete removal of cohesin in meiosis I led to nondisjunction [Ishiguro et al., 2010; Katis et al., 2010; Rumpf et al., 2010; Phadnis et al., 2015]. We hypothesize that the occurrence of nondisjoined chromosomes in our system resulted from the defects in congression, since the distant position of the chromosome on the meiotic spindle further from the metaphase plate was shown to be linked to co-segregation of both univalents [Holt et al., 2012]. Moreover, the elevated levels of cohesin proteins on hybrid oocytes might exacerbate this situation. In conclusion, our experiments showed that congression defects, together with the lack of cold resistant microtubule attachment, cause true chromosome nondisjunction. Despite that this situation almost certainly would lead to aneuploidy and embryo loss, the SAC is unable to properly respond to such errors and prevent propagation of aneuploidy in the embryo.

Acknowledgments

The authors are grateful to all members of the Martin Anger laboratory for helpful discussion and useful comments. This work was supported by Czech Science Foundation Projects P502/12/2201 and 15-04844S and by the Ministry of Education, Youth, and Sports of the Czech Republic under the project CEITEC 2020 (LQ1601). We acknowledge the core facility Cellular Imaging supported by the MEYS CR (LM2015062 Czech-BioImaging).

Statement of Ethics

The authors declare that all experiments performed in this study comply with the current laws of the Czech Republic. All institutional and national guidelines for the care and use of laboratory animals were followed. All animal work was conducted according to Act No 246/1992 Coll. on the protection of animals against cruelty under supervision of Central Commission for Animal Welfare, approval ID 018/2010 1285/2011 and 1505/2013.

Disclosure Statement

The authors have no conflicts of interest to declare.

References

Chiang T, Duncan FE, Schindler K, Schultz RM, Lampson MA: Evidence that weakened centromere cohesion is a leading cause of age-related aneuploidy in oocytes. Curr Biol 20: 1522–1528 (2010).

Chmátal L, Gabriel SI, Mitsainas GP, Martínez-Vargas J, Ventura J, et al: Centromere strength provides the cell biological basis for meiotic drive and karyotype evolution in mice. Curr Biol 24: 2295–2300 (2014).

Chmátal L, Yang K, Schultz RM, Lampson MA: Spatial regulation of kinetochore microtubule attachments by destabilization at spindle poles in meiosis I. Curr Biol 25: 1835–1841 (2015).

Collins J, Jones KT: DNA damage responses in mammalian oocytes. Reproduction 152: R15–R22 (2016).

Danadova J, Matijescukova N, Danylevska AM, Anger M: Increased frequency of chromosome congression defects and aneuploidy in mouse oocytes cultured at lower temperature. Reprod Fertil Dev DOI: 10.1071/RD1530 (2016).

Eichenlaub-Ritter U: Oocyte ageing and its cellular basis. Int J Dev Biol 56: 841–852 (2012).

Hassold T, Hunt P: To err (meiotically) is human: the genesis of human aneuploidy. Nat Rev Genet 2: 280–291 (2001).

Herbert M, Kalleas D, Cooney D, Lamb M, Lister L: Meiosis and maternal aging: insights from aneuploid oocytes and trisomy births. Cold Spring Harb Perspect Biol 7: a017970 (2015).

Holt JE, Lane SI, Jennings P, García-Higuera I, Moreno S, Jones KT: APC (FZR1) prevents nondisjunction in mouse oocytes by controlling meiotic spindle assembly timing. Mol Biol Cell 23: 3970–3981 (2012).

Hornak M, Jeseta M, Musilova P, Pavlok A, Kubelka M, et al: Frequency of aneuploidy related to age in porcine oocytes. PLoS One 6: e18892 (2011).

Ishiguro T, Tanaka K, Sakuno T, Watanabe Y: Shugoshin-PP2A counteracts casein-kinase-1-dependent cleavage of Rec8 by separase. Nat Cell Biol 12: 500–506 (2010).

Jones KT, Lane SI: Molecular causes of aneuploidy in mammalian eggs. Development 140: 3719–3730 (2013).

Katis VL, Lipp JJ, Imre R, Bogdanova A, Okaz E, et al: Rec8 phosphorylation by casein kinase 1 and Cdc7-Dbf4 kinase regulates cohesin cleavage by separase during meiosis. Dev Cell 18: 397–409 (2010).

Kovacovicova K, Awadova T, Mikel P, Anger M: In vitro maturation of mouse oocytes increases the level of Kif11/Eg5 on meiosis II spindles. Biol Reprod 95: 18 (2016).

Kudo NR, Wassmann K, Anger M, Schuh M, Wirth KG, et al: Resolution of chiasmata in oocytes requires separase-mediated proteolysis. Cell 126: 135–146 (2006).

Kudo NR, Anger M, Peters AH, Stemmann O, Theussl HC, et al: Role of cleavage by separase of the Rec8 kleisin subunit of cohesin during mammalian meiosis I. J Cell Sci 122: 2686–2698 (2009).

Lane SI, Yun Y, Jones KT: Timing of anaphase-promoting complex activation in mouse oocytes is predicted by microtubule-kinetochore attachment but not by bivalent alignment or tension. Development 139: 1947–1955 (2012).

Lister LM, Kouznetsova A, Hyslop LA, Kalleas D, Pace SL, et al: Age-related meiotic segregation errors in mammalian oocytes are preceded by depletion of cohesin and Sgo2. Curr Biol 20: 1511–1521 (2010).

Mailhes JB: Faulty spindle checkpoint and cohesion protein activities predispose oocytes to premature chromosome separation and aneuploidy. Environ Mol Mutagen 49: 642–658 (2008).

Nagaoka SI, Hassold TJ, Hunt PA: Human aneuploidy: mechanisms and new insights into an age-old problem. Nat Rev Genet 13: 493–504 (2012).

Petronczki M, Siomos MF, Nasmyth K: Un ménage à quatre: the molecular biology of chromosome segregation in meiosis. Cell 112: 423–440 (2003).

Phadnis N, Cipak L, Polakova S, Hyppa RW, Cipakova I, et al: Casein kinase 1 and phosphorylation of cohesin subunit Rec11 (SA3) promote meiotic recombination through linear element formation. PLoS Genet 11: e1005225 (2015).

Revenkova E, Herrmann K, Adelfalk C, Jessberger R: Oocyte cohesin expression restricted to predictyate stages provides full fertility and prevents aneuploidy. Curr Biol 20: 1529–1533 (2010).

Rumpf C, Cipak L, Dudas A, Benko Z, Pozgajova M, et al: Casein kinase 1 is required for efficient removal of Rec8 during meiosis I. Cell Cycle 9: 2657–2662 (2010).

Sebestova J, Danylevska A, Novakova L, Kubelka M, Anger M: Lack of response to unaligned chromosomes in mammalian female gametes. Cell Cycle 11: 3011–3018 (2012).

Simunić J, Tolić IM: Mitotic spindle assembly: building the bridge between sister K-fibers. Trends Biochem Sci 41: 824–833 (2016).

Tachibana-Konwalski K, Godwin J, van der Weyden L, Champion L, Kudo NR, et al: Rec8-containing cohesin maintains bivalents without turnover during the growing phase of mouse oocytes. Genes Dev 24: 2505–2516 (2010).

Touati SA, Wassmann K: How oocytes try to get it right: spindle checkpoint control in meiosis. Chromosoma 125: 321–335 (2015).

Tsutsumi M, Fujiwara R, Nishizawa H, Ito M, Kogo H, et al: Age-related decrease of meiotic cohesins in human oocytes. PLoS One 9: e96710 (2014).

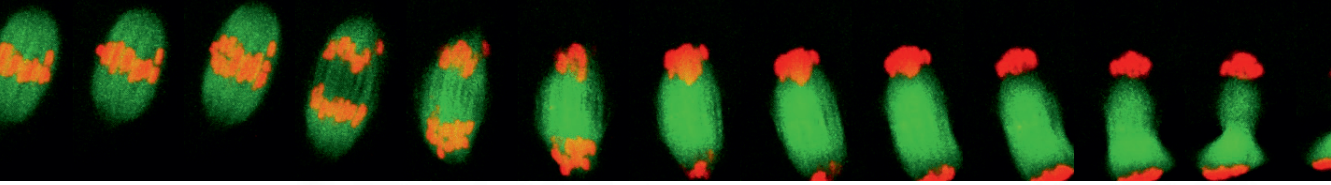

MASARYK UNIVERSITY
FACULTY OF SCIENCE
DEPARTMENT OF EXPERIMENTAL BIOLOGY

BRNO 2019